

Site investigation SFR

Water-rock interaction and mixing modelling in the SFR

María J. Gimeno, Luis F. Auqué,
Javier B. Gómez, Patricia Acero
University of Zaragoza, Spain

October 2011

Svensk Kärnbränslehantering AB
Swedish Nuclear Fuel
and Waste Management Co
Box 250, SE-101 24 Stockholm
Phone +46 8 459 84 00



Site investigation SFR

Water-rock interaction and mixing modelling in the SFR

María J. Gimeno, Luis F. Auqué,
Javier B. Gómez, Patricia Acero
University of Zaragoza, Spain

October 2011

This report concerns a study which was conducted for SKB. The conclusions and viewpoints presented in the report are those of the authors. SKB may draw modified conclusions, based on additional literature sources and/or expert opinions.

Data in SKB's database can be changed for different reasons. Minor changes in SKB's database will not necessarily result in a revised report. Data revisions may also be presented as supplements, available at www.skb.se.

A pdf version of this document can be downloaded from www.skb.se.

Abstract

During 2008, the Swedish Nuclear Fuel and Waste Management Company (SKB) initiated an investigation programme for a future expansion of the final repository for low and medium level radioactive operational waste, SFR, located about 150 km north of Stockholm. The purpose of the investigations was to define and characterise a bedrock volume large enough to allow further storage of operational waste from existing Swedish nuclear power plants and future waste from the decommissioning and dismantling of nuclear power plant reactors (SKB 2008). Of several alternatives, a selected location was investigated southwest of the present SFR tunnel system.

As part of the SFR Site Descriptive Model, the objective of the hydrogeochemical site description is to describe the chemistry, origin and distribution of groundwaters in the bedrock and the hydrogeochemical processes involved in their evolution. Hydrogeochemical information (salinity distribution, groundwater residence time, palaeohydrogeochemical input, etc.) are also of importance to help constrain the hydrogeological descriptive model.

The hydrogeochemical modelling work has been performed in three steps, resulting in three model versions (0.1, 0.2 and 1.0). In versions 0.1 and 0.2, explorative analyses using traditional geochemical approaches (trend plots, x-y scatter plots, 3D visualisations, etc.) were performed to describe the data and to provide an early insight and understanding of the site. The final hydrogeochemical site description version 1.0 (Nilsson et al. 2011) includes data from the previous versions, as well as subsequent complementary data from the SFR extension project, and all these data are further evaluated using additional modelling approaches and techniques.

In this context, the present report gives a more detailed analysis of the available data for some hydrogeochemical systems and a detailed description of the results of the geochemical and statistical modelling. One of the main aims is to establish the major geochemical processes controlling the behaviour of variables such as pH and Eh and, in general, all the parameters controlled by microbial or water-rock interaction processes. Thus, an integration of the mineralogical and microbiological data has also been performed.

The other aim is to characterise the mixing processes that have affected the groundwaters over time. Thus, a statistical analysis has been performed with M3 in order to obtain a more quantitative approach to the mixing processes in the system, as well as to provide a mathematical basis to take into account all the variability of the system and to evaluate the reliability of the categorised groundwater types which are based on expert judgement (Nilsson et al. 2010). Therefore, this report should be considered as a supporting document to the final hydrogeochemical site description version 1.0 (Nilsson et al. 2011).

Most of the main geochemical characters and trends observed in the SFR groundwaters are similar to those observed at Forsmark, especially if only groundwaters with marine contributions are compared. This applies to the carbonate, sulphate, silica and fluoride systems. No clear pH trend with depth has been found in these waters which may reflect the lateral heterogeneity of the groundwater system. The high and variable HCO_3^- values found in groundwaters with a marine signature seem to be the result of the biological activity during infiltration of marine waters through seabed sediments. Calcite equilibrium is the main pH controlling process, and its presence has been detected at all depths. Marine waters are the main source of sulphur, and neither heterogeneous reactions with sulphate minerals (undersaturated, in the case of gypsum or in equilibrium in the case of barite), nor sulphate reducing microbial activity have played an important role on the control of dissolved sulphate concentrations (conditioned, therefore, mainly by mixing). Dissolved silica and fluoride concentrations are mainly subject to mineralogical and solubility controls. For silica, this involves incongruent dissolution of feldspars with formation of secondary clays, clay mineral transformations, silica adsorption-desorption reactions in clays and chalcedony equilibrium, and for fluoride, equilibrium with fluorite.

The potentiometric Eh measurements in the SFR groundwaters provide oxidising and reducing values. Reducing values (from -140 to -190 mV) are in line with those measured in the Forsmark groundwaters and are apparently controlled by the occurrence of an iron phase with an intermediate crystallinity and/or by ferrous clay minerals, both of which have been identified. Oxidising values of

groundwaters (from +30 to +110 mV) appear to be controlled by amorphous Fe(III) oxyhydroxides and should represent the existence of present or recent oxic environments, since these phases quickly recrystallise to less soluble and more stable phases under reducing conditions.

The overall main characteristics of the redox sensitive elements would support the existence of anoxic reducing conditions in the groundwaters from the SFR. As for Forsmark, iron and sulphur represent two very important redox systems. Their evolution and behaviour are linked to bacterial activity (iron reducing bacteria –IRB, and sulphate reducing bacteria –SRB) and to some inorganic processes, such as equilibrium conditions with respect to Fe(II)-monosulphides and to siderite and reductive dissolution of ferric oxyhydroxides by hydrogen sulphide. Different inorganic reactions and microbial processes could participate in the control of dissolved manganese in the groundwaters. However, there is a clear link between manganese concentrations, equilibrium with rhodochrosite and *Littorina* signatures, i.e. preservation of hydrochemical conditions imposed by rhodochrosite formation during the infiltration of *Littorina* waters through the marine sediments. The nitrogen system also supports these anoxic reducing conditions with meaningful nitrite and ammonium contents. High nitrate concentrations detected in some SFR groundwaters (compared to those found in Forsmark or Laxemar) may be related to anthropogenic disturbances associated with the SFR facility.

The M3 results have been very helpful in supporting the discrimination of groundwater types based on expert judgment. However, it has failed in obtaining a unique set of end member waters to explain the mixing contribution to the chemical composition of the SFR groundwaters. The limited chloride concentration range, the hydraulic conditions due to the tunnel and the presence of two relatively similar brackish sea waters, complicate the calculations of the mixing proportions. These waters comprise a complex mixture of different end members and can be explained by many different combinations of end members. From all the possible mixing models identified by M3, two proved superior at predicting concentrations and both are equally suitable and reasonable from a hydrogeochemical point of view, but for different sets of samples. Additional studies using five end members together with the systematic analyses of different sets of input compositional variables, failed to resolve the best tradeoff between *accuracy* in computing the concentration of conservative elements and *resolution* in identifying all the end members that contribute to the chemistry of the groundwaters.

Contents

1	Introduction	7
1.1	Background	7
1.2	Objectives and scope	7
1.3	Hydrochemical data set	7
1.4	Report layout	8
2	Present understanding of the system	9
2.1	Geology and hydrogeology	9
2.2	Palaeohydrogeological evolution	11
2.3	Hydrogeochemistry	13
3	Assessment of mixing in the SFR area	17
3.1	Principal components analysis of water types	17
3.2	M3 analysis: selection of end-member waters and calculation of mixing proportions	21
3.2.1	Selection of input compositional variables	21
3.2.2	Selection of end-member waters	22
3.2.3	Test of mixing models	27
4	Non-redox geochemical systems	39
4.1	Carbonate system	39
4.1.1	Hydrogeochemical trends	39
4.1.2	Mineralogical data	43
4.1.3	Processes: Thermodynamic approach	44
4.1.4	Discussion and conclusions	45
4.2	Sulphate system	46
4.2.1	Hydrochemical trends	46
4.2.2	Speciation-solubility calculations	48
4.2.3	Conclusions	51
4.3	Silica system	52
4.3.1	Hydrochemical trends	53
4.3.2	Speciation-solubility calculations	54
4.3.3	Conclusions	55
4.4	Fluoride system	56
4.4.1	Hydrochemical trends	57
4.4.2	Speciation-solubility calculations	57
4.4.3	Conclusions	57
5	Redox geochemical systems	59
5.1	Selection of redox data	59
5.1.1	Selection of representative Eh and pH values	59
5.1.2	Selection of samples for redox modelling	60
5.2	Redox potentials	61
5.2.1	Potentiometric Eh measurements	61
5.2.2	Redox pair calculations	63
5.2.3	Conclusions	67
5.3	Sulphur and iron systems	67
5.3.1	Hydrochemical trends	68
5.3.2	Mineralogical data	69
5.3.3	Processes: Thermodynamic approach	71
5.3.4	Conclusions	75
5.4	Manganese system	76
5.4.1	Hydrochemical trends	76
5.4.2	Mineralogical data	76
5.4.3	Processes: Thermodynamic approach	78
5.4.4	Conclusions	79

5.5	The Nitrogen system (nitrate, nitrite and ammonium)	80
5.5.1	Hydrochemical data	80
5.5.2	Comparison with other crystalline systems and with the Baltic Sea waters	82
5.5.3	Microbiological data	83
5.5.4	Conclusions	83
5.6	Molecular hydrogen and methane	84
6	Conclusions	87
7	References	91
Appendix 1	Searching for suitable compositions of the Baltic and the Old Meteoric end members	99
Appendix 2	M3 results	107
Appendix 3	pH uncertainties in speciation-solubility calculations	123
Appendix 4	Review of on-line Eh measurements in the SFR	131

1 Introduction

1.1 Background

With the objective of a future expansion of the final repository for low and medium level radioactive operational waste, SFR, the Swedish Nuclear Fuel and Waste Management Company (SKB) initiated in 2008 an investigation programme for defining and characterising a bedrock volume large enough to allow further storage of operational waste from existing Swedish nuclear power plants, and future waste from the decommissioning and dismantling of nuclear power plant reactors.

The investigation programme within the SFR extension project was performed between 2007 and 2009 with some complementary studies conducted during 2010. Although the approach shows close similarities to the Forsmark site investigations, the area is much smaller, the rock volume studied is mostly at shallow depths (down to ~ 400 m.a.s.l.) and almost completely covered by the Baltic Sea, and the location is close to an existing repository facility, the construction of which has had a marked impact on the groundwater chemistry, and to some extent continues to do so. Together, these conditions present a special set of circumstances which have not been addressed before within the SKB site investigation programmes (Nilsson et al. 2011).

As part of the SFR Site Descriptive Model, a thorough hydrogeochemical site description has been conducted to describe the chemistry, origin and distribution of groundwaters in the bedrock and the hydrogeochemical processes involved in their evolution. The hydrogeochemical modelling work has been performed in three steps, resulting in three model versions (0.1, 0.2 and 1.0). In versions 0.1 and 0.2, explorative analyses using traditional geochemical approaches (trend plots, x-y scatter plots, 3D visualisations, etc.) were performed to describe the data and to provide an early insight and understanding of the site. The final hydrogeochemical site description version 1.0 (Nilsson et al. 2011) includes data from the previous versions, as well as subsequent complementary data from the SFR extension project, and all these data are further evaluated using additional modelling approaches and techniques.

This report should be considered as a supporting document to the final hydrogeochemical site description version 1.0 (Nilsson et al. 2011).

1.2 Objectives and scope

The main objectives of the present work are; (1) to identify the main geochemical processes controlling the behaviour of variables such as pH and Eh and, in general, all the parameters controlled by microbial or water-rock interaction processes, and (2) to characterise the mixing processes that have affected the groundwaters with time.

The integration of the fracture filling and microbial data has also been considered an important aim since they may provide important information for the site understanding. Finally, a special effort has been made in analysing the processes and uncertainties associated with the present input of Baltic Sea waters into the bedrock as the main anthropic effect in the SFR system.

1.3 Hydrochemical data set

The dataset forming the basis for the modelling stage version 1.0 in the SFR extension project (and used in this report) contains quality assured data from the recent investigation phase in the target area south-west of the repository (Jönsson et al. 2008, Thur and Nilsson 2009a, b, Thur et al. 2009, Lindqvist and Nilsson 2010) as well as from earlier studied boreholes in the present SFR facility (Nilsson 2009), from two PLU boreholes (Gustavsson et al. 2006) and from complementary investigations in the present SFR in the Autumn of 2010 (Nilsson 2011). This hydrochemical dataset has been obtained from 12 recent borehole sections in five boreholes (and from the entire length of two open boreholes in connection with hydraulic tests) together with data from a total of 18 early boreholes in the present SFR tunnel system.

The main part of the data consists of basic groundwater analyses including isotopes, although a few gas, microbe and redox data are also available. Quality checked data were extracted from the Sicada database (Sicada-10-077 (0:1)), complemented with later data (Sicada-11-056 (0:1)) and compiled to produce the

Hydrogeochemistry Data Table version 1.0. This data table, in Excel format, is used for all the interpretation and modelling work and is stored in the SKB model database SKBDoc for traceability.

The quality assurance of the hydrochemical data and the selection criteria of groundwater samples in the available hydrochemical database delivered by SICADA for the SFR site are detailed in Nilsson (2009) and Nilsson et al. (2010, 2011). In these reports, analytical uncertainties, impacts on sampling and sampling conditions (e.g. from grouting, drilling, drilling water) or effects from the use of different sampling techniques, have been evaluated and discussed.

Additional review of the hydrochemical database delivered by SICADA has been performed in this work. For the speciation-solubility calculations, samples with a charge balance error exceeding $\pm 5\%$ have been eliminated, in common with the Site Descriptive Models for Forsmark, Laxemar-Simpevarp and SFR (Nilsson 2009, Nilsson et al. 2010).

An important source of uncertainty associated with the available hydrochemical data is related to the pH determinations. Apart from the pH measurements obtained with the Chemmac probe for 7 borehole sections, field measurements for pH are available only for 78 of the 416 samples from the studied area (i.e. 19% of the total number of samples). This situation represents an important limitation to the development and interpretation of speciation-solubility calculations, affecting in particular the characterisation of redox processes and the carbonate system. Thus, an analysis of the effects of pH uncertainty on the results and interpretations has been performed for each of the speciation-solubility calculations presented in this work (Appendix 3).

The selection of the representative pH and Eh values from Chemmac log data for each specific borehole section from the SFR area has also been performed in this work. It has been based on a careful analysis of the data delivered by SICADA and those data available in the methodological P-reports. The whole selection procedure, similar to that used in the Site Characterisation Programmes from the PLU and Laxemar-Simpevarp areas (Gimeno et al. 2008, 2009), is described in Appendix 4.

The groundwaters in the SFR dataset cover a maximum depth down to about -400 m.a.s.l. and represent a relatively limited salinity range (1,500 to 5,500 mg/L chloride). Overall, this hydrochemical dataset is less comprehensive than for the previous site investigation programme at Forsmark (henceforth referred to as the 'Forsmark site investigations' or 'PLU' (SKB 2001)), reflecting the fact that the number of drilled boreholes is comparatively few. Furthermore, the candidate area in the SFR is relatively small and the issues to consider in the safety assessment are somewhat different from PLU (see Nilsson et al. 2011).

1.4 Report layout

In addition to this introductory Chapter 1, a summary of the present understanding of the system is presented in Chapter 2 with special emphasis on present knowledge of the geological, hydrogeological and structural features of the SFR site and their effects on the groundwater evolution. This will help to understand the different modelling work performed later on.

Chapter 3 presents the statistical analysis performed with M3 for the study of the mixing processes with a thorough explanation of the methodology and the uncertainties and limitations involved.

Water-rock interaction processes are studied in Chapters 4 and 5. Chapter 4 describes the geochemical modelling of the non redox systems, including carbonates, sulphates, silica and fluoride. Chapter 5 deals with the redox parameters including the potentiometrical measurements and the description and modelling of the redox sensitive elements (sulphur and iron, manganese and nitrogen and the dissolved gases). Chapter 6 summarises the main conclusions of this work.

Finally, a series of appendices has been added to complement the information shown in this report. Appendix 1 presents the calculation of the chemical composition of the Baltic and the Old Meteoric end members. Appendix 2 lists the mixing proportions for the selected mixing models and the theoretical compositions obtained with them assuming only mixing. Appendix 3 deals with the uncertainty analysis performed with respect to the use of the pH values. Results of speciation solubility calculations (saturation indices and redox pair values) using both measured pH (mostly laboratory values) and pH calculated assuming calcite equilibrium, are compared. Appendix 4 reports the selection of Eh and pH values performed by the University of Zaragoza (UZ) group. A comparison with the values proposed in the SICADA database is also reported where P-reports are available.

2 Present understanding of the system

The general presentation of the data, the hydrogeochemical explorative analysis and the conceptual model, are all thoroughly described in the final hydrogeochemical site description version 1.0 (Nilsson et al. 2011). Here, only a short summary of the main geological and hydrogeological features of the system and the present conceptual hydrogeochemical model are presented to put this present work into context.

2.1 Geology and hydrogeology

The SFR bedrock is dominated by different types of metamorphosed granitoid with subordinate felsic to intermediate metavolcanic rocks, metamorphosed diorite or gabbro, and pegmatite or pegmatitic granite formed between 1.89 and 1.85 billion years ago (Curtis et al. 2010). Ductile-brittle and brittle deformation occurred several times during the Proterozoic (Svecokarelian, Gothian and Sveconorwegian orogenies) and other secondary geological processes (loading by sedimentary rocks or by ice during glacial periods, unloading related to denudation of this younger sedimentary material and/or melting of an accumulated ice mass) have also affected the bedrock at several times during the Proterozoic and Phanerozoic. This has resulted in the activation and subsequent reactivation of the different fracture systems and the exposure of the Proterozoic crystalline bedrock accompanied by stress release effects.

The major structures comprising the SFR area are shown in the magnetic total field image in Figure 2-1. The site is divided into three structural domains to facilitate localisation for the reader (Curtis et al. 2010); (1) the Southern Boundary Belt or Southern Belt, dominated by the deformation zone ZFMWNW0001 (Singö zone), (2) the Northern Boundary Belt or Northern Belt, dominated by the deformation zones ZFMNW0805A and B (formerly Zone 8), and (3) the SFR Central Block or the Central Block which corresponds to the domain between the Southern and Northern belts.

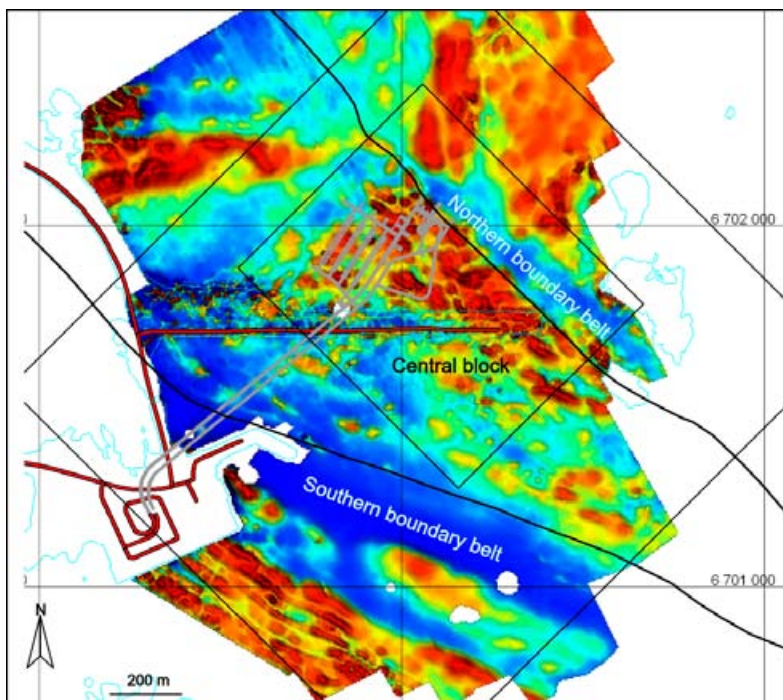


Figure 2-1. Magnetic total field demarcating the SFR Central Block containing the existing SFR storage facility, the Northern Boundary Belt (dominated by deformation zone ZFMNW0805A) and the Southern Boundary Belt (dominated by deformation zone ZFMWNW0001). Taken from Curtis et al. (2010).

Therefore, the Northern and Southern Boundary Belts delimit the SFR site/target area. These two steeply dipping deformation zones (ZFMWNW0001 and ZFMNW0805A, B), together with the other steeply dipping zones (i.e. ZFMNE0870A and B – formerly Zone 9 –, ZFMN1209 – formerly Zone 6 – and ZFMNNE0869 – formerly Zone 3 – within and close to the target area, i.e. the Central Block; Figure 2-2), have served as important groundwater flow pathways over long periods of geological time. Some of these steeply dipping zones (e.g. ZFMNNE0869, ZFMNW0805A, B and ZFMNE0870), have some hydraulic contact with the gently dipping deformation zone ZFM871 (formerly Zone H2) which is located just beneath the silo at the SFR.

From a hydrological point of view, the bedrock at the SFR has been divided at about –200 m.a.s.l. into the shallow bedrock aquifer (SBA), with a high frequency of interconnected transmissive fractures, and the underlying bedrock characterised by a decrease of interconnected fracture frequency with depth and therefore of lower transmissivity (Figure 2-3). The SBA is considered to play an important role in the hydraulic connectivity of the rock mass in the vicinity of the Northern Boundary Belt, but is of less significance further away in the Central Block towards the Southern Belt and below –60 m.b.s.l. (Öhman et al. 2011).

Most of the hydrogeochemical data from the SFR site originates from deformation zones or possibly shallow bedrock aquifer (SBA) features and only a limited amount comes from discrete single fractures in the bedrock mass between zones.

The present groundwaters in the SFR are a result of complex mixing and reactions over a long period of geological time. In addition, the situation of the SFR (under the Baltic Sea¹) has led to the present intrusion of Baltic Sea waters due to drawdown related to the present SFR tunnel system. This artificially induced mixing is superimposed to the natural groundwater mixing patterns established prior to the SFR construction, of similar palaeohydrogeochemical origin to those described at Forsmark (see Section 2.2).

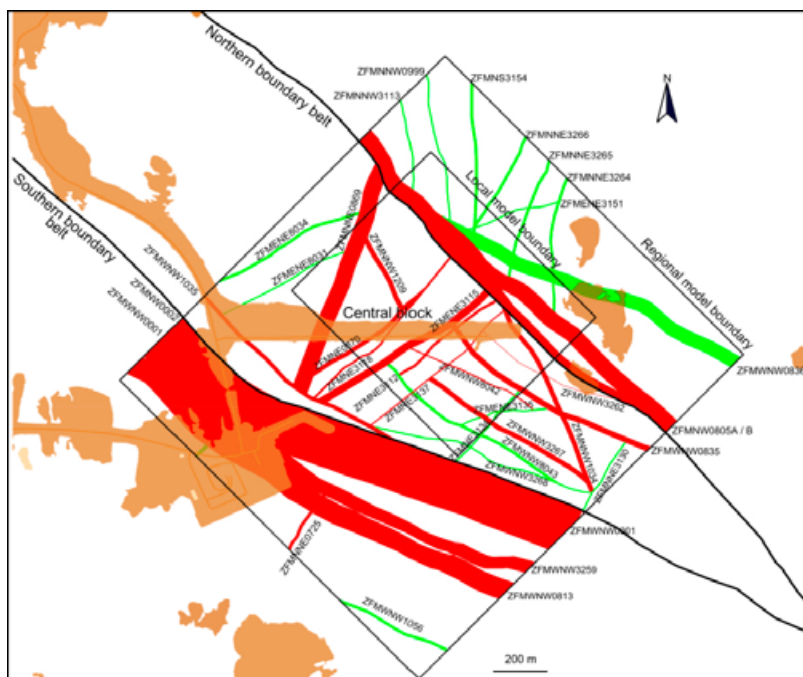


Figure 2-2. Intersection at the current ground surface of deformation zone traces of all sizes inside the regional model area, i.e. a combined model version. The regional deformation zones ZFMWNW0001 and ZFMNW0805A, along with their major splays, form the southern and northern boundaries of the central SFR tectonic block. Confidence in existence; high=red, medium=green). Taken from Curtis et al. (2010).

¹ Fresh groundwater of present meteoric origin is almost absent because the SFR is located under the Baltic Sea.

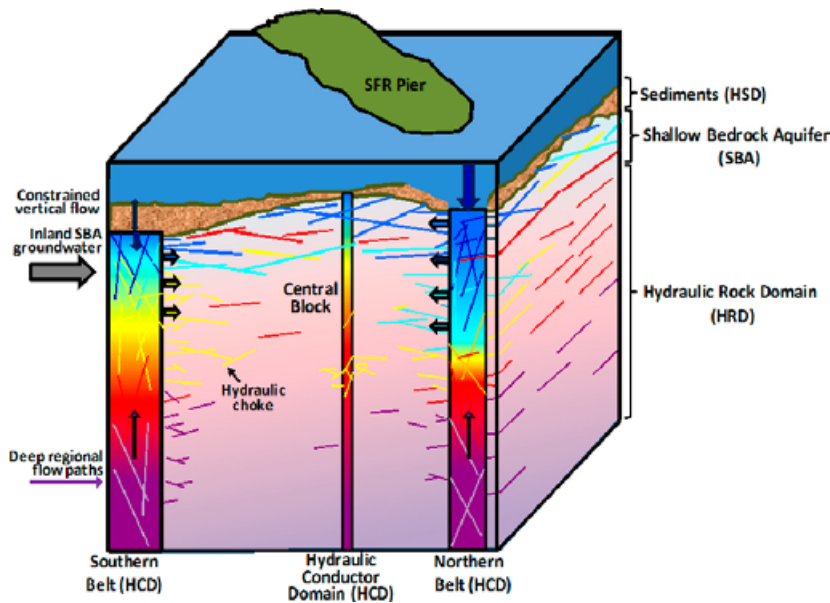


Figure 2-3. Conceptual block model (0–1,000 m depth) integrating the major hydrogeological and hydrogeochemical features of the investigated SFR rock volume. The different groundwater types are indicated by the same colour scheme used in the rest of the plots with the exception of the deeper saline groundwater which is indicated by lilac and is not present as a dominant groundwater type in the SFR rock volume (taken from Nilsson et al. 2011).

Hydrostructural properties of the bedrock and the regolith features have an important role in controlling the mixing paths and the degree of superposition of old and recent (Baltic intrusion) mixing events. The sea bottom above the SFR is characterised by recent sea sedimentation and still older Quaternary deposits. The nature and thickness of these overlying sediments are quite heterogeneous; the sediment layers (including low conductive glacial clays) are considerably thicker on the south side of the pier (Southern Boundary Belt; Figure 2-3) compared to the north side of the pier (Northern Boundary Belt) where there are areas with no, or only partial, sediment coverage (see Öhman et al. 2011). Therefore, the character of these overlying sediments may regulate the hydraulic connection between the Baltic Sea and the underlying rock mass (Öhman et al. 2011) and, thus, they may be important to explain past and present hydrogeochemical conditions, for example, the presence, or not, of Baltic type groundwater in the underlying bedrock.

2.2 Palaeohydrogeological evolution

Past climatic changes, which in the Forsmark region have involved both glaciations/deglaciations and marine transgressions/regressions, are the major driving forces for long term hydrogeochemical changes and are, therefore, of fundamental importance in understanding the palaeohydrogeological, palaeohydrogeochemical and present evolution of the groundwater in the region. Figure 2-4 shows the conceptual model for the Forsmark region following the last deglaciation.

Based on this, an overall evolutionary model has been proposed for the SFR area. Prior to the last deglaciation, the groundwaters at the SFR are considered to have comprised non-marine types changing from brackish to saline with increasing depth. Mixed components of old meteoric waters, derived from both temperate and cold climate events, are also thought to have been present at shallow to intermediate depths. Figure 2-5a shows a tentative distribution of groundwater types and salinity gradients in the SFR area before the intrusion of the last deglaciation meltwater just prior to the Holocene.

During the last deglaciation dilute glacial meltwaters under high hydraulic gradients (Figures 2-4a and 2-5b) penetrated to maximum depths investigated at the SFR (~ -400 m.a.s.l.) and probably to still greater depths in common with observations at Forsmark (Laaksoharju et al. 2008).

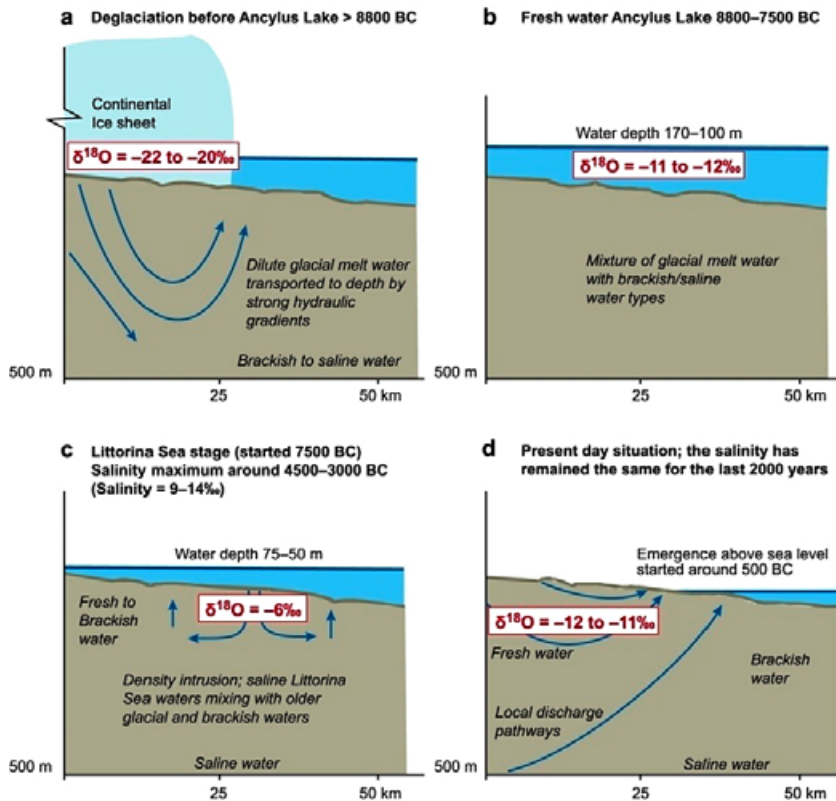


Figure 2-4. Conceptual model for the Forsmark region following the last deglaciation. The different stages are; a) deglaciation before the Ancylus Lake (>8800 BC), b) freshwater Ancylus Lake between 8800 to 7500 BC, c) density intrusion of Littorina Sea water between 7500 BC to 0 AD, and d) the present day situation where the SFR is situated below sea-level just outside the coast line. Blue arrows indicate possible groundwater flow patterns. After Laaksoharju et al. (2008).

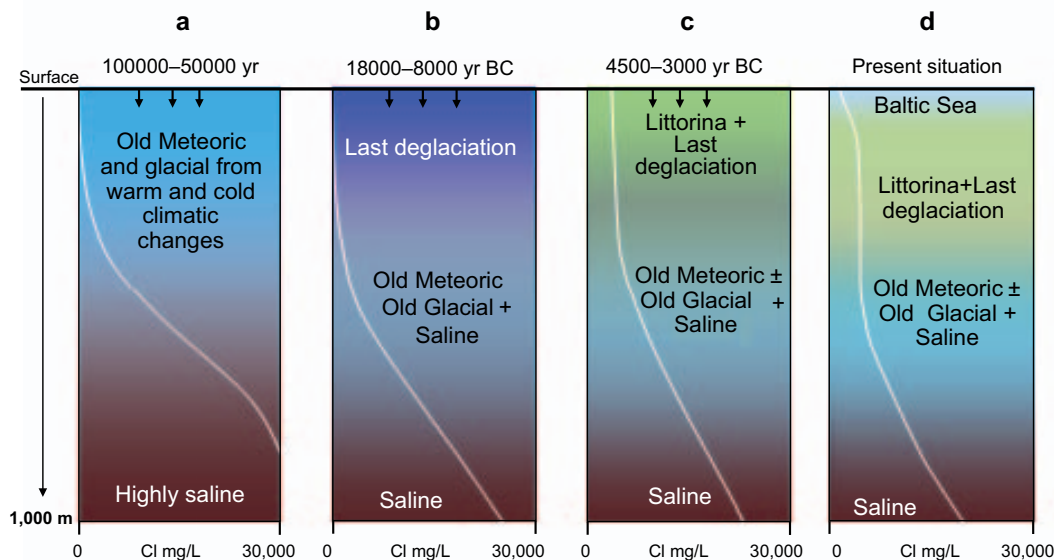


Figure 2-5. Sketch showing tentative salinities and groundwater-type distributions versus depth for the transmissive deformation zones at the SFR. From left to right; a) situation prior to the last deglaciation, b) last deglaciation and intrusion of Late Weichselian meltwater, c) the Littorina Sea water penetration caused by density intrusion, and d) the present situation with possible penetration of local Baltic Sea water. After Nilsson et al. (2011).

These waters mixed with the resident non-marine brackish to saline and old meteoric groundwaters resulting in a range of brackish glacial types. The largest components of glacial waters are found between –100 and –250 m.a.s.l.

Subsequently during the Holocene, the Ancylus Lake (years 8800 to 7500 BC) was developed after the deglaciation (Figure 2-4b) although there are no signs of Ancylus lake water in the bedrock. This period was followed by the brackish Littorina Sea transgression that resulted in the density driven infiltration of saline waters into the bedrock along many of the same transmissive flow paths that earlier channelled the glacial meltwaters (Figures 2-4c and 2-5c). This produced varying degrees of mixing, whilst sometimes in less hydraulic conductive fractures or less transmissive rock mass areas between the major deformation zones, the glacial meltwater appears to have been preserved.

Following the Littorina stage (and the subsequent transition to Baltic Sea conditions), the area continued to be submerged, and slowly moving, deep regional discharge flow paths within the highly transmissive deformation zones were once again dominant. This was the likely hydrogeological situation prior to commencement of the SFR investigation phase in 1985 (Figure 2-4d).

The present situation is shown in Figure 2-5d which illustrates the intrusion of present Baltic Sea water in some fractures down to about –100 m.a.s.l. (Figure 2-3). This intrusion is probably to a large extent driven by the hydraulic gradient created by the existing SFR storage facility.

The impact of changes in flow paths and groundwater drawdown effects during and following construction of the SFR tunnel system has influenced the groundwater chemistry. These changes have been addressed in terms of observed changes in chemistry, based on sample time series data from commencement of the SFR excavation/construction phase, and the hydrochemistry of present day groundwater compositions related to different bedrock features influenced by drawdown effects.

2.3 Hydrogeochemistry

The previous palaeoclimatic considerations form the basis for the explorative analyses and, especially, for the identification of the different groundwater types defined in Nilsson et al. (2011). This subdivision was performed by expert judgement similar to that conducted within the site modelling (e.g. Smellie et al. 2008) at Forsmark. However, in order to further test this subdivision, a principal component analysis of the waters has also been carried out and discussed in this report (see Section 3.1).

Four different groundwater types are differentiated in the SFR from the perceived main origin of the waters (Baltic Sea water, Littorina Sea water, glacial meltwater etc.) although their compositions have subsequently been altered by mixing and reaction processes²:

- Local Baltic Sea type (blue)³: Brackish marine water with a Cl content of 2,500 to 3,500 mg/L and $\delta^{18}\text{O}$ at –9 to –7.5‰ VSMOW (these Cl and $\delta^{18}\text{O}$ ranges correspond to that of Baltic Sea water sampled off the coast at the SFR). This is a brackish water of marine origin with some modification caused by ion exchange and microbial reactions which has resulted in the lowering of Mg, K, Na and SO_4^{2-} and enrichment of Ca and HCO_3^- compared with the Baltic Sea. Some samples referred to the Local Baltic Sea type also contain components of Littorina and Brackish-glacial water types.
- Littorina type (turquoise): Brackish marine water with a Cl content of 3,500 to 6,000 mg/L and $\delta^{18}\text{O}$ at –9.5 to –7.5‰ V-SMOW. This is a brackish water also of marine origin (infiltrated during the Littorina period) with some modification caused by interaction with the seabed sediments, ion exchange and dilution from the contributing glacial meltwater (as deduced from the depleted $\delta^{18}\text{O}$ values compared to the Littorina end member, at around –5‰ V-SMOW). It has a higher salinity than the present Baltic Sea although some samples may also contain portions of Baltic Sea water.

²The groundwater types differentiated in the SFR should not be mistaken for the end members or “original groundwaters” which represent the original composition of the waters (glacial meltwaters, Baltic Sea water, Littorina Sea waters, etc.) that subsequently will be mixed in the bedrock. Therefore, when using and describing the groundwater types it is important to remember that, for example, the Littorina type groundwater is a mixture of different groundwaters with a significant (dominating) component of Littorina Sea water (see also Section 3.1).

³The colour indicated between brackets for each water type is the one used in all the plots where waters are colour coded.

- Brackish-glacial type (red): Brackish groundwaters with a Cl content of 1,500 to 5,000 mg/L and $\delta^{18}\text{O} < -12.0\text{‰}$ V-SMOW. This water type has low Mg, K, SO_4 and HCO_3 and shows higher Br/Cl ratios than marine waters. It is a mixture of glacial (last deglaciation or older) + brackish non-marine water \pm Littorina. The marine signature is generally weak and this type represents the oldest present at the SFR with small amounts of post-glacial components.
- Mixed Transition type (yellow): Brackish groundwater with a Cl content of 2,500 to 6,000 mg/L and $\delta^{18}\text{O}$ at -12.0 to -9.5‰ V-SMOW. Waters in this group result from the mixing of the above three groundwater types (the mixing may either be natural or artificially created by the drawdown caused by the SFR repository or during the drilling and sampling procedures). Most of these waters contain components of brackish marine waters (maybe of different ages but mostly Littorina in type) + glacial waters (from the last deglaciation or older) \pm weakly brackish waters.

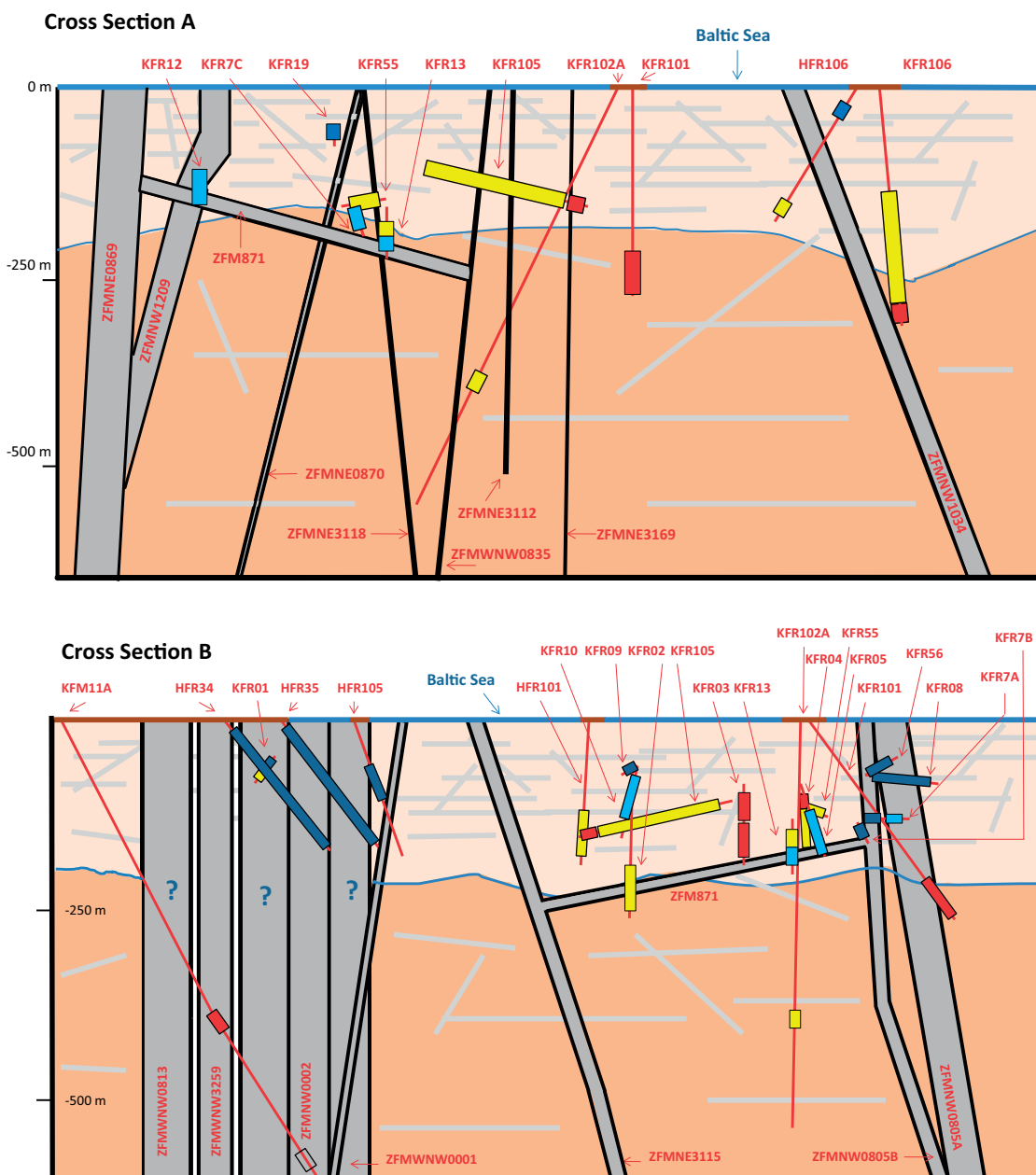


Figure 2-6. Vertical cross sections A (NW-SE) and B (SW-NE) showing a simplified visualisation of the SFR volume area. Groundwater types are colour coded and the upper bedrock division (light beige colour with high fracture intensity) represents the Shallow Bedrock Aquifer. The actual intersections of the structural zones are indicated and the boreholes when not aligned along the section are extrapolated onto the same 2D plane (taken from Nilsson et al. 2011).

In Figure 2-6 two vertical 2D sections with a simplified visualisation of the distribution of the different groundwaters types and their relation to the important transmissive deformation zones in the SFR site are shown. A division at about –200 m.a.s.l. is also indicated between the shallow bedrock aquifer (light beige colour) with a high frequency of interconnected transmissive fractures, and the underlying bedrock (darker beige colour) characterised by a decrease of interconnected fracture frequency with depth and therefore of lower transmissivity.

Glacial meltwater was hydraulically injected under considerable head pressure into the bedrock during the deglaciation stage, approximately 18,000 BC to 8000 BC. The exact penetration depth is still unknown, but will depend on the hydraulic properties of the bedrock. Because of the shallow depth of the investigated SFR site, penetration of glacial meltwater has been widespread, certainly down to zone ZFM871 (formerly Zone H2) facilitated by the intersecting vertical to steeply dipping transmissive deformation zones. These glacial meltwaters underwent mixing with the older, pre-existing groundwaters comprising old meteoric waters and deeper non-marine brackish to saline types (depending on depth) to form a range of brackish-glacial groundwater types (Figure 2-6; boreholes KFM11A, KFR03, KFR04, KFR101, KFR105 and KFR106).

During the subsequent Littorina Sea transgression, density driven marine waters preferentially followed the same major transmissive pathways to zone ZFM871 and potentially beyond. Mixing with the earlier resident old meteoric and non-marine brackish-glacial groundwaters led to the formation of a range of mixed groundwater types with the brackish-glacial types. The strongest Littorina signatures seem to have been preserved in the steeply dipping zones of ZFMNNE0869 (formerly Zone 3) and ZFMW0805A, B (formerly Zone 8a and b), and within or close to zone ZFM871 (formerly Zone H2). The importance of this hydraulic connection with subhorizontal zone ZFM871 can be seen in both visualisations, namely, where the main concentration of the Littorina type groundwaters with a variable glacial component are present (Figure 2-6; boreholes KFR05, KFR7A, KFR7C, KFR09, KFR10, KFR12, KFR13).

The division of the SFR groundwaters into different types has facilitated interaction and integration with the hydrogeological models. The distribution of these types shows that the major deformation zones have served as important groundwater flow pathways over long periods of geological time, whilst single fractures in rock volumes between zones generally contain older and more isolated groundwater that still retain evidence of the older groundwater mixing patterns. The major groundwater features can be summarised as follows:

- Baltic Sea waters have been infiltrating the SFR since its construction and mixing with near surface Littorina type groundwaters and, possibly, also brackish glacial-type groundwaters along the more hydraulically conducting pathways (Figure 2-6). Therefore, as seen in Figure 2-6, local Baltic type groundwaters are present at shallow levels and associated with the large scale transmissive deformation zones ZFMWNNW0001 (Singö zone) and ZFMNW0805A and B (formerly Zone 8), that is, the major steeply dipping Northern and Southern Boundary Belts.
- However, whilst the Northern Boundary Belt (with thin sedimentary cover and rapid intrusion of local Baltic type water) strictly follows a mixing line between Littorina and local Baltic type groundwaters, the Southern Belt (with thick sedimentary cover which impedes rapid intrusion of local Baltic type water) shows a less marine signature. This is also seen in the groundwaters related to the gently dipping heterogeneous zone ZFM871 (formerly Zone H2) which show a more marine character when close to the Northern Boundary Belt, whilst groundwaters located further away show a non-marine character.
- The strongest Littorina signatures appear to characterise the junctions between the vertical zones ZFMNNE0869 and ZFMNW0805A, B and the gently dipping zone ZFM871 (formerly Zone H2).
- In the Southern Boundary Belt a discharge of shallow groundwater from the inland via the upper conductive shallow bedrock aquifer may supply a groundwater mixture of young meteoric and Littorina origin to this depth interval. However, it is not clear at the moment whether this mixture could progress further to the northeast beyond the Southern Belt.
- Variable mixing of the three major groundwater types (Local Baltic type, Littorina type and Brackish-glacial type) under both natural and anthropogenic conditions corresponds to the Mixed Transition type groundwaters. The boreholes associated with this type of groundwaters are HFR101, KFR01, KFR02, KFR04, KFR7A, KFR7C, KFR10, KFR13, KFR55, KFR102A, KFR105, KFR106; Figure 2-6. These groundwater types are often located where there is a more dynamic groundwater circulation conducive to mixing processes.

- There are still scarce data in the Central Block and the area southeast of zones ZFMENE0870 and ZFM871 (the recently investigated SFR extension project area), but it appears that the overall hydrochemistry of groundwaters in this domain have not undergone any major changes due to the Baltic Sea water intrusion.

Thus, deformation zones and SBA properties, as well as sea sediment thickness, play important roles in explaining the distribution and mixing of different groundwater types, including the Baltic Sea intrusion, during and following construction of the SFR.

Collectively, the obtained results indicate that the greatest mixing effects with Baltic Sea waters have occurred soon after construction of the SFR reflecting changes in groundwater pressure and inflow to boreholes and the tunnel system. Since then, conditions have slowly stabilised to reach close to equilibrium around year 2000 (Nilsson et al. 2011).

Overall, both recent and old mixing events appear to control some of the main hydrochemical features of the groundwaters at the SFR further modified by the dynamic hydrogeological properties of the regolith and the bedrock. In this report, the importance of the water-rock interaction processes associated to those mixing events is explored.

3 Assessment of mixing in the SFR area

3.1 Principal components analysis of water types

Each sample in the general data table has been assigned by expert judgment to one of the four water categories described above (Nilsson et al. 2010, 2011), using the letter and colour coding listed in Table 3-1. To these groundwater types, a set of Baltic Sea waters (sampled near SFR during the PLU activities) has been added and allocated a black colour code.

The objective of this section is to compare the categorisation obtained by expert judgment (based on detailed knowledge of the hydrogeochemistry of the site) with a “blind” categorisation obtained by a multivariate statistical analysis.






Figure 3-1 shows three principal component projections of the complete dataset using the original colour code for each sample. The principal components analysis was carried out using Cl, SO₄, δ²H and δ¹⁸O as input compositional variables (ICVs). The first principal component (axis labelled “Component 1” in Figure 3-1) stores information on the “lightness” of the isotopes (isotopically light samples plot on the left and heavy samples on the right); the second component (Component 2) carries information on TDS (very dilute samples plot in the lower part of the axis and less dilute ones in the upper part); the third (Component 3) on sulphate concentration (with low SO₄ samples plotting in the upper part and high SO₄ samples in the lower part); and finally component 4 carries information on the isotopic ratio (with high ²H/¹⁸O ratio samples plotting in the lower part of the axis and samples with a low ratio in the upper part).

Lines have been added to these three graphs marking the boundaries between water categories. They actually represent planes in the three-dimensional volume. The top graph (plotting component 1 against component 2) has three lines; one marks the boundary between the Brackish Glacial (red) and Transition (yellow) water types, other marks the boundary between the Transition and the Littorina+Local Baltic water types, and the last one (horizontal) marks the boundary between the Littorina and the Local Baltic water types. The middle and bottom graphs in Figure 3-1 only have two lines; one marks the boundary between the Brackish-Glacial and the Transition water types, and the other marks the boundary between the Transition and the Littorina+Local Baltic water types.

These lines have been drawn to minimise the number of colour (i.e. water type) changes with respect to the original categorisation. In other words, the position of the lines is such that they separate the categories (by statistical means) matching as close as possible the previous categories (defined by expert judgment). As Table 3-2 shows and Figure 3-1 confirms, only a very small number of samples belong to a different water category by both methods.

From the 15 samples recorded in Table 3-2, three (ID samples: 216, 254, and 324) are virtually on the line separating two categories and thus their type could be either one (T or L); two other samples (40 and 312) have an anomalous composition (very high SO₄ concentration for their Cl content) and, although they have been changed from water type T to L, they could as well have been assigned to a brand new water type (see their anomalous position in the middle graph of Figure 3-1). This leaves only 10 samples with a “reassigned” water category, which confirms the overall quality of the initial categorisation based on expert judgement.

Table 3-1. Letter and colour code for the different water types, including sea water (not groundwater) from the Baltic Sea (black).

Water type	Letter	Colour
Local Baltic type	B	
Littorina type	L	
Mixed transition type	T	
Brackish-glacial type	G	
Baltic Sea water	BS	

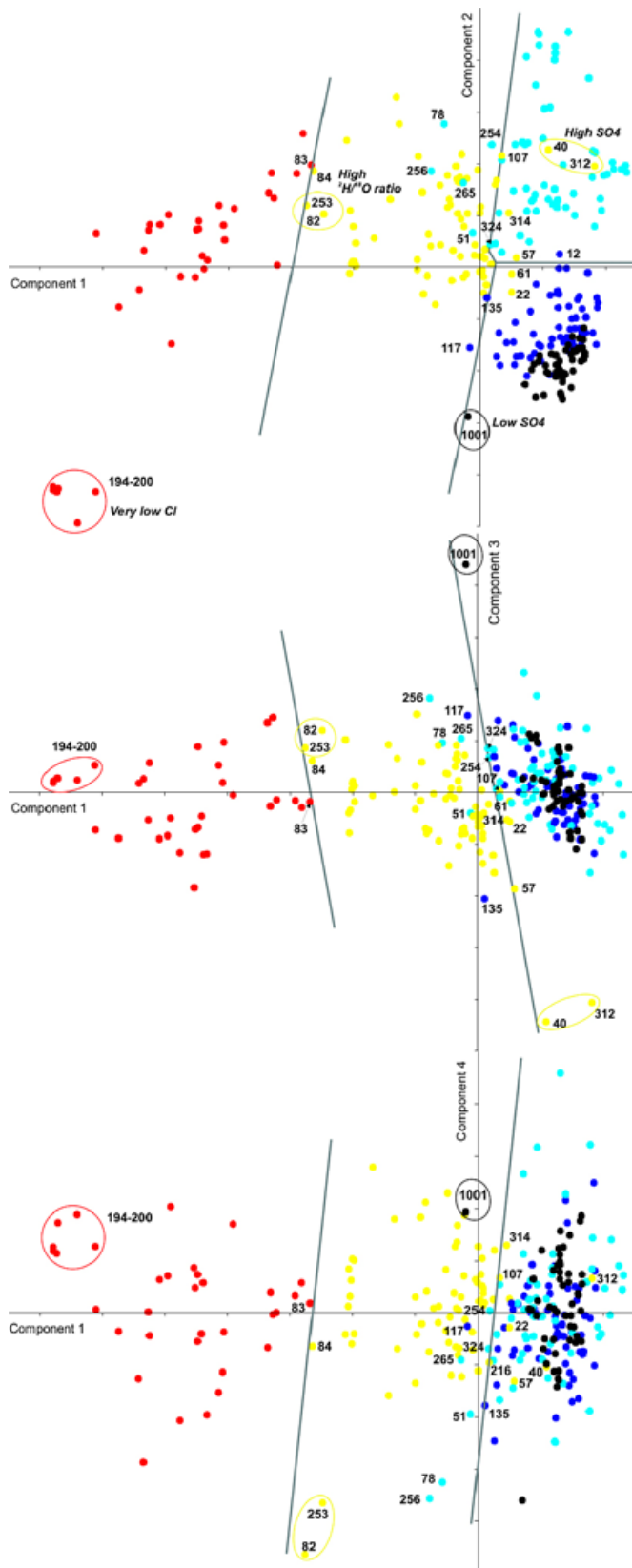


Figure 3-1. Three PC projections (all with the first principal component as the horizontal axis) showing the boundaries between water types. Samples plotting in the “wrong” PC area are labelled. Also labelled are several samples with anomalous compositions (encircled). The PCA has been performed with Cl, SO₄, δ²H and δ¹⁸O as input compositional variables.

Table 3-2. Samples with reassigned water type. ID Sample is the identification number (in correlative order) as it appears in the Hydrogeochemistry Data Table version 1.0 (in Excel format and stored in the SKB model database SKBDoc for traceability).

ID Sample	ID code	Sample Number #	Old water type	New water type
22	KFR01	13948	T	B
40	KFR01	13446	T	L*
51	KFR01	17034	L	T
57	KFR01	17074	T	L
61	KFR01	12651	T	B
107	KFR04	13957	T	L
117	KFR08	3219	B	T
135	KFR08	17000	B	T
216	KFR105	16362	T	T/L
254	KFR13	13967	L	T/L
256	KFR13	12663	L	T
265	KFR55	3204	L	T
312	KFR7A	16094	T	L*
314	KFR7A	16585	T	L
324	KFR7C	3223	L	T/L

Figure 3-1 also identifies several samples with anomalous compositions (encircled and labelled in the upper graph). Two of these samples have been discussed already in the previous paragraph (40 and 312). Besides them, there is a group of 6 samples (194–200) with very low Cl contents (ranging from 1,610 to 1,880 mg/L, whereas the next less dilute sample in the dataset has a Cl content of 2,464.7 mg/L). In fact, as will be seen below, this group of samples can not be easily explained as a mixture of any of the selected end-member waters. Samples 82 (T) and 253 (T) have a $^2\text{H}/^{18}\text{O}$ ratio (> 9) which is much higher than any other Transition type groundwater; finally, sample 1001, a Baltic sea water sample, has a concentration of sulphate which is half of the average SO_4 concentration of all Baltic sea water samples (196 mg/L against 400 mg/L). As all the other elements in the chemical analysis of this sample are in concentrations close to the average one, it seems that the anomalous SO_4^{2-} content could be an analytical artefact.

Figure 3-2 shows again the PC1 vs PC2 projection but now the position of the end members has also been added. As shown in these plots, SFR groundwaters form a very narrow concentration fairly well lined up between the Littorina and the Glacial end members, which are at a similar distance to the group of samples. Baltic Local and the two meteoric end members plot roughly on the Glacial-Littorina line and close to the groundwater samples. On the other hand, the Deep Saline end-member plots very far from the group.

So, in general, the relative position of the samples and the end members is indicative of two facts; (1) that these waters are a complex mixture of the different end members, and (2) that, as will be shown below, they can be explained by many different combinations of end members.

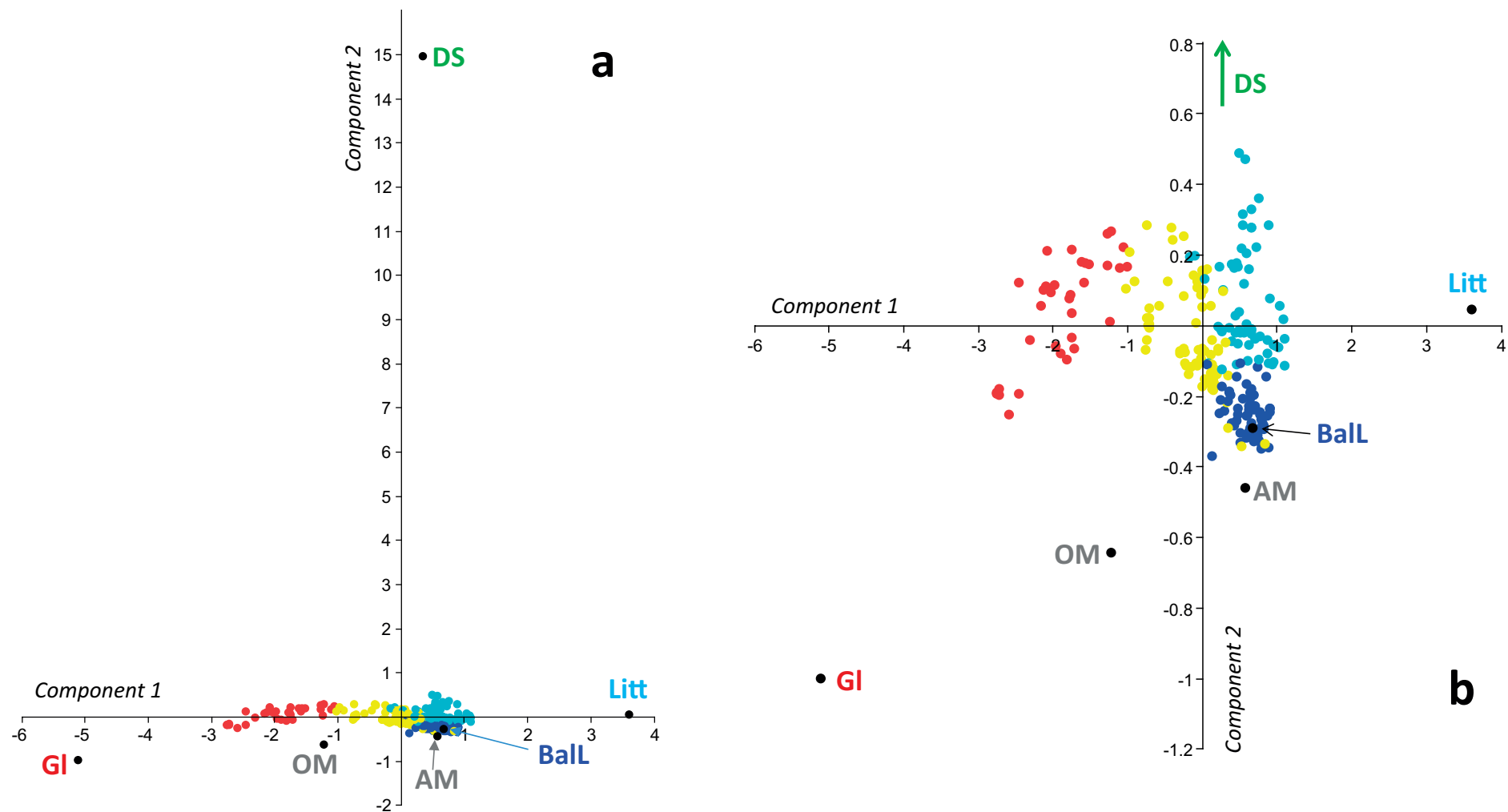


Figure 3-2. Location of the end members (open circles) in the PCA projection that shows Component 1 (x axis) vs Component 2 (y axis) for the SFR groundwaters. The difference between this figure and Figure 3-1 is the inclusion of the end members and the exclusion of the Baltic Sea waters; this has slightly changed the position of the samples. The PCA has been performed with Cl, SO₄, ²H and ¹⁸O as input variables.

3.2 M3 analysis: selection of end-member waters and calculation of mixing proportions

M3 is a Principal Component Analysis code that approaches the modelling of mixing and mass balance from a purely geometrical perspective (Laaksoharju et al. 1999, Gómez et al. 2006, 2009). As opposed to standard geochemical codes, M3 tries first to explain the chemical composition of a parcel of water by pure mixing, and only then are deviations from the pure mixing model interpreted as chemical reactions.

The M3 multivariate approach uses several chemical and physicochemical variables (conservative and non-conservative) to construct an ideal linear mixing model of the groundwater system. This is done by performing a Principal Component rotation of an $n \times n$ covariance matrix, where n is the number of chemical and physicochemical variables (e.g. Gershenfeld 1999). Each element of the covariance matrix expresses the degree of correlation of a pair of variables. Graphically, this is equivalent to the rotation of a reference frame composed of n orthogonal axes (one axis for every variable) until one axis, the first principal component, points in the direction of the maximum variability of the dataset; another axis, the second principal component, points in the perpendicular direction with the second largest variability, and so on for the other axes. Once the samples and the end-members have been expressed in the Principal Component coordinates, mixing proportions are calculated in a straightforward way as the local coordinates of each sample in a $k-1$ dimensional hypertetrahedron whose vertices are the k end-member waters (Gómez et al. 2006). This hypertetrahedron is a simplex and therefore always has as many dimensions as end members minus one.

Because there is one coordinate (i.e. one axis) for each input variable, at least as many input variables as end members minus one are needed to obtain the mixing proportions (e.g. if three input variables are being used, say the concentration of Cl, Br, and ^{18}O , it would be possible to give mixing proportions between two, three or a maximum of four end-member waters, although this latter case only works in ideal conditions).

Once the mixing proportions are calculated, the constituents that cannot be described by mixing are described using reactions by simple elemental mass balance supported by independent knowledge of the system. Reactions are inferred heuristically (by inspection) from the difference, for each sample, between the actual value of an input compositional variable and the value computed by M3 assuming pure mixing. For example, if there is a deficit of both Ca and HCO_3^- in the computed composition compared with the actual Ca and HCO_3^- contents, it could be inferred that calcite has dissolved. Unfortunately, there is no rigorous statistical test to decide whether a deviation between the computed and the measured concentrations of an element in a sample is sufficient to invoke a reaction.

3.2.1 Selection of input compositional variables

An important step in the correct application of M3 methodology is the proper selection of the *input compositional variables* (ICVs). Because M3 is based on a principal components analysis, which is a *linear* statistical technique, in principle only linear trends and correlations can be correctly interpreted. Mixing is such a linear process and thus, provided all ICVs are mostly controlled by mixing, results (mixing proportions and deviations) are meaningful. This by no means is equivalent to saying that only conservative elements can be used as ICVs in M3. Any element can be used as long as its concentration in the mixed water is *to the first order* controlled by the mixing process and not by subsequent reactions; *it is the relative intensity of the two processes (mixing and reaction) what matters*.

An example would clarify this sentence. Two waters with Ca contents of 10 mg/L and 10,000 mg/L mix in a 50:50 proportion; thus, the concentration of Ca in the final water is 5,005 mg/L. This mixing event occurs in an aquifer composed of altered tuffs with zeolites. After (or during) mixing, the water reacts with the altered tuffs by Ca-Na cation exchange and the concentration of Ca in the water is reduced by 10 mg/L before the exchange complex in the zeolites becomes saturated with Ca. So, both mixing and reaction have taken place and Ca is obviously not a conservative element. But because the potential change in Ca concentration due to mixing is $\Delta\text{Ca}_{\text{mixing}} = 10,000 - 10 = 9,990$ mg/L and the potential change in concentration due to reaction is $\Delta\text{Ca}_{\text{reaction}} = 10 - 0 = 10$, mixing is the most intense process and the Ca content in the mixed water is mostly controlled by the mixing event and not by the subsequent reaction. In the specific case of a 50:50 mixing proportion,

the Ca content from mixing is 5,005 mg/L, which is reduced to 4,995 mg/L after cation exchange, a relative change of 0.002 (or 0.2%). On the other hand, the low Ca water has changed its Ca concentration due to mixing by $(5,005 - 10)/5,005 = .998$ (or 99.8%), and the high Ca water by $(10,000 - 5,005)/10,000 = 0.499$ (or 49.9%). As the change in Ca concentration due to mixing is orders of magnitude larger than the change due to reaction, it can be concluded that a good prediction of the Ca content of the final water can be made if just the change due to mixing is considered, ignoring that due to reaction. In this situation Ca would be a useful ICV for M3.

A preliminary exploratory analysis of the groundwater system is thus compulsory before using M3. The exploratory analysis would point to the relative importance of reaction and mixing in the system and serve as an exclusion filter for highly reactive elements. In the particular case of the SFR dataset, Cl, Br, $\delta^2\text{H}$ (D), $\delta^{18}\text{O}$ (O^{18}), and SO_4 can be considered, after the exploratory analysis, as elements not affected to first order by reactions. So, the following sets of ICVs have been used:

S1: Cl+Br+D+ O^{18}

S2: Cl+ SO_4 +D+ O^{18}

S3: Cl+ SO_4 +Br+D+ O^{18}

Apart from these three sets, two additional ones, with conservative and non-conservative elements, have also been included in order to test; (1) the resolution of the first three sets (remember that the less input compositional variables in a set, the fewer number of end-member waters that can be used in a single simulation), and (2) the effect of non-conservative elements among the input variables in the predicted concentrations for the *conservative* elements. These two additional sets of ICVs are:

S4: Na+Ca+K+Mg+ HCO_3 +Cl+ SO_4 +D+ O^{18}

S5: Na+Ca+K+Mg+ HCO_3 +Cl+ SO_4 +D+ O^{18} +Tr

Tritium (Tr) has been included in the last combination because two of the end-member waters are very similar (Littorina and Baltic Sea) except in their tritium content (zero for the Littorina end member, above zero for the Baltic Sea end member).

3.2.2 Selection of end-member waters

Based on the palaeohydrogeological conceptual model (Section 2.2) the water types identified in SFR (see Section 2.3) can be chemically described using several end-member waters (Table 3-3). Some of these end-member waters are represented by real samples from natural systems and some others are estimated from diverse geological sources (for more detailed information see Gimeno et al. 2008, 2009).

Table 3-3. Potential end-member waters used in the M3 analysis.

End-member	Abbr	Na	K	Ca	Mg	HCO_3	Cl	SO_4	Br	$\delta^2\text{H}$	$\delta^{18}\text{O}$	Tr
Deep Saline	DS	8,500	45.5	19,300	2.12	14.1	47,200	10	323.6	-44.9	-8.9	0
Glacial meltwater	GI	0.17	0.4	0.18	0.1	0.12	0.5	0.5	0.001	-158	-21	0
Littorina Sea	Lit	3,674	134	151	448	93	6,500	890	22.2	-38.0	-4.7	0
Altered Meteoric (Forsmark)	AM	274	5.6	41.1	7.5	466	181	85.1	0.572	-80.6	-11.1	12.1
Old Meteoric (Forsmark)	OM	274	5.6	41.1	7.5	14.1	181	85.1	0.572	-50.0	-5.0	0
Baltic Sea (average)	BalP	1,760	66	82	219	78.7	3,025	450	10.3	-60.8	-7.55	15.4
Baltic Sea Local (sample #4330; PFM000064)	BalL	1,410	48.6	69.5	172.0	80.5	2,494.6	345.2	9.42	-60.2	-8.0	14.2

The **Deep Saline end member (DS)** corresponds to the deepest and most saline water sampled in Laxemar (from borehole KLX02 at 1,631–1,681 m depth with a salinity of 75 g/L TDS). It is old (at least 1.5 million years), has a Ca-Na-Cl composition and a significant deviation from the MWL (Meteoric Water Line in $\delta^{18}\text{O}$ vs $\delta^2\text{H}$ plots) due to its long interaction with the bedrock in a near-stagnant environment (Laaksoharju and Wallin 1997). For Forsmark, the sulphate content of this end member has been changed to a very low value of 10 mg/L (Gimeno et al. 2008).

The **Old Meteoric end member (OM)**. The SDM-Site Forsmark hydrogeochemical investigations showed that changes in the groundwater chemistry during the Quaternary were not restricted to post glacial time as there is groundwater and porewater evidence that indicates an old, warm climate derived meteoric water component. Without recognising this older component the hydrogeochemistry (and hydrogeology) cannot be adequately explained (Laaksoharju et al. 2009a). Therefore, an old dilute water (“**Old meteoric end member**”) has been included. Its composition is similar to the Altered Meteoric end member but with a longer residence time (zero tritium content).

Glacial end member (GI). The composition adopted for the Glacial end member corresponds to present meltwaters from one of the largest glaciers in Europe, the Josterdalsbreen in Norway, located on a crystalline granitic bedrock (Laaksoharju and Wallin 1997). These waters represent the chemical composition of surface meltwaters prior to the water-rock interaction processes undergone during their infiltration into the bedrock. They have a very low content of dissolved solids, even lower than present-day meteoric waters, and an isotopically light signature ($\delta^{18}\text{O} = -21\text{‰}$, $\delta^2\text{H} = -158\text{‰}$) (Gimeno et al. 2009).

Littorina end member (Lit). The Littorina stage in the postglacial evolution of the Baltic Sea commenced at ≈ 6500 BC. The salinity increased more or less continuously until ≈ 4500 – 4000 BC, reaching estimated maximum values twice as high as modern Baltic Sea and this maximum prevailed at least from 4000 to 3000 BC. The chemical composition of the Littorina Sea used here is based on the maximum salinity estimation of 12‰ or 6,500 mg/L Cl^- , while the concentration of other main elements were obtained by diluting the global mean ocean water (Pitkänen et al. 2004).

The **Altered Meteoric end member (AM)** corresponds to a real sample (Gimeno et al. 2008, 2009) which represents a typical shallow dilute groundwater (less than 100 m depth) of recent meteoric origin and, therefore, it should reflect the chemical characteristics of meteoric waters after a short interaction with soils, overburden and granite. Its tritium content and low chloride concentrations are representative of its recent meteoric origin and the absence of mixing processes with more saline waters.

The **Baltic Sea (average) end member (BalP)** corresponds to the average Baltic Sea water defined by Pitkänen et al. (2004).

The **Baltic Sea (local) end member (BalL)** is a real water sample collected in the Baltic Sea near the SFR site (sample #4330, PFM000064).

Comment on the Baltic Sea end members. The average Baltic Sea water composition of Pitkänen et al. (2004) is a good compromise for the Baltic Sea end member as it gives a spatial (and, in some way, a temporal) average which eliminates short-lived and local variations. However, due to the fact that infiltration of Baltic Sea water into the SFR bedrock has increased during the construction and operation of the SFR, it seems also reasonable to use a local Baltic Sea sample as the end member. Because of this difficulty in selecting a proper Baltic Sea end member, both the average Baltic Sea and the local one have been included in the list of potential end-member waters. The selection of the most appropriate local Baltic Sea sample (among the 51 samples of Baltic Sea waters taken from the PLU and included in the final SFR dataset) was carried out with the help of M3’s End-member Variability Module (Gómez et al. 2006). A summary of the procedure can be found in Appendix 1.

How can one select the correct combination of end members? If the end members have been correctly chosen for the given dataset, all samples should plot inside the volume defined by the end members (Gómez et al. 2006). Only samples inside the “mixing volume” can be “explained” by pure conservative mixing of the selected end members. The closer the number of explained samples is to the total number of samples, the better the combination is (in the sense that more samples can be explained as a mixture of the selected end members). In other words, a set of end members are properly selected for a specific dataset when most of the waters in the dataset are inside the mixing volume. For three end

members, the mixing “volume” is simply a triangle; for four end members a tetrahedron, and for five or more end members a hypertetrahedron (Gómez et al. 2006). The corners of these mixing volumes are occupied by the end members.

M3 performs a systematic search of combinations, starting from two end members and ending with the maximum number of potential end members (Gómez et al. 2006). The total number of combinations increases rapidly with this maximum number. For 7 potential end members, those collected in Table 3-3, the total number of combinations is 127. In other words, M3 solves the mixing problem for all the samples in the dataset a total of 127 times for each set of ICVs, selecting each time a different combination of potential end members and computing the percentage of samples (coverage) that can be explained by mixing the chosen end members. The “best” combinations of end-member waters are, *a priori*, those with a higher coverage, i.e. with a higher percentage of samples inside the mixing polyhedron. Table 3-4 shows all the combinations of end-member waters with a coverage of at least 80%. Calculations were made using the 5 different sets of ICVs listed in Section 3.2.1. Table 3-4 includes the coverage and the list of end members that define the corners of the mixing volume. The pair defined by a set of ICVs and a combination of end members is called a **mixing model** (MM). Table 3-4 contains 37 different mixing models.

Table 3-4 shows that only mixing models with three and four end-member waters have coverage > 80%. Considering that M3 has systematically computed all the possible combinations, starting with 2 end members and ending with 7 end members, *this is a clear indication that the SFR groundwater system must be the result of mixing a maximum of four different water types*. The best combination of 5 end members for each set of ICVs is listed in Table 3-5. Sets with four ICVs (Cl+Br+²H+¹⁸O and Cl+SO₄+²H+¹⁸O) have no 5 end-member combination (i.e. not even one sample is inside a mixing volume defined by 5 end-member waters), whereas the other three sets (with 5, 9 and 10 ICVs) have maximum coverages of 52.7%, 33.6% and 42.7% respectively, i.e. quite low values.

Although a high coverage is a *necessary* condition for a mixing model to be good, it is not a *sufficient* condition. Figure 3-3 shows on pc1–pc2 plots two examples of high-coverage combinations that are considered bad combinations. It is clear from the figure that the two mixing models plotted, with coverage > 80%, omit from the mixing volume an important subset of samples (black circles), i.e. on the left graph those with a glacial signature and on the right graph those with a high salinity. It seems obvious that in the left hand graph an end member to the left of the selected ones is needed (the Glacial end member) and in the right hand graph an end member above the selected ones is needed (the Deep Saline end member). Thus, only those mixing models that include both the Glacial and the Deep Saline end members can be considered capable of explaining SFR groundwaters. Table 3-6 lists these mixing models; an important reduction of mixing models has been achieved, i.e. from 37 in Table 3-4 to 21 in Table 3-6.

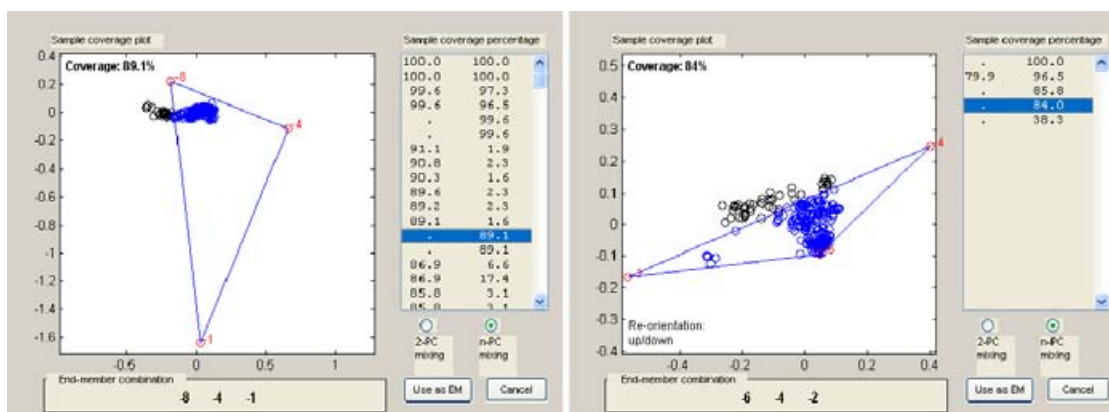


Figure 3-3. M3 screenshots showing two high coverage combinations of end members that do not include the Glacial end member (left) or the Deep Saline end member (right). Results of the principal components analysis are projected onto the pc1–pc2 plane (pc1 runs horizontally and pc2 vertically). The end members that define each combination are labelled (–1: DS; –2: GI; –4: Lit; –6: Ball; –8: AM). Samples inside the mixing polyhedron are coloured in blue and those outside in black.

Table 3-4. Mixing models with coverage >80%. Combinations of three end members are in black and combinations of four end members are in red.

Input compositional variables									
S1: Cl+Br+ ² H+ ¹⁸ O		S2: Cl+SO ₄ + ² H+ ¹⁸ O		S3: Cl+SO ₄ +Br+ ² H+ ¹⁸ O		S4: Na+Ca+K+Mg+HCO ₃ + Cl+SO ₄ + ² H+ ¹⁸ O		S5: Na+Ca+K+Mg+HCO ₃ + Cl+SO ₄ + ² H+ ¹⁸ O +Tr	
Cov %	Combination	Cov %	Combination	Cov %	Combination	Cov %	Combination	Cov %	Combination
100	[BalP GI DS]	100	[OM Lit GI DS]	100	[OM Lit GI DS]	100	[AM Lit GI DS]	99.1	[BalP GI DS]
100	[BalL GI DS]	100	[Lit GI DS]	100	[Lit GI DS]	99.6	[BalP GI DS]	97.2	[AM BalP GI DS]
100	[OM GI DS]	100	[BalP GI DS]	100	[BalP GI DS]	97.3	[AM BalP GI DS]	90	[AM Lit DS]
		96.5	[BalL Lit GI DS]	94.5	[BalL Lit GI DS]	89.1	[AM Lit DS]	89.6	[AM BalP DS]
		89.4	[AM Lit DS]	91.7	[BalL GI DS]	89.1	[AM BalP DS]	88.2	[BalL GI DS]
		89.4	[AM BalP DS]	87.8	[AM Lit DS]	85.6	[OM Lit DS]	85.3	[OM BalP DS]
		85.8	[BalL GI DS]	87.8	[AM BalP DS]	85.6	[OM BalP DS]	82.1	[AM OM Lit DS]
		85.5	[OM Lit GI]	86.2	[OM BalP GI DS]	84.1	[AM OM Lit DS]	80.6	[OM Lit DS]
		84	[BalL Lit GI]			82.1	[BalL GI DS]		

Table 3-5. Best 5end-member combination for each set of ICVs.

S1: Cl+Br+ ² H+ ¹⁸ O		S2: Cl+SO ₄ + ² H+ ¹⁸ O		S3: Cl+SO ₄ +Br+ ² H+ ¹⁸ O		S4: Na+Ca+K+Mg+HCO ₃ +Cl+ SO ₄ + ² H+ ¹⁸ O		S5: Na+Ca+K+Mg+HCO ₃ +Cl+ SO ₄ + ² H+ ¹⁸ O +Tr	
Cov %	Combination	Cov %	Combination	Cov %	Combination	Cov %	Combination	Cov %	Combination
	None		None	52.7	[OM BalL Lit GI DS]	33.6	[AM OM Lit GI DS]	42.7	[AM BalL Lit GI DS]

Table 3-6. Mixing models with coverage > 80%. Only combinations including DS and GI are shown.

S1: Cl+Br+ ² H+ ¹⁸ O		S2: Cl+SO ₄ + ² H+ ¹⁸ O		S3: Cl+SO ₄ +Br+ ² H+ ¹⁸ O		S4: Na+Ca+K+Mg+HCO ₃ + Cl+SO ₄ + ² H+ ¹⁸ O		S5: Na+Ca+K+Mg+HCO ₃ + Cl+SO ₄ + ² H+ ¹⁸ O +Tr	
Cov	Combination	Cov	Combination	Cov	Combination	Cov	Combination	Cov	Combination
100	[BalP GI DS]	100	[OM Lit GI DS]	100	[OM Lit GI DS]	100	[AM Lit GI DS]	99.1	[BalP GI DS]
100	[BalL GI DS]	100	[Lit GI DS]	100	[Lit GI DS]	99.6	[BalP GI DS]	97.2	[AM BalP GI DS]
100	[OM GI DS]	100	[BalP GI DS]	100	[BalP GI DS]	97.3	[AM BalP GI DS]	88.2	[BalL GI DS]
		96.5	[BalL Lit GI DS]	94.5	[BalL Lit GI DS]	82.1	[BalL GI DS]		
		85.8	[BalL GI DS]	91.7	[BalL GI DS]				
				86.2	[OM BalP GI DS]				

From the remaining 21 mixing models in Table 3-6, 13 have three end members (in black in the table) and 8 four end members (in red in the table). In these 21 mixing models only 9 combinations of end members are different (Table 3-7). In other words, from the 127 possible combinations of end members, just 9 have coverage > 80%. Two of these 9 combinations are common to all 5 sets of ICVs, four combinations appear in two different sets, and three appear in only one set. Four of the nine combinations are 3 end-member combinations, and the other five are 4 end-member combinations.

Table 3-7. Combinations of end members with coverage > 80%, indicating the specific sets of input compositional variables (ICVs) where they appear.

ID	End-member combination	Set of ICVs
C1	[BalL GI DS]	S1, S2, S3, S4, S5
C2	[BalP GI DS]	S1, S2, S3, S4, S5
C3	[Lit GI DS]	S2, S3
C4	[OM GI DS]	S1
C5	[AM BalP GI DS]	S4, S5
C6	[AM Lit GI DS]	S4
C7	[BalL Lit GI DS]	S2, S3
C8	[OM BalP GI DS]	S3
C9	[OM Lit GI DS]	S2, S3

S1: Cl+Br+D+O¹⁸

S2: Cl+SO₄+D+O¹⁸

S3: Cl+SO₄+Br+D+O¹⁸

S4: Na+Ca+K+Mg+HCO₃+Cl+SO₄+D+O¹⁸

S5: Na+Ca+K+Mg+HCO₃+Cl+SO₄+D+O¹⁸+Tr

The analysis carried out in this section has shown that only three end-member and four end-member mixing models have coverage > 80% (Table 3-6). No five end-member mixing model has coverage > 53%, thus casting serious doubts on the possibility of more than four end-member waters being responsible of the chemistry of SFR groundwaters. The 21 mixing models listed in Table 3-6 have several properties in common, which are important to stress here:

- 13 mixing models are based on 3 end-member combinations and 8 mixing models are based on 4 end-member combinations.
- Only 9 different combinations of end members appear in the 21 mixing models (Table 3-7). Four of the nine combinations are 3 end-member combinations, and the other five are 4 end-member combinations.
- All 9 end-member combinations have Deep Saline and Glacial as end members.
- Except in one mixing model, the third end member in 3 end-member combinations is always a marine end member (Baltic Sea or Littorina).
- Both Baltic Sea end members (BalP and BalL) are equally good *a priori*. BalP appears in 8 mixing models and BalL in 7, both in three and in four end-member combinations.
- The Old Meteoric (OM) end member only appears in conservative sets of ICVs, whereas the Altered Meteoric (AM) only appears in non-conservative sets of ICVs.
- Only two end-member combinations have at the same time two marine end members (BalL and Lit).
- Set 1 of ICVs (Cl+Br+δ²H+δ¹⁸O) has no four end-member combination with coverage > 80%. All the other sets have both three and four end-member combinations. This situation points to a lack of resolution of the mixing models based on Set 1 of ICVs.
- Sets 2 and 3 of ICVs share five of the six combinations of end members. Only combination [DS GI BalP OM] differs. Both sets have only conservative compositional variables.

Without any *a priori* knowledge of the site, three end-member and four end-member combinations are equally possible, and no one can be eliminated. Also, no set of ICVs can be eliminated beforehand without a more detailed analysis of each mixing model, specifically without a quantitative assessment of the differences between the actual contents of the conservative elements and those predicted by each mixing model. This is the topic of the next section, where all 21 mixing models are compared.

3.2.3 Test of mixing models

Coverage, as already seen in the previous section, is not the only attribute of a “good” mixing model. Obviously, a key aspect for classifying a mixing model as good or bad is how well the chemical composition of conservative elements (like chloride) can be reproduced. This is easily performed once the mixing proportions have been computed. An example using Cl as the conservative element will clarify the procedure.

Let us assume that the mixing proportions of sample 15 as calculated with one of the mixing models (Set1 of ICVs: Cl+SO₄+δ²H+δ¹⁸O; end-member combination: DS-Gl-Lit-BalL) are: DS = 1.5%, Gl = 14.6%, Lit = 11.0%, and BalL = 72.9%. The chloride content in the end members is (Table 3-3): DS = 47,200 mg/L; Gl = 0.5 mg/L; Lit = 6,500 mg/L, and BalL = 2,494.6 mg/L. Thus, the predicted chloride concentration of sample 15 under this mixing model is:

$$Cl_{\text{Sample \#15}} = \frac{Cl_{\text{DS}} \times 1.5\% + Cl_{\text{Gl}} \times 14.6\% + Cl_{\text{Lit}} \times 11.0\% + Cl_{\text{BalL}} \times 72.9\%}{100} = 3255.7 \text{ mg/L}.$$

As the actual chloride concentration of sample 15 is Cl = 3,250.0 mg/L, the mixing model overestimates the Cl content by 5.7 mg/L (0.18%). If the calculated Cl concentration of each sample is plotted against its actual concentration on an XY graph, a good model should have most samples along the 1:1 diagonal line.

Figure 3-4 plots the measured and calculated chloride concentrations in all 21 mixing models, with the measured concentration in the vertical axis and the calculated one in the horizontal axis. Visually, it seems clear that some mixing models are better than others, in the sense that samples plot closer or farther from the diagonal line (note that the diagonal line represents the “perfect” model).

Obviously, a more quantitative assessment of the quality of each mixing model than the mere visual inspection is needed. The whole procedure can be reduced to a “goodness-of-fit” exercise, where the “model” is the diagonal line in Figure 3-4 and the “observations” are the water samples; the closer to the diagonal line the samples are, the better the fit and the smaller the mismatch between measured and computed concentrations (residuals). The chi-square statistics, χ^2 , has been used as a measure of the “goodness-of-fit” because it is useful for assessing relative deviations.

The χ^2 “goodness-of-fit” statistics is defined as:

$$\chi^2 = \sum_{i=1}^N \frac{(x_i^{\text{ob}} - x_i^{\text{cal}})^2}{x_i^{\text{ob}}},$$

where x is the variable to be fitted, and superscripts “ob” and “cal” refer to observed and calculated values for each of the N entries in the dataset. Because models with a different number of samples are being compared, a better measure of the “goodness of fit” in this case is the reduced χ^2 , χ_r^2 :

$$\chi_r^2 = \frac{1}{\nu} \sum_{i=1}^N \frac{(x_i^{\text{ob}} - x_i^{\text{cal}})^2}{x_i^{\text{ob}}},$$

where ν is the number of degrees of freedom, $\nu = N - n - 1$, being n the number of fitted parameters in the model. Here, n is zero because both the intercept and the slope of the diagonal line (the model) cannot be chosen; thus, $\nu = N - 1$. The advantage of the reduced chi-squared is that it already normalises for the number of data points and model complexity (i.e. it is a misfit measure in a per sample basis). When comparing different models, the best model is the one with lowest χ_r^2 . The reduced χ^2 for the 21 mixing models is also included in the graphs in Figure 3-4, and Table 3-8 lists the mixing models in increasing order of reduced chi-square.

Table 3-8. “Goodness-of-fit” with respect to Cl of the 21 mixing models listed below and plotted in Figure 3-4. Combinations of four end members are in red.

Reduced χ^2	Set of input compositional variables	End-member combination
0.6	Cl+SO ₄ + ² H+ ¹⁸ O	[DS GI Lit OM]
1.1	Cl+SO ₄ + ² H+ ¹⁸ O	[DS GI Lit BalL]
14.2	Cl+SO ₄ +Br+ ² H+ ¹⁸ O	[DS GI BalP]
16.5	Cl+SO ₄ +Br+ ² H+ ¹⁸ O	[DS GI Lit OM]
19.2	Cl+SO ₄ +Br+ ² H+ ¹⁸ O	[DS GI BalP OM]
19.6	Cl+SO ₄ +Br+ ² H+ ¹⁸ O	[DS GI Lit BalL]
20.6	Na+Ca+K+Mg+HCO ₃ +Cl+SO ₄ + ² H+ ¹⁸ O	[DS GI BalP AM]
21.3	Cl+Br+ ² H+ ¹⁸ O	[DS GI BalP]
25.2	Cl+Br+ ² H+ ¹⁸ O	[DS GI OM]
26.4	Na+Ca+K+Mg+HCO ₃ +Cl+SO ₄ + ² H+ ¹⁸ O+Tr	[DS GI BalP]
35.3	Na+Ca+K+Mg+HCO ₃ +Cl+SO ₄ + ² H+ ¹⁸ O+Tr	[DS GI BalL]
38.1	Cl+SO ₄ + ² H+ ¹⁸ O	[DS GI BalP]
48.6	Na+Ca+K+Mg+HCO ₃ +Cl+SO ₄ + ² H+ ¹⁸ O	[DS GI BalP]
53.8	Na+Ca+K+Mg+HCO ₃ +Cl+SO ₄ + ² H+ ¹⁸ O+Tr	[DS GI BalP AM]
69.6	Na+Ca+K+Mg+HCO ₃ +Cl+SO ₄ + ² H+ ¹⁸ O	[DS GI Lit AM]
71.6	Cl+SO ₄ + ² H+ ¹⁸ O	[DS GI BalL]
81.9	Na+Ca+K+Mg+HCO ₃ +Cl+SO ₄ + ² H+ ¹⁸ O	[DS GI BalL]
98.5	Cl+SO ₄ +Br+ ² H+ ¹⁸ O	[DS GI BalL]
154.8	Cl+Br+ ² H+ ¹⁸ O	[DS GI BalL]
497.2	Cl+SO ₄ +Br+ ² H+ ¹⁸ O	[DS GI Lit]
499.0	Cl+SO ₄ + ² H+ ¹⁸ O	[DS GI Lit]

Table 3-8 (and also Figure 3-4) demonstrates two things; (1) four end-member combinations are superior to three end-member ones (6 of the 8 four end-member combinations occupy the 7 first positions in the table), and (2) sets of ICVs with only conservative elements are superior to sets with conservative and non-conservative elements (the first 6 mixing models are based on conservative input compositional variables).

Apart from these two important conclusions, Table 3-8 also shows that the first two models are far superior to the rest from a chi-square point of view. The top mixing model has a reduced- χ^2 of 0.6 and the second a reduced- χ^2 of 1.1, whereas the third has a reduced- χ^2 of 14.2, more than ten times larger. Thus, it is concluded that only the first two mixing models reproduce in a quantitatively satisfactory way the mixing behavior of SFR groundwaters. Figure 3-5 plots the comparison between the measured and the calculated chloride values in both mixing models (coverage and reduced χ^2 value are included in the plots).

Figure 3-6 plots deviations with respect to all conservative elements (Cl+SO₄+²H+¹⁸O) for mixing models MM1 and MM2. Sulphate is reproduced even better than chloride, which can be a little surprising as its behaviour is not usually as conservative as chloride. The isotopes are also well reproduced, although the scatter is slightly larger than for chloride.

Overall, the match between the predicted and measured concentrations of chloride, sulphate, deuterium and oxygen-18 can be considered as excellent. Thus, it could be concluded that only the first two mixing models reproduce in a quantitatively satisfactory way the mixing behaviour of SFR groundwaters. The question is which of them is better. This will be analysed in the next section.

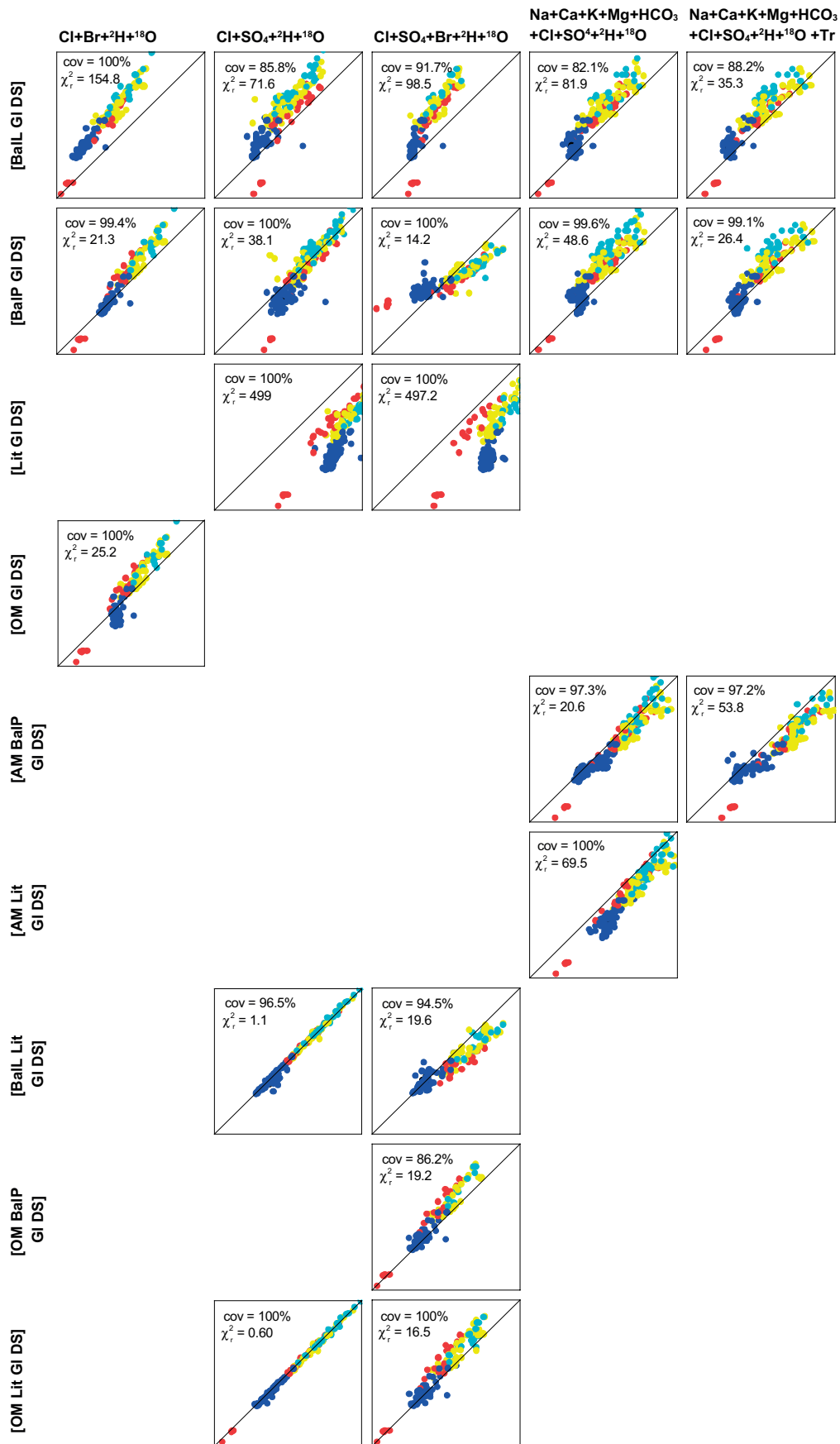


Figure 3-4. Comparison of mixing models using deviations with respect to Cl as the measure of goodness (chi-square statistics).

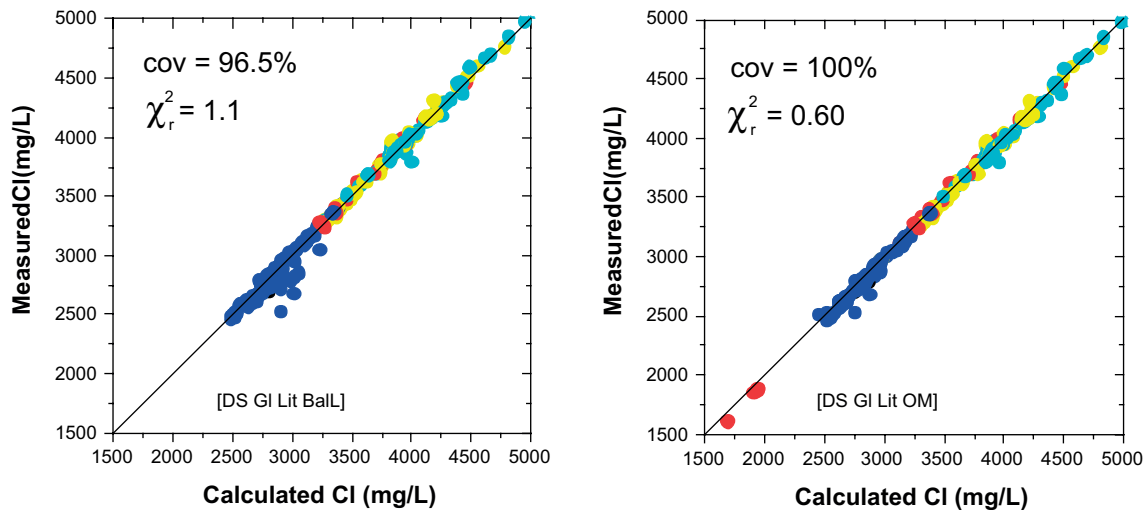


Figure 3-5. The two selected mixing models. Left; mixing model 1 (MM1) with DS, Gl, Lit and BalL end members. Right; mixing model 2 (MM2) with DS, Gl, Lit and OM end members. Both have $Cl+SO_4+\delta^2H+\delta^{18}O$ as input compositional variables.

Mixing proportions

The two selected mixing models (model 1, MM1, and model 2, MM2) are based on four conservative input compositional variables (Cl , SO_4 , 2H , and ^{18}O) and have four end-members; model 1 consisting of Deep Saline, Glacial, Littorina and Baltic Sea (local), and model 2 including Old Meteoric instead of Baltic Sea. Figure 3-7 summarises in a graphical way the mixing proportions predicted by the two best mixing models. Samples are separated into four groups according to the water type; within each group they are sorted by increasing depth and, for the same depth, by date of sampling. The horizontal axis only indicates a numeric order. White gaps in the graphs correspond to samples that can not be explained by the corresponding mixing model (≈ 10 samples). Mixing proportions computed with models MM1 and MM2 for all samples in the dataset are tabulated in Appendix 2.

As shown in the plots, model 1 (with BalL end member) indicates that the most abundant component in the SFR groundwaters is BalL, followed by the Gl (only dominant in some of the waters of Brackish-glacial type) and Lit components; the DS component is, by far, the less abundant (this is clearly seen in the PCA plots, Figure 3-2, where the DS end member plots very far from the locations of the set of samples). Although correct for many samples (mainly those affected by the hydraulic drawdown effects resulting from the SFR) this is erroneous for most of the Brackish-glacial type waters, where the influence of the local Baltic Sea waters is negligible.

Model 2, with the Old Meteoric end member, generally indicates similar abundances for the Litt and the OM components for almost all samples. These abundances increase as the proportion of Gl decreases. Gl is clearly dominant, even more so than in model 1, in the case of the Brackish-glacial type groundwaters. The DS component of each sample is exactly the same as in model 1. This model appears suitable for the samples that were not well explained by model 1 (the ones with the highest glacial signature) but it gives erroneous results for the set of samples at the right side of the plot, those with a clear Baltic Sea water component in them.

Another way to explore these results is by representing the mixing proportions of each end member with respect to the others (two by two) for each of the selected mixing models (Figures 3-8 and 3-9). For model 1 (Figure 3-8), the BalL end member is plotted against the other three end members in the first column. For model 2 (Figure 3-9), it is the OM end member that is plotted against the other three. For both models, the Lit end member is plotted against the two remaining end members (Gl and DS) in the second column, and in the third column the Gl end member is plotted against DS.

The diagonal line on each plot represents a binary mixture of the two end members occupying the axes. In other words, samples that can be explained as a mixture of only two end-member waters will plot on the diagonal line when the two end members contributing to its composition define the axes of the graph.

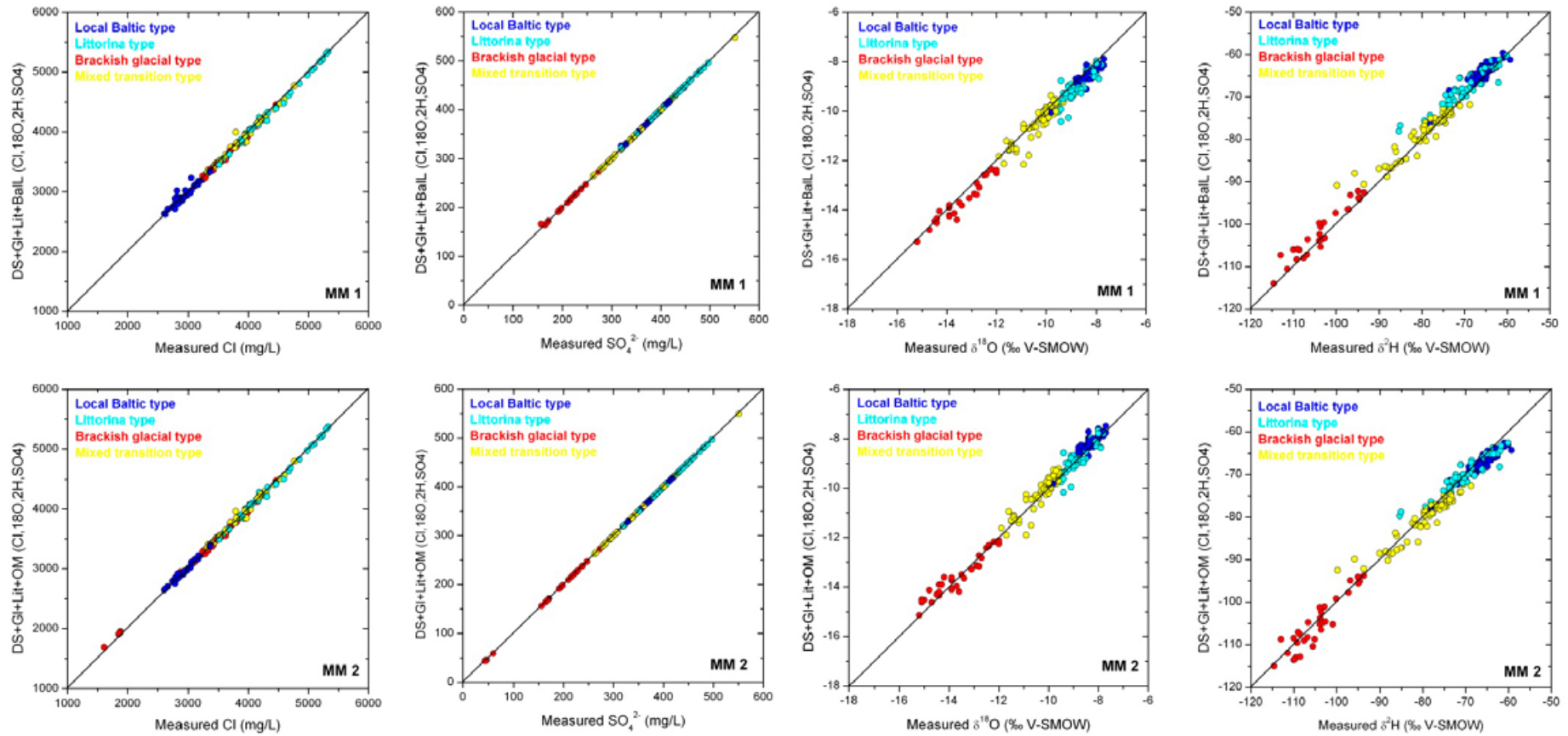


Figure 3-6. Measured and calculated chloride, sulphate, deuterium and oxygen-18 values in the finally selected 2 mixing models (MM1 first row, MM2 second row), with the measured concentration in the vertical axis and the calculated one in the horizontal axis. The closer to the diagonal line the better the reproducibility of the measured values. Both models have $\text{Cl}+\text{SO}_4+\delta^2\text{H}+\delta^{18}\text{O}$ as input compositional variables. Apart from Cl and the isotopes, sulphate behaves as a conservative element in this system, as clearly shown in the corresponding plots.

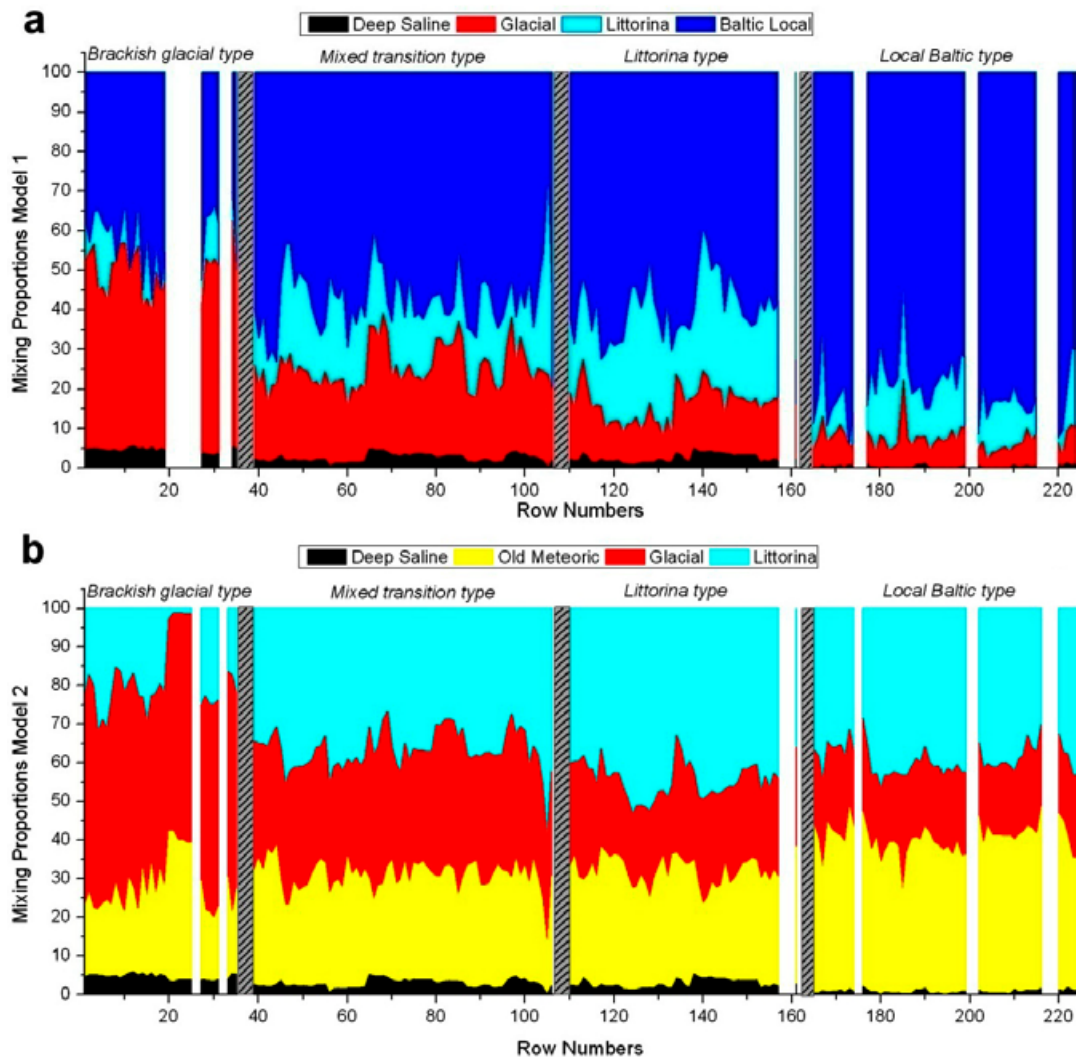


Figure 3-7. Mixing proportions predicted by the two selected mixing models. Samples are separated into four groups according to the water type, and within each group they are sorted by increasing depth (and date of sampling). Grey dashed rectangles separate one group from the other. Horizontal axis labels are not sample IDs, they only represent a numeric order. White gaps in the graph correspond to samples that can not be explained by the selected mixing model (≈ 10 samples).

A sample plotted on one axis has a zero contribution from the end member occupying the other axis, a sample near the origin of coordinates has zero contribution from the two end members that define the axes in the corresponding graph, and a sample located in the interior of the triangular area defined by the two axes and the diagonal line has contributions from at least three (possibly four) different end-member waters (the two end members defining the axis plus, at least, one end member more).

Apart from the visualisation of the mixing proportions corresponding to the different water types (colour coded in the plots), these plots show the relative distribution of these groups. One of the clearest observations is that here the meaning of “Transition” is made clear; these waters are basically a complex mixture with contributions from the Gl, Lit and BalL or Gl, Lit and OM end members, although basically their location fills the gap between waters dominated by the Gl and the Lit end members.

The Baltic and Littorina water types follow a clear trend that starts in the BalL end member (lower left corner in Figure 3-8a) and evolves towards the Lit end member by increasing at the same time the Lit and Gl contributions. On the other hand, neither the Brackish-glacial nor the Transition water types follow any clear trend. A final interesting observation is the trend followed by all water types when Glacial proportions are plotted against DS (Figures 3-8f and 3-9f). To better appreciate this trend, these graphs have been replotted in Figures 3-8g and 3-9g with the vertical axis expanded.

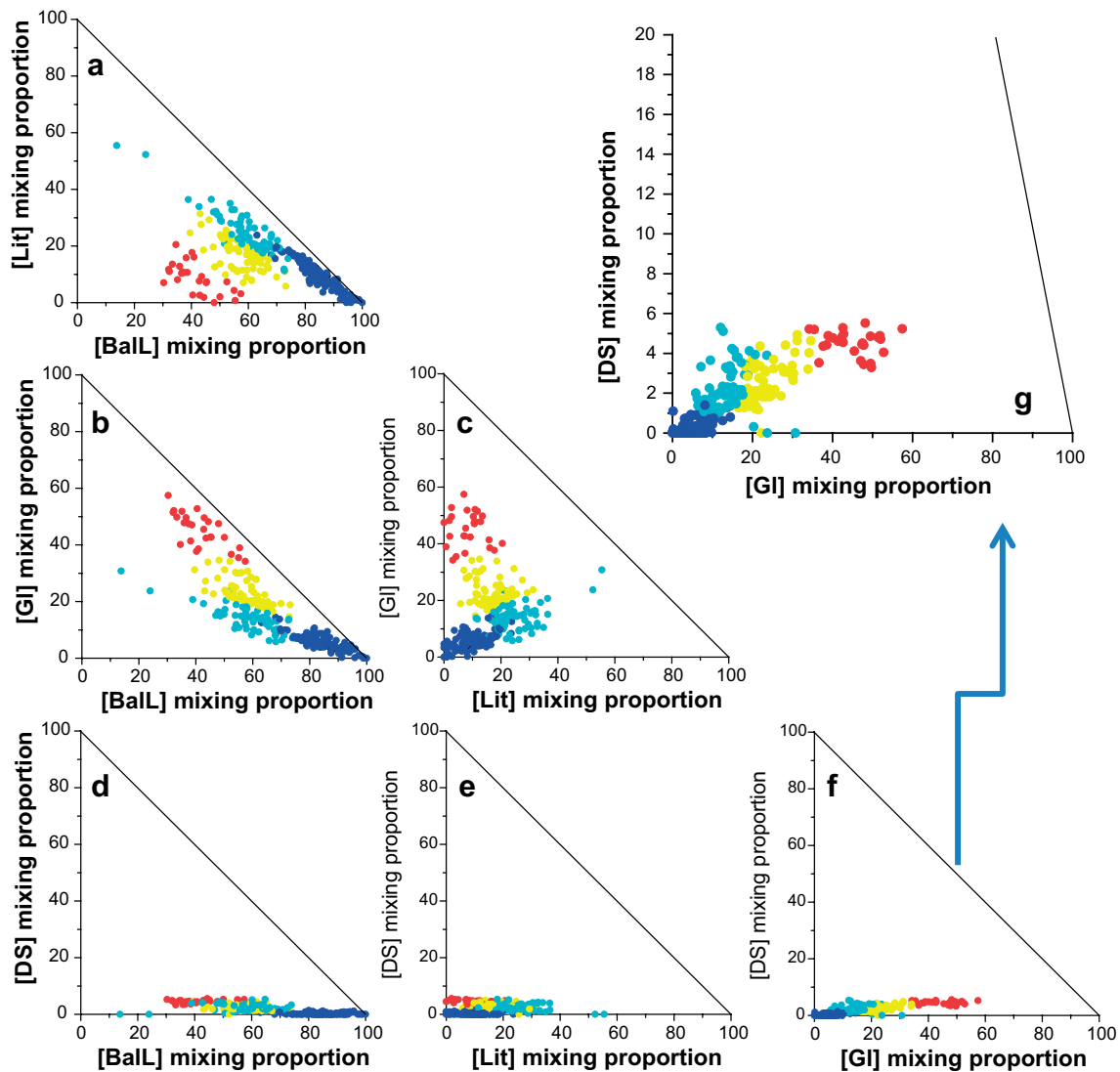


Figure 3-8. Mixing proportions for mixing model 1 (MM1). Colours refer to the water types defined in Section 2.3 (red, Brackish-glacial water type; blue, local Baltic water type; cyan, Littorina water type; yellow, Transition water type). Panel 'g' shows the Gl vs DS plot in an expanded view where the slanted line ending in 100% Gl is the diagonal line shown in the rest of the graphs.

There is an obvious continuous increasing trend starting at the origin of coordinates in Figure 3-8g, and slightly displaced to the right (higher Gl proportion) in Figure 3-9g. In both cases, Baltic type waters are the first ones in the trend, followed by Littorina waters, then by the Transition waters and finally by the Brackish-glacial ones. This trend implies a parallel increase in the contribution of both the Gl and the DS end members (and a decrease in the contribution of the Lit end member). In other words, those samples with the strongest glacial signature are, at the same time, those with the largest percentage of the Deep Saline end member, in agreement with what could be expected from an original salinity gradient established between glacial waters and deep saline waters occupying the lower reaches of the groundwater system. Here, the “transitional” character of the Transition water type is also evident, filling the gap between the Brackish-glacial and the Littorina water types.

Analysing in detail the difference in the mixing proportions between models MM1 and MM2 some interesting conclusions can be highlighted (Figure 3-10). The Deep Saline mixing proportions obtained with both models are almost identical (Figure 3-10a). However, the proportions obtained for the Litt and Gl end members are higher in model 2 than in model 1 and higher for the Local Baltic type groundwaters than for the others. This is obviously due to the fact that model MM2 does not use the BalL end member but the OM instead, which is considerably more dilute. This affects the mixing proportions of the other end members (except the DS).

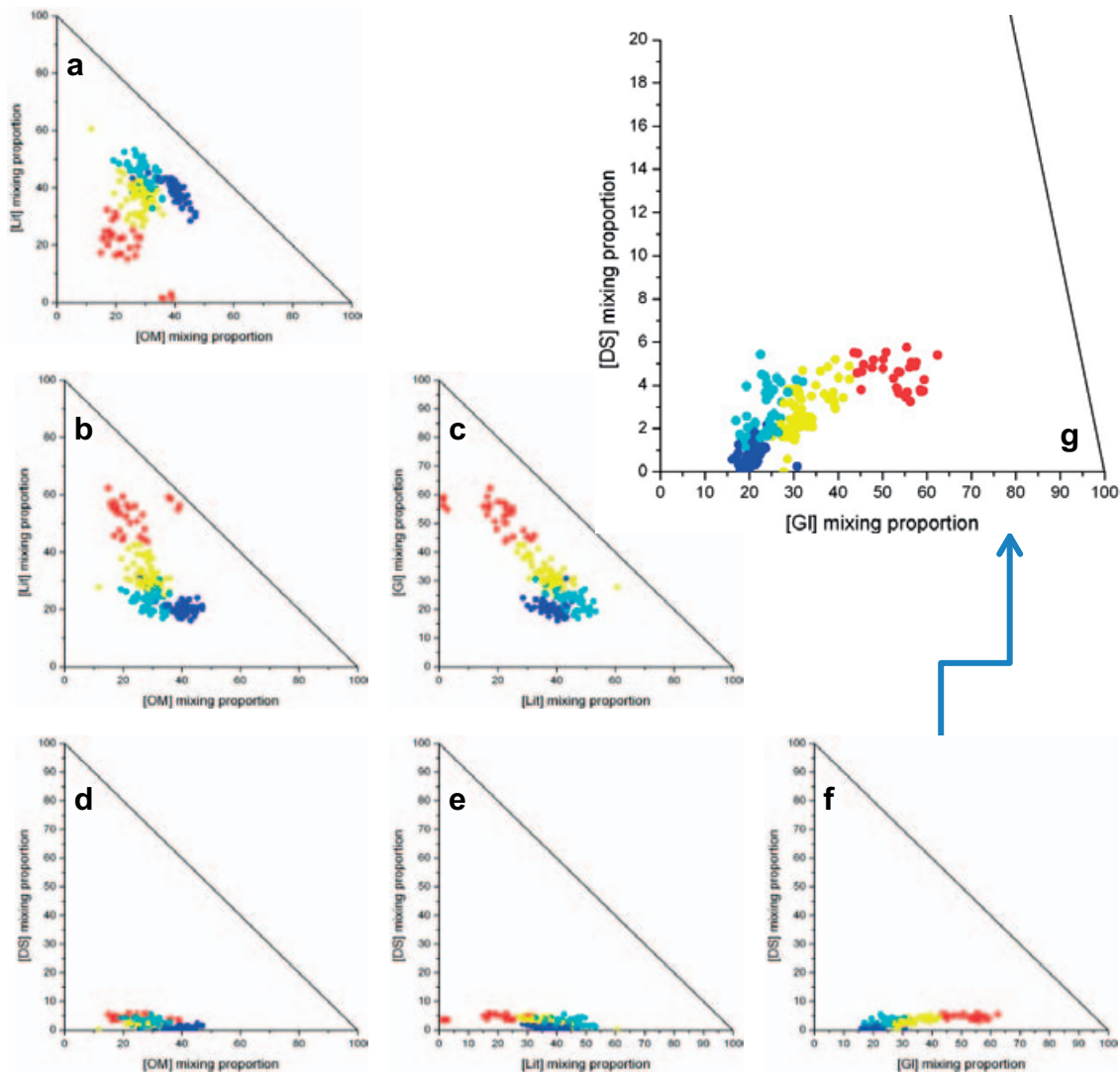


Figure 3-9. Mixing proportions for mixing model 2 (MM2). Colours refer to the water types defined in Section 2.3. (red, Brackish-glacial water type; blue, local Baltic water type; cyan, Littorina water type; yellow, Transition water type). Panel 'g' shows the Gl vs DS mixing plot in an expanded view where the slanted line ending in 100% Gl represents the diagonal line shown in the rest of the graphs.

Looking in more detail at this change, the proportion of the Baltic Local end member obtained in model MM1 is converted to Old Meteoric plus additional Littorina and Glacial proportions to the ones predicted with model MM1 (Figure 3-10d).

Discussion

As presented above, these models are very good when comparing calculated and measured concentration values (Figure 3-6), but they are less successful when comparing mixing proportions because each model has a different set of end members. A multivariate statistical approach alone does not seem to be enough to discriminate which mixing model is best. However, statistics is not the only viewpoint that should be used here. The hydrogeochemical history of the site is also of utmost importance. Based on the hydrogeochemical and palaeohydrogeological knowledge of the system (Nilsson et al. 2010), old meteoric water components, represented by the Old Meteoric end member, are thought to have been present at shallow to intermediate depths, supporting the use of mixing model MM2, but the effects of Baltic Sea water components are also clear in some parts of the system, either having been present in the fracture zones before construction of the SFR tunnels, or, mainly, as a result of the recent drawdown as a consequence of its construction, which means that this end member should also be used, supporting the use of mixing model MM1.

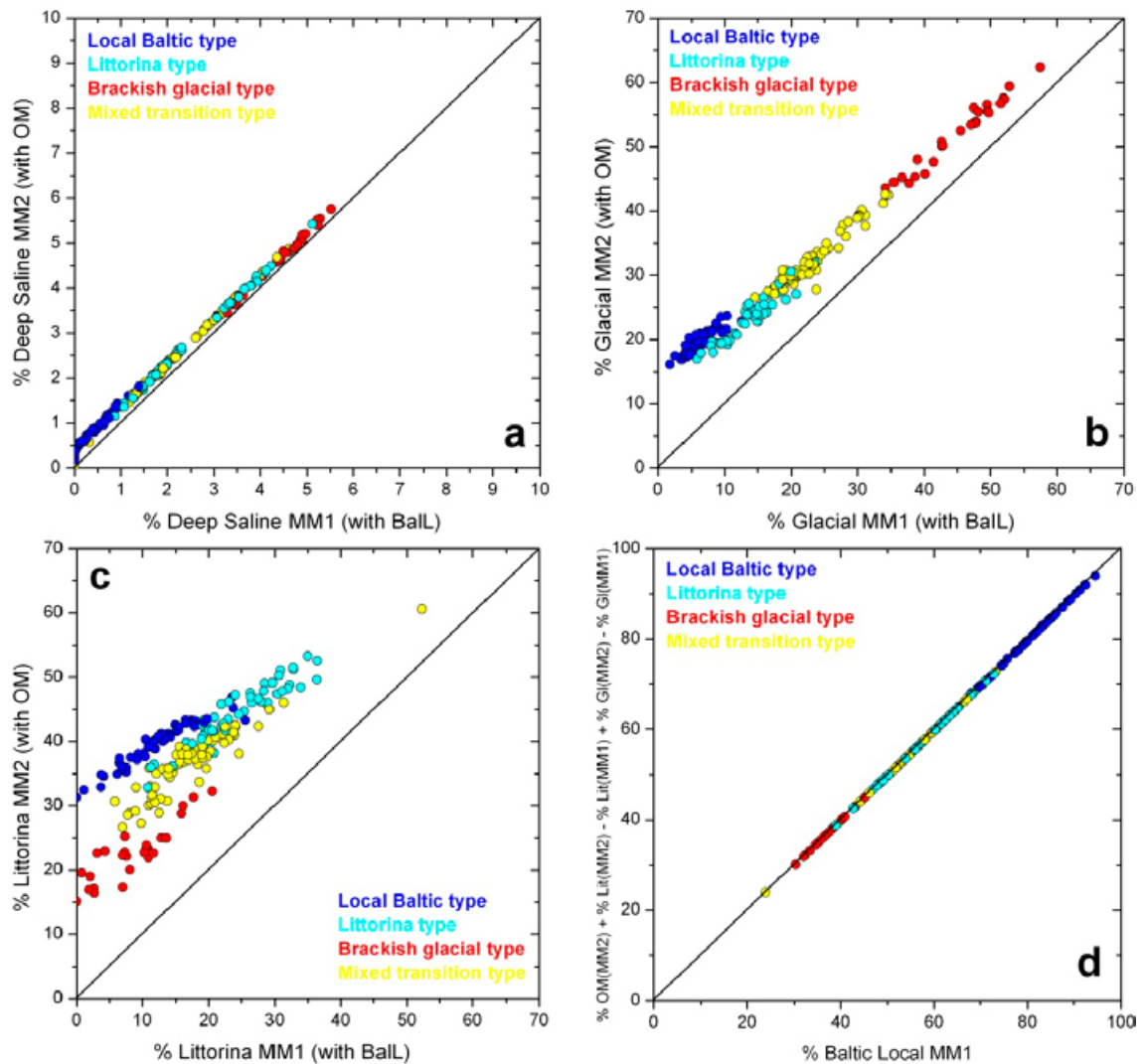


Figure 3-10. Comparison of the mixing proportions obtained for the end members in mixing models MM1 (x axis) and MM2 (y axis). Deep Saline, Glacial and Littorina are easily compared as they are present in both models. The two remaining end members Ball and OM cannot be compared in a straightforward way, but panel 'd' shows that the Ball proportion obtained with mixing model MM1 is translated as a combination of OM and an excess of Litt and Gl proportions in model 2 with respect to their proportions in model 1.

Therefore, both models, MM1 and MM2, are equally suitable and reasonable from a hydrogeochemical point of view but, and this is the main point for *different sets of samples*. With additional data, a more specific analysis could be carried out applying the above procedure to two different sets of data.

Notwithstanding the apparent inconclusiveness of the above analysis, there is a very interesting piece of information that can be extracted to enhance the accuracy of the hydrogeological models. Despite the different end members and mixing proportions obtained with the two mixing models, it is quite remarkable that the predicted chemical composition as a result of mixing (without reaction) is very similar irrespective of the model used. This is shown in Figure 3-11, where the composition calculated with mixing model MM1 is plotted against the one calculated with mixing model MM2. Except for bicarbonate, where results are completely different when computed with both models, all the other main chemical variables give almost the same value.

This fact allows us to create a hypothetical composition for each sample only due to mixing, including not only the conservative elements, but also other more reactive ones such as magnesium, sodium, calcium or potassium. This composition could in turn be used to calibrate the hydrogeological simulations of mixing over time. These theoretical compositions are listed in Table A2-3 in Appendix 2.

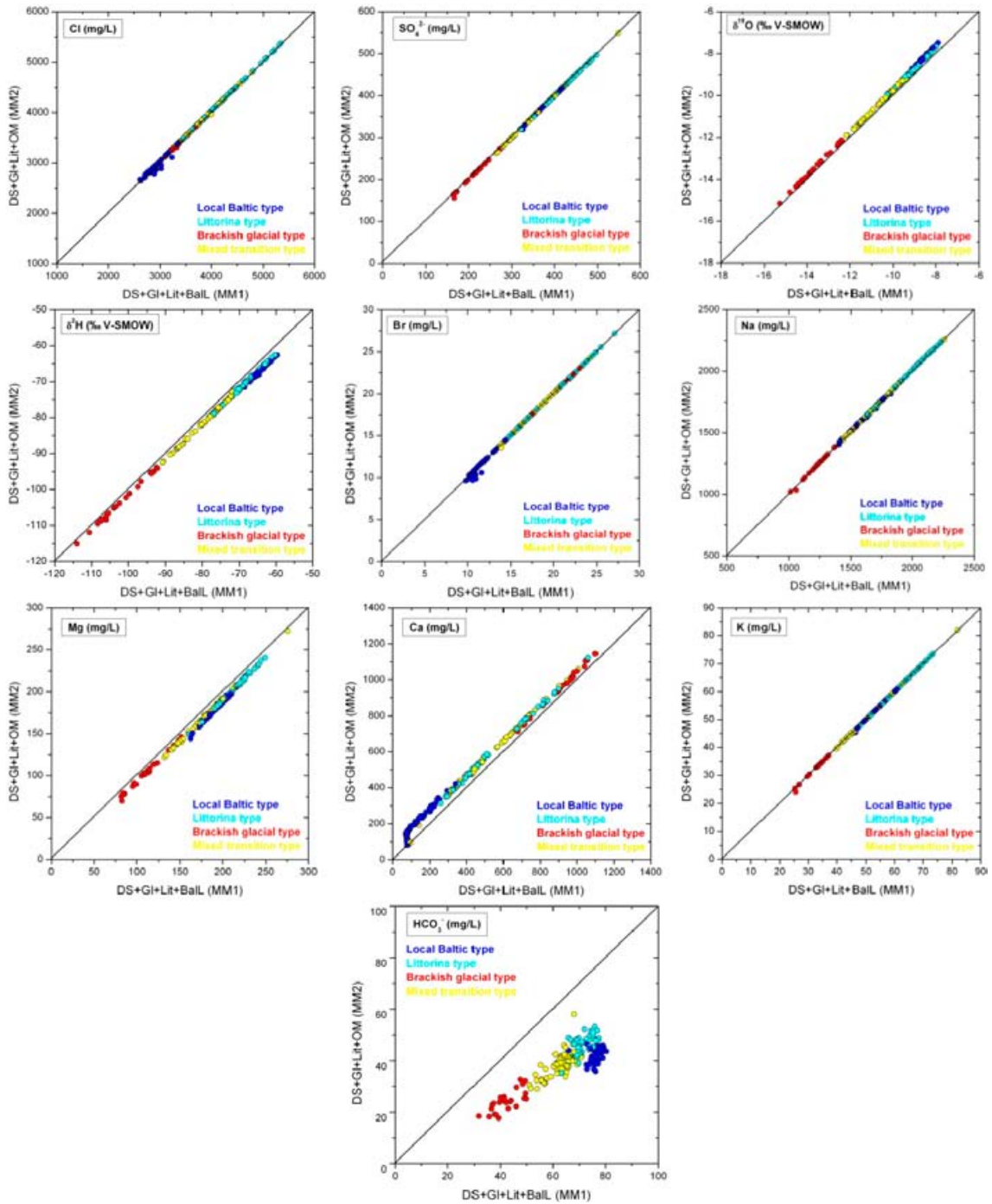


Figure 3-11. Comparison of the values for the main chemical components calculated with models MM1 (x) and MM2 (y). Except for bicarbonate, the values obtained for all the others are almost the same. Even for the other non-conservative elements, whose contents obtained by mixing are different from the values measured in the system.

Results obtained with five end members

The alternative possibility that is being analysed is to try and work with 5 end members. Had good mixing models with the 5 end members (including always OM and Ball) been found, mixing proportions for these five end-member waters could have been obtained for all the samples. However, as explained in Section 3.2.2, the best 5 end member combination of DS+GI+Ball+Lit+OM was obtained with the set of 5 ICVs (Cl+SO₄+δ²H+δ¹⁸O+ Br), but the coverage was very low, only 52.7%. Analysing the results, apart from the fact that half of the samples in the data set were not explained, those would still have a too high proportion of the Baltic end member exceeding what would be reasonable for most of the groundwaters (mainly in the case of the brackish-glacial type samples). Mixing proportions obtained with this mixing model (MM3) are shown in Figure 3-12a.

Additional analyses were performed in order to test the unusual behaviour of the results. Trying to increase the coverage of the 5 end-member combination, and considering that the most uncertain end member is the old meteoric, a search for the most appropriate old meteoric composition was carried out with the help of M3's End member Variability Module (Gómez et al. 2006) (cf. Appendix 1). Apart from the difficulties in finding a reasonable composition for this end member, the mixing proportions obtained when using the optimal OM composition did not improve on those previously found with the original OM end member, except in the coverage which increases to 90%.

The final test performed in order to improve the results obtained with five end members was the use of a different set of ICVs. Bromide was a good *a priori* conservative element, but few samples were analysed for bromide, so the initial dataset was already small. Accordingly, a different compositional variable, sodium, more commonly analysed and with a more or less conservative behaviour, was tried instead of bromide. Thus, the final set of ICVs to be tested was composed by Cl+SO₄+δ²H+δ¹⁸O+Na. For the same set of 5 end members as above, but using this new set of variables, the coverage is 68.6% (still quite low). The mixing proportions resulting from this new mixing model (MM4) are shown in Figure 3-12 together with the results obtained with mixing model MM3 for comparison.

Though not very impressive, the slight improvement in coverage when including an element like sodium to the set of ICVs (and still maintaining the adjusted concentrations of the conservative elements), indicates that more M3 work must be done in order to systematically analyse which is the best set of ICVs, i.e. being as conservative as possible to maintain a satisfactory fit to the measured concentrations, and at the same time give the highest resolution of the model.

This systematic search should be done in combination with the addition of an alternative end member discarded in Section 3.2.2; the Altered Meteoric end member. This member was discarded based on available information and considering the palaeogeographical history of the site, which assumes that recent meteoric waters can not be present in the system. However, the new hydrogeological models (Öhman et al. 2011) indicate the possibility of some input of mixed water from Forsmark containing both a Littorina and a present meteoric component. If this is the case, some of the groundwaters, at least those close to the Southern Boundary Belt, could be explained by a mixture of these waters. The results presented in Section 3.2.2. indicate that this end member only appears in mixing models when all the standard set of parameters (including all the non-conservative ones) are used in the calculations. So, this end member should be taken into consideration if more "non-conservative" elements are going to be included in the simulations. Again, a tradeoff between resolution (which increases with the number of ICVs) and accuracy (which increases when only conservative ICVs are used) should be sought in order to find an optimal model.

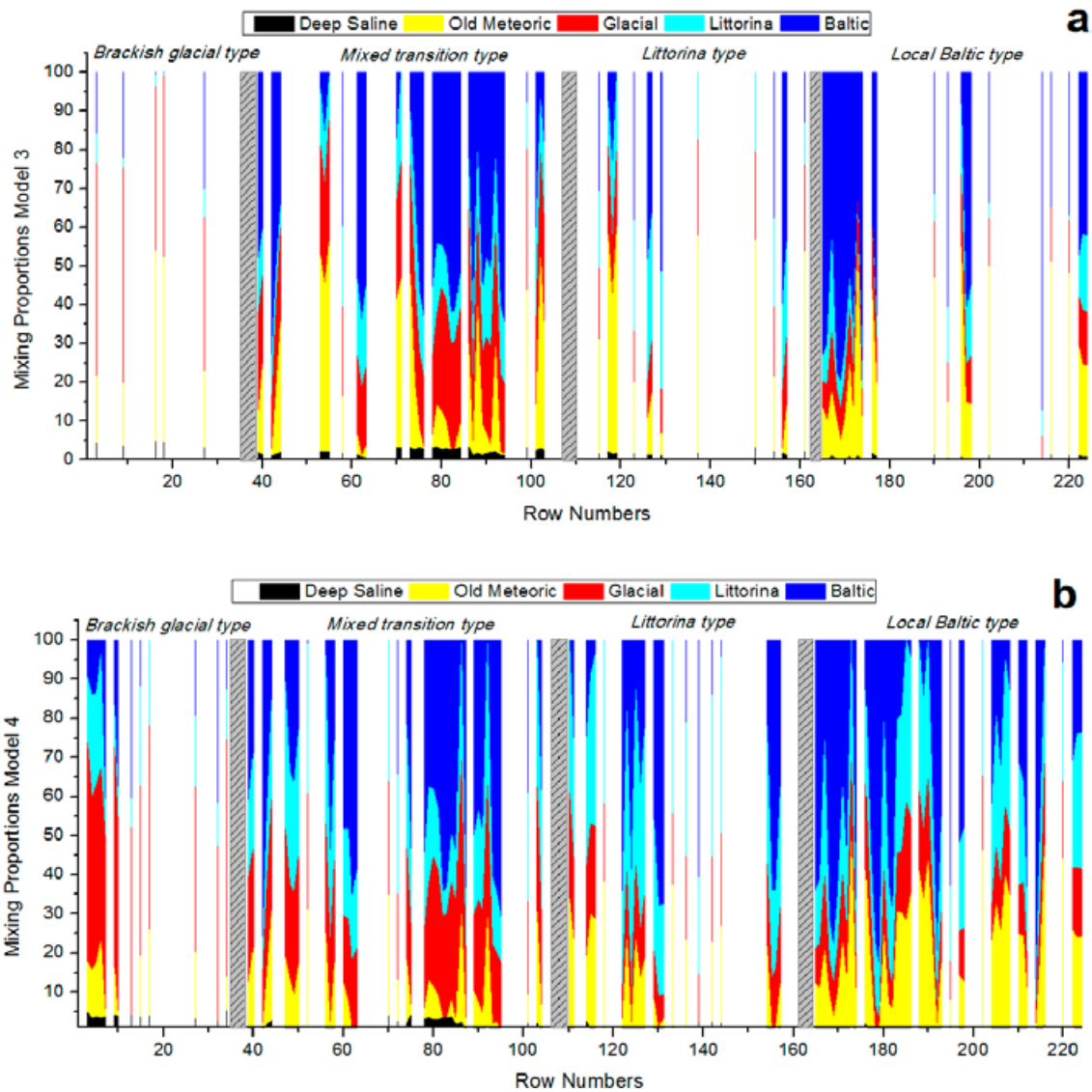


Figure 3-12. Mixing proportions predicted by the mixing models 3 and 4. White gaps in the graphs correspond to samples whose composition cannot be explained. Samples are ordered in four groups according to the water type, and within each group they have been sorted by increasing sample number. Note: the labels shown are not the sample ID, only a numeric order.

4 Non-redox geochemical systems

This section presents the results of the modelling work performed using all available data (see Section 1.3). A summary of the main conclusions on the distribution of the chemical elements, their main controls and the results of geochemical modelling, is also presented.

The chapter is subdivided into several sections to provide a thorough description and discussion of the different compositional systems, carbonates (Section 4.1), sulphates (Section 4.2), silica (Section 4.3) and fluoride (Section 4.4). Importantly, in all the cases an effort has been made to integrate the already existing information concerning the hydrochemistry and mineralogy of the site.

Hydrogeochemical modelling has been performed with the PHREEQC code (Parkhurst and Appelo 1999) and using the WATEQ4F thermodynamic database (Ball and Nordstrom 2001), with the modifications reported in Gimeno et al. (2008, 2009). As a first step, modelling has focussed on speciation-solubility calculations related to the carbonate, sulphate, silica and fluoride systems. These calculations were used to; (a) investigate the processes that control water composition and the main hydrochemical trends, (b) to test the hypotheses emerging from all the previous study, and (c) to perform uncertainty analysis.

Following the same approach used in the site characterisation programme (Gimeno et al. 2009), the evaluation of the SFR dataset commenced with a general analysis of the different groundwater variables based on the conceptual understanding of the system (including the description of the water types) presented and discussed in the previous work performed by Nilsson et al. (2010). Studies of bedrock fracture fillings and microbes in groundwater have also been considered since they may provide important information for the site description.

4.1 Carbonate system

The carbonate system has been demonstrated to be fundamental in understanding the evolution of groundwater parameters such as alkalinity, dissolved calcium and pH in the Site Descriptive Programmes both in Finland and in Sweden. Moreover, calcite is particularly important for understanding the carbonate system in the groundwaters from these and other similar crystalline rock systems (e.g. Nordstrom et al. 1989, Pitkänen et al. 1999, 2004, Iwatsuki et al. 2005, Gimeno et al. 2008, 2009). Calcite is one of the most abundant minerals in fracture fillings in these sites and it plays an integral role in the pH-buffering of the recharge groundwaters. CO₂ partial pressure (usually referred as pCO₂ in this document) is another relevant parameter for understanding the evolution of the carbonate system and for evaluating possible uncertainties in measured pH values.

In this section, the hydrogeochemical parameters pH, alkalinity and dissolved calcium, and the results of the geochemical modelling (pCO₂ and calcite saturation index) are discussed. As many pH values for the SFR groundwaters are measured in laboratory, theoretical pH and pCO₂ values assuming calcite equilibrium are also discussed (see also Appendix 3).

4.1.1 Hydrogeochemical trends

The bicarbonate concentrations in the SFR groundwaters range from 40 to 160 mg/L (0.65 to 2.62 mmol/L) and their trends with respect to depth and chloride contents almost perfectly reflect those of the PLU groundwaters (Figure 4-1). However, bicarbonate does not show the high concentrations found in the fresh and mixed groundwaters above 150 m depth in PLU where the carbonate system and the biogenic production of CO₂, related to the infiltration of meteoric waters, are very active (Gimeno et al. 2008).

The highest bicarbonate contents in the SFR are found in the shallow brackish marine groundwaters of Local Baltic type (blue circles) and they are usually higher than the 70–90 mg/L (1.15–1.47 mmol/L) found in the Baltic Sea water at the surface (black circles). Littorina type groundwaters (cyan circles) show variable and also high bicarbonate contents (reaching 134 mg/L; 2.2 mmol/L), frequently higher

than the estimated value for Littorina marine waters (92.5 mg/L; 1.52 mmol/L). Some of the Transition type groundwaters (yellow circles) also show high bicarbonate contents and the Brackish-glacial groundwaters (red circles) have concentrations well above 50 mg/L (0.82 mmol/L). The extremely low values encountered in the PLU dataset (Figure 4-1b, d) do not appear in the SFR groundwaters.

Higher (and more variable) HCO_3^- values than the estimated value for Littorina waters were also found in the groundwaters with clear marine Littorina signatures from the Laxemar-Simpevarp and PLU sites (Gimeno et al. 2008, 2009). During infiltration of marine waters through the sediments, biological activity promotes an important increase in HCO_3^- contents. For example Carman and Rahm (1997) found HCO_3^- contents as high as 488 mg/L (8 mmol/L) just 10 cm below the water-sediment interface in the present Baltic Sea. Thus, these high HCO_3^- values in the groundwaters with marine signatures can be considered a trace of marine contribution not eliminated by water-rock interaction processes (see Gimeno et al. 2009 for further discussion). Thus, the Local Baltic type groundwaters analysed in the SRF system show the highest bicarbonate values as a clue of their marine origin. Furthermore, some transition type groundwaters with high bicarbonate contents have also been influenced by the present intrusion of Baltic Sea waters in the SFR groundwaters.

Dissolved calcium concentrations range from 87 to 1,220 mg/L (2.17 to 30.5 mmol/L) and their trends with respect to depth and chloride contents are also similar to those of the PLU groundwaters (Figure 4-2).

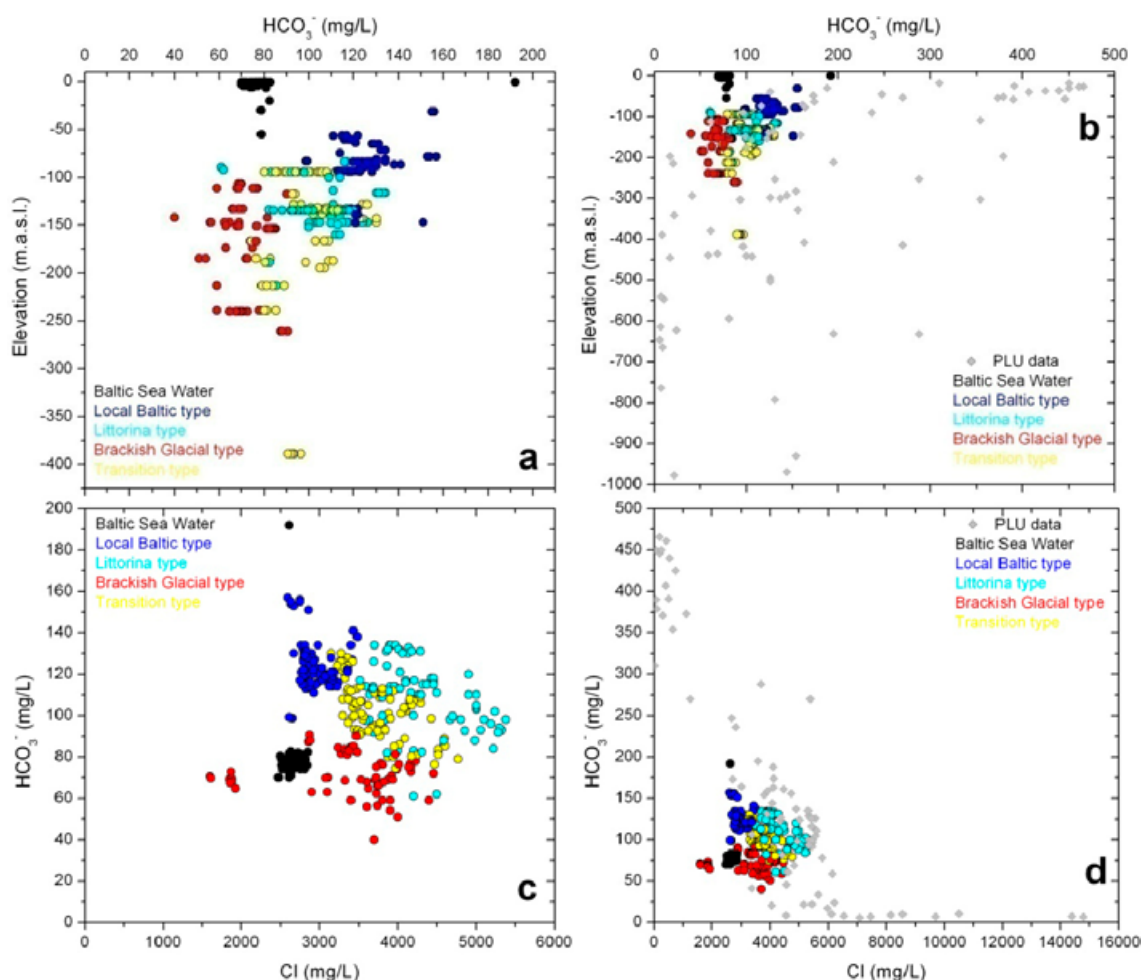


Figure 4-1. Bicarbonate contents vs depth (a, b) and chloride concentrations (c, d) in the SFR groundwaters colour coded by water types. The diagrams to the left (a and c) show the SFR data where the scales are restricted to those relevant to the SFR extension data. The diagrams to the right show these data integrated in the general distribution of the PLU data (Forsmark). Note the change in scales in the graphs to the right.

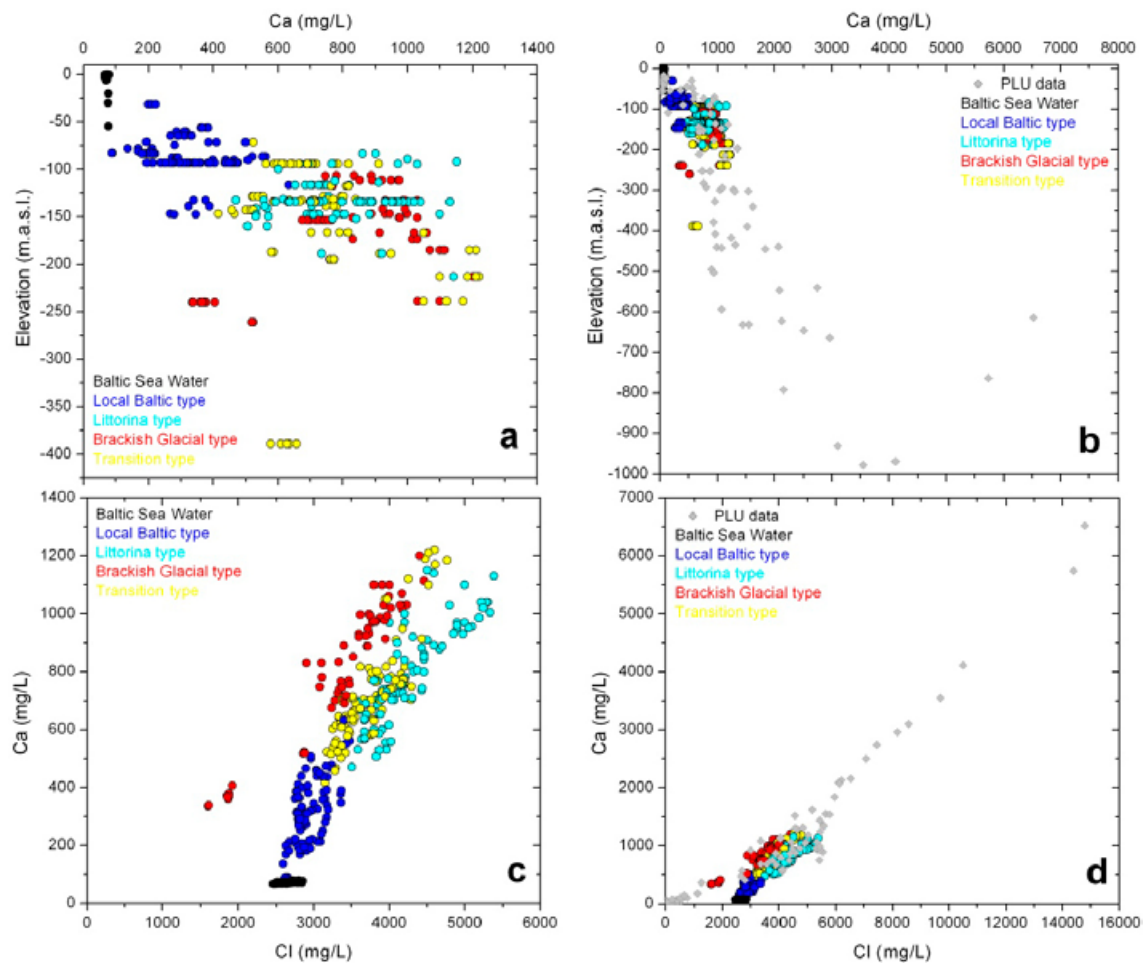


Figure 4-2. Calcium contents vs depth (a, b) and chloride concentrations (c, d) in the SFR groundwaters colour coded by water types. The diagrams to the left (a and c) show the SFR data where the scales are restricted to those relevant to the SFR extension data. The diagrams to the right show these data integrated in the general distribution of the PLU data (Forsmark). Note the change in scales in the graphs to the right.

The lowest calcium concentrations in the SFR groundwaters are associated with some Local Baltic type groundwaters. These show calcium contents slightly higher (87–90 mg/L or 2.17–2.24 mmol/L in the HFM34 at 82.9 m depth) than the present Baltic Sea waters (around 75–80 mg/L, 1.87–2.0 mmol/L), which can be attributed to their dominant Baltic signature slightly modified by water-rock interaction processes (calcite dissolution, mainly). However, calcium content in most of these Local Baltic type groundwaters mostly ranging between 200 and 600 mg/L (5.0 and 15.0 mmol/L), are clearly higher than the present Baltic Sea waters, showing a rough positive correlation with chloride contents (Figure 4-2c). Thus, although modified by heterogeneous reactions (e.g. calcite dissolution-precipitation, cation exchange), a mixing control seems to be still noticeable.

Mixing control for dissolved calcium is also apparent for the whole set of the SFR groundwaters. A certain positive correlation between chloride and calcium contents can be deduced by comparison with the PLU groundwaters characterised by similar chloride contents (Figure 4-2d) ranging between 2,000 and 6,000 mg/L (56.4 and 169.2 mmol/L). The “simple” trend formed by binary mixing between a saline and a dilute end member is invalid for the PLU groundwaters within that chloride range by Littorina intrusions and, in the case of the SFR groundwaters, by Littorina and Baltic intrusions. These additional mixing events would promote different heterogeneous processes (cation exchange, calcite reequilibrium) modifying the dissolved calcium contents attributable to conservative mixing.

Measured pH in the SFR groundwaters ranges from 6.6 to 8.0 (Figure 4-3; values up to 8.3 have been measured in the Baltic Sea waters). As already indicated before, the available data for SFR were recorded at different occasions over the last 25 years and in the case of pH it means that the type of measurement, and therefore its quality, varies considerably. Out of the 416 samples studied in

this work, only 245 have laboratory measurements and 40 samples do not have any pH value. Field pH measurements have been performed for 78 samples, and data representing 12 pH (and Eh) values from Chemmac measurements, corresponding to seven borehole sections, are also available⁴.

The same selected Chemmac pH has been used for all the samples corresponding to the same section and date (53 samples in total).

There is no a clear pH trend with depth (Figure 4-3a, b), which might be due to the heterogeneity of the system, to the frequent horizontal dispersion of this parameter in the examined sections and to the possible uncertainty in the measurements. In general, values determined in the field are higher and constitute a narrower range (7.3 to 8) than the pH values measured in the laboratory, and they roughly show an increasing trend with depth. Field pH values measured for similar depths in the PLU groundwaters (Figure 4-3b) reach higher values, mainly in the case of brackish-saline non-marine groundwaters (below 400 m depth), absent in the SFR system.

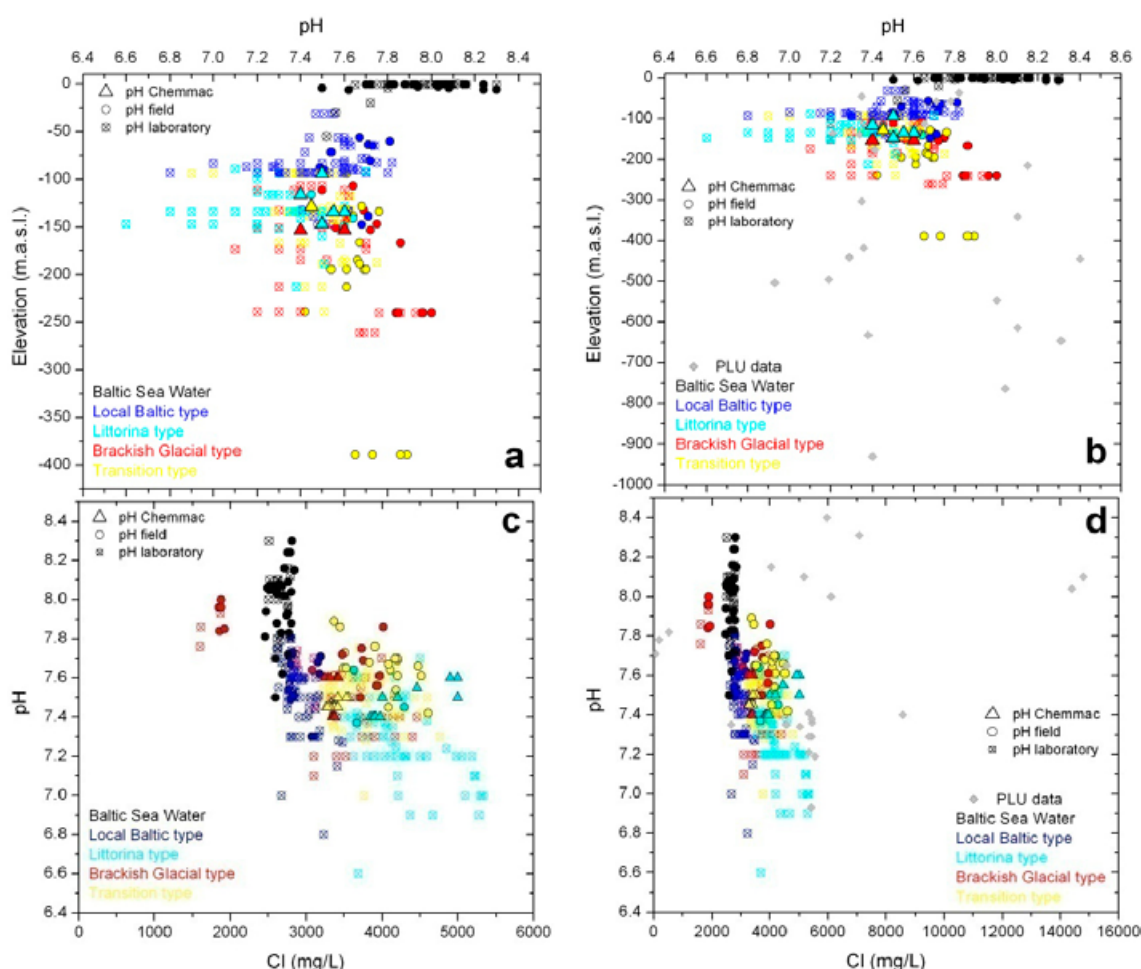


Figure 4-3. Measured pH values with respect to depth (a, b) and chloride (c, d) in the SRF groundwaters colour coded by water types. The diagrams to the left (a and c) show the SFR data where the scales are restricted to those relevant to the SFR extension data. The diagrams to the right show these data integrated in the general distribution of the PLU data (Forsmark). Note the change in scales in the graphs to the right.

⁴Chemmac measurements were conducted in three of the early SFR boreholes (KFR01 at 44.5–62.3 m.b.l. KFR7A at 48.0–74.7 m.b.l. and KFR10 at 87.0–107.28 m.b.l.) in 1986–87 and repeated in the same three borehole sections in 2000 (Nilsson 2009). Additionally, six recent chemmac measurements were conducted in two sections from the KFR105 borehole (120–130 and 265–306.8 m.b.l.), drilled from the SFR construction tunnel within the SFR extension project (Lindquist and Nilsson 2010, Nilsson et al. 2010), and in sections from boreholes KFR08 (63–104 m.b.l.), KFR19 (95 to 110 m.b.l.) and KFR07 (48–74.7 m.b.l.) (Chapter 5 and Appendix 4).

The rough pH decrease with the increase of chloride contents (Figure 4-3c, d) suggests that the Baltic Sea water intrusion and mixing with the older and more saline groundwaters at depth, may promote a pH increase. This aspect would merit further studies in future studies. An uncertainty analysis to the pH measurements has been performed (Appendix 3) and the trends obtained with the theoretical pH values (assuming calcite equilibrium; Appendix 3) do not change the above results.

4.1.2 Mineralogical data

Mineralogical data from two different domains are of particular interest to understand the SFR hydrochemical evolution; (1) from the seabed sediments above the SFR facility (through which present Baltic waters intrude), and (2) from the fracture fillings in the bedrock (in contact with all identified groundwater types in the SFR).

The SFR site is located 50 metres beneath the bottom of the Baltic Sea and adjacent to the Forsmark Nuclear Power Plant. The Baltic Sea is only 2–6 metres deep at about 600 metres off the shoreline, at the area where the SFR deposition tunnels are located.

Investigations of the seabed at the SFR reveal that the distribution and extent of marine sediments are quite heterogeneous (Section 2.1). The sediment layers are considerably thicker on the south side of the pier (Figure 2-3) and include low conductive glacial clays and a bottom layer of till. On the north side of the pier there are areas with no, or only partial, sediment coverage (see Nilsson et al. 2011). There is no more detailed information on the mineralogy of the glacial till in this area, but soils and glacial till deposits in the Forsmark area show an important influence of calcareous materials from Ordovician limestones present on the seabed towards the north of the area⁵ (Lundin et al. 2004, SKB 2005).

Limestone clasts and boulders can be observed on the surface of the regolith. Most till samples in the Forsmark area contain between 10–30% calcite (calcium carbonate) per dry weight, which is about 30 times higher than the median value of the Swedish reference data (SKB 2006). Sandy tills have an average calcite content of 18%, whereas clay-rich till deposits present even higher contents (24%; SKB 2005). Mineralogical data of the seabed deposits at the SFR are needed in order to see if they contain calcite (or if calcite still remains in the subaqueous environment).

The available mineralogical information for the fracture fillings present in the SFR bedrock, indicates that, together with chlorite, calcite is one of the most abundant fracture filling minerals and is widely distributed at all examined depths (reaching 520 m.a.s.l.) without significant variations with depth (Sandström and Tullborg 2011). Clay minerals, mainly mixed layer smectite-illite and illite, also appear in dominant amounts in open fractures (Döse 2009, Döse et al. 2009a, b, Winell 2009, Winell et al. 2009a, b, Sandström and Tullborg 2011). Overall, these characteristics are similar to those found in the fracture fillings from the PLU and Laxemar-Simpevarp sites (Drake et al. 2006, Sandström et al. 2008, Drake and Tullborg 2009, Sandström and Tullborg, 2009, 2011) although, in contrast, mixed layer smectite-illite (poorly ordered) and illite are much more abundant at the SFR (Sandström and Tullborg 2011).

Due to the fast dissolution kinetics of calcite compared with silicates and aluminosilicates, the presence of this mineral in significant amounts is important as it provides buffering capacity against acidification. On the other hand, the surface Baltic waters are undersaturated with respect to calcite and, thus, dissolution processes could be feasible during the intrusion of these marine waters. It is unknown, at present, whether calcite dissolution occurs during the inflow of Baltic waters through the seabed sediments or through the bedrock (with the available data of calcite distribution with depth, calcite dissolution cannot be deduced at shallower levels in the bedrock) and this issue should be addressed in future studies.

Finally, the important presence of clay minerals in the open, water conducting fractures would support the probable existence of cation exchange processes during the groundwater evolution and their participation in the control of calcium and other cations (calcium and potassium appear in significant amounts in the usually poorly ordered, mixed layer clays of smectite-illite type (Sandström and Tullborg 2011)).

⁵ Calcite at Forsmark originates from the seafloor of Gävlebukten, a bay to the Baltic Sea located about 100 km north of the Forsmark site and covered by Cambrian and Ordovician sedimentary bedrock. The calcium-rich material was transported from Gävlebukten and deposited in the Forsmark area during the latest glacial period (Tröjbom and Söderbäck 2006).

4.1.3 Processes: Thermodynamic approach

Speciation-solubility calculations performed with the available data for the SFR area indicate that all the sampled groundwaters are equilibrated with higher $p\text{CO}_2$ than the atmospheric value (Figure 4-4). The same results were obtained when using a theoretical pH value obtained assuming calcite equilibrium (Appendix 3). Thus, there is an absence of groundwaters with lower $p\text{CO}_2$ than the atmosphere, which otherwise has been reported for the PLU or other crystalline systems (Gimeno et al. 2008, 2009) characterised by more saline waters than those found in the SFR.

Groundwaters are, in general, in equilibrium or slightly oversaturated with respect to calcite (Figure 4-5) and 45 of the 128 samples with pH field data (field and Chemmac) show SI values higher than +0.3 units. These oversaturation values may be either “real” (due to kinetic effects, retarded precipitation of calcite, or microbiological activity, see Gimeno et al. 2009), or resulting from CO_2 -outgassing during sampling of groundwaters originally equilibrated with respect to calcite, or even both. The possible effects of the uncertainty in the pH measurements are discussed in Appendix 3.

A few Local Baltic type groundwaters seem to be undersaturated with respect to calcite (Figure 4-5). This could be attributed to a very fast infiltration process of the present Baltic Sea waters (some of them clearly undersaturated with respect to this mineral) which did not allow the attainment of equilibrium with respect to calcite. This issue merits further studies given the possible uncertainty associated with the pH measurements in the cases when they were performed in the laboratory.

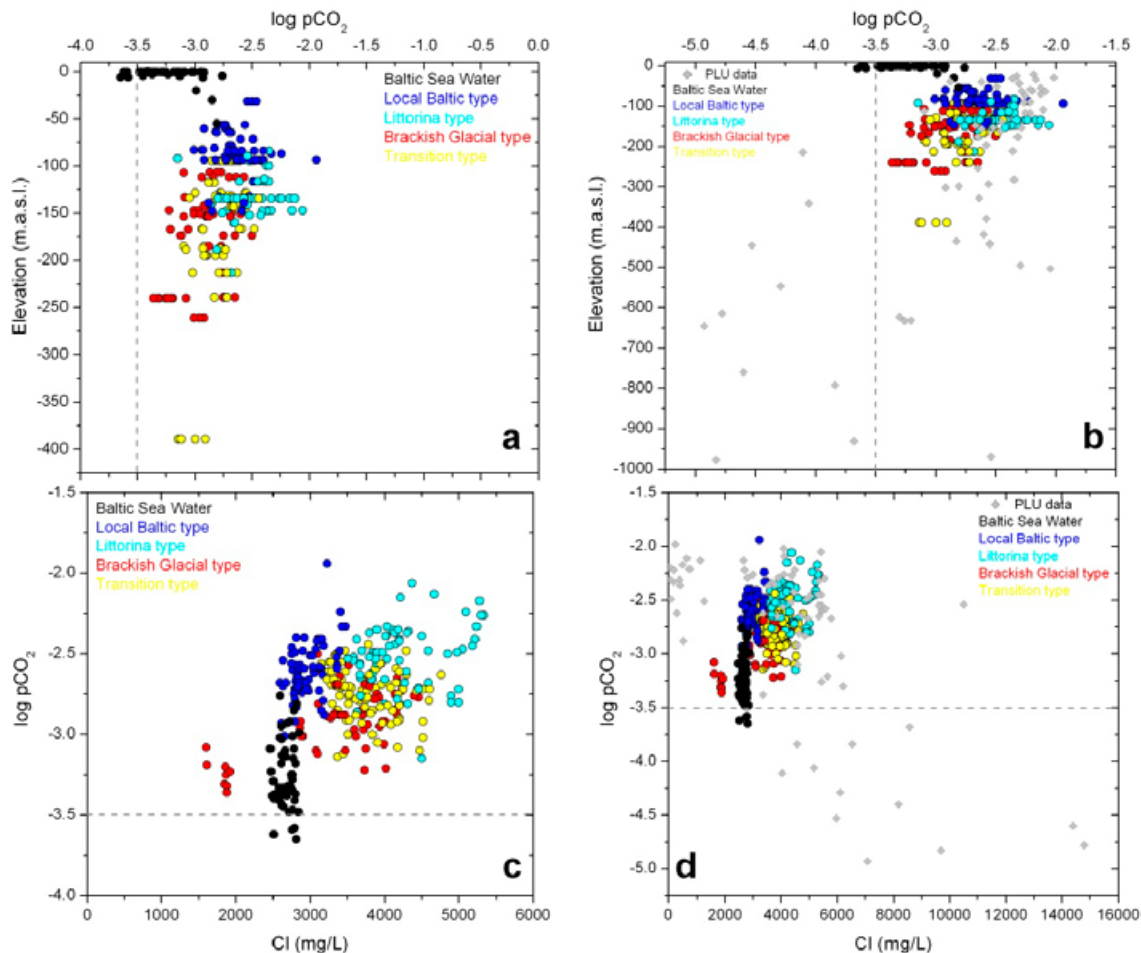


Figure 4-4. Calculated $\log p\text{CO}_2$ versus depth (a, b) and chloride content (c, d) for the SFR groundwaters colour coded by water types. The diagrams to the left (a and c) show the SFR data where the scales are restricted to those relevant to the SFR extension data. The diagrams to the right show these data integrated in the general distribution of the PLU data (Forsmark). Note the change in scales in the graphs to the right. Dashed line indicates the atmospheric $\log p\text{CO}_2$ value.

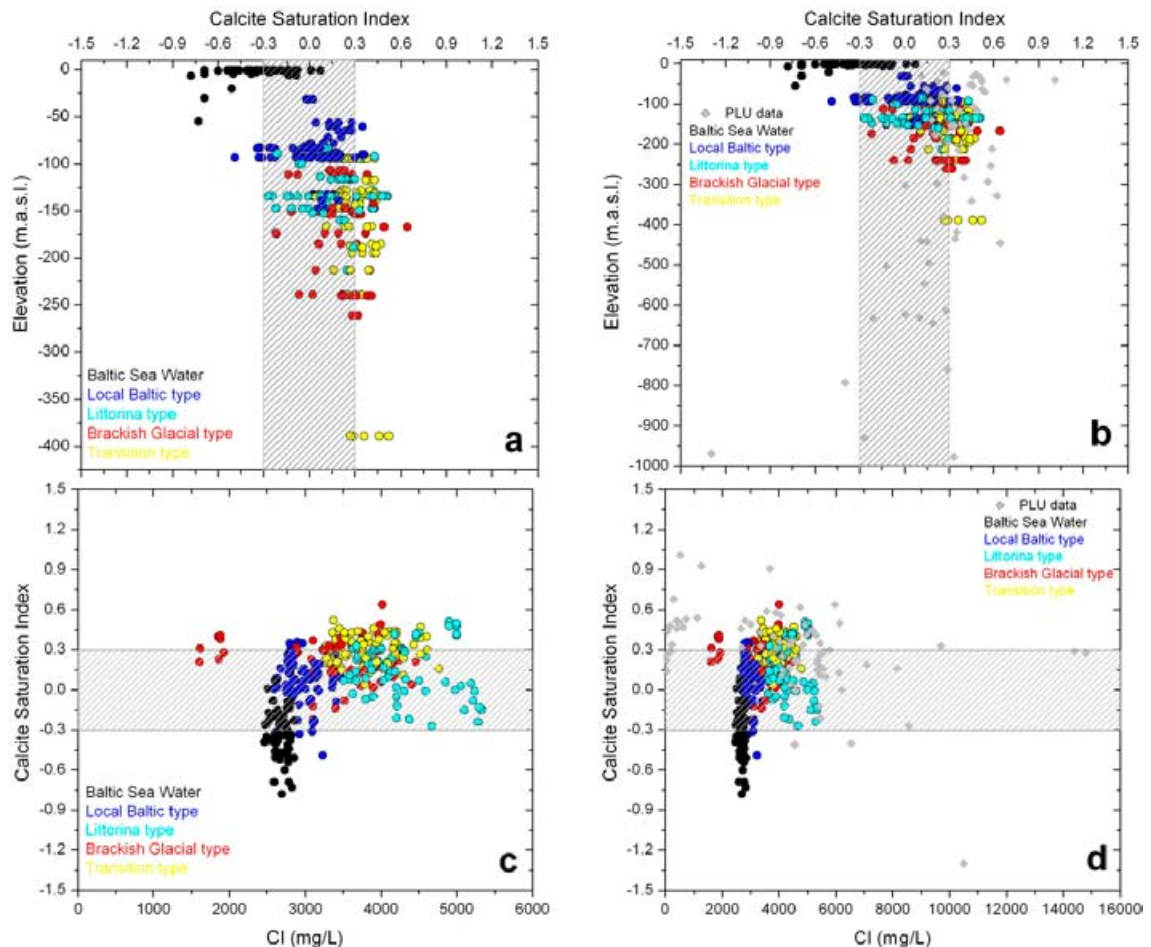


Figure 4-5. Calculated saturation index for calcite versus depth (a, b) and chloride content (c, d) for the SFR groundwaters colour coded by water types. The diagrams to the left (a and c) show the SFR data where the scales are restricted to those relevant to the SFR extension data. The diagrams to the right show these data integrated in the general distribution of the PLU data (Forsmark). Note the change in scales in the graphs to the right. Rastered areas correspond to the uncertainty range (± 0.3 units) associated with the calcite saturation index calculations.

In any case, most of the Local Baltic type groundwaters (as also for the majority of the other types) are in equilibrium with respect to calcite. Thus, some calcite dissolution is expected to have occurred during the intrusion of the Baltic waters, in agreement with the observed increases in calcium and alkalinity. Calcite reequilibrium appears to be effective in almost all groundwater samples following mixing events (e.g. mixing of the intruding Baltic waters with the preexisting groundwaters) as it occurs in the PLU and Laxemar-Simpevarp groundwaters.

4.1.4 Discussion and conclusions

Most of the parameters related to the carbonate system in the SFR groundwaters show similar trends to those observed in the PLU, especially if only groundwaters with marine contributions are compared. Some differences are evident but they are mostly associated with the sampled groundwater types. For instance, pH in the SFR groundwaters never reaches values as high as the ones reported for the brackish to saline non-marine PLU groundwaters. Therefore, SFR groundwaters never display the extremely low dissolved bicarbonate values or the pCO_2 lower than the atmospheric value that otherwise can be found in the above-mentioned types of PLU groundwaters.

Dissolved calcium and bicarbonate and the pH values do not show any clear correlation with depth. Only a rough decrease in bicarbonate and an increase in calcium with depth and chloride content can be observed. The few field pH measurements also indicate a slight increase with depth and a rough decrease with chloride.

Although heterogeneous reactions (calcite reequilibrium, cation exchange) may have noticeably modified the dissolved calcium concentrations, a mixing control is still evident. High and variable HCO_3^- values are found in groundwaters with a marine (both Littorina and present Baltic) signature as a result of the biological activity during infiltration of marine waters through seabed sediments.

Overall, most of the SFR groundwaters seem to be in equilibrium or slightly oversaturated with respect to calcite, which can either represent a real situation or a result of CO_2 outgassing during pH measurements. A few Local Baltic type groundwaters are (slightly) undersaturated with respect to calcite. This could be attributed to an infiltration time for present Baltic Sea waters (some of them clearly undersaturated with respect to calcite) which has been too fast to allow equilibration with respect to this mineral. However, this issue should be considered further, given the possible uncertainty associated to the pH measurements.

Although some calcite dissolution may occur during the infiltration of Baltic Sea waters, the intensity of this process must be low due to the high alkalinity content and near neutral pH in seawaters (7.5–8.3). Moreover, if anaerobic oxidation of organic matter occurred during the infiltration of these Baltic Sea waters, as supported by the evidence of sulphate reduction processes (see Section 5.3), this would lead to calcite precipitation (Luukkonen et al. 2004). Thus, the effects of Baltic Sea intrusion need to be further examined, together with the mineralogy and porewater hydrogeochemistry of the seabed above the SFR.

4.2 Sulphate system

Dissolved sulphate in crystalline systems may be affected or controlled by multiple processes or reactions such as weathering reactions (e.g. pyrite), surface processes, sulphate reduction activity or equilibrium situations with respect some mineral phases (e.g. gypsum, barite, etc). For the sites included in the Site Characterisation Programmes in Sweden and Finland (PLU, Laxemar and Olkiluoto), mixing processes throughout their palaeohydrological history may also exert a fundamental control on dissolved sulphate, especially if marine waters are involved (e.g. Pitkänen et al. 2004, Gimeno et al. 2008, 2009), as it also occurs in the SFR site (Nilsson et al. 2010).

In this section, the dissolved sulphate trends and controls in the SFR groundwaters are studied, including even processes with low influence *a priori* on them (e.g. gypsum equilibrium) and with special emphasis on mixing processes. Barium and strontium trends, commonly coupled to the sulphate system, are also examined.

4.2.1 Hydrochemical trends

Dissolved sulphate contents in the SFR groundwaters show a wide variation, ranging from 44 to 551 mg/L (0.46 to 5.74 mmol/L) and their trends with respect to depth and chloride contents are closely similar to those of the PLU groundwaters (Figure 4-6). The highest sulphate concentrations⁶ are associated with groundwaters with clear Littorina signatures and with chloride contents about 5,000–5,500 mg/L (141–155.1 mmol/L), as described for the PLU groundwaters.

Groundwaters with a more distinct present Baltic contribution appear in the shallower 150 m of the bedrock (Figure 4-6a, b). This Baltic contribution seems to diminish the variability of sulphate and to decrease the chloride contents from around 5,000–5,500 mg/L (in the groundwaters with clear Littorina signature) towards lower values (around 3,000 mg/L of chloride \approx 84.6 mmol/L; Figure 4-6c, d).

This vertical trend would indicate an important effect of past and present seawater intrusion on the dissolved sulphate contents, as documented in Olkiluoto (Pitkänen et al. 1999) or in the PLU groundwaters (see Gimeno et al. 2008 for details). This is also consistent with the significant correlations observed between dissolved sulphate and other marine derived components in the SFR (e.g. Mg with $R^2 = 0.52$, or HCO_3^- with $R^2 = 0.51$).

⁶Except for the sample with the highest sulphate value but, otherwise, with clear transition characteristics.

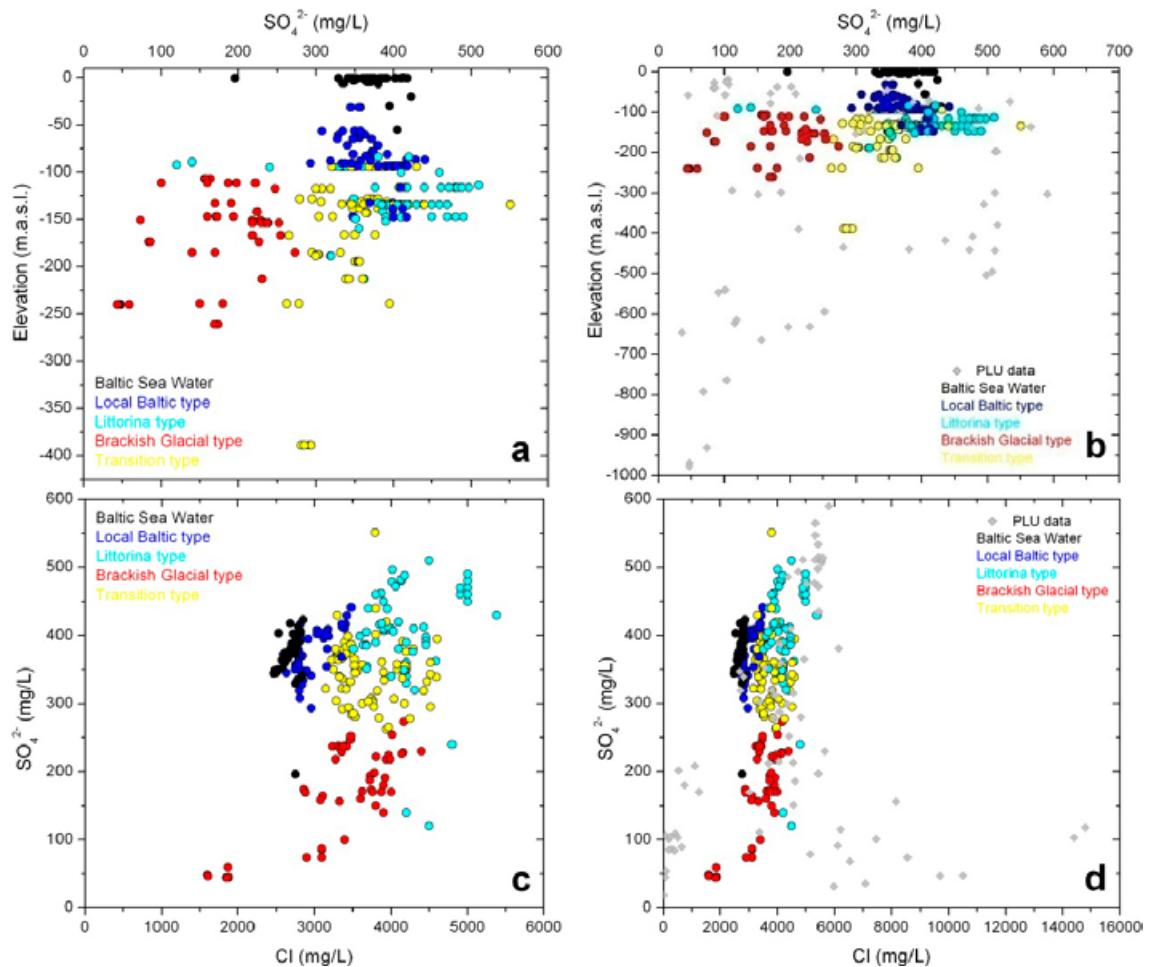


Figure 4-6. Sulphate concentrations versus depth (a, b) and chloride contents (c, d) in the SFR groundwaters colour coded by water types. The diagrams to the left (a and c) show the SFR data where the scales are restricted to those relevant to the SFR extension data. The diagrams to the right show these data integrated in the general distribution of the PLU data (Forsmark). Note the change in scales in the graphs to the right.

Reaction processes may also play a key role in the control of dissolved sulphate contents. One of the main influences seems to be the SRB activity, which promotes sulphur (^{32}S and ^{34}S) isotope fractionation and results in a larger portion of the heavy isotope remaining in the sulphate (e.g. Clark and Fritz 1997). Available $\delta^{34}\text{S}$ values versus depth and dissolved sulphate contents are plotted in Figure 4-7 for the SFR and the PLU data. Most of the SFR data show the same trends as the PLU data and values higher than marine ($\delta^{34}\text{S} \sim 21\text{‰}$ CDT, Clark and Fritz 1997) are common.

The highest $\delta^{34}\text{S}$ value (+37.5‰ CDT) is observed in one of the samples with lower chloride (1,870 mg/L, 52.7 mmol/L) and sulphate (22.4 mg/L, 0.23 mmol/L) contents from the KFR101 borehole at section 271.5–341.76 m.b.l. Such an extreme $\delta^{34}\text{S}$ value is a strong indicator of sulphate reducing activity under closed system conditions. The closed system behaviour is also supported by the presence of a glacial meltwater component in these samples ($\delta^{18}\text{O}$ values between -14.4 and -15.1‰ in two samples), indicative of long term hydraulic isolation (in common with groundwaters from the PLU or from Laxemar (Smellie et al. 2008, Gimeno et al. 2009). Values of $\delta^{34}\text{S}$ between 22.4 and 24.4‰, also indicative of sulphate reduction activity, can be found in other groundwaters with glacial signatures, as well as in Littorina and Transition groundwater types.

The $\delta^{34}\text{S}$ data from the four analyses presently available for the Local Baltic type groundwaters (from 20.8 to 21.4‰) are in the range usual for seawaters (compare the black and the blue circles in Figure 4-7a), which excludes the existence of sulphate reducing activity. However, the molal Cl/SO_4 ratio for seawaters is around 19 whereas the values for these type of groundwaters range from 18.9 to 23.5 (with an average value of 21), suggesting that some sulphate could have been consumed by SRB activity.

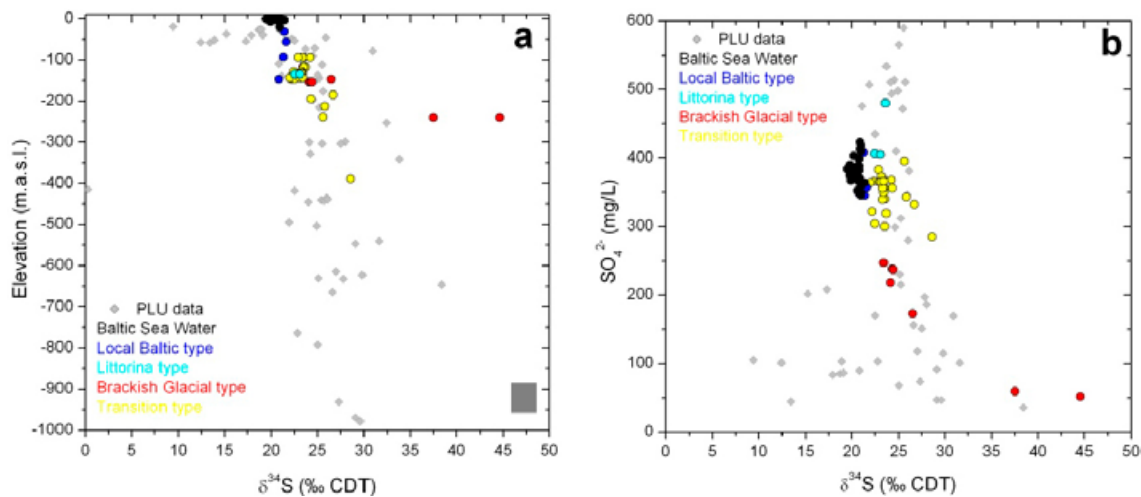


Figure 4-7. $\delta^{34}\text{S}$ values (‰ CDT) versus depth (a) and sulphate contents (b) in the SFR groundwaters integrated in the general distribution of the PLU.

The presence of sulphate reduction activity during the intrusion of present Baltic Sea waters is also supported by the existence of dissolved S(-II) in some Local Baltic groundwater types (see Section 5.3) and merits further studies.

With regard to the strontium behaviour, its dissolved concentration trends with depth are closely similar to those observed in the PLU groundwaters (Figure 4-8). Dissolved strontium shows a weak correlation with dissolved sulphate and chloride (R^2 lower than 0.4; Figure 4-8c), when present in PLU groundwaters with similar chloride contents (between 3,000 and 6,000 mg/L or 84.6 and 169.2 mmol/L; Figure 4-8d). However, its correlation with calcium is quite remarkable ($R^2 = 0.918$; Figure 4-8e, f).

This group of groundwaters with chloride $< 6,000$ mg/L (< 169.2 mmol/L) has been more affected by mixing processes, which has triggered more variable and complex ion exchange processes than the ones observed for deeper groundwaters with chloride contents higher than 6,000 mg/L (Figure 4-8d). This would explain the greater dispersion in the relation of Cl-Sr and the lower dispersion in the correlation of Sr-Ca, given that these elements behave geochemically similarly. Such evidence points towards the participation of common water-rock interaction processes (e.g. cation exchange) superimposed on the influence of mixing during control of the calcium and strontium contents.

Finally, barium contents in the SFR groundwaters show a general increasing trend with depth down to 250 m (Figure 4-9a). Then, deeper down, the few samples analysed in the SFR fit with the lower limit of contents found in the PLU where an increasing trend extends down to 430 m depth (Figure 4-9b). Barium contents do not show any correlation with chloride concentrations (Figure 4-9c). Dissolved barium concentrations in the SFR groundwaters are commonly below 0.2 mg/L ($1.46 \cdot 10^{-3}$ mmol/L) except in the old and isolated groundwaters from the KFR101 borehole (Cl contents around 1,800 mg/L, 50.8 mmol/L), where contents between 0.5 and 0.55 mg/L ($3.6 \cdot 10^{-3}$ and $4.0 \cdot 10^{-3}$ mmol/L) are recorded. These high dissolved barium contents, or even higher, are only reached in the brackish groundwaters with an important Littorina contribution in the PLU (Figure 4-9d).

4.2.2 Speciation-solubility calculations

The concentrations of many dissolved elements, such as calcium, strontium, barium and, obviously, sulphate, can be controlled or regulated by processes affecting sulphate minerals in natural groundwaters. The most common controlling phases are gypsum, celestite and barite (e.g. Nordstrom et al. 1989). Thus, saturation states of the SFR groundwaters with respect to the aforementioned minerals have been calculated and the results are presented here. The uncertainty ranges considered for these saturation indices are: ± 0.2 SI units for gypsum, ± 0.3 SI units for celestite and ± 0.5 SI units for barite (Langmuir and Melchior 1985, Deutsch 1997).

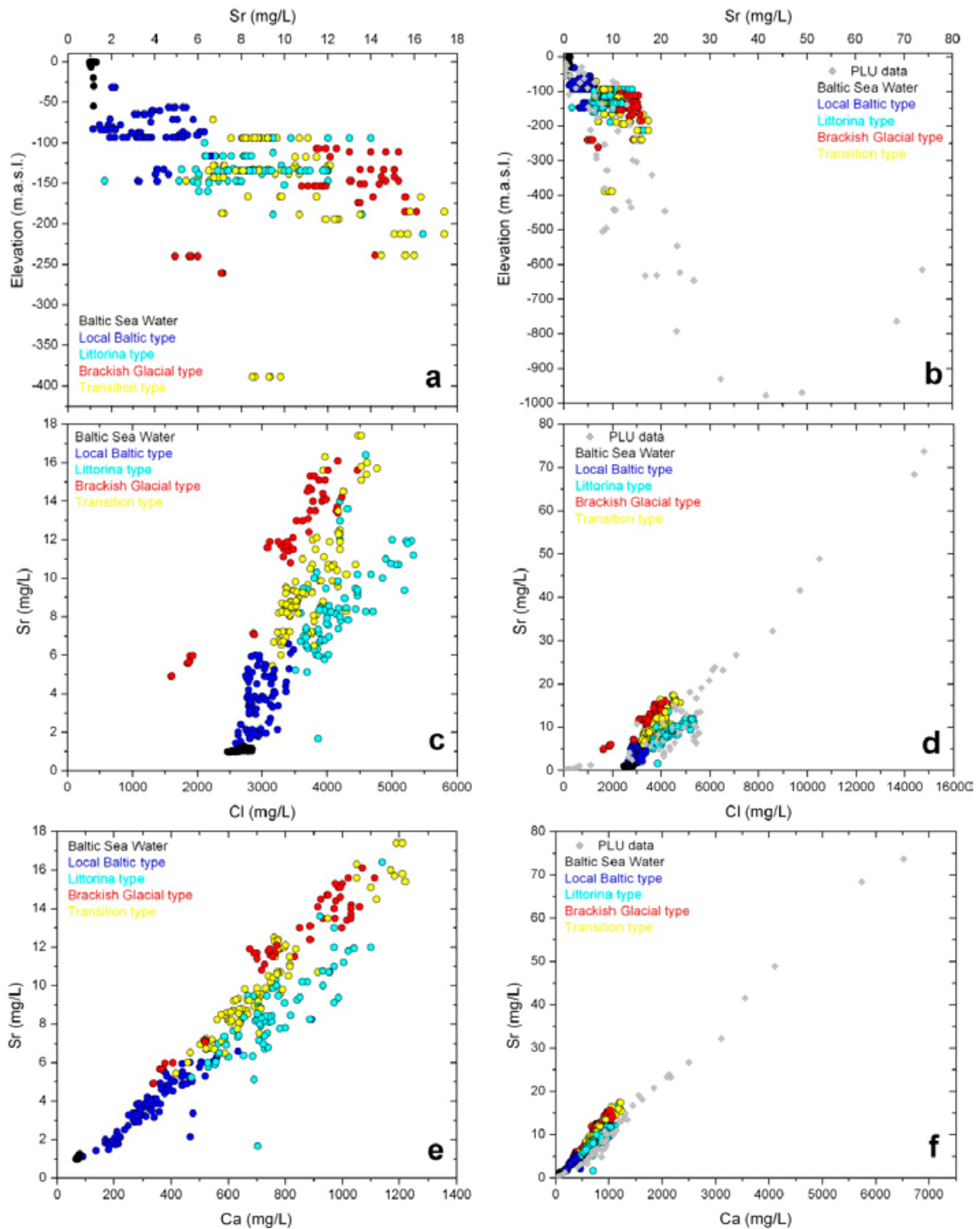


Figure 4-8. Strontium concentrations versus depth (a, b), chloride (c, d) and calcium contents (e, f) in the SFR groundwaters colour coded by water types. The diagrams to the left (a, c, e) show the SFR data where the scales are restricted to those relevant to the SFR extension data. The diagrams to the right show these data integrated in the general distribution of the PLU data (Forsmark). Note the change in scales in the graphs to the right.

Groundwaters from the SFR area are always undersaturated with respect to gypsum and the SI trends with depth are the same as observed for the PLU groundwaters (Figure 4-10). Littorina type and Transition type waters are the closest to equilibrium although clearly undersaturated, as reported for groundwaters with clear Littorina contributions in the PLU (Gimeno et al. 2008) or in other crystalline rock systems (Olkiluoto and Laxemar-Simpevarp; Pitkänen et al. 2004, Gimeno et al. 2009).

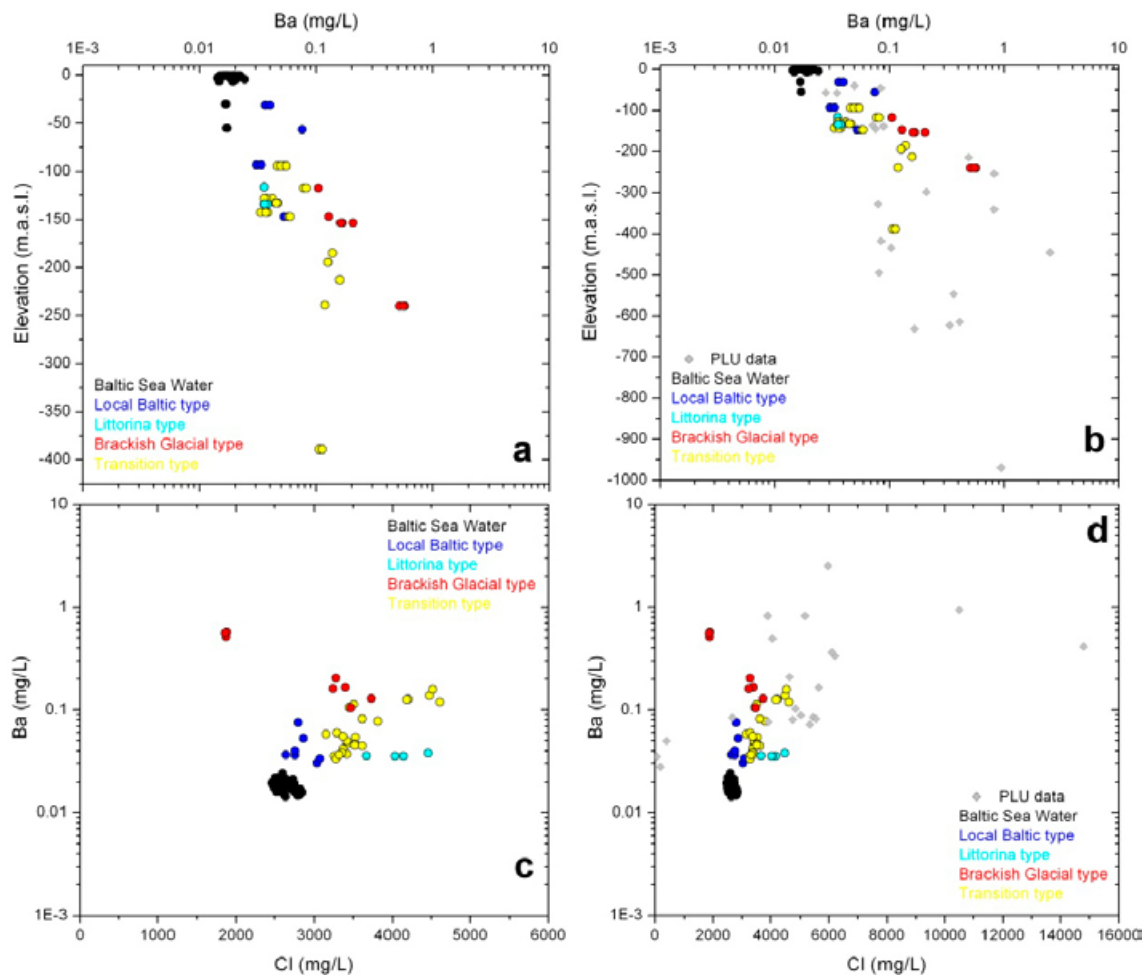


Figure 4-9. Dissolved barium contents versus depth (a, b) and chloride concentrations (c, d) in the SFR groundwaters colour coded by water types. The diagrams to the left (a and c) show the SFR data where the scales are restricted to those relevant to the SFR extension data. The diagrams to the right show these data integrated in the general distribution of the PLU data (Forsmark). Note the change in scales in the graphs to the right.

Local Baltic type waters are the farthest to equilibrium (except the less concentrated Brackish-glacial type waters from the KFR101 borehole; Figure 4-10a). The same overall undersaturation state in the SFR groundwaters can be deduced with respect to celestite (data not shown).

Even though there are no data relative to SFR groundwaters deeper than 400 m and with dissolved chloride contents higher than 5,000 mg/L (141.0 mmol/L), the general trends observed for the gypsum saturation states or the sulphate contents with respect to dissolved chloride concentrations suggest that they may be similar to the ones observed in the PLU groundwaters.

Overall, these results indicate, as also reported for the PLU groundwaters, that gypsum and celestite do not participate in the control of dissolved sulphate in the SFR groundwaters. To date, none of these minerals have been identified from the mineralogical studies carried out on this site (Döse et al. 2009a, b, Winell 2009, Winell et al. 2009a, b, Sandström and Tullborg 2011) or thorough studies focussed on fracture filling minerals from the PLU area down to 1,000 m depth⁷ (e.g. Sandström et al. 2008, Sandström and Tullborg 2009, 2011).

⁷The presence of gypsum and celestite has been reported for the Laxemar-Simpevarp area, where the corresponding equilibria are reached in groundwaters deeper than 800 m and with chloride contents higher than 8,000 mg/L (225.67 mmol/L; Gimeno et al. 2009).

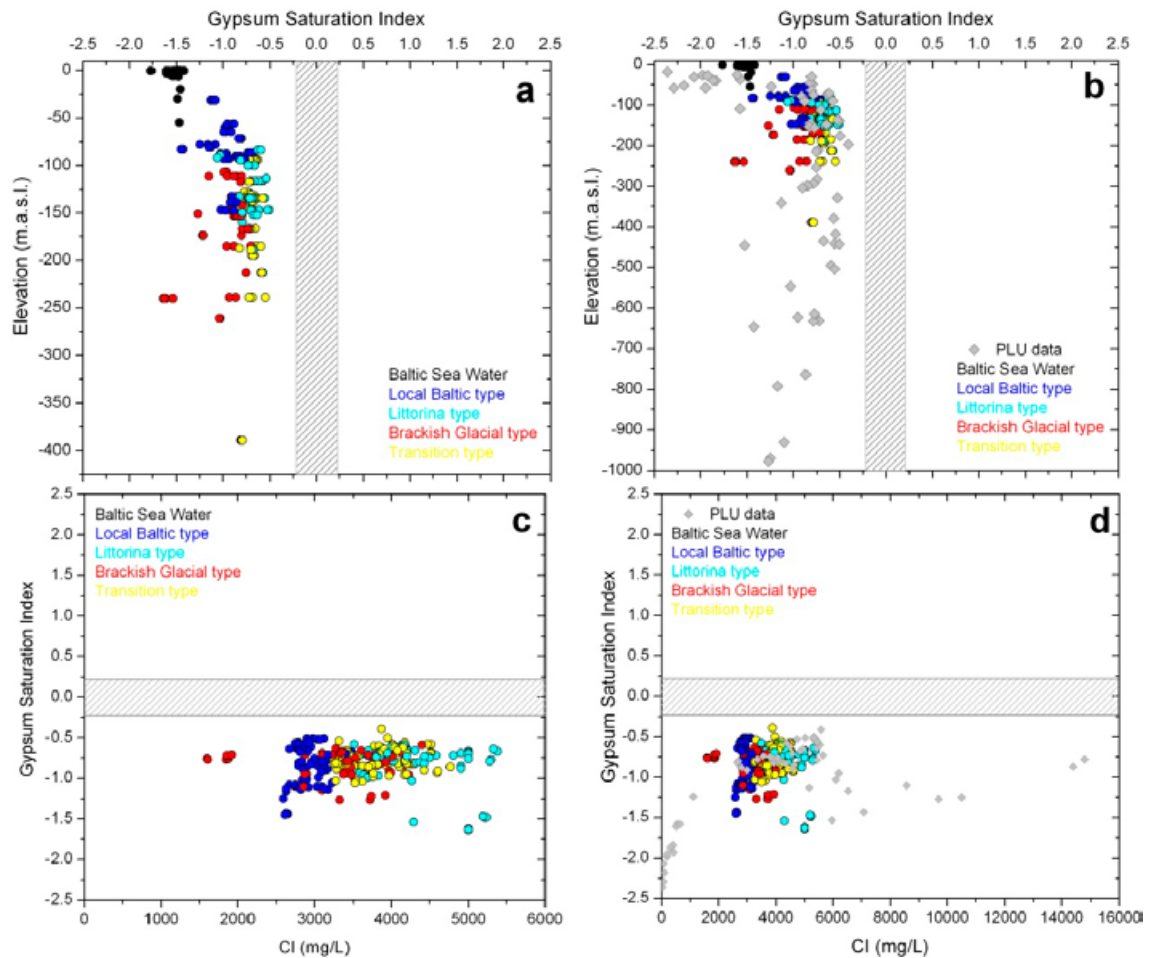


Figure 4-10. Gypsum saturation index versus depth (a, b) and chloride contents (c, d) for the SFR groundwaters colour coded by water types. The diagrams to the left (a and c) show the SFR data where the scales are restricted to those relevant to the SFR extension data. The diagrams to the right show these data integrated in the general distribution of the PLU data (Forsmark). Note the change in scales in the graphs to the right. Rastered areas correspond to the uncertainty range (± 0.2 units) associated with the gypsum saturation index calculations.

On the contrary, most of the SFR groundwaters are in equilibrium with respect to barite (Figure 4-11), as reported for other low temperature granitic groundwater systems such as the PLU groundwaters (Figure 4-11a, b), Stripa (Nordstrom et al. 1989), or Laxemar-Simpevarp (Gimeno et al. 2009).

Mineralogical studies in drillcores indicate that barite is even more common in the SFR than in the PLU (Sandström and Tullborg 2011). However, some of the groundwaters below 150 m depth and with the highest barium concentrations, including those from the KFR01 borehole, are clearly oversaturated with respect to barite. The same degree of oversaturation is present in some groundwaters from the PLU (Figure 4-11b). More studies are needed to assess the influence of other barium-rich mineral phases, such as harmotome (a soluble Ba-zeolite locally detected in the fracture fillings of the Simpevarp and Laxemar subareas down to 300–400 m depth and also locally found at SFR (Drake and Tullborg 2009, Gimeno et al. 2009, Sandström and Tullborg 2011), or the possibility of analytical errors in these samples.

4.2.3 Conclusions

In the light of the observed compositional trends for the dissolved sulphate concentrations, the main source of sulphur in the SFR groundwaters is the intrusion of past (Littorina) and present (Baltic) seawaters, which have mixed with the preexistent groundwaters.

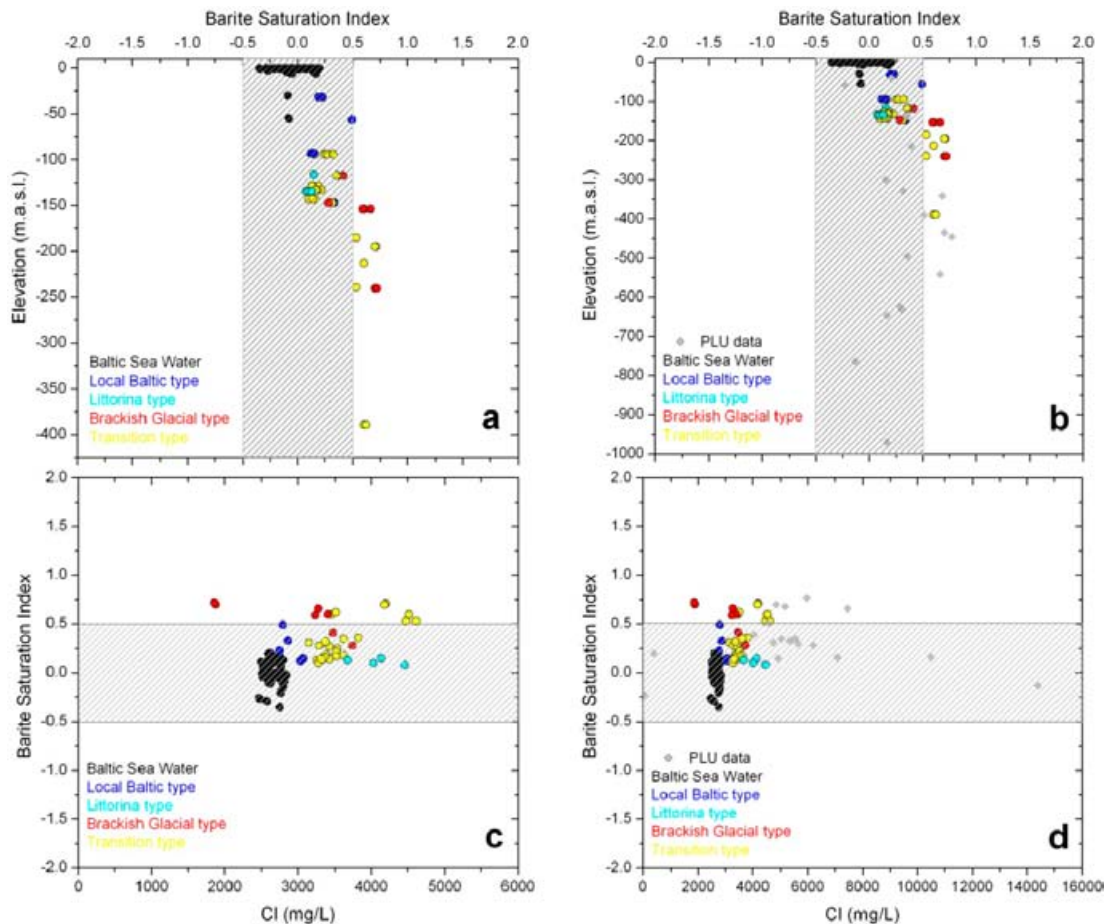


Figure 4-11. Barite saturation index versus depth (a, b) and dissolved barium contents (c, d) for the SFR groundwaters colour coded by water types. Rastered areas correspond to the uncertainty range (± 0.5 units) associated with the barite saturation index calculations. See Figure 4-10 caption for more details.

Apart from these mixing processes and the lack of isotopic data ($\delta^{34}\text{S}$), sulphate reducing microbial activity seems to have played a very minor role on the control of dissolved sulphate concentrations. For some of the groundwaters more affected by the intrusion of present Baltic Sea waters, even though the isotopic data are not fully supportive, the Cl/SO_4 ratios point towards the existence of active sulphate reducing processes.

As also reported for the PLU groundwaters, all the SFR groundwaters are undersaturated with respect to gypsum and celestite and in equilibrium with respect to barite. However, none of these minerals appear to have appreciably affected the dissolved sulphate contents derived from mixing processes in the studied groundwaters.

4.3 Silica system

Previous studies in the PLU and Laxemar areas have indicated that dissolved silica contents in the near surface and shallow groundwaters are mainly controlled by mineral reactions with no clear limiting equilibrium situations. On the contrary, dissolved silica in deeper groundwaters seems to be generally controlled by equilibrium with respect to a silica phase (quartz or chalcedony), although the influence of seawater intrusion and mixing on the silica content of both systems has also been detected (Gimeno et al. 2009 and references therein).

In the case of the SFR area, the existence of past (Littorina stage) and recent (Baltic Sea) seawater intrusion and mixing may have also influenced the dissolved silica trends. The effect of these processes on dissolved silica and the possible mineralogical controls in the SFR groundwaters will be evaluated in this section.

4.3.1 Hydrochemical trends

Silica concentrations in the SFR groundwaters range from 2.4 to 17.5 mg/L (0.04 to 0.29 mmol/L), with the lowest values in one of the Local Baltic type groundwaters and the highest in some Local Baltic and Littorina type groundwaters (Figure 4-12a). However, more than 98% of the samples display silica contents between 7 and 14 mg/L (0.12 and 0.23 mmol/L). This variability range decreases with depth in such a way that at 250 m depth, the silica contents range from 10 to 13 mg/L (0.17 to 0.22 mmol/L).

Silica values in the SFR groundwaters are similar to the ones reported for other crystalline rock systems (e.g. PLU, Laxemar, Olkiluoto, Palmottu or the Lac du Bonnet granitic batholith in Canada) at levels shallower than 500 m depth⁸ (Figure 4-10b, c). In the case of the PLU and Laxemar groundwaters, this variability is frequently related to the variable seawater influence. For instance, the widest variability and highest silica contents (up to 24 mg/L or 0.4 mmol/L; Figure 4-12b) in the PLU groundwaters are related to the brackish groundwaters characterised by an important Littorina contribution, also displaying high and variable contents of dissolved sulphate, magnesium and manganese, inherited from their marine origin (Gimeno et al. 2008).

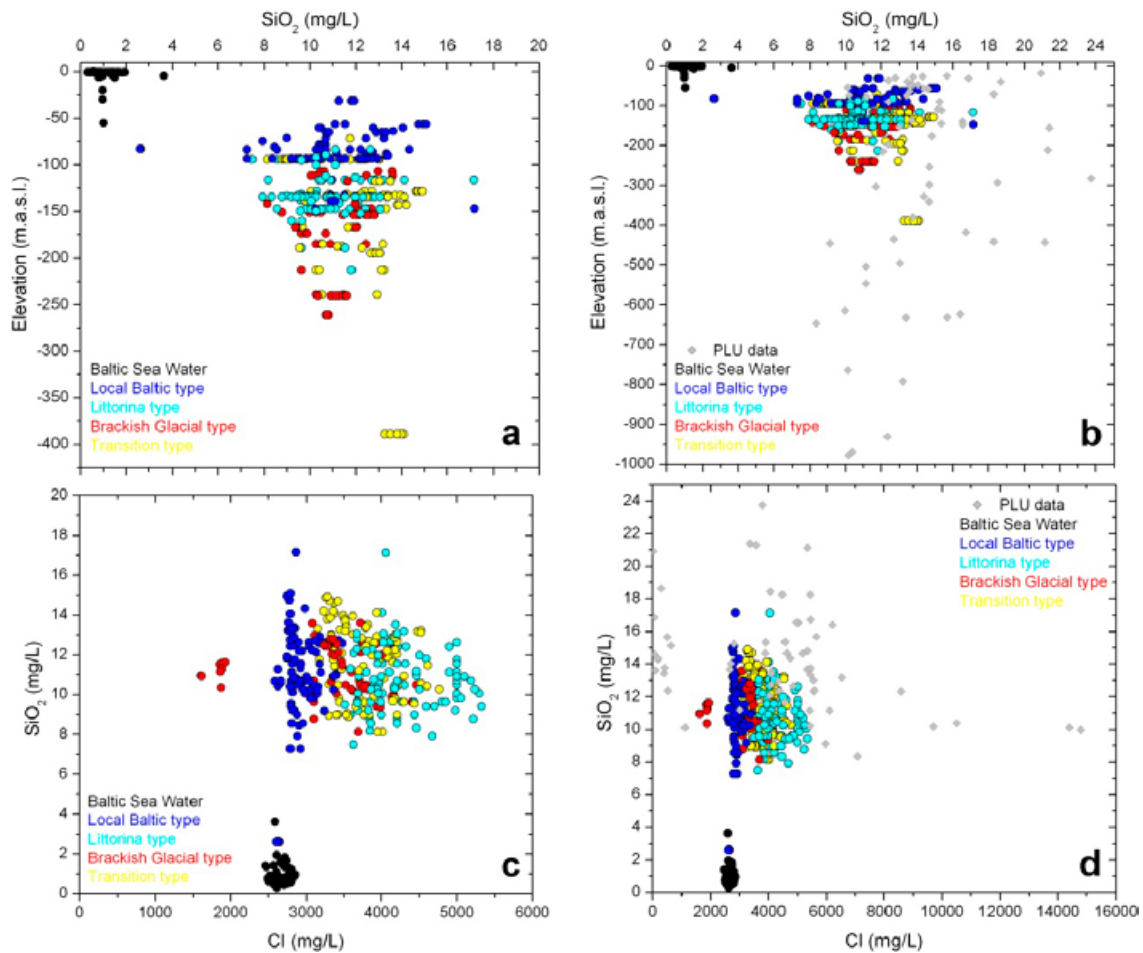


Figure 4-12. Dissolved silica contents versus depth (a, b) and chloride contents (c, d) in the SFR groundwaters colour coded by water types. The diagrams to the left (a and c) show the SFR data where scales are restricted to those relevant to the SFR extension data. The diagrams to the right show these data integrated in the general distribution of the PLU data (Forsmark) down to 1,000 m (b) and wider concentration scales (d).

⁸ The silica values observed in the most saline (Cl > 7,000 mg/L or 197.4 mmol/L) and deep groundwaters of these systems are relatively constant between 6.4 and 10.7 mg/L (0.11 and 0.18 mmol/L) (Gimeno et al. 2009).

High silica concentrations can be acquired by marine waters when passing through sea-bottom sediments with highly soluble diatom skeletons (made of amorphous silica) and diatom ooze and diatomaceous muds are frequently present in the Littorina sediments (Burke and Kemp 2002 and references therein). As these silica rich recharge waters flow through the bedrock, silica concentrations would decrease by reaction with the fracture filling minerals, especially with clays (e.g. McKenzie et al. 1967). However, in the PLU area it is clear that these reactions have not been able to eliminate the high dissolved silica contents, which remain as a fingerprint of an old mixing process.

In the Laxemar-Simpevarp area the Littorina imprint on silica concentrations seems to have been weaker and/or more easily removed (e.g. through sorption processes in fracture filling clays) as there is no clear relation between waters with high Littorina mixing proportion and high silica contents. However, the lowest contents of dissolved silica (4 mg/L, 0.07 mmol/L) were found in KAS02 (Äspö; sample #1418) at 307.68 m depth in groundwaters with an important contribution of present Baltic Sea waters (Glynn and Voss 1999, Gimeno et al. 2009) with depleted silica concentrations due to biological extraction (present Baltic Sea waters show very low silica contents, usually below 1 mg/L or 0.017 mmol/L).

Thus, marine influences can promote the existence of both high or low dissolved silica contents depending on the heterogeneous reactions during the infiltration of seawaters through the marine sediments. In the SFR groundwaters, both types of marine influences are also present. The two highest silica concentrations (around 17 mg/L or 0.29 mmol/L) have been measured in Littorina type and Local Baltic type groundwaters, and the lowest silica concentrations are also associated with Local Baltic type groundwaters (HFM34 borehole at 83 m depth). The hydrochemistry of these Local Baltic type groundwaters is almost identical to the Baltic Sea waters sampled in the SFR site (samples #16375, #16376 and #16377) but with silica contents two or three times higher (around 2.6 mg/L or 0.043 mmol/L). Therefore, those groundwaters from the HFM34 borehole would correspond to present Baltic Sea waters without any mixing with older groundwaters, but their higher silica contents would be derived from water-rock interaction processes, probably with clay minerals present in the fracture fillings.

Despite the marine influences on the SFR groundwaters, dissolved silica contents are not correlated with dissolved chloride (Figure 4-12c), which is common in the rest of the systems considered above (e.g. Figure 4-12d). Thus, mineralogical control as a source or as a limiting phase of this element appears to be clearly superimposed on the mixing effects.

4.3.2 Speciation-solubility calculations

The speciation-solubility results presented here are focussed on the saturation indices of chalcedony, as the most frequent silica phase involved in the control of dissolved silica in the groundwaters of this type of crystalline rock systems, and quartz. The uncertainty range considered for both saturation indices is ± 0.2 SI units (Deutsch 1997).

Results are presented in Figure 4-13. Overall, most groundwaters in the SFR area would be closer to equilibrium with chalcedony than with quartz, irrespective of their depth and salinity (Figure 4-13a, c), in common with Forsmark (Figure 4-13b, d) and in other “similar” crystalline environments such as Olkiluoto or Lac du Bonnet (Gimeno et al. 2009). Only the recent Baltic groundwaters from the HFM34 borehole (together with present day Baltic Sea waters) are clearly undersaturated with respect to both phases, which suggests that water-rock interaction processes have not had either the time (i.e. Baltic waters are typically about 13.5 TU) or the intensity necessary to impose the dissolved silica contents found in other groundwaters.

Another observation is the slightly broader range of saturation indices in the shallower and less saline samples compared with the deeper and more saline groundwaters, both in the SFR and in the PLU (Figure 4-13b, d) and also in the Laxemar-Simpevarp groundwaters (Gimeno et al. 2009). This slightly greater dispersion in the chalcedony SI values in all these systems at shallow depths may be related to the superposition of other processes controlling the dissolved silica (e.g. aluminosilicate reactions and/or mixing processes such as the previously mentioned “disturbance” induced by the marine contributions). In these cases, dissolved silica concentrations might not be controlled by chalcedony equilibrium but by incongruent dissolution reactions or surface processes involving clay minerals in fracture fillings (see Gimeno et al. 2009 for further discussion).

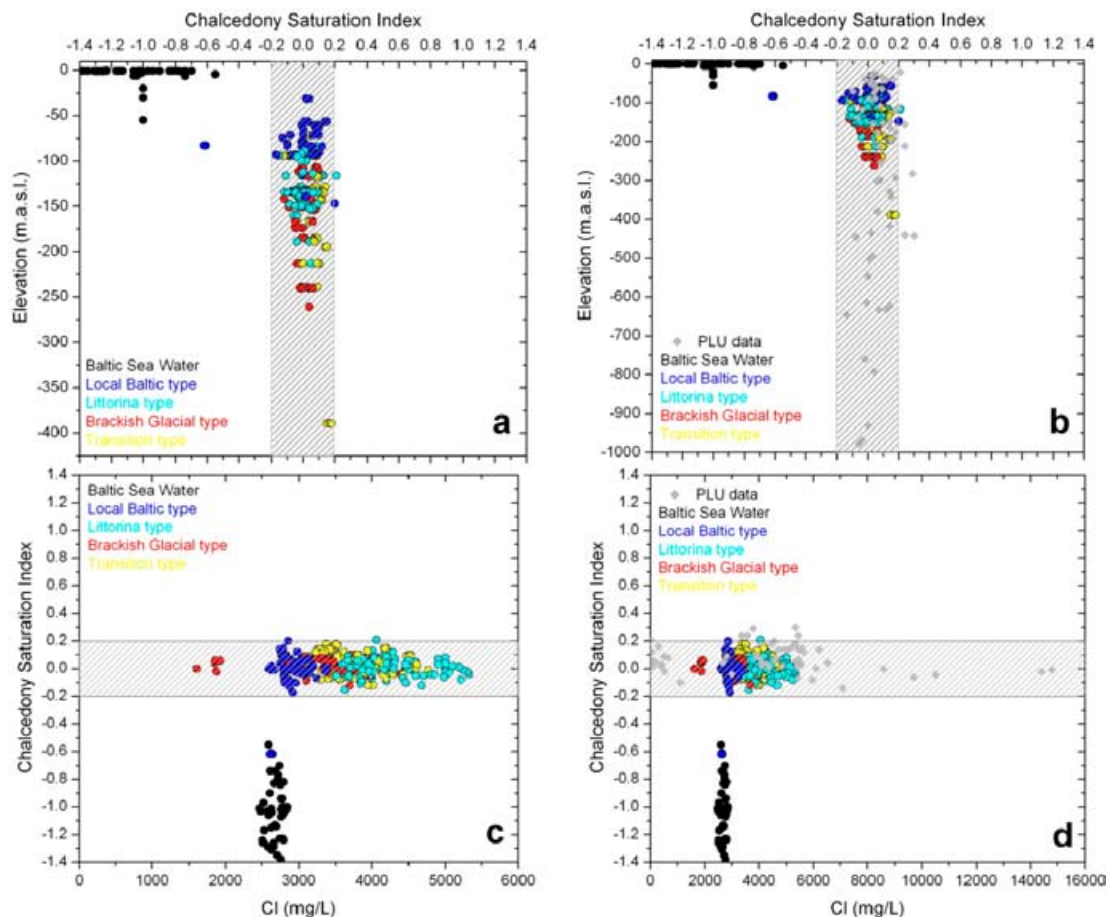


Figure 4-13. Chalcedony saturation index versus depth (a, b) and chloride contents (c, d) for the SFR groundwaters colour coded by water types. The diagrams to the left (a and c) show the SFR data where scales are restricted to those relevant to the SFR extension data. The diagrams to the right show these data integrated in the general distribution of the PLU data (Forsmark). Note the change in scales in the graphs to the right. Rastered areas correspond to the uncertainty range (± 0.2 units) associated with the chalcedony saturation index calculations.

Groundwaters from the KFR101 borehole at section 271.5–341.76 m.b.l. with long term hydraulic isolation, high $\delta^{34}\text{S}$ values and presence of an important glacial melt water component (see above) indicate clear equilibrium situations with respect to chalcedony. The long residence times of these groundwaters, without marine perturbations, would favour an effective equilibrium control of dissolved silica, as it occurs in the glacial derived groundwaters or in the deepest and more saline groundwaters from the PLU or Laxemar-Simpevarp areas.

4.3.3 Conclusions

Dissolved silica concentrations in the SFR groundwaters are not correlated with chloride contents, which would indicate the presence of a mineralogical control as a source of this element or as a limiting phase. Therefore, dissolved silica represents a typical reactive component whose control is kinetically or thermodynamically determined by heterogeneous processes.

Depending on the groundwater residence time, different water-rock interaction processes can participate in the control of dissolved silica. In groundwaters with short residence times, the main processes that can participate in the control of silica contents are incongruent dissolution of feldspars with formation of secondary clays, clay mineral transformations and silica adsorption-desorption reactions in clays (Langmuir 1997 and references therein). For the SFR, this type of situation can be inferred for recent Baltic waters circulating in some fractures (with or without minor mixing), for which silica contents are probably controlled by surface reactions in clays.

Control by a more stable solid silica phase (e.g. chalcedony) occurs in groundwaters with longer residence times. This is the case, for example, of the old glacial derived groundwaters with a long term hydraulic isolation (KFR101 borehole).

However, mineralogical controls of this type may be overlapped with mixing, as the effects of marine intrusions with distinctive silica contents (e.g. very high in some Littorina waters and very low in present Baltic waters) are still apparent in the present concentrations of this element in some groundwaters. Mixing processes could be responsible for the present dispersion of silica contents at least in some of the SFR groundwaters.

4.4 Fluoride system

Fluoride concentrations in waters from crystalline environments are usually strongly controlled by dissolution-precipitation or exchange processes involving fluoride bearing minerals (e.g. biotite, hornblende, micas, fluorite, clays with exchangeable fluoride, etc). Amongst these minerals, fluorite is the most common mineral limiting phase in crystalline groundwaters (Nordstrom and Jenne 1977, Nordstrom et al. 1989, Iwatsuki et al. 2005, Chae et al. 2007), including those studied in the Site Characterisation Programmes (Gimeno et al. 2008, 2009). Moreover, fluorite has been detected in the fracture fillings from the SFR (Sandström and Tullborg 2011). For these reasons, special attention has been paid in this section to the evaluation of equilibrium or disequilibrium situations with respect to fluoride.

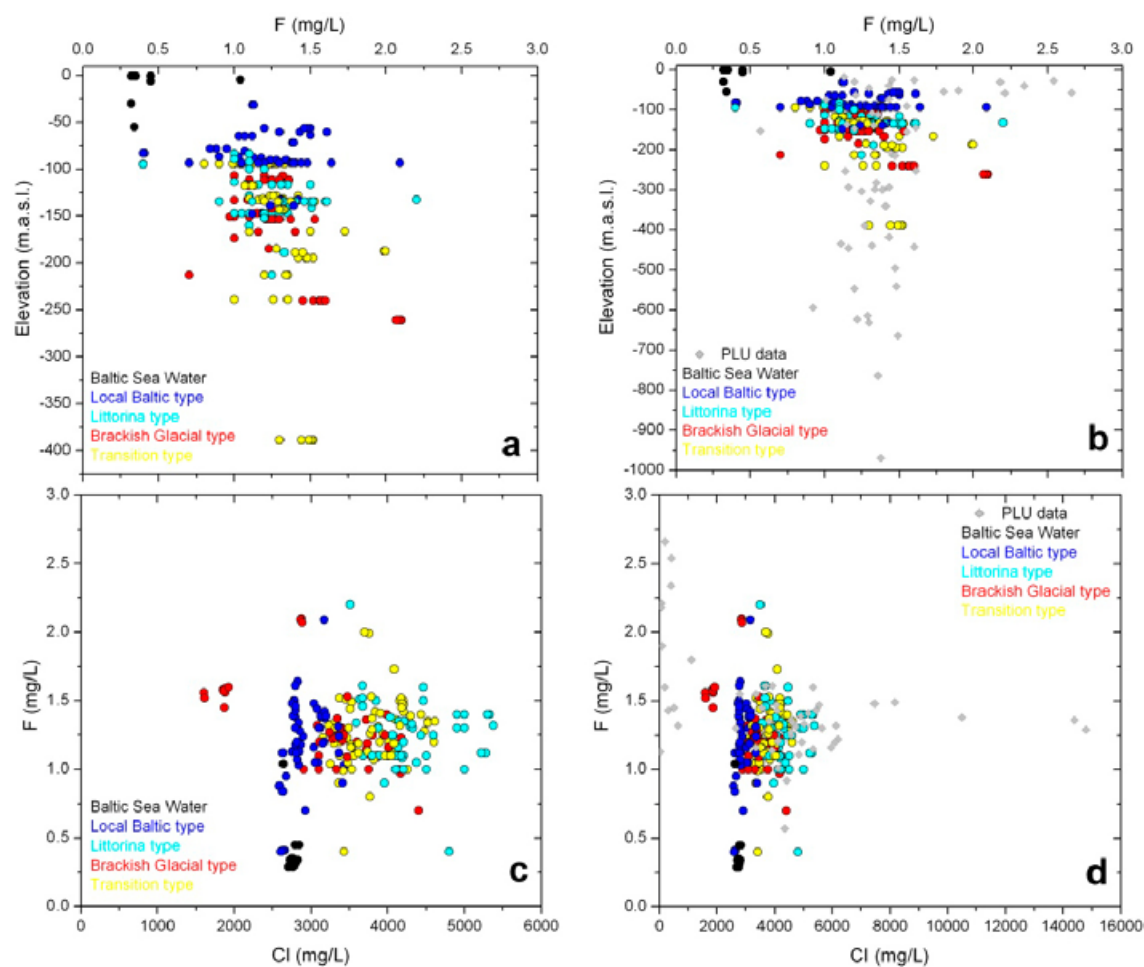


Figure 4-14. Fluoride contents with respect to depth (a, b) and chloride (c, d) in the SFR groundwaters colour coded by water types. The diagrams to the left (a and c) show the SFR data where the scales are restricted to those relevant to the SFR extension data. The diagrams to the right show these data integrated in the general distribution of the PLU data (Forsmark). Note the change in scales in the graphs to the right.

4.4.1 Hydrochemical trends

Fluoride concentrations in the SFR groundwaters range from 0.4 to 2.2 mg/L (0.02 to 0.11 mmol/L), with most values ranging between 1 and 2 mg/L (0.05 and 0.1 mmol/L; Figure 4-14 a, c). These ranges are within those reported for the PLU groundwaters, where fluoride contents are always lower than 2.6 mg/L (0.14 mmol/L; Figure 4-14b, d; Gimeno et al. 2009).

In common with the silica contents, some of the lowest fluoride contents (below 1 mg/L or 0.05 mmol/L in the HFM34 borehole) have been measured in groundwaters derived exclusively from present Baltic Sea water, for which similar values have also been reported in the vicinity from Forsmark (usually below 0.45 mg/L or 0.024 mmol/L) or from the SFR area (below 0.3 mg/L or 0.016 mmol/L). Low fluoride contents have also been observed in some Littorina type or Transition type groundwaters from the SFR area (Figure 4-14c), which could also be related to the dilution effect caused by Baltic Sea intrusion.

In any case, the overall narrow range of dissolved fluoride in most of the SFR groundwaters, together with the lack of correlation between fluoride and chloride, would suggest the existence of a “*mineral solubility control*” on dissolved fluoride in the groundwaters of the SFR.

4.4.2 Speciation-solubility calculations

Since fluorite is usually the fluoride solubility-limiting phase in most crystalline groundwaters, the speciation-solubility calculations presented here are focussed on this mineral.

As displayed in Figure 4-15, the vast majority of the SFR and PLU groundwaters are in equilibrium with respect to this mineral within the uncertainty range accepted for the saturation index, which is ± 0.53 SI units (Nordstrom and Jenne 1977, Hem 1985) and the same observation stands for the Laxemar groundwaters (Gimeno et al. 2009). This situation is especially clear for the old, isolated, glacial derived groundwaters from borehole KFR101, whose fluoride contents remained very stable during the 5-month sampling as well as their associated saturation states with respect to fluorite. As already described in Section 4.3.2, a similar situation can be deduced with respect to chalcedony equilibrium, consistent with the longer residence time of these waters.

In most of the cases for which undersaturation with respect to fluorite is inferred, the samples correspond to Local Baltic type groundwaters from depths shallower than 100 m (Figure 4-14a, c). This behaviour is consistent with the short residence time of these waters which would prevent them reaching equilibrium with respect to fluorite, and with the expected dilution effect caused by the infiltration of present Baltic Sea waters with low fluoride contents.

4.4.3 Conclusions

The narrow concentration ranges and the lack of correlation with chloride concentrations observed for the fluoride contents in the SFR groundwaters are indicative of the existence of a “*mineral solubility control*”.

According to speciation-solubility calculations, most of the analysed groundwaters at the SFR are equilibrated with respect to fluorite and a similar behaviour can be observed in the PLU and Laxemar groundwaters. This behaviour is especially clear for the groundwaters with longer residence times, which have remained isolated from present or past marine intrusion events. It is noteworthy that this fluoride solubility control superimposes onto the control that calcite exerts on dissolved calcium, giving rise to a relationship between pH, alkalinity, calcium contents and fluoride contents.

In the cases for which undersaturation with respect to fluorite has been obtained, they correspond mostly to shallow groundwaters affected by the dilution effect associated with the intrusion of present Baltic Sea waters with very low fluoride contents. Moreover, the short residence time of these shallow groundwaters would have prevented their reequilibration with respect to fluoride minerals.

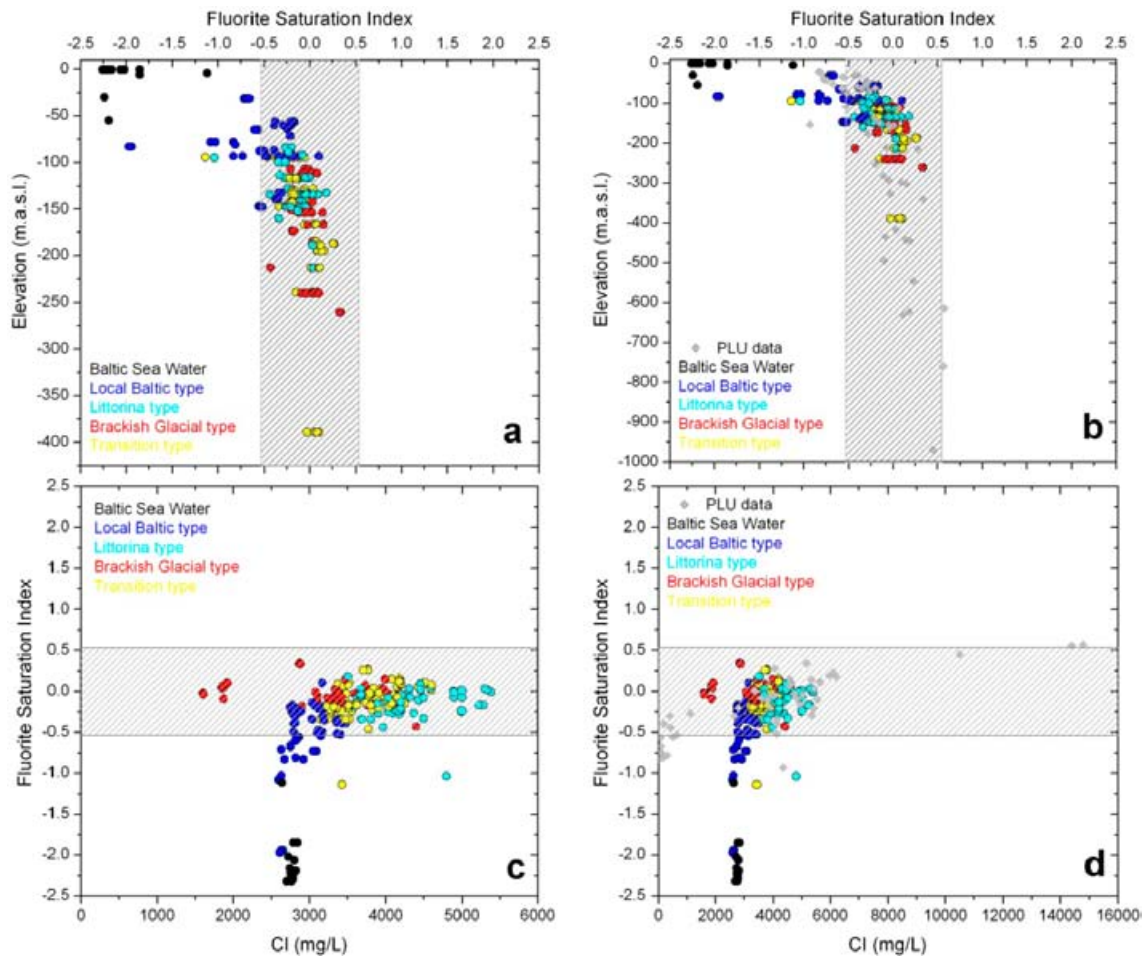


Figure 4-15. Fluorite saturation indices vs. depth (a, b) and chloride contents (c, d) in the SFR groundwaters colour by water types. The diagrams to the left (a and c) show the SFR data and where the scales are restricted to those relevant to the SFR extension data. The diagrams to the right show these data integrated in the general distribution of the PLU data (Forsmark). Note the change in scales in the graphs to the right. Rastered areas correspond to the uncertainty range (± 0.53 units) associated with the fluorite saturation index calculations.

5 Redox geochemical systems

The understanding of redox systems, especially in crystalline rock environments, is one of the most complicated items in hydrogeochemistry and, therefore, the only way to deal with them is to know, understand, interpret and integrate all the related information (hydrochemical, mineralogical and microbiological) as a whole. This type of integration has been extremely useful for the identification of the main flaws and problems during the study of effective redox processes in the target sites during the Site Characterisation Programmes (Gimeno et al. 2008, 2009).

This section integrates the results obtained from the potentiometrical Eh measurements, the redox pair calculations, the speciation-solubility calculations and the microbiological analysis to identify the main controls of the redox state in the SFR groundwaters.

5.1 Selection of redox data

The available redox data include total Fe, Fe(II), S(-II), Mn, N(III), N(V), N(-III) and U concentrations in the groundwaters. Other types of redox data such as potentiometric Eh measurements, dissolved hydrogen and methane contents or microbiological analyses, are still scarce.

Twelve potentiometric Eh values are available from logs of on-line Eh measurements for seven different borehole sections (see Appendix 4). Gas analyses are presently available for seven sections (KFR01 at 44.5–62.3 m.b.l.⁹, KFR10 at 0.0–107.28 m.b.l. KFR7A at 48.0–74.4 m.b.l. KFR08 at 62.9–104 m.b.l. KFR19 at 95.6–110 m.b.l. and KFR105 at 120–137 and 265–306.5 m.b.l.). Molecular hydrogen contents are below the detection limit except in samples taken in the two sections from the KFR105 borehole. Methane concentrations were measured with duplicate analysis in all the aforementioned sections except in sections from KFR105 where only single analyses are available.

Comprehensive microbiological data (comprising determinations of total number of cells, concentration of ATP, number of cultivable, heterotrophic aerobic bacteria and most probable number of cultivable metabolic groups, i.e. iron, manganese, sulphate and nitrate reducing bacteria, as well as acetogens and methanogens) are available only from two sections in the borehole drilled from the SFR tunnel system (KFR105). For other sections (KFR01 at 44.5–62.3 m.b.l. KFR10 at 0.0–107.28 m.b.l. KFR7A at 48.0–74.4 m.b.l.) only data on the total number of cells are available.

As stated in previous sections, the mineralogical information for the SFR area is less complete than for the PLU or Laxemar-Simpervarp areas. However, some information about key redox minerals in the water conducting fractures can be obtained from the Boremap mapping activities in the SFR zone (Döse et al. 2009a, b, Winell 2009, Winell et al. 2009a, b) and from the preliminary results obtained by Sandström and Tullborg (2011).

Therefore, with these limitations in mind, the interpretation of the redox data and parameters available for the SFR based on the framework of the general results for the PLU area seems to be the most appropriate approach.

5.1.1 Selection of representative Eh and pH values

The selection of the representative pH and Eh values for each specific borehole section from the SFR area has been based on a careful analysis of the data delivered by SICADA and those available in the methodological P-reports. The detailed selection procedure, similar to that used in the Site Characterisation Programmes from the PLU and Laxemar-Simpevarp areas (Gimeno et al. 2008, 2009), is described in Appendix 4.

⁹Metres along the borehole length; this is used when describing or referring to the borehole sections. When talking about depths, the elevation of the middle of the section is indicated as metres above sea level (m.a.s.l.).

Chemmac equipment was used for the continuous Eh (and pH) logging in the SFR. The measurements were performed at the SFR facility, where the outlet in the tunnel from each borehole section was connected directly to the Chemmac measurement cell. Pumping was not required since the groundwater was discharged by natural over-pressure (Nilsson 2009).

Twelve Eh (and pH) logs, corresponding to seven borehole sections, are available. Potentiometric Eh measurements were conducted in three of the early SFR boreholes (KFR01 at 44.5–62.3 m.b.l. KFR7A at 48.0–74.7 m.b.l. and KFR10 at 87.0–107.28 m.b.l.) in 1986–87 and repeated in the same three borehole sections in 2000 (Nilsson 2009). Additionally, six recent potentiometric Eh measurements were conducted in two sections from KFR105 borehole (120–130 and 265–306.8 m.b.l.), drilled from the SFR construction tunnel within the SFR extension project (Lindquist and Nilsson 2010. Nilsson et al. 2010), and in sections from boreholes KFR08 (63–104 m.b.l.), KFR19 (95 to 110 m.b.l.) and KFR07 (48–74.7 m.b.l.).

In the data review, only one dubious Eh result was detected (see Appendix 4). The other eleven retained Eh values agree very well with the recommended values in the specific P-reports (Nilsson 2009, Lindquist and Nilsson 2010).

5.1.2 Selection of samples for redox modelling

The quality assurance of the hydrochemical data (including redox data) and the selection criteria of groundwater samples in the available hydrochemical database for the SFR site are detailed in Nilsson (2009) and Nilsson et al. (2010). Problems affecting some of the selected redox data, and especially the dissolved sulphide, whose mere presence allows the characterisation of a specific redox environment, were identified in these works:

- Sulphide analyses were not performed regularly in the early SFR boreholes although there are some data from a few selected borehole sections dating from 1986, 2000 and 2006. The recent sampling programme in the SFR extension boreholes has included sulphide analyses. However, the number of dissolved sulphide analyses is scarce for the spatial dimensions of the studied system.
- Most of the available sulphide data are difficult to evaluate due to uncertainties related to sampling conditions (see Nilsson et al. 2010), as it may also occur in the Site Characterisation Programmes (Gimeno et al. 2009, Tullborg et al. 2010).
- The groundwater analyses treated in the present report have been carried out during more than twenty years. The analytical methods, detection limits and the performing laboratories have changed several times during this time period. In most cases, this situation does not represent an important problem (see the discussion in Nilsson et al. 2010). However, this is not the case of dissolved sulphide, for which several different detection limits have been reported in the SICADA database (e.g. 0.01 and 0.006 mg/L).

The available dissolved sulphide data above the reporting detection limit ($0.03 \text{ mg/L} \approx 1 \cdot 10^{-3} \text{ mM}$; e.g. Nilsson 2009) used in the Site Characterisation Programmes (Gimeno et al. 2008, 2009) have also been used in this present study.

Finally, as stated in Section 4.1, most of the available pH data were measured in laboratory and this situation may represent a serious uncertainty in redox pair modelling and speciation-solubility calculations for the redox systems. Selecting samples with available *in situ* pH values (as it is usually done in the Site Characterisation Programmes (Gimeno et al. 2008, 2009) would result in an extremely reduced set of samples to deal with the redox systems. Thus, samples with both field and laboratory pH values have been selected and, in the cases where pH and Eh values were obtained with Chemmac probe, they have been used for all the samples corresponding to the same section and sampling date. However, in order to check the uncertainty associated with the pH values, redox pair modelling and speciation solubility calculations have been performed both with the measured and with the calculated pH values (in equilibrium with calcite), identical to that done for the carbonate system (Appendix 3).

Thus, with these cautions in mind, all samples with available redox data were selected, including Eh and pH data from continuous logging, analytical data for Fe(II), S(-II), Mn and CH_4 , and microbiological information.

5.2 Redox potentials

The available potentiometric Eh data and the potentials deduced using different redox couples are presented and discussed in this section. The relation between different types of redox potentials is also evaluated and some inferences on the redox conditions (and on their associated uncertainties) are presented.

5.2.1 Potentiometric Eh measurements

As stated in Section 5.1, twelve Eh logs in seven borehole sections from depths between 94 and 154 m from the SFR are presently available. The selected Eh values for these sections (see Appendix 4) are presented in Table 5-1. Six of the twelve revised Eh values show a mildly reducing character whereas the rest indicate slightly oxidising conditions. The sections with reducing values correspond to Littorina and Baltic type groundwaters except the one with the most reducing value (−190 mV), which is a Brackish-glacial type groundwater from the KFR105 borehole at the deepest section (154 m depth). These reducing values are in line with the measured Eh values from the PLU investigation and, mainly, with those of Littorina type brackish marine waters (Figure 5-1), but they are higher than the Eh values found at the Laxemar-Simpevarp area (between −200 and −310 mV).

Oxidising Eh values, similar to those measured in the SFR, have been neither reported in the PLU nor in the Laxemar-Simpevarp groundwaters. These oxidising values do not show a homogeneous trend with the rest of the time series measurements; Eh measured in KFR01 shifts from initially reducing values to oxidant values, while in KFR105 (section 265.0 to 306.8 m.b.l.) the opposite has been found. Eh measured in KFR7A changes from reducing to oxidising to again reducing conditions with time (Table 5-1).

Oxygen diffusion into the tubes connecting the borehole outlet and the measurement cell (e.g. due to long tubing or to a poor choice of tubing material) cannot be entirely discarded for the Eh measurements carried out in 1986–1987 and 2000 (Nilsson 2009) and this might be an explanation for the oxidising values obtained during those campaigns. Unfortunately, there are no dissolved oxygen data for these measurement periods. However, during the more recent measurements performed in 2009, oxidising values were also obtained in the KFR105 borehole despite the fact that dissolved oxygen was below detection limit. Thus, these oxidising values may, alternatively, be representative of the true groundwater situation at the measurement time. Several possibilities exist to explain them.

The KFR01 section (with a value of −140 mV in 1986 and +110 mV in 2000) is associated with the Southern Boundary Belt, intersecting the large vertical Singö deformation zone (ZFMWNW0001) and representing a transition from Littorina type to Baltic type groundwaters. The KFR7A and KRF10 sections (the first one showing two shifts from reducing to oxidising and again reducing conditions, and the second one just oxidising) are related to the Northern Boundary Belt and to the gently dipping, subhorizontal zone ZFM871 (formerly H2) and other major highly transmissive vertical zones (ZFMNNE869 and ZFMNW0805A, formerly Zone 3 and Zone 8, respectively) intersecting or in close vicinity to the deposition tunnels. The presence of the SFR tunnel system has enhanced the importance of those zones as downward transport paths for modern Baltic Sea water.

Table 5-1. Selected Eh values (mV) for the borehole sections in the SFR where the SKB methodology (Chemmac) has been used. The value measured during 1986–87 in KFR10 at −87.0 to −107.28 m.a.s.l. does not perfectly fulfill the criteria indicated in Appendix 4 but it has been included for discussion purposes.

	KFR01 (44.5–62.3 m.b.l.)	KFR7A (48.0–74.7 m.b.l.)	KFR10 (87–107.28 m.b.l.)	KFR105 (120–137 m.b.l.)	KFR105 (265 – 306.8 m.b.l.)	KFR08 (63–104 m.b.l.)	KFR19 (95–110 m.b.l.)
1986–87	−140.0	−180.0	+60.0				
2000	+110.0	+30.0	+70				
2009				+40.0	+50.0		
2010		−150.0			−190.0	−157.0	−165.0

Groundwaters in the KFR7A and KRF10 sections still retain their Littorina signatures but their initial character has changed due to the intrusion of present Baltic Sea water. For instance, an increment in the tritium contents and a general “dilution” of all the dissolved components, including redox sensitive elements like Fe or Mn, are apparent between the 1986–87 and the 2000 samples in the KFR105 borehole or between the 1986–87 and the 2010 samples in the KFR7A borehole.

Sections in boreholes KFR08 and KFR19 (both with reducing Eh values) are also associated with the Northern Boundary Belt and are related to a major deformation zone (ZFMNW0805A, formerly Zone 8) and to the bedrock between zones, respectively. Groundwaters at these sections were, even at the beginning of the monitoring, clearly Local Baltic type and they probably represent a major flow path for the presently intruding Baltic Sea waters.

The KFR105 sections (with oxidising and reducing values) pass through Zones ZFMENE3115, ZFMENE3112 and ZFMENE3137. At section 120–134 m.b.l. (with an oxidising Eh value), the present Transition type groundwaters showed a dilution effect and an increment in the tritium contents during the measurement period. However, at section 265.0–306.8 m.b.l. (with oxidising and then reducing values) the composition of the Brackish-glacial groundwater type present there was fairly stable during the measurement periods in 2009 and 2010, with tritium very low or below the detection limit, but iron contents clearly increasing during these measurement campaigns and Eh values shifting from oxidising to reducing (Table 5-1).

Thus, the observed oxidising conditions could be related to the intrusion of modern Baltic Sea waters through favourable fracture or deformation zones, which could have been promoted by the drawdown and altered hydraulic conditions caused by the repository. However, sections with a clear influence of Baltic type groundwaters (KFR08 and KFR19) provide reducing values and borehole sections without apparent marine influence and stable hydrochemical composition (KFR105 borehole at section 265.0–306.8 m.b.l.) record both oxidising and reducing values. Moreover, most of the Baltic type groundwaters show hydrochemical “anoxic” characters (e.g. with dissolved Fe(II) or S(-II); See Section 5.3.2) which suggest that some other processes may be involved.

The influential effects of the oxygenated environment of the SFR tunnel system during more than 20 years in an otherwise, reducing natural system, could be also responsible for some of the oxidising measured values (e.g. at section 265.0–306.8 m.b.l. in the KFR105 borehole). These possibilities are further discussed in the next section.

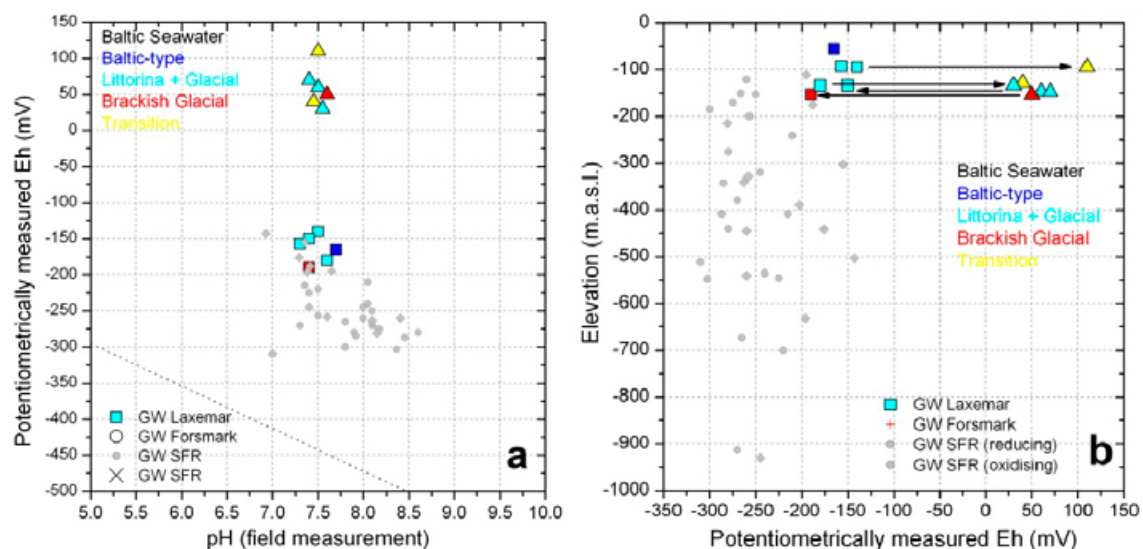


Figure 5-1. Potentiometrically measured Eh values versus pH (a) and depth (b) for the SFR and the PLU and Laxemar groundwaters.

5.2.2 Redox pair calculations

The redox pairs that have been analysed are similar to those addressed in the Site Descriptive Models from Forsmark and Laxemar-Simpevarp, i.e. the dissolved homogeneous $\text{SO}_4^{2-}/\text{HS}^-$ and CO_2/CH_4 redox pairs, and the heterogeneous couples $\text{Fe}^{2+}/\text{Fe}(\text{OH})_3$, $\text{S}_{(\text{c})}/\text{HS}^-$, $\text{SO}_4^{2-}/\text{FeS}_{\text{am}}$, $\text{SO}_4^{2-}/\text{pyrite}$ and $\text{Fe}^{3+}\text{-clay}/\text{Fe}^{2+}\text{-clay}$. These are the most suitable redox pairs to explain the reducing conditions of these groundwaters and in similar systems elsewhere in the Scandinavian Shield (see Gimeno et al. 2008, 2009 and references therein). Also, they include those pairs that can be participating in the control of the potentiometrically measured Eh values (both reducing and oxidising) recorded in the target areas.

The PHREEQC code (Parkhurst and Appelo 1999) and the thermodynamic data included in the WATEQ4F database (Ball and Nordstrom 2001) have been used for the calculations, except in the cases of the heterogeneous pairs $\text{SO}_4^{2-}/\text{FeS}_{\text{am}}$ and $\text{Fe}^{2+}/\text{Fe}(\text{OH})_3$. For the $\text{SO}_4^{2-}/\text{FeS}_{\text{am}}$ pair, a $\log K = -3.0$ for FeS_{am} has been used, as recommended by Chen and Liu (2005) and Gimeno et al. (2006). In the case of the $\text{Fe}^{2+}/\text{Fe}(\text{OH})_3$ pair, three different sets of $\log K$ values have been used for the solid; 1) the set of values proposed by Nordstrom et al. (1990), corresponding to amorphous-microcrystalline hydrous ferric oxides, 2) the value derived from the calibration proposed by Grenthe et al. (1992) for a crystalline phase (such as hematite or goethite), and 3) the value defined by Banwart (1999) using the same methodology as Grenthe et al. (1992) but based on a representative iron phase of intermediate crystallinity.

The redox potential corresponding to the $\text{Fe}^{2+}/\text{Fe}(\text{OH})_3$ heterogeneous redox pair has been obtained in all these calculations using the above equilibrium constants and the Fe(II) activity calculated with PHREEQC. A detailed explanation on the selected solubilities (for the iron oxyhydroxides and $\text{FeS}_{(\text{am})}$) and on the overall methodological approach can be found in Gimeno et al. (2009).

The $\text{Fe}^{3+}\text{-clay}/\text{Fe}^{2+}\text{-clay}$ redox pair was proposed by Banwart (1999) from results obtained in the 'Large-Scale Redox Experiment' carried out at the Äspö HRL. The redox pair is based on the reversible one-electron transfer between oxidised and reduced smectites. For this reaction, the conditional redox potential (Eh, V) as a function of pH at 10°C is defined by the equation:

$$\text{Eh} = 0.280 - 0.056 \text{ pH}. \quad (5-1)$$

From the available analytical determinations in the studied groundwaters, other redox pairs could be considered, such as nitrogen couples (e.g. $\text{NO}_3^-/\text{NO}_2^-$, $\text{NO}_3^-/\text{NH}_4^+$, $\text{NO}_2^-/\text{NH}_4^+$) or manganese redox pairs ($\text{MnO}_2/\text{Mn}^{2+}$). However, the obtained redox potentials with those redox couples are much more oxidant than the measured ones or than those obtained with the aforementioned redox couples¹⁰ (e.g. for the nitrogen redox pairs, calculated redox potential values between +300 to +500 mV are obtained even for clearly reducing conditions). Thus, the values obtained for the nitrogen and manganese redox couples will not be considered in the discussion below.

Redox pairs and potentiometric measured Eh values

Potentiometric Eh measurements can be influenced by both technical and interpretative problems. However, SKB has developed over the last 25 years one of the best available methodologies for the measurement of this parameter (Auqué et al. 2008), and its careful use provides, at the very least, extremely helpful information in understanding something as complex as the redox systems.

The comparison between potentiometrically measured Eh values and those obtained by different redox couples may allow the identification of the redox couples probably involved in the control of measured Eh (e.g. Langmuir 1997, Nordstrom 2005). Moreover, potentiometric Eh values can be used to deduce the type of oxyhydroxide that may control these measured values (oxyhydroxides/ Fe^{2+} are clearly electroactive redox pairs) and this methodology has been successfully used in previous works (e.g. Grenthe et al. 1992, Banwart 1999, Trotignon et al. 2002, Gimeno et al. 2008, 2009). Thus, some deductions on the redox environment can be made based on this information.

In this section, potentiometric Eh values are compared with the results of different redox couples. Reducing and oxidising values are analysed separately, since they may involve control by different possible redox couples.

¹⁰ This wide variation in the potential values obtained by using different redox couples reflects the typical redox disequilibrium repeatedly observed in natural waters (Lindberg and Runnells 1984, Langmuir 1997, Stefánsson et al. 2005) even in those with long residence time (Thorstenson et al. 1979, Thorstenson 1984, Stefánsson et al. 2005).

Reducing potentiometric Eh values measured in the SFR groundwaters are compared with the redox potentials obtained from the different redox couples, using the available pH field measurements (some of them measured with the Chemmac probe) for the groundwater samples (Table 5-2). The Eh values calculated with the Fe²⁺/Fe(OH)₃ redox pair using the equilibrium constant proposed by Grenthe et al. (1992) are too reducing to be consistent with the measured ones. However, the Eh calculated with the same redox pair but using the equilibrium constant for the oxyhydroxide proposed by Banwart (1999) are in agreement with the measured values within the uncertainty range for Eh measurements considered acceptable in the SKB methodology and in the scientific literature, which is around ± 50 mV (SKB 2001, Kölling 2000). The same happens with the Fe³⁺-clay/ Fe²⁺-clay redox couple proposed by the same author (Banwart 1999), which also provides good agreement with the potentiometric Eh values for the three reducing samples (Table 5-2).

Compared with that found during the studies performed in the PLU and Laxemar-Simpevarp Site characterisations, the Fe²⁺/Fe(OH)₃ redox pair (using Banwart's data) also provided similar potentials to the potentiometrically measured Eh in some of these groundwaters (Gimeno et al. 2008, 2009); however, the Fe³⁺-clay/ Fe²⁺-clay redox couple, always gave different values to the potentiometrically measured ones. Thus, the observed agreement between the Fe²⁺/Fe(OH)₃ and the Fe³⁺-clay/ Fe²⁺-clay redox couples in the SFR groundwaters would suggest a closer situation to the one reported for the 'Large-Scale Redox Experiment' carried out at Äspö than to the characterised candidate sites.

Dissolved sulphide was not analysed or was below the reporting limit in most cases for the monitoring sections. Only in the KFR19 borehole was a concentration of 0.03 mg/L analysed and the SO₄²⁻/HS⁻ redox pair provides a potential of -211 mV. Dissolved sulphide concentrations of 0.01 and 0.02 mg/L were determined in the KFR105 and KFR08 boreholes, respectively, i.e. below the accepted reporting limit (0.03 mg/L). However, using these values, the SO₄²⁻/HS⁻ redox pair would provide a potential of -210 and -184 mV, respectively, also in agreement with the potentiometrically measured ones.

Table 5-2. Comparison of the reducing Eh values potentiometrically measured with the Chemmac probe and the Eh values calculated with different redox pairs. For the Fe²⁺/Fe(OH)₃ redox pair, the equilibrium constant for the hematite defined by Grenthe et al. (1992), and the equilibrium constant for the solid phase defined by Banwart (1999), are used.

	Sample #	Measured Eh (mV)	Fe(II) (mg/L)	S(-II) (mg/L)	pH	Fe ³⁺ -clay/ Fe ²⁺ -clay	Fe ²⁺ / Fe(OH) ₃		SO ₄ ²⁻ /HS ⁻
							Banwart (1999)	Grenthe et al. (1992)	
KFR01	1321	-140	0.46	—	7.5	-140	-139	-270	
KFR105	16651	-190	0.76	0.01	7.70	-152	-187	-318	-210
KFR7A (1987)	1334	-181	5.17	bdl	7.58	-145	-212	-343	
KFR7A (2010)	16917	-153	2.55	bdl	7.4	-134	-184.5	-320	
KFR08	16943	-157	1.93	0.02	7.3	-129	-160	-296	-184
KFR19	16937	-167	0.932	0.03	7.7	-151	-213	-349	-211

Table 5-3. Selected Eh values for the examined Chemmac logs in different boreholes and sections and results of the Fe²⁺/Fe(OH)₃ redox pair considering an amorphous and a microcrystalline phase. Redox pair results using both measured pH and pH calculated in equilibrium with calcite are shown also.

	Sample #	Measured Eh (mV)	With measured pH		With calculated pH	
			Fe ²⁺ /Fe(OH) ₃	Fe ²⁺ /Fe(OH) ₃	Fe ²⁺ /Fe(OH) ₃	Fe ²⁺ /Fe(OH) ₃
			3 microcrystalline	3 amorphous	3 microcrystalline	3 amorphous
KFR01	1987	-140	-37	+77	+16	+130
44.5–62.3	2000	+110	-30 to -54	+60 to +84	+4 to +13	+118 to +126
KFR7A	1987	-180	-109	+5	-32	+82
48.0 –74.7	2000	+30	-87 to -125	-11 to -27	-29 to -33	+81 to +85
KFR10	1986	+60	-28 to -99	+15 to +86	-29 to -34	+80 to +87
87.0–107.3	2000	+70	-28 to -69	+45 to +86	-17 to -21	+93 to +97

For the oxidising values potentiometrically measured in some of the analysed sections, redox pair calculations would seem to support a control by amorphous Fe(III)-oxyhydroxides (Table 5-3). The potentiometric value obtained for the $\text{Fe}^{2+}/\text{Fe}(\text{OH})_3$ redox pair using the equilibrium constant for a microcrystalline phase or for the phases proposed by Grenthe et al. (1992) and Banwart (1999), provide too low (more reducing) values, as also indicated for the $\text{Fe}^{3+}\text{-clay}/\text{Fe}^{2+}\text{-clay}$ redox couple (Table 5-2).

The possible control by an amorphous Fe(III)-oxyhydroxide would imply the existence of present or very recent oxic environments associated with the studied sections. Oxygen intrusion in reducing media usually induces the precipitation of amorphous Fe(III)-oxyhydroxides (ferrihydrite or hydrous ferric oxides, Langmuir 1997). This is not affected by the pH uncertainties (Table 5-3) and it would support the reliability of the oxidising Eh measurement; the $\text{Fe}^{2+}/\text{Fe}(\text{OH})_3$ heterogeneous redox pair is the most clearly electroactive (specially with amorphous phases) and, therefore, one of the most feasible to control the Eh measurements in natural systems (see Gimeno et al. 2008, 2009 and references therein). In this context, the key point is to identify and explain the possible oxygen source:

- Contamination problems during the Eh measurements cannot be excluded and this could be an explanation for the apparent existence of oxic environments in the SFR groundwaters.
- Oxidising conditions could also be related to the intrusion of modern oxygenated Baltic Sea waters through favourable fracture or deformation zones. The rapid penetration of oxidising Baltic waters is feasible especially in sections associated with the Northern Boundary Belt, where marine sediments in the seabed above the SFR are virtually absent, providing local hydraulic connections between the seawater and the fracture network in the bedrock (Nilsson et al. 2011, Öhnman et al. 2011). In this situation, the amount of fine-grained organic debris, which could favour the development of a reducing environment, would also be very small. However, the most recent measurements performed in preferential “Local Baltic type” groundwater paths (KFR08 and KFR19 boreholes in sections associated with the Southern Boundary Belt) indicate that this type of “recent” marine groundwater is anoxic and clearly reducing. Oxygen consumption in saturated soils and sediments is well documented (e.g. Drew 1983, Silver et al. 1999, Pedersen 2006) and the Äspö Redox Zone experiment (Banwart 1999, Molinero-Huguet et al. 2004) also showed that microbial respiration, in the upper metres of a fracture zone, effectively consumes the oxygen in infiltrating waters.
- Oxidising values controlled by the precipitation of amorphous Fe(III)-oxyhydroxides can also be related to the influence of the oxic environment created by the presence of the SFR tunnels. In fact, the precipitation of these minerals was also observed in the Äspö Underground Laboratory when reducing groundwaters were put in contact with the oxygen-rich atmosphere of the tunnel. Moreover, it was found that microbes (e.g. *Gallionella ferruginea*, an iron-oxidising chemolithotrophic microbe species adapted to low oxygen conditions) may catalyse the formation of iron oxides from dissolved ferrous iron in groundwaters reaching an oxidising environment. The formation of these *bacteriogenic iron oxides* (BIOS), constituted by ferrihydrite (Ferris et al. 1999, Martínez et al. 2004), was significant for groundwaters with dissolved oxygen concentrations between 0.3 mg/L and 1.5 mg/L, pH between 7.4 and 7.7 and Eh values above approximately +100 mV (Anderson and Pedersen 2003, Anderson et al. 2006, Laaksoharju et al. 2009b). These ranges are very similar to the ones found in the SFR groundwaters with oxidising potentials. Thus, these types of “alterations” in the monitored sections could justify the measurement of stable oxidising values during the measurement periods and would highlight the need for extended pumping and measurement periods in order to obtain Eh values corresponding to pristine and undisturbed conditions.

Redox pairs and overall redox conditions at the SFR

The advantage of using Eh values derived from a redox pair is that tentative Eh values, for samples without potentiometrically measured Eh data, can be obtained. Moreover, redox potentials calculated from redox couples are usually considered the only way to approach meaningful Eh values in natural waters (Thorstenson 1984, Nordstrom and Munoz 1986, Langmuir 1997, Drever 1997, Nordstrom 2005 etc).

Thus, as the available Eh measurements for the SFR are still scarce, redox potentials from the redox couples have been calculated for the whole set of groundwater samples with suitable data. The selected redox couples are those of sulphur and iron (including the $\text{Fe}^{2+}/\text{Fe}(\text{OH})_3$ and $\text{Fe}^{3+}\text{-clay}/\text{Fe}^{2+}\text{-clay}$ redox pairs), which have provided meaningful results in this and in previous studies. Calculations have been performed with both the measured and the calculated pH values (in equilibrium with calcite) and the results are presented in Figure 5-2.

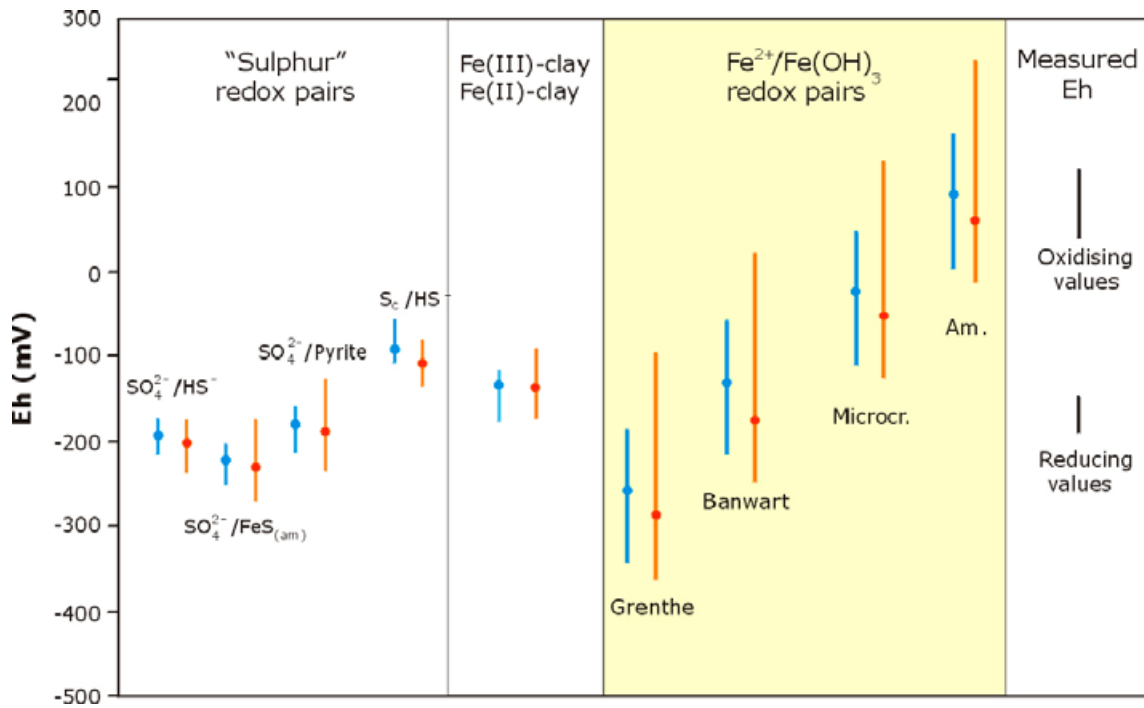


Figure 5-2. Eh values calculated from different redox couples for the whole suitable set of SFR groundwaters, compared with the potentiometrically measured Eh values. Red lines represent the range of values obtained with the measured pH and blue lines the range of Eh values obtained with the calculated pH. Circles represent the mean value for each case.

Sulphur redox pairs would provide reducing values for the SFR groundwaters. Values from the $\text{SO}_4^{2-}/\text{HS}^-$ and $\text{SO}_4^{2-}/\text{FeS}_{\text{am}}$ redox couples, which have generally shown a good agreement with the potentiometrically measured Eh values in the Site Characterisation Programmes (Gimeno et al. 2008, 2009), would be around -200 mV. The $\text{Fe}^{3+}\text{-clay}/\text{Fe}^{2+}\text{-clay}$ redox pair would lead to less reducing values (mean around -120 mV).

From the limited data available of methane (four samples) values for the CO_2/CH_4 redox pair can be obtained. Redox potential results for this pair are very similar to those obtained with the sulphur couples (from -208 to -233 mV) even taking into account the possible impact of pH uncertainty on the calculated values (11 mV of Eh uncertainty in the worst case). A similar agreement has also been reported for the PLU and the Laxemar-Simpevarp groundwaters.

The redox potential defined by the $\text{Fe}^{2+}/\text{Fe}(\text{OH})_3$ heterogeneous redox pair depends on the mineral phase characters (solubility, particle size, etc.) of the specific ferric oxyhydroxide included in the calculations. For a crystalline Fe(III)-oxyhydroxide (i.e. hematites, frequently found in the fracture fillings of the SFR), the results obtained using the Grenthe's solubility value are between -100 and -350 mV. Results using the Banwart's solubility value provide less reducing values, but usually lower than 0 mV.

Only the calculations considering microcrystalline or amorphous phases, representative of oxic or post-oxic environments, provide oxidising values (Table 5-3 and Figure 5-4).

Overall, most of the selected redox pairs suggest the existence of reducing Eh values for the SFR groundwaters. For sulphidic and methanic groundwaters, Eh values between -200 and -220 mV could be proposed. For the rest, values below -100 mV could be feasible. Finally, in agreement with the results in the previous section, oxidising Eh values controlled by an amorphous or microcrystalline Fe(III)-oxyhydroxide could be obtained if oxygen intrusion existed.

5.2.3 Conclusions

The potentiometric Eh measurements in the SFR groundwaters provide oxidising and reducing values. Reducing values (from -140 to -190 mV) are in line with those measured in the PLU groundwaters. They are apparently controlled by the occurrence of an iron phase of intermediate crystallinity and/or by ferrous clay minerals. The coincidence in the results of the $\text{Fe}^{2+}/\text{Fe}(\text{OH})_3$ and the $\text{Fe}^{3+}\text{-clay}/\text{Fe}^{2+}\text{-clay}$ redox pairs would be similar to that observed in the 'Large-Scale Redox Experiment' (Banwart 1999), where the effects of the intrusion of meteoric waters in the Äspö tunnels were studied.

Moreover, mineralogical studies at the SFR indicate that mixed layer clays (poorly ordered smectite-illite) are the most abundant minerals in the fracture fillings from water conducting fractures. Also, the presence of hematite and other unclassified iron oxyhydroxides has been identified at almost all examined depths (Sandström and Tullborg 2011). These observations would probably support the good results obtained with the $\text{Fe}^{2+}/\text{Fe}(\text{OH})_3$ and the $\text{Fe}^{3+}\text{-clay}/\text{Fe}^{2+}\text{-clay}$ redox pairs. However, more data are needed on these mineral phases and, especially, on the type and particle size (crystallinity) of the iron oxyhydroxides (see also Section 5.3.2).

The measured oxidising Eh values in the SFR groundwaters (from $+30$ to $+110$ mV) appear to be controlled by amorphous Fe(III)-oxyhydroxides. They would represent the existence of present or very recent oxic environments, since these phases quickly recrystallise to less soluble and more stable phases under reducing conditions. The chemical character (e.g. pH and Eh values) of these groundwaters is very similar to that observed in the Äspö Underground Laboratory when reducing groundwaters were put in contact with the oxygen-rich atmosphere of the tunnel and microbes were observed to catalyse the formation of amorphous Fe(III)-oxyhydroxides.

Thus, these oxidising conditions would be representative of the groundwater situation close to the oxic environment in the tunnels and they would change towards more reducing ones in the case of pumping. Furthermore, the gradual removal of the groundwater from the tunnel section and the progressive input of pristine formation water may have caused a disequilibrium and the observed long stabilisation periods towards reducing conditions (see Appendix 4). The results in the more recent measurements performed in the KFR19 and KFR7A boreholes, also displaying long stabilisation periods, would support this interpretation. The Eh calculation results for the suitable redox pairs in the SFR groundwaters point also towards the existence of overall reducing conditions (below -100 mV), especially in the case of sulphidic and methanic groundwaters (below -200 mV).

5.3 Sulphur and iron systems

Iron and sulphur represent two very important systems for the understanding of the redox processes in groundwaters of crystalline rocks similar to those studied in the Swedish programme for the geological disposal of spent nuclear fuel (e.g. Nordstrom and Puigdomenech 1986, Grenthe et al. 1992, Banwart 1999, Trotignon et al. 2002, Gimeno et al. 2008, 2009).

The evolution and behaviour of these elements are frequently linked to bacterial activity. Typical bacterial activities, represented by iron reducing bacteria (IRB) and sulphate reducing bacteria (SRB), are common sources of dissolved Fe(II) and S(-II). Both microbial groups have been identified in the PLU and Laxemar-Simpevarp groundwater systems (Hallbeck and Pedersen 2008 a, b) and their presence could either be mutually exclusive (dominance of one of the metabolic activities and, thus, of one of the redox systems, as it occurs in the classic sequence of redox zones; e.g. Langmuir 1997, Appelo and Postma 2005) or be effective at the same time (see Gimeno et al. 2009 for further discussion).

Moreover, iron and sulphur systems may also be interrelated through inorganic processes, such as sulphide precipitation and reductive dissolution of ferric oxyhydroxides by hydrogen sulphide (Canfield 1989, Canfield et al. 1992, Poulton et al. 2004), which may exert an important control on the dissolved Fe(II) and S(-II) contents.

In this section, both redox systems are evaluated together and the possible sources of dissolved iron and sulphur are discussed. With these aims, speciation-solubility calculations have been performed with the PHREEQC code (Parkhurst and Appelo 1999) and the WATEQ4F database (Ball and Nordstrom 2001) with the modifications presented in Gimeno et al. (2009) to identify some other effective processes controlling dissolved iron and sulphide concentrations.

Saturation indices have been calculated for siderite, amorphous Fe(II)-monosulphide¹¹ and mackinawite, phases whose control on Fe(II) and S(II) has been identified in the studied systems (e.g. Gimeno et al. 2009) and in other groundwater systems (e.g. Chen and Liu 2005, Jakobsen and Cold 2007). A detailed description of the thermodynamic data used for these phases can be found in Gimeno et al. (2009, Appendix C). An uncertainty range of 5% of the log K value (Deutsch 1997) has been fixed for siderite, which is ± 0.55 ¹². The uncertainty range considered for ferrous iron monosulphides (FeS_(am) and mackinawite) has been given as ± 0.36 , as recommended by Gimeno et al. (2006).

5.3.1 Hydrochemical trends

Dissolved iron and sulphide contents in the SFR groundwaters show patterns with respect to depth and chloride contents very similar to those observed in the PLU groundwaters. Fe(II) contents are always above the detection limit, ranging between 0.25 and 7.5 mg/L ($4.5 \cdot 10^{-3}$ and 0.13 mmol/L) for groundwaters at depths between 100 and 150 m (Figure 5-3a), as also observed for the analogous PLU groundwaters (Figure 5-3b). The highest and more variable dissolved Fe(II) contents appear in Littorina type groundwaters with chloride contents between 3,500 and 5,000 mg/l (Figure 5-3c), as also reported for the PLU groundwaters (Figure 5-3d). Dissolved Fe(II) contents in Local Baltic type groundwaters are lower (between 0.25 and 4.5 mg/L; $4.5 \cdot 10^{-3}$ and 0.08 mmol/L).

Dissolved sulphide contents range between 0.03 and 2.2 mg/L ($9.4 \cdot 10^{-4}$ and 0.069 mmol/L), being mostly below 0.5 mg/L (0.016 mmol/L) and very frequently even below detection (0.01 or 0.006 mg/L – $3.1 \cdot 10^{-4}$ or $1.9 \cdot 10^{-4}$ mmol/L-, depending on the date of the analysis) or reporting limits (0.03 mg/L or $9.4 \cdot 10^{-4}$) in SICADA. The values corresponding to these limits, 0.006 and 0.03 mg/L are indicated in the plots as dashed lines. Unless otherwise expressed, calculations and interpretations have always considered samples with sulphide values above the reporting limit.

The highest S(-II) content is associated with a Littorina type groundwater with chloride concentrations about 5,000 mg/L (Figure 5-4c) at a depth around 100 m, in common with the PLU groundwaters (Figure 5-4d). However, in general, the proportion of sulphidic samples in Littorina type groundwaters (around 16% of all analysed samples of this type) is much lower than in the Brackish-glacial type (45%, including here the hydraulically isolated waters from the KFR101 borehole at section 271.5–341.76 m.b.l.) or in Local Baltic type groundwaters (27%).

Some of the most sulphidic Local Baltic type groundwaters appear in sections with an important or even exclusive contribution of present Baltic Sea waters, to which they are very similar in composition. This could be due to the existence of sulphate reduction processes during the inflow of Baltic Sea waters, either through the marine seabed sediments or along the bedrock fractures receiving recent and continuous input of organic matter associated with the marine intrusion.

Overall, the concentration ranges and distribution of dissolved Fe(II) and S(-II) are very similar to those observed in the PLU groundwaters. Some mixing control or marine inheritance from the Littorina intrusion is apparent for the dissolved Fe(II) contents. On the other hand, the existence of sulphate reducing activity appears to affect most groundwater types from 60 to 240 m depth.

From a hydrostructural point of view, some preliminary remarks on the distribution of S(-II) and Fe(II) concentrations can be made. Groundwaters associated with the Southern Boundary Belt do not show dissolved sulphide concentrations and the iron contents are low and constant (between 0.3 and 0.5 mg/L; 0.01 and 0.016 mmol/L). Groundwaters associated with the rest of the hydrostructural domains, and especially those related to the Northern Boundary Belt, show a wider range and higher concentrations of dissolved Fe(II) and also more samples with a sulphidic character.

¹¹ Under the term “iron mono-sulphides” the amorphous mono-sulphide (FeS(am) or FeS(ppt)), more properly named disordered mackinawite (Wolthers et al. 2003, 2005) or nanocrystalline mackinawite (Rickard 2006, Rickard and Luther 2007), and the ordered or crystalline mackinawite (tetragonal FeS) and greigite (Fe₃S₄), are included. Only amorphous monosulphide and crystalline mackinawite have been considered in this work.

¹² The solubility value of siderite used in the calculations is the one included in the WATQE4F database (Ball and Nordstrom 2001), log K = -10.89. This value is similar to the more recent experimental values proposed by Jensen et al. (2002), from -11.03 ± 0.1 to -10.34 ± 0.15 under anaerobic conditions.

High contents of dissolved iron, and even of dissolved sulphide, are usually related to the Littorina marine intrusion in the PLU groundwaters. Therefore, the differences observed in the Southern Boundary Belt groundwaters could be associated with the presence of a thicker sediment cover in that area, constricting the intrusion of Littorina and Baltic Sea waters. In any case, this will need further study.

5.3.2 Mineralogical data

Mineralogical studies on iron and sulphur minerals provide an important input in the understanding of the geochemical redox evolution in the studied groundwaters. The amount and character of these minerals shed light on those factors influencing not only the present situation, but also the palaeohydrological or future evolution of the redox state.

Iron and sulphur minerals are critical in assessing the inorganic reducing capacity of the bedrock against the intrusion of oxic waters. The study of redoxsensitive iron and/or sulphur minerals, such as pyrite and specially Fe-oxides and Fe-oxyhydroxides (e.g. goethite) can be used, for instance, to trace the redox front position and the depths reached by oxygenated waters (e.g. Drake and Tullborg 2009, Drake et al. 2008, 2009). Moreover, these phases are related to some fundamental metabolic processes such as iron reducing activity (conditioned by the presence of suitable Fe(III)-bearing minerals as the necessary terminal electron acceptors) or sulphate reduction activity (promoting the formation of iron sulphides).

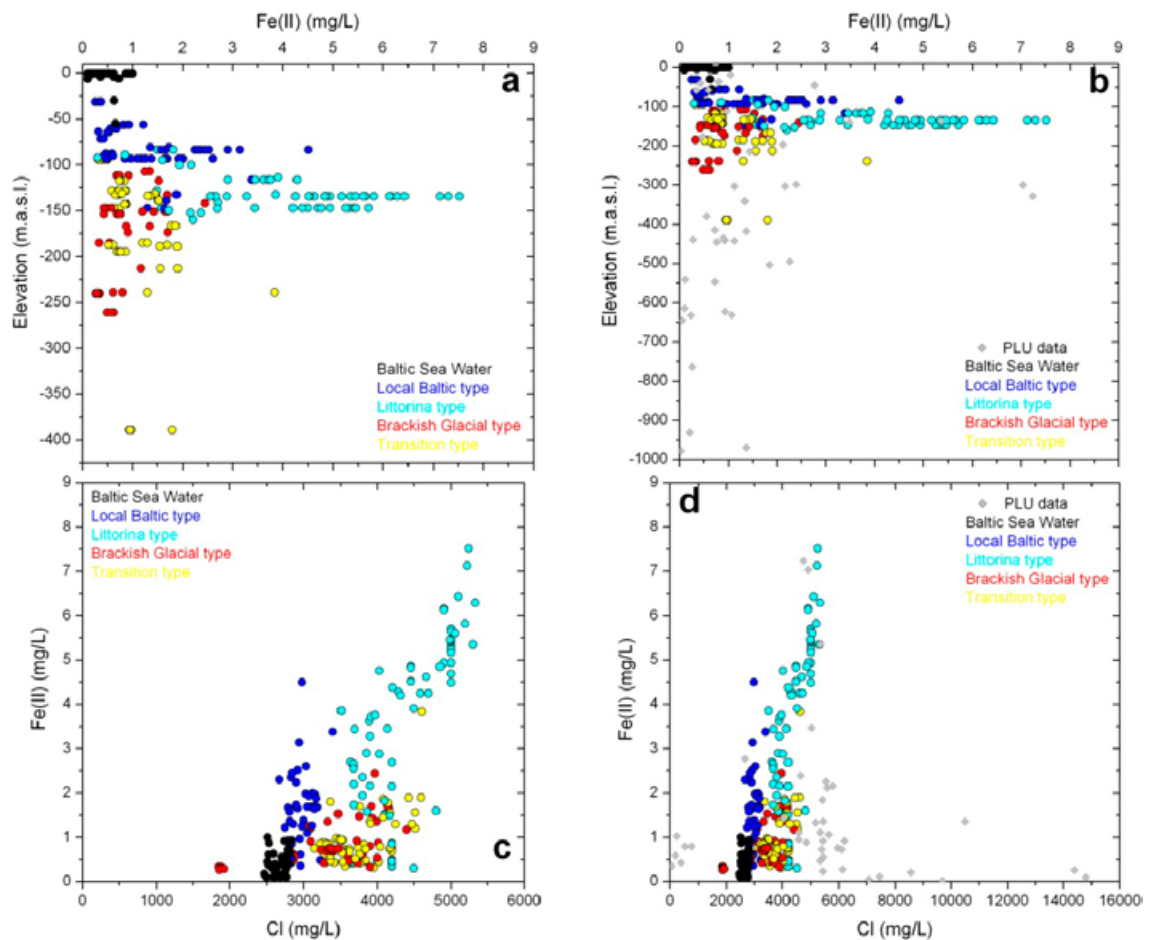


Figure 5-3. Dissolved Fe(II) concentrations versus depth (a, b) and chloride contents (c, d) in the SFR groundwaters colour coded by water types. The diagrams to the left (a and c) show the SFR data where the scales are restricted to those relevant to the SFR extension data. The diagrams to the right show these data integrated in the general distribution of the PLU data (Forsmark). Note the change in scales in the graphs to the right.

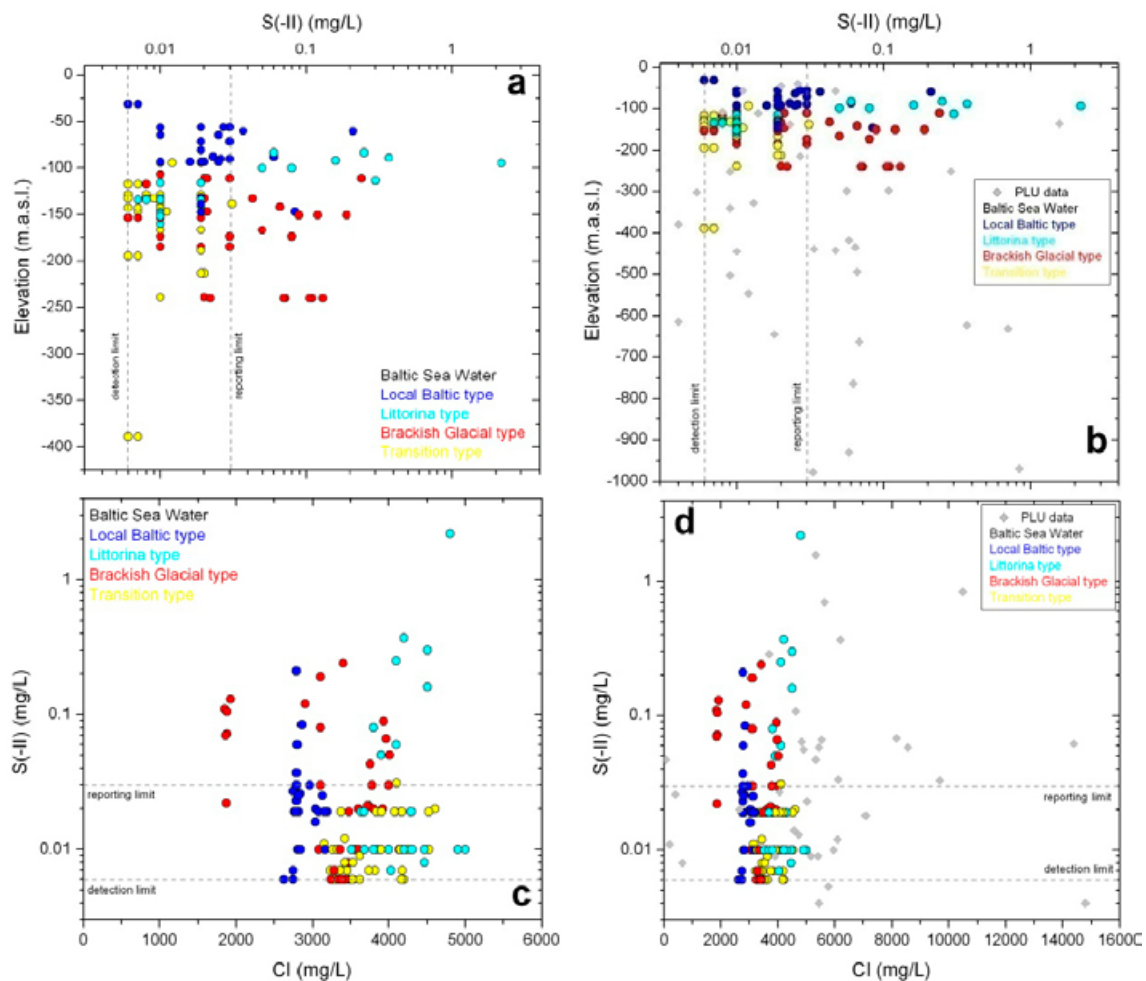


Figure 5-4. Dissolved $S(-II)$ concentrations versus depth (a, b) and chloride contents (c, d) in the SFR groundwaters colour coded by water types. The diagrams to the left (a and c) show the SFR data where the scales are restricted to those relevant to the SFR extension data. The diagrams to the right show these data integrated in the general distribution of the PLU data (Forsmark). Note the change in scales in the graphs to the right.

The performed mineralogical studies indicate the existence of hematite and other unclassified iron oxyhydroxides (probably goethite) at almost all examined depths. Moreover, mixed layer clays (smectite-illite) and chlorites with low Mg/Fe ratios are the most abundant minerals (together with calcite) in the fracture fillings from water conducting fractures (Döse et al. 2009a, b, Winell 2009, Winell et al. 2009a, b, Sandström and Tullborg 2011).

There are still no data on the Fe(II) contents associated with chlorite and clay minerals in the SFR fracture zones and the available data from the Site Characterisation Programmes are very scarce. However, the chlorite analyses performed in the Äspö subarea indicate that Fe(II) represents more than 55% of the total Fe content in all the samples and that the largest inorganic reducing capacity seems to be provided by the Fe(II)-bearing Al-silicates and clay minerals (chlorite, corrensite, smectite, mixed layer clays, illite/smectite; e.g. Drake et al. 2006). Moreover, this inorganic reductive capacity may be enlarged by the presence of iron reducing bacteria because iron oxyhydroxides and Fe(III)-bearing clay minerals may be suitable terminal electron acceptors for iron reducing bacteria (IRB) (Gimeno et al. 2009 and references therein).

Sulphide phases have also been found in the SFR fracture fillings. They occur as pyrite (though the presence of, arsenopyrite, chalcopyrite and galena has been sporadically described; (Winell et al. 2009a; Sandström and Tullborg 2011) which appears unevenly distributed in the open fracture fillings in common with the PLU or in the Laxemar-Simpevarp areas (Sandstrom et al. 2008, Drake and Tullborg 2009, Gimeno et al. 2009). Based on the drillcore mapping, pyrite is only absent in

water conductive fractures in the upper 10 metres, probably having been dissolved during events of intrusion of oxygenated fluids, but the amount of data from the upper part of the bedrock is limited (Sandström and Tullborg 2011). Overall, the presence of pyrite at most depths would indicate prevailing reducing conditions.

However, the presence of iron oxyhydroxides in water conductive zones at depths down to about 500 m.a.s.l. as indicated by the drillcore mapping (Sandstrom and Tullborg 2011), could indicate that oxidising conditions have prevailed, at some period, in some parts of the fracture system. The presence of well-crystalline, low particle size iron oxyhydroxides (e.g. goethite) would indicate the presence of past oxidising events and, by now, they are detected down to ~110 m in the PLU and Laxemar-Simpevarp areas (Dideriksen et al. 2007, 2010). Thus, a better characterisation of these phases is needed as it is also possible that at least some of them are iron oxides (haematite) that can be difficult to distinguish from iron hydroxides by visual inspection (Sandström and Tullborg 2011) and would indicate completely different conditions.

5.3.3 Processes: Thermodynamic approach

With respect to the carbonate system (Section 4.1), two domains can be distinguished in the redox processes evolution of the SFR site; (1) the marine sediments through which present Baltic waters infiltrate, and (2) the deeper bedrock zone. As stated above, significant contents of dissolved Fe(II) and S(-II) in some “pure” Local Baltic type groundwaters would indicate the development of anoxic or reducing environments already during the infiltration of the marine waters through the sediments and/or along the shallow bedrock fractures.

Microbial activity and organic matter decay in marine sediments may lead to complete redox sequences (from oxic to post-oxic, sulphidic and methanic environments) even at centimetre scales (e.g. Berner 1981, Van Cappellen and Wang 1996, Konovalov et al. 2007) and IRB and SRB activities are the main source of Fe(II) and S(-II) in these environments. Dissimilatory IRB can reduce the low crystallinity iron oxyhydroxides using organic matter (e.g. acetate, Equation 5-2) or hydrogen (Equation 5-3) as electron donors:



and sulphate-reducing bacteria can reduce the dissolved SO_4^{2-} through reactions 5-4 and 5-5:



Additionally, sulphate reduction processes can indirectly produce dissolved Fe^{2+} through reaction 5-6:



All these reactions may be involved as sources of dissolved Fe(II) and S(-II) in marine sediments. However, under the increased hydraulic gradient conditions promoted by the presence of the SFR facility, marine waters may penetrate through these sediments or infiltrate directly along the bedrock fractures¹³ too quickly to allow the development of these reactions.

Other redox processes may also influence the Fe (II) and S(-II) contents of the recently infiltrated Baltic waters and of the older groundwaters in the bedrock. For instance, the inorganic or biotically induced reductive dissolution of Fe(III)-oxyhydroxides and Fe-silicates (e.g. Fe^{3+} -bearing clay minerals; Banwart 1999) or the biogenic S(-II) production, may also be effective.

The only two available microbiological data from the SFR suggest the existence of minor amounts (as most probable numbers) of most of the analysed metabolic groups, including IRB and SRB (this

¹³ On the north side of the pier there are areas with no, or only partial, sediment coverage that would represent direct hydraulic connections between the fracture network and the Baltic Sea (Öhman et al. 2011, Nilsson et al. 2011).

last group being below the detection limit despite the detected presence of dissolved S(-II)). This situation is clearly contrary to the one reported for other similar systems. For instance, sulphate reducing bacteria have been found in the PLU and the Laxemar-Simpevarp groundwaters at almost all depths (Hallbeck and Pedersen 2008a, b) and IRB activity appears to be particularly high in the shallower 200 m of the systems studied in the Fennoscandian Shield (Pedersen 2008).

Additional processes can be involved in the control of these components in the SFR groundwaters, such as the equilibrium with respect to iron and sulphur minerals. Speciation-solubility results indicate that most of the Littorina- and Local Baltic type groundwaters are in equilibrium with respect to siderite (Figure 5-5a, c), as also observed in the PLU groundwaters with clear Littorina contributions (Figure 5-5b, d).

In the case of Littorina type groundwaters, this equilibrium situation appears to be mostly inherited from their infiltration stage through the marine sediments and maintained during mixing with the preexisting groundwaters. The “peculiar” vertical trend of the Fe(II) contents versus chloride (Figure 5-3), similar to the one found with respect to other “inherited” components such as Mn or NH_4^+ (Sections 5.4.1 and 5.5.1), would support this interpretation.

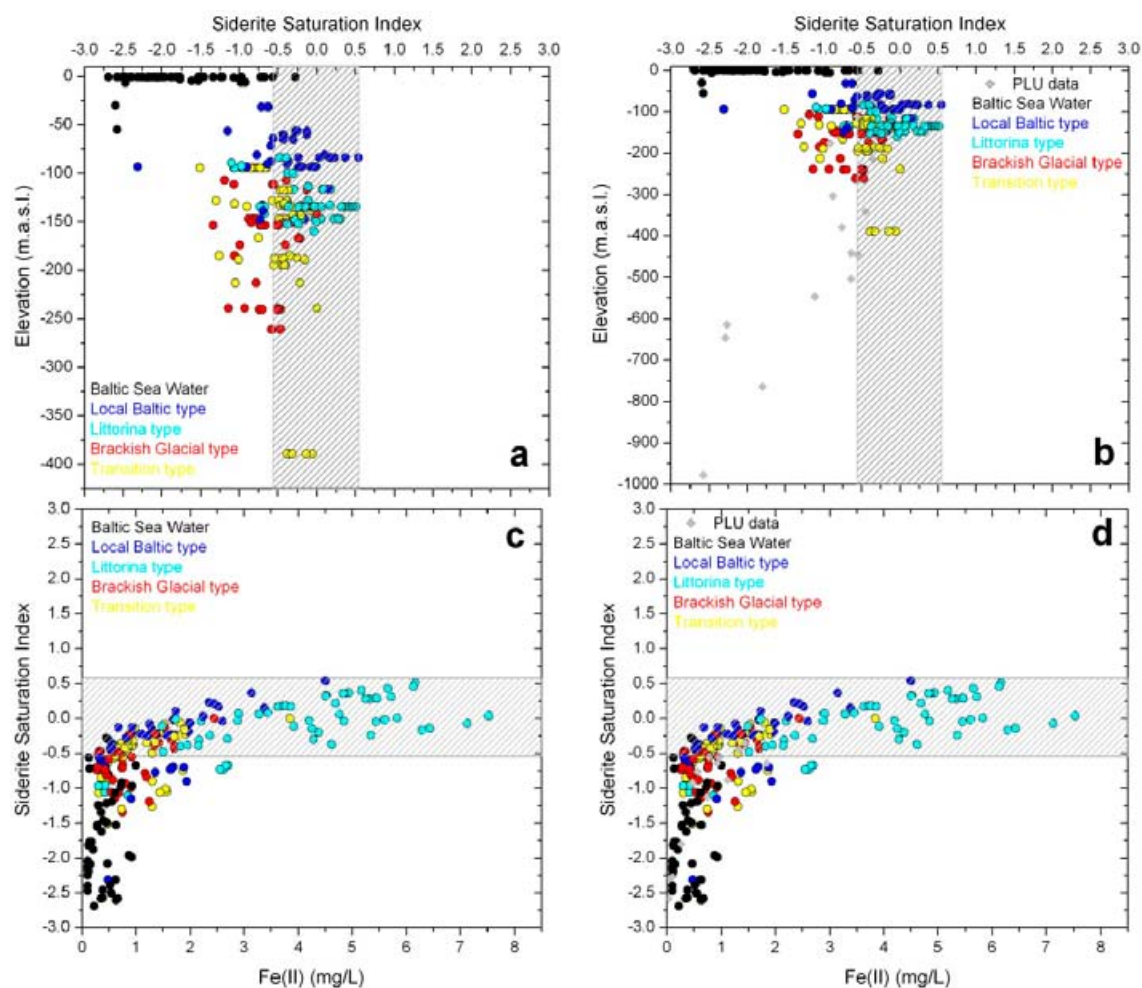


Figure 5-5. Siderite saturation index versus depth (a, b) and chloride contents (c, d) in the SFR groundwaters colour coded by water types. The diagrams to the left (a and c) show the SFR data where the scales are restricted to those relevant to the SFR extension data. The diagrams to the right show these data integrated in the general distribution of the PLU data (Forsmark. Note the change in scales in the graphs to the right. Rastered areas correspond to the uncertainty range (± 0.54 units) associated with the siderite saturation index calculations.

In the case of the Local Baltic type groundwaters, siderite equilibrium may have been attained during their circulation through marine sediments or bedrock materials or even during mixing with preexistent groundwaters with higher dissolved Fe(II) contents. However, the influence of siderite equilibrium on Fe(II) contents still merits further studies¹⁴.

On the contrary, the SFR groundwaters with the clearest glacial signatures, including the less saline groundwaters from the KFR101 borehole at section 271.5–341.76 m.b.l. (with a long term hydraulic isolation), are undersaturated with respect to this mineral. This is consistent with the undersaturation observed in the most saline and deep groundwaters (not affected by marine intrusion) in the PLU and Laxemar systems (Gimeno et al. 2009). Groundwaters associated with the Northern Boundary Belt are undersaturated with respect to siderite, supporting minor influence of past (Littorina) and present (Baltic) intrusions.

Equilibrium situations with respect to amorphous Fe(II)-monosulphides have been reached only in some SFR groundwaters (of Local Baltic, Littorina or Brackish-glacial type; Figure 5-6). These equilibrium situations would indicate the effective and present precipitation of these phases¹⁵ through the reaction:



and the unmistakable presence of microbial sulphate reduction presently active in those groundwaters (Gimeno et al. 2008, 2009 and references therein) is just as scarce as in the PLU groundwaters (Gimeno et al. 2008). Moreover, some of these results are affected by pH uncertainties (see Appendix 3), reducing even more the number of samples in equilibrium with respect to amorphous Fe(II)-monosulphides. More studies are needed in order to decide whether this situation corresponds to the real one or if it is an artefact of sampling conditions (Gimeno et al. 2009, Nilsson et al. 2010, Tullborg et al. 2010).

Most groundwaters are in equilibrium with respect to mackinawite (a crystalline and less soluble iron monosulphide). These situations could correspond either to a low SRB activity, where H₂S production would not be high enough to reach the amorphous monosulphide solubility product (but large enough to reach mackinawite equilibrium) or to the presence of environments with an important SRB activity in the past that is no longer existent but which produced the original amorphous phase that has been recrystallised (Gimeno et al. 2008, 2009).

This might be the case for the long term hydraulically isolated groundwaters from the KFR101 borehole at section 271.5–341.76 m.b.l. which are equilibrated with respect to mackinawite and which display isotopic δ³⁴S values (reaching +37.5‰ CDT) strongly indicative of SRB activity under closed system conditions (see Section 4.2). Most probably, saturation with respect to amorphous monosulphides was reached in this environment due to SRB activity in the past but, once this activity ceased, the amorphous FeS recrystallised quickly to mackinawite¹⁶, affecting the dissolved sulphide contents in the corresponding groundwaters (e.g. Gimeno et al. 2007 and references therein).

In any case, these results must be considered with caution as dissolved sulphide contents may be affected by uncertainties related to the sampling conditions. More data and further studies are needed to clarify the importance of sulphate reduction processes in the SFR groundwaters.

¹⁴ Purely coincidental apparent equilibrium with siderite was described in the ‘Large-Scale Redox Experiment’ carried out at the Äspö HRL (Banwart 1999).

¹⁵ The precipitation kinetics of amorphous iron monosulphides is very fast and their metastability, becoming mackinawite or pyrite in a short time lag, has been demonstrated in the field and in the laboratory. Therefore, the occurrence of this equilibrium indicates a continuous and present supply of H₂S derived from SRB activity. When dissolved Fe(II) (or a source for this component) is also present, waters become oversaturated with respect to the amorphous monosulphides, which quickly precipitate, maintaining the equilibrium in the system. Therefore, the equilibrium observed in the SFR groundwaters could correspond to a present monosulphide precipitation process. See Gimeno et al. (2008, 2009) for a review on this subject.

¹⁶ This recrystallisation starts within a few days and can be completed in two years (Rickard 1995, Wilkin and Barnes 1997). More recent works suggest that the recrystallisation time is even shorter. For instance, the ripening experiments performed by Benning et al. (2000) on amorphous monosulphides indicate that mackinawite transformation occurs in less than three months and waters in contact reach the solubility product of mackinawite.

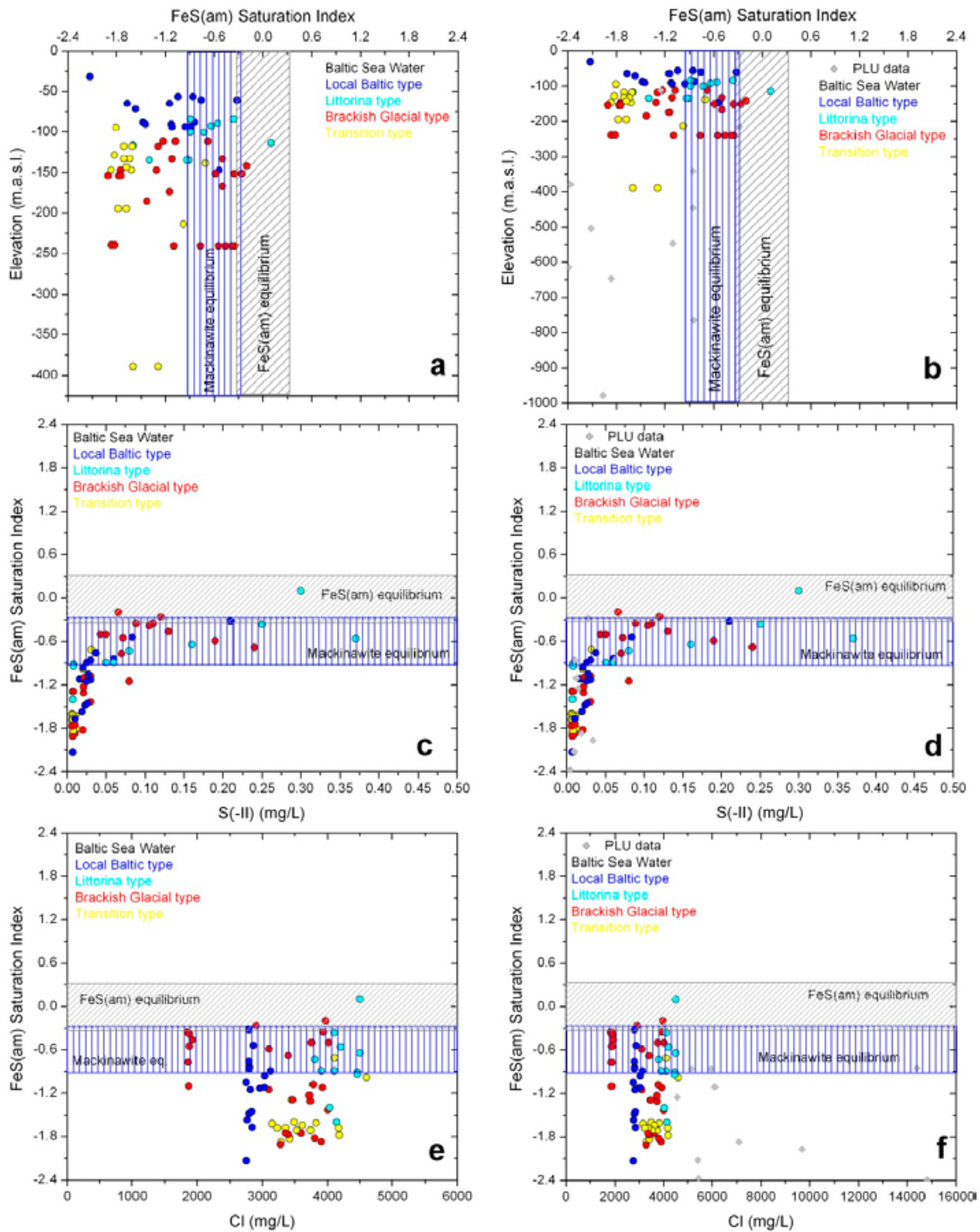


Figure 5-6. Saturation indices for amorphous ferrous iron monosulphide (FeS) versus depth (a, b), dissolved sulphide (c, d) and chloride contents (e, f) in the SFR groundwaters colour coded by water types. The diagrams to the left (a, c, e) show the SFR data where the scales are restricted to those relevant to the SFR extension data. The diagrams to the right show these data integrated in the general distribution of the PLU data (Forsmark). Note the change in scales in the graphs to the right. Rastered areas correspond to the uncertainty range (± 0.36 units) associated with the $FeS(am)$ (grey inclined lines) and mackinawite (blue vertical lines) saturation index calculations.

5.3.4 Conclusions

The contents and distribution of dissolved Fe(II) and S(-II) in the SFR groundwaters are very similar to the ones reported for the PLU groundwaters, which is apparently related to the presence of similar controlling factors. Moreover, the dissimilarities can be feasibly attributed to the existence of an important input of present Baltic Sea waters to the SFR groundwaters which is not the case in the PLU area.

The presence of dissolved Fe(II) and S(-II) in some “pure” Local Baltic type groundwaters would indicate the acquisition of an anoxic or reducing character during the infiltration of marine waters through the marine seabed sediments and/or along the bedrock fractures prior to mixing with the preexistent, reducing groundwaters.

Equilibrium situations with respect to amorphous Fe(II)-monosulphides have been reached only in some groundwaters. These equilibrium situations with respect to the amorphous and metastable iron monosulphides would indicate the local presence of an iron source combined with a continuous and present supply of H₂S produced by SRB activity in the system. However, these results are affected by pH uncertainties and by problems in the measurements of dissolved sulphide. Thus, more data and further studies are needed.

Inorganic or biotically induced reductive dissolution of Fe-silicates (e.g. Fe³⁺ bearing clay minerals; Banwart 1999) or ferric oxyhydroxides in the fracture fillings appear to be the main sources of dissolved Fe(II). However, the highest Fe(II) contents and their larger variability are associated with Littorina type groundwaters, as also described for the PLU groundwaters. This could indicate a participation of a Littorina intrusion in the control of the Fe(II) dissolved contents.

Additionally, siderite could also participate on the control of dissolved Fe(II) in groundwaters with a marine component (i.e. Local Baltic- and Littorina types), since most of these groundwaters are in equilibrium with respect to this mineral. However, more detailed studies would be necessary to ascertain whether this equilibrium is effective in the bedrock or if it is only an inherited feature from the inflow of marine waters through seabed sediments.

All the described features would be indicative of anoxic and reducing environments in the SFR groundwaters. Mineralogy would support this situation as there are no definite indications of a significant inflow of oxygenated waters, such as oxidation and/or dissolution of sulphides (pyrite is only absent in water conductive fractures in the upper 10 metres) have been identified in the SFR fracture system (Sandstrom and Tullborg 2011). However, more detailed studies on the presence and degree of alteration of sulphide minerals in the fracture fillings would be advisable to assess the effect of the repository construction and the induced Baltic Sea water intrusion. Moreover, the presence of iron hydroxide at depths down to about 500 m and the age of these occurrences must be studied in order to clarify the extent of (probably) past oxygen intrusion events.

Finally, the reducing effect of organic matter decay in the marine sediments above the SFR should also be clarified by further studies. The nature and thickness of these overlying sediments are quite heterogeneous; the sediment layers (including low conductive glacial clays) are considerably thicker on the south side of the pier whereas on the north side of the pier there are areas with no, or only partial, sediment coverage (see Nilsson et al. 2011). Thus, it is possible that marine waters may penetrate rapidly or, even infiltrate directly into the fractures of bedrock too quickly to allow any reactions occurring. A more detailed study of the redox evolution of the intruding Baltic waters is recommended.

On the other hand, groundwaters associated with the Southern Boundary Belt appear to show a distinctive character (low Fe(II) contents, no sulphidic evidence, undersaturation with respect to siderite, etc.) that could be related to the thicker sediment cover in this zone, constraining the intrusion of Littorina and Baltic Sea waters. Thus, also the nature and thickness of the overlying sediments are probably important to explain some of the observed redox characters and this aspect must be explored in future work as the available data are still scarce.

5.4 Manganese system

Manganese is a redox sensitive element that can exist in different oxidation states; the most widely occurring forms in the environment are soluble Mn(II), when reduced, and insoluble Mn(IV), when oxidised. Mn(II) can be mobilised under anoxic conditions (manganese oxide reduction occurs after denitrification in the usual redox sequence) and, thus, the presence of dissolved Mn(II) can be considered as an indicator of anoxic or reducing conditions in the groundwaters.

Mn(II) contents in the groundwaters from the studied sites in Sweden and Finland can be controlled by different inorganic reactions and microbial processes (e.g. manganese reducing bacteria, MRB). However, they may also be influenced by marine intrusions through mixing processes with the preexisting groundwaters (Gimeno et al. 2008, 2009).

In this section, the manganese system is evaluated and the possible sources and sinks of dissolved manganese are discussed.

5.4.1 Hydrochemical trends

Manganese contents show variable but high values in the SFR groundwaters (around 4 mg/L \approx 0.07 mmol/L); Figure 5-7a, c), reaching values even slightly higher than those observed in the PLU groundwaters (Figure 5-7b, d). The highest manganese concentrations are related to groundwaters with Cl contents around 4,000–5,000 mg/L and with a clear Littorina signature (Figure 5-7c), in common with those reported for the PLU groundwaters (Figure 5-7d) or for other crystalline rock systems also affected by a Littorina recharge period (e.g. Laxemar-Simpevarp, Forsmark, Olkiluoto and Finnsjön; see the reviews by Gimeno et al. (2007, 2009).

As expected from their oxic conditions, present Baltic Sea waters in the surrounding areas of Forsmark and the SFR, display extremely low Mn contents (below 0.05 mg/L or $9.1 \cdot 10^{-4}$ mmol/L and frequently below the detection limit). However, the Mn contents in groundwaters with a clear component of present Baltic Sea waters are notably higher (between 0.5 and 2.3 mg/L; 0.01 and 0.042 mmol/L), and this seems to be related to an evolution towards anoxic and more reducing conditions during their infiltration and/or mixing in the bedrock. This is consistent with the clear sulphidic character of many of these Local Baltic type groundwaters.

As observed for Fe(II), groundwaters associated with the Southern Boundary Belt show homogeneous values (between 0.6 and 0.9 mg/L; 0.011 and 0.016 mmol/L) in the lower range of the values observed in the rest of hydrostructural domains. These low values would support a minor influence of marine intrusions in this zone, in agreement with the observations performed in Section 5.3

5.4.2 Mineralogical data

Manganese may occur as manganese oxides or oxyhydroxides, as carbonate minerals (as rhodochrosite; MnCO_3 , or in solid solution with siderite or calcite) and, also, as a trace constituent in many other minerals. It can be associated with iron minerals, such as iron or mixed Mn-Fe oxyhydroxides, and with chlorites and other clays.

As stated above, the presence of hematite and other iron oxyhydroxides has been described in almost all the boreholes and sections studied during the Boremap mapping activities in the SFR area. Moreover, calcite and chlorite constitute some of the most abundant minerals in those fracture fillings and clay minerals appear in dominant amounts in open fractures (Döse et al. 2009a, b, Winell 2009, Winell et al. 2009a, b, Sandström and Tullborg 2011), as it occur in the fracture fillings from the PLU and Laxemar-Simpevarp zones (Drake et al. 2006, Sandström et al. 2008, Drake and Tullborg 2009).

During the mineralogical analyses performed throughout the Site Characterisation Programmes in the fracture fillings from the PLU and Laxemar-Simpervarp areas, manganese has been found associated with clay minerals (e.g. chlorite, corrensite) and, occasionally, with calcite. Chemical analyses of bulk fracture filling material in the PLU area indicate that the highest MnO values are found below \sim 300 m (up to 0.45%wt MnO) and that the values at the shallower levels are mostly below 0.2%wt MnO (Sandström et al. 2008). In the Laxemar Simpevarp area, the MnO values in the bulk fracture filling material at shallower depths than 50 m are always below 0.4%wt (Drake and

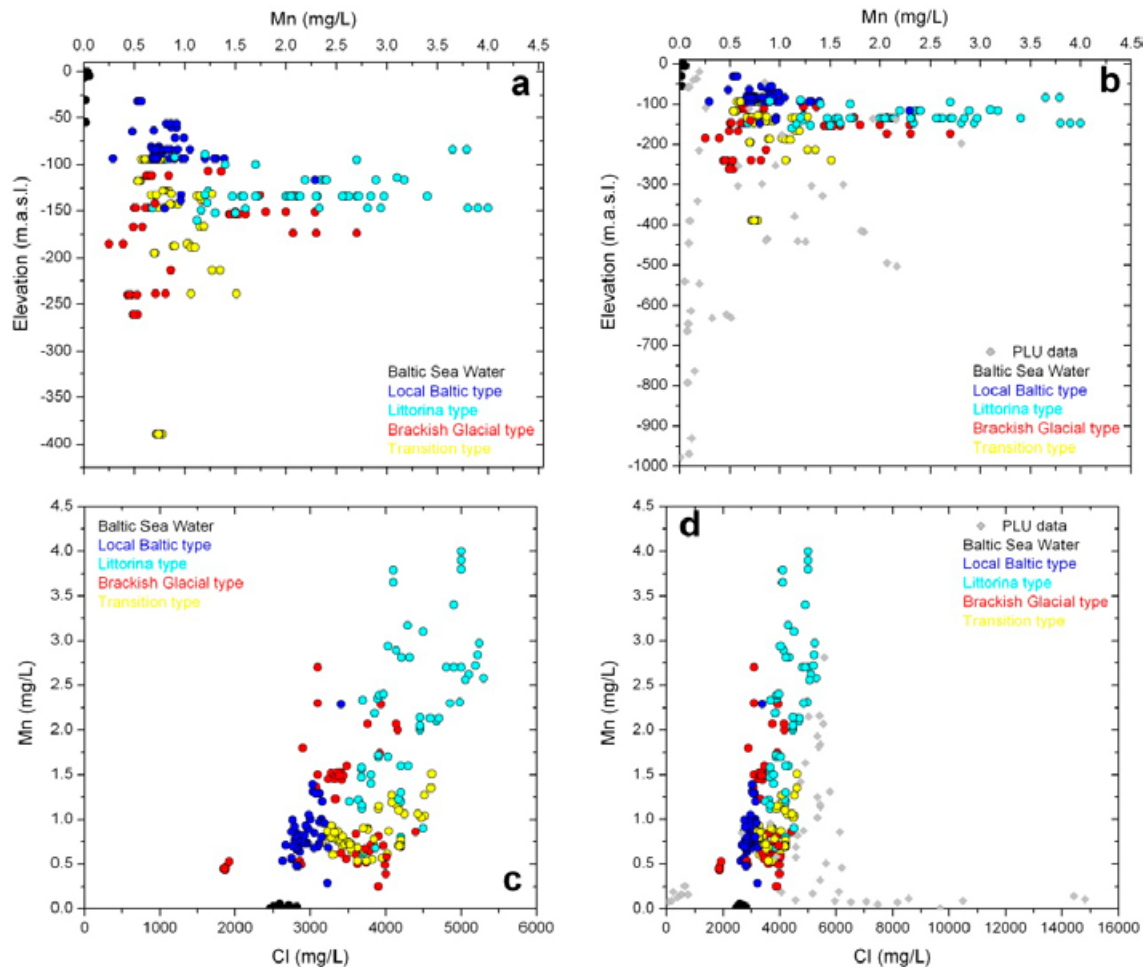


Figure 5-7. Dissolved Mn(II) concentrations versus depth (a, b) and chloride contents (c, d) in the SFR groundwaters colour coded by water types. The diagrams to the left (a and c) show the SFR data where the scales are restricted to those relevant to the SFR extension data. The diagrams to the right show these data integrated in the general distribution of the PLU data (Forsmark). Note the change in scales in the graphs to the right.

Tullborg 2009). These observations can be extrapolated to the SFR, where iron oxyhydroxides and clay phases with traces of manganese may participate in the control of dissolved manganese through different types of reactions, including surface processes.

Manganese reducing activity could also exert an important control on dissolved manganese contents in the presence of the appropriate terminal electron acceptors (TEAs). Manganese reducing bacteria (MRB) may use a wide number of Mn oxides and oxyhydroxides as TEAs, including mixed valence and trivalent oxides and hydroxides and MnO₂ oxides (see Gimeno et al. 2009 and references therein). However, the presence of Mn-oxides or oxyhydroxides has not been detected in the fracture fillings¹⁷ in the SFR or in the extensive mineralogical studies performed in the PLU and Laxemar-Simpevarp areas. This would represent a major limitation to the significant MRB activity in the SFR groundwaters.

¹⁷ Mn-oxyhydroxides have only occasionally been detected in the shallower 10 m of bedrock from the Laxemar zone (Drake and Tullborg 2008).

5.4.3 Processes: Thermodynamic approach

As already indicated, mixing with old marine waters appears to exert an important control on the dissolved manganese contents in the SFR groundwaters. However, mineralogical or microbiological controls may also participate, or even be dominant, especially during the present intrusion of Baltic waters.

Under anoxic conditions, the dissolution of Mn(II)-bearing minerals and the reductive dissolution of manganese oxyhydroxides may increase dissolved manganese concentrations in the present marine sediments above the SFR. Depending on the groundwater residence time in these sediments and on the degree of development of a redox sequence in them, manganese oxyhydroxides may also quickly react with dissolved S(-II) and Fe(II) (Postma 1985, Yao and Millero 1993), through the following reactions:



or even with some metabolic products excreted by bacteria or with other dissolved components (e.g. siderophores), which may promote an increase in the dissolved Mn(II) contents. Likewise, dissimilatory manganese reducing processes may reduce manganese oxyhydroxides using hydrogen or organic matter (e.g. acetate) as electron donors:



thereby increasing the dissolved Mn concentrations during the present infiltration of Baltic waters through the marine seabed sediments.

All these processes could justify the observed increase in Mn dissolved contents in the Local Baltic type groundwaters. However, more data on the sediment and porewater characteristics above the SFR would be needed to assess their existence and possible relevance in the studied system.

The influence of MRB on dissolved Mn contents in the remaining groundwaters is not supported by the mineralogical results, which do not show the presence of Mn-oxyhydroxides (see Section 5.4.2) or by the observed hydrochemical trends, which do not show the correlation between Mn(II) and HCO_3^- that would be expected in the case of MRB activity according to reaction (5-11).

Additional controls on dissolved manganese contents in the groundwaters may involve surface processes or solubility constraints. Overall, dissolved manganese shows a meaningful correlation with dissolved Fe(II) contents, mainly in Littorina type groundwaters. The contribution of this old marine component through mixing processes may partially explain this correlation, although the “simultaneous” control by iron phases with traces of manganese (oxyhydroxides, clays) or by the operation of surface processes between dissolved manganese and iron oxyhydroxides may also be effective. However, the intensity of these simultaneous controls has generally not been effective enough to eliminate the marine signature of many of the SFR groundwaters, and these processes may even have contributed to preserve it in reactive elements such as Fe and Mn. This issue merits further studies.

Among the rest of controls that may influence the final dissolved manganese contents in the SFR groundwaters, the one most clearly present is rhodochrosite equilibrium. Speciation-solubility calculations indicate strong undersaturation states with respect to all the Mn oxides and oxyhydroxides included in the WATEQ4F database. The only Mn mineral that reaches equilibrium in the studied groundwaters, considering a SI uncertainty range of ± 0.55 (Gimeno et al. 2008) is rhodochrosite (Figure 5-8) and this result is not significantly affected by the pH uncertainty (see Appendix 3). Littorina type groundwaters may have inherited this character from their infiltration stage through the marine sediments, since authigenesis of Mn-carbonates has been an active process in the Baltic Sea since 7,000–8,000 year ago (Kulik et al. 2000, Neumann et al. 2002 and references therein). The same possibility has already been proposed by Gimeno et al. (2006, 2008, 2009) for these types of groundwaters in the PLU and Laxemar-Simpervap areas.

Most of the Local Baltic type groundwaters are also in equilibrium with rhodochrosite (Figure 5-8) and most of the groundwaters related to the Southern Boundary Belt are clearly undersaturated with respect to this mineral, supporting a lower influence of marine waters in this zone.

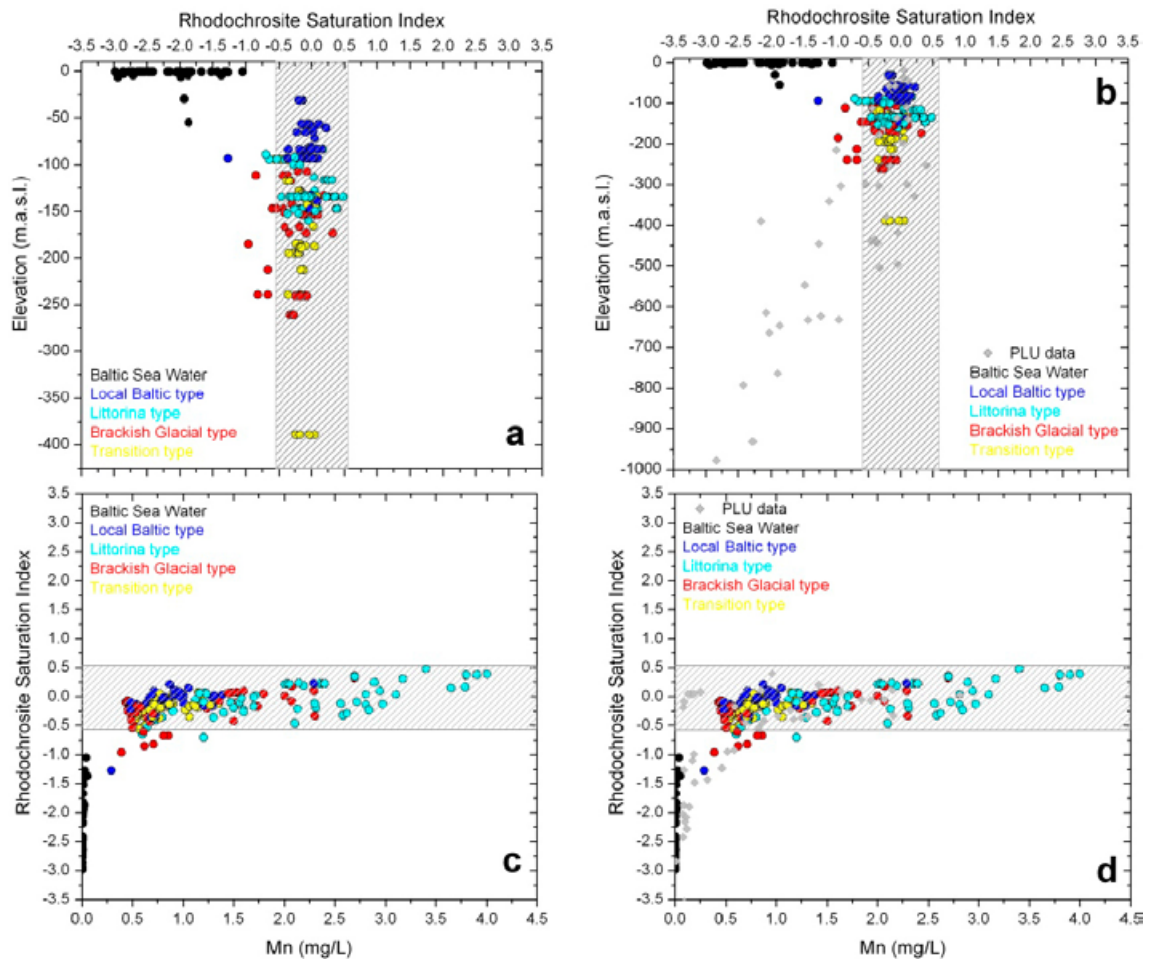


Figure 5-8. Rhodochrosite saturation index versus depth (a, b) and manganese contents (c, d) calculated for the SFR groundwaters colour coded by water types. The diagrams to the left (a and c) show the SFR data where scales are restricted to those relevant to the SFR extension data. The diagrams to the right show these data integrated in the general distribution of the PLU data (Forsmark). Note the change in scales in the graphs to the right. Rastered areas correspond to the uncertainty range (± 0.55 units) associated with the rhodochrosite saturation index calculations.

5.4.4 Conclusions

As it occurs with dissolved S(-II) and Fe(II), the contents, distribution and controlling factors of dissolved manganese in the SFR groundwaters are very similar to the ones reported for the PLU groundwaters. Meaningful amounts of dissolved manganese have been found in most of the samples, supporting the existence of a generalised anoxic/reducing environment in the SFR groundwaters. This interpretation is also valid for groundwaters with a clear component of present Baltic Sea waters, which suggests the existence of an evolution towards anoxic and more reducing conditions during the infiltration of Baltic waters and/or mixing in the bedrock.

Different inorganic reactions and microbial processes could participate in the control of dissolved manganese in the SFR groundwaters. However, there is a clear link between manganese concentrations, equilibrium with rhodochrosite and Littorina signatures, as also reported for the PLU groundwaters. These relationships can be interpreted as an inheritance of the hydrochemical conditions imposed by rhodochrosite formation during the infiltration of Littorina waters through the marine sediments. Thus, an “old” mixing control on manganese contents is still evident in the SFR groundwaters.

Dissolved manganese contents and the frequent undersaturation state with respect to rhodochrosite in the groundwaters related to the Southern Boundary Belt also suggest less influence of marine waters in this zone, in agreement with the iron and sulphur systems (see Section 5.3).

5.5 The Nitrogen system (nitrate, nitrite and ammonium)

In natural waters, nitrogen occurs in various oxidation states from nitrate (+V) to ammonium (-III) and the transformation between those species is almost exclusively facilitated by microorganisms (Kehew 2001). Organic nitrogen is converted to ammonium (ammonification process) and, under oxidising conditions, ammonium is oxidised to nitrite (NO_2^-) or further oxidised to nitrate (NO_3^-) by specialised nitrifying bacteria. Under aerobic conditions, nitrate behaves as a conservative anion and nitrification may lead to nitrate accumulation.

Under anaerobic conditions, nitrate is the most thermodynamically favoured electron acceptor for the oxidation of organic substrates and it may be used by nitrate reducing bacteria (NRB) for respirative energy production (denitrification) in the presence of reduction potential (in the form of organic matter, pyrite or Fe(II)-bearing phases e.g. Appelo and Postma 2005). Denitrification occurs in different steps, each of which is catalysed by specific NRB producing nitrite, nitrous oxide, ammonium or nitrogen gas (Hallberg and Keeney 1993, Chapelle 2001) and usually resulting in nitrate depletion and, in general, in a global depletion in nitrogen species (Chapelle 2001).

Moreover, NO_3^- contents in groundwater systems characterised by very low concentrations (as occurs in many crystalline systems) has led to their use to indicate groundwater sample contamination (Gascoyne 2004).

In the case of nitrite, it is a metastable intermediate product in the overall denitrification processes under anaerobic conditions and, thus, it may be detected at low levels in most aqueous systems under anoxic conditions (Appelo and Postma 2005, Rivett et al. 2008). With regard to ammonium (NH_4^+), it is the most stable nitrogen form under reducing conditions and it is less mobile than nitrate (e.g. it participates in exchange reactions).

The available data on the analytical contents of nitrogen species from the SFR are examined and interpreted in this section with the aim of gaining some information from their particular properties and “contrasting” behaviour.

5.5.1 Hydrochemical data

Available analytical data for dissolved nitrogen species in the groundwater samples from the SFR include NO_2^- , NO_3^- , and NH_4^+ . Nitrate and nitrite contents in the SFR groundwaters are low (Figure 5-9) and, in many cases, below the detection limit. Nitrate contents are generally between $8.7 \cdot 10^{-4}$ and 0.9 mg/L ($1.4 \cdot 10^{-5}$ and $1.4 \cdot 10^{-2} \text{ mM}$), being most of the values below 0.1 mg/L ($1.6 \cdot 10^{-3} \text{ mmol/L}$). Brackish-glacial and Local Baltic type groundwaters tend to display the largest nitrate concentrations within this general range. The highest nitrate content (13 mg/L ; 0.21 mmol/L ; Figures 5-9c, d) has been recorded in a sample from section 44.5–62.3 m in the KFR01 borehole during 2000, the section in which redox measurements performed in the same year indicated a stable and oxidising Eh value around 110 mV (Section 5.2.2; Table 5-3).

Nitrite concentrations vary between $6.6 \cdot 10^{-4}$ and $2.9 \cdot 10^{-2} \text{ mg/L}$ ($1.43 \cdot 10^{-5}$ and $6.4 \cdot 10^{-4} \text{ mmol/L}$), with most of the measured values below $7.5 \cdot 10^{-3} \text{ mg/L}$ ($1.6 \cdot 10^{-4} \text{ mmol/L}$; Figures 5-9a, b). The highest nitrite contents within this range are associated with Brackish-glacial and, especially, Littorina type groundwaters with large chloride contents (above 100 mmol/L or $3,500 \text{ mg/L}$).

Although, the largest variability in the nitrate and nitrite contents seems to be associated with groundwaters shallower than 200 m, this observation could be biased by the small number of sample analyses below this depth.

With respect to NH_4^+ concentrations (Figures 5-9e, f), they range between $6.5 \cdot 10^{-3}$ and 0.72 mg/L ($3.6 \cdot 10^{-4}$ and $4 \cdot 10^{-2} \text{ mmol/L}$), the highest contents being, in this case, associated with groundwaters with an important contribution from Littorina or Local Baltic type waters or to some of the Transition type groundwaters. In contrast, Brackish-glacial type groundwaters always display NH_4^+ concentrations below 0.18 mg/L (10^{-2} mmol/L). NH_4^+ contents show the maximum concentrations (0.5 and 0.7 mg/L ; $2.8 \cdot 10^{-2}$ and $3.9 \cdot 10^{-2} \text{ mmol/L}$; Figure 5-10a) for chloride contents between $3,000$ and $6,000 \text{ mg/L}$, associated with the important contribution of the present Baltic waters and the old Littorina waters, respectively. The association between high and variable contents of ammonium and

the marine character of the groundwaters is even more clearly seen in the Littorina groundwaters (around 5,000 mg/L Cl) from the PLU (Figure 5-10b).

No meaningful differences in the contents of dissolved NO_2^- , NO_3^- , and NH_4^+ can be observed among the different hydrostructural domains in the SFR.

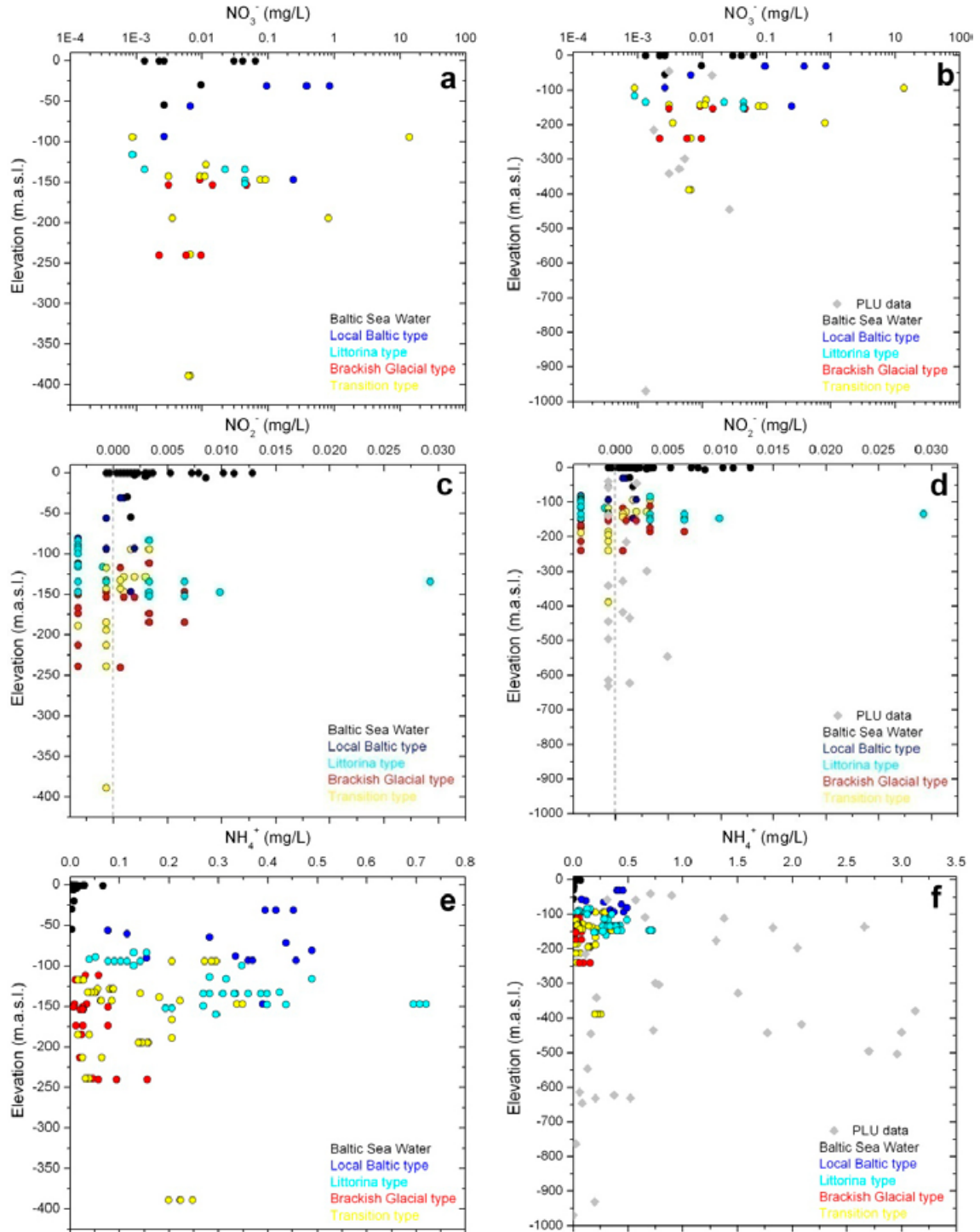


Figure 5-9. Distribution of NO_3^- (a, b), NO_2^- (c, d) and NH_4^+ concentrations (e, f) versus depth in the SFR groundwaters colour coded by water types. The diagrams to the left (a, c, e) show the SFR data where scales are restricted to those relevant to the SFR extension data. The diagrams to the right show these data integrated in the general distribution of the PLU data (Forsmark). Note the change in scales in the graphs to the right.

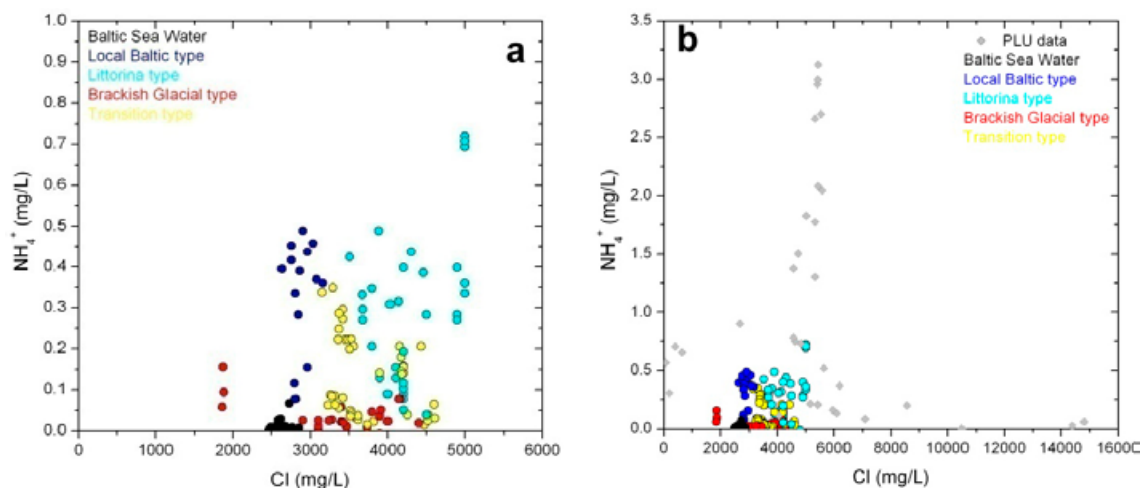


Figure 5-10. Dissolved NH_4^+ concentrations versus chloride contents in the SFR (a) and the PLU (b) groundwaters.

5.5.2 Comparison with other crystalline systems and with the Baltic Sea waters

Some groundwaters from the SFR show higher concentrations of nitrate and nitrite than the groundwaters from the PLU (the highest analysed contents are 0.025 and 0.005 mg/L, $4 \cdot 10^{-4}$ mmol/L and 10^{-4} mmol/L for NO_3^- and NO_2^- , respectively), Laxemar (with maximum contents of dissolved NO_3^- and NO_2^- around 0.005 mg/L, 10^{-4} mmol/L) or Finnsjön (with maximum nitrate and nitrite contents of 0.018 and 0.04 mg/L, $2.9 \cdot 10^{-4}$ mmol/L and $8.57 \cdot 10^{-4}$ mmol/L, respectively, in groundwaters with $\text{Cl} > 2,000$ mg/L).

Nitrate contents seem to be higher in the Local Baltic type groundwaters than in the present Baltic shore waters from the PLU (Figures 5-9c and 5-11), which may imply either the existence of larger nitrate concentrations in the marine waters from SFR or nitrate enrichment resulting from the leaching of wastes from the SFR facilities (e.g. blasting residues). This second possibility would be in line with the higher nitrate contents detected in the Transition type groundwaters.

Nitrite concentrations in the SFR groundwaters are similar to the Baltic Sea water contents which could be entering the SFR area (Figures 5-9a and 5-11). However, groundwaters with the clearest

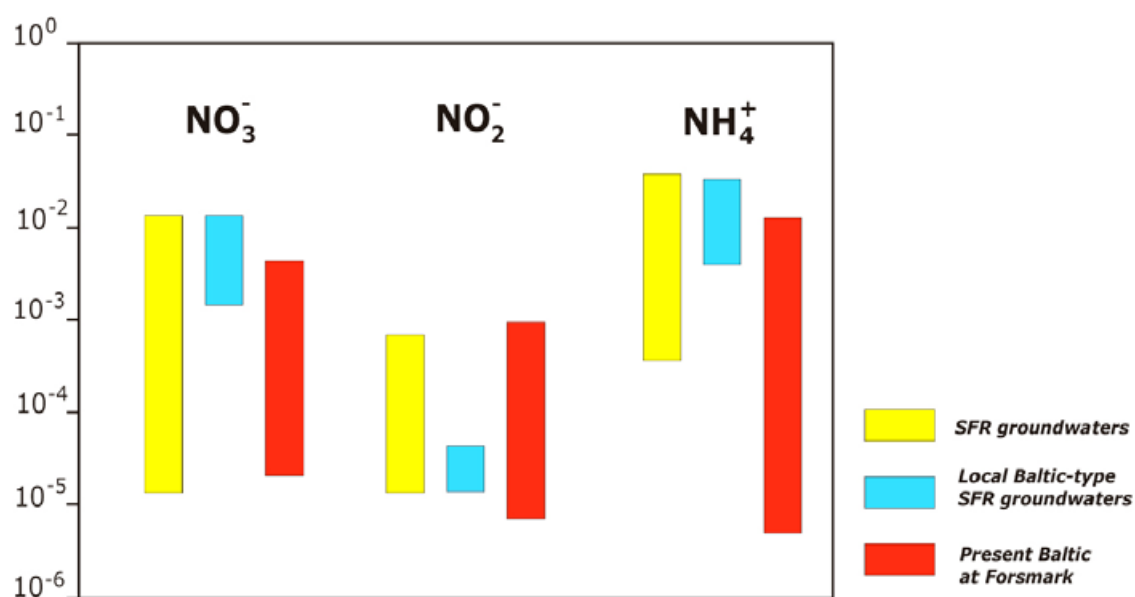


Figure 5-11. Ranges of nitrate, nitrite and ammonium concentrations based on the whole SFR groundwater set and on the Local Baltic type groundwaters and the Baltic Sea data from the PLU.

Baltic signature (Local Baltic type groundwaters) show the lowest nitrite contents whereas groundwaters with Littorina or Glacial signatures display the highest concentrations. Thus, the highest nitrite contents in the SFR groundwaters are probably related to *in situ* bacterial denitrification (see below).

Finally, the highest ammonium contents in the SFR groundwaters are related to groundwaters with a clear marine signature (both Littorina and present Baltic), as it occurs in the PLU groundwaters or in the Olkiluoto groundwaters (Pitkänen et al. 2004) although the contents are not as high as in the Littorina groundwaters from the PLU (Figures 5-9f and 5-11). The largest ammonium contents in the SFR groundwaters are higher than those observed in the range of the present Baltic Sea. However, increasing ammonium concentrations with depth in the interstitial waters from marine sediments is a common observation. In marine sediments with organic matter, bacterial activity promotes the transformation of organic nitrogen compounds and the formation of NH_4^+ . It also occurs in the present deep sediments of the Baltic Sea, where NH_4^+ concentrations from 4 to 16 mg/L (0.22 to 0.9 mmol/L) are frequent (Carman and Rahm 1997).

All these observations suggest that the NH_4^+ amounts found in the SFR groundwaters mostly represent an inherited character from the marine contribution. The variability in this component, both in the Local Baltic type and in the Littorina type groundwaters, may be related to different intensities of bacterial activity in the percolated marine sediments and/or to a variable extent of water-rock interaction (exchange processes) during percolation in the bedrock.

5.5.3 Microbiological data

As indicated at the beginning of this section, there are only two microbiological analyses with determinations of the most probable number (MPN) of cultivable metabolic groups in the SFR. However, the results indicate that nitrate reducing bacteria (NRB) show the highest MPN (3.3 and 70 cells/mL) of all analysed metabolic groups (iron, manganese and sulphate reducing bacteria, acetogens and methanogens) at depths between 128 and 154 m.

Analyses of nitrate reducing bacteria (NRB) were also recently incorporated in the MPN analyses protocols performed in the Site Characterisation Programmes. The results show the presence of meaningful amounts of nitrate reducing microorganisms at depths between 200 and 700 m, with higher MPN in Forsmark and in Laxemar than in the SFR (Hallbeck and Pedersen 2008a, b). As stated above, the nitrate contents in the groundwaters of Forsmark and Laxemar are extremely low and the presence of nitrate reducers does not necessarily imply that nitrate reduction is occurring, since this bacterial group may use other electron acceptors in the absence of nitrate, such as oxygen, Fe(III) and Mn(IV) (Hallbeck and Pedersen 2008a, b).

However, all these results would indicate the usual presence of NRB in these types of groundwater systems. Thus, if the amounts of nitrate increase in the system and anoxic conditions are maintained or restored, nitrate reducing activity would be enhanced, decreasing the nitrate concentrations and generating some characteristic metabolic by-products (e.g. nitrite), as it appears to occur in some of the SFR groundwaters.

5.5.4 Conclusions

Higher concentrations of nitrate and nitrite have been detected in some SFR groundwaters compared to those found in Forsmark (PLU) and Laxemar. These higher nitrate concentrations may be related to anthropic disturbances related to the SFR facility and probably favoured by the existence of some localised oxic or suboxic environments as occurs in other crystalline systems (Stotler et al. 2009). In fact, in the section where the sample with higher nitrate contents was taken in 2000 (section 44.5–62.3 m.b.l. in KFR01A), the redox measurements performed that year indicate a stable Eh value (using three electrodes) around 110 mV (see Section 5.2.2).

Nevertheless, nitrate and nitrite contents in the SFR groundwaters are generally in the usual range for uncontaminated groundwaters and, furthermore, they are similar or even lower than those found in other crystalline rock systems (e.g. Pitkänen et al. 2004, Stotler et al. 2009). It is also clear that the influence of blasting residues is minimal, if any, in the present SFR groundwaters, some twenty years after the SFR excavation and construction.

The highest nitrite contents are consistent with the existence of *in situ* bacterial denitrification. Nitrate reducing microorganisms are very common in surface waters, soils and groundwaters (Rivett et al. 2008 and references therein) and they have been identified in the still scarce analysis at the SFR, as well as in the Forsmark and Laxemar microbiological investigations.

The active presence of this metabolic activity would imply the existence of anoxic environments.

Finally, ammonium contents are always clearly detectable (except in a few Brackish- glacial and Transition type groundwaters) and, in fact, it is the most common analysed nitrogen component in the SFR groundwaters. This would support the existence of generalised reducing conditions in the SFR groundwaters. On the other hand, the high ammonium concentrations found in the Local Baltic type and Littorina type groundwaters seem to be an inherited character from those marine contributions, as also is observed in the PLU or in the Olkiluoto groundwaters (Gimeno et al. 2008, Pitkänen et al. 2004).

5.6 Molecular hydrogen and methane

As stated above, the available methane and hydrogen data from the SFR are still very scarce and cover a limited range of depths (from 94.23 to 134.43 m) in KFR01, KFR10 and KFR7A boreholes.

Hydrogen contents in four of the six available analyses are below the detection limit. Concentrations in the two sections of the KFR105 are 7.4 and 8.9 $\mu\text{L/L}$ (0.33 and 0.4 $\mu\text{mol/L}$). This situation qualitatively agrees with the low hydrogen contents found in the Site Characterisation Programmes at Forsmark (PLU) and Laxemar. In the PLU, only six of the sixteen analysed samples have detectable values (ranging between 5.4 and 213 $\mu\text{L/L}$; 0.24 and 19.2 $\mu\text{mol/L}$, with maximum values between 300 and 500 m depth; Figure 5-12a). In Laxemar, the maximum hydrogen concentrations detected are even lower than in the PLU (Figure 5-12b).

Molecular hydrogen, like methane, can be generated by biological and inorganic processes in deep crystalline rock systems. In the degradation sequence of organic matter, biogenic molecular H_2 and simple organic molecules (e.g. acetate) are continuously produced by fermentative bacteria and heterotrophic acetogens from complex organic compounds. In turn, the produced H_2 or acetate are quickly metabolised by other microorganisms (e.g. turnover times from minutes to hours; Konhauser 2007) using different terminal electron acceptors (TEAs). This strong coupling justifies that the maximum hydrogen concentrations from biogenic origin are below 50–150 nM in low temperature systems (e.g. marine sediments, soils aquifers, etc; Lovley and Goodwin 1988, Hoehler et al. 1998, Christensen et al. 2000, Lin et al. 2005, Heimann et al. 2010).

Overall, the maximum detected amounts of hydrogen in the PLU and in Laxemar are several orders of magnitude higher than the maximum values from biogenic origin and, thus, additional sources of H_2 are required. Even though abiogenic H_2 may be produced by, at least, six different inorganic processes (see Pitkänen and Partamies 2007, Hallbeck and Pedersen 2008a, b and references therein), these additional sources and the promoted heterogeneity and variability in the distribution of hydrogen contents in these systems are still not well understood (Gimeno et al. 2009).

In the SFR such “high” hydrogen contents have not been detected although this situation could be related to the small number of available data.

Furthermore, it would be advisable to improve the detection limits for hydrogen and to explore the nanomolar range of this component in the SFR and in the other sites. The hydrogen contents in the “biogenic range” may be used as a diagnostic value to identify the dominant redox processes that exist in a particular location of the system, and therefore would contribute to the overall understanding of their redox processes.

Methane contents in the available SFR gas data range between 0.02 and 0.119 mL/L ($8.9 \cdot 10^{-4}$ and $5.3 \cdot 10^{-3}$ mmol/L) and increase apparently between 50 and 134 m depth. The lowest values are measured in a Local Baltic type groundwater whereas the highest contents correspond to the Brackish-glacial type groundwaters. More data would be needed to confirm the possible correlation between methane contents and groundwater type.

Overall, methane contents in the SFR are in agreement with those found in the PLU. They are below 0.12 mL/L ($5.9 \cdot 10^{-3}$ mmol/L) except in the sample from the KFM01D borehole at 445 m depth, where there is a reported value as high as 4.6 mL/L (0.2 mmol/L; Figure 5-13a). Moreover, they do not display any correlation with depth or with the MPN of methanogens (usually below 10 cell/mL; Hallbeck and Pedersen 2008a). A similar situation can be observed in the Laxemar-Simpevarp area (Figure 5-13b) where methane contents are usually below 0.1 mL/L ($4.5 \cdot 10^{-3}$ mmol/L) and the highest values below 0.88 mL/L ($4 \cdot 10^{-2}$ mmol/L).

As hydrogen and methane may be generated by organic processes (methanogenic microorganisms) and inorganic processes in deep crystalline rock systems (Pitkänen and Partamies 2007, Hallbeck and Pedersen 2008a, b and references therein). Moreover, inorganic methane may diffuse upwards towards the surface and mix with biogenic methane. Methane from both sources seems to be present in the Forsmark, Laxemar and Olkiluoto sites (Pitkänen and Partamies 2007, Hallbeck and Pedersen 2008a, b) and probably also at the SFR. However, much more analytical and microbiological data are needed to clarify the origin and distribution of methane not only at the SFR but also in the PLU and Laxemar sites (Gimeno et al. 2009).

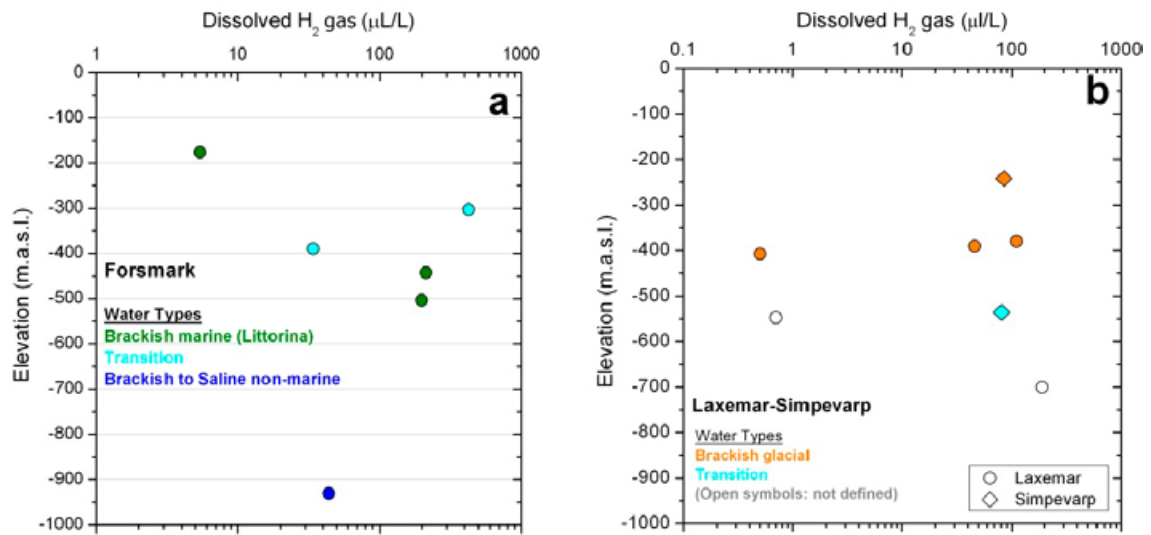


Figure 5-12. Distributions of hydrogen with depth in Forsmark (a) and Laxemar-Simpevarp (b). Available data for the SFR are below the detection limit (except for two samples with values of 7.4 and 8.9 μL/L).

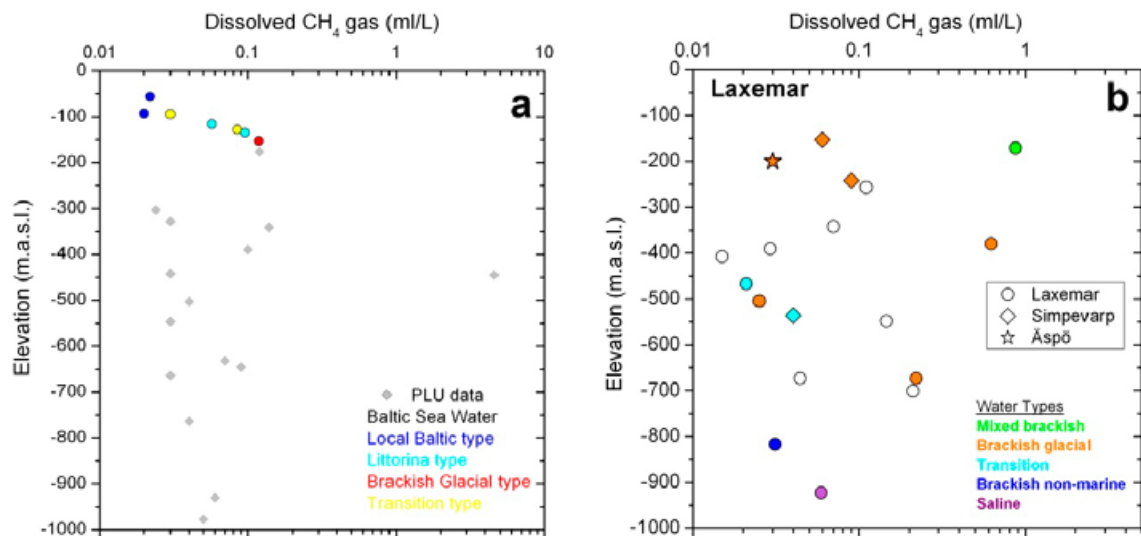


Figure 5-13. Depth distributions of methane in the SFR and PLU (a) and in Laxemar (b) groundwaters.

6 Conclusions

Most of the hydrogeochemical features and trends observed in the SFR groundwaters are similar to those observed in the PLU in agreement with the common palaeohydrogeological evolution of both systems. Some clear differences arise from the sampling depths at SFR as the brackish to saline non-marine groundwaters characterised in the PLU have not been sampled in the SFR. Thus, some of the characteristics related to this type of groundwaters (extremely low dissolved bicarbonate values or the $p\text{CO}_2$ lower than the atmospheric value) have not been observed in the SFR groundwaters. Two additional important differences are; 1) the drawdown of Baltic Sea waters into the SFR groundwaters caused by the repository excavation and construction, and 2) the effects of the actual presence of the repository at the present time. The intrusion of modern Baltic Sea waters does not seem to drastically alter the major compositional trends related to the past Littorina intrusion, still visible in many groundwaters from the SFR. However, some effects in the redox state, specially associated with the SFR facilities, can be deduced.

The main conclusions obtained from the study of the different compositional systems in the SFR groundwaters are summarised.

Most of the parameters related to the carbonate system in the SFR groundwaters show similar trends to those observed in the PLU, especially if only groundwaters with marine contributions are compared:

- There is no a clear pH trend with depth which may reflect the lateral heterogeneity of the groundwater system. In general, values determined in the field or *in situ* are higher and fall in a narrower range (7.3 to 8) than the pH values measured in the laboratory (6.8 to 8 with the majority of samples in the interval 7.2 to 7.7).
- High and variable HCO_3^- values are found in groundwaters with a marine (both Littorina and present Baltic) signature, as a result of the biological activity during infiltration of marine waters through seabed sediments.
- Although heterogeneous reactions (calcite reequilibrium, cation exchange) may have noticeably modified the dissolved calcium concentrations; mixing control is still evident.
- Baltic Sea waters are clearly undersaturated with respect to calcite.
- Overall, most of the SFR groundwaters seem to be in equilibrium or slightly oversaturated with respect to calcite. A few Local Baltic type groundwaters are (slightly) undersaturated with respect to calcite. This could be attributed to an infiltration time for present Baltic Sea waters too fast to allow equilibration with respect to calcite. However, this issue should be considered further, given the possible uncertainty associated to the pH measurements.
- Although some calcite dissolution may occur during the infiltration of Baltic Sea waters, the intensity of this process must be low due to the high alkalinity content and near neutral pH in seawaters. Calcite is one the most abundant minerals in the fracture fillings of the bedrock and it is widely distributed at all examined depths (reaching 520 m depth) without significant variations with depth. Thus, no obvious clues of calcite dissolution can be deduced with the present data although more detailed analysis are needed mainly in the shallowest part of the bedrock.

The sulphate system in the SFR groundwaters shows also similar trends to those observed in the PLU:

- The main source of sulphur in the SFR groundwaters is the intrusion of past (Littorina) and present (Baltic) seawaters, which have mixed with the preexistent groundwaters.
- Available isotopic data ($\delta^{34}\text{S}$) indicate that sulphate reducing microbial activity seems to have played a minor role on the control of dissolved sulphate concentrations except in some isolated groundwaters.
- All the SFR groundwaters are undersaturated with respect to gypsum and celestite and are in equilibrium with respect to barite. Water-rock interaction processes seem to have modified the strontium contents derived from mixing processes. However, none of these minerals appears to have appreciably affected the dissolved sulphate contents derived from mixing processes.

Dissolved silica concentrations in the SFR groundwaters are not correlated to chloride contents, which would indicate the presence of a mineralogical control as a source of this element, or as a limiting phase:

- In groundwaters with short residence times, the main processes that can participate in the control of silica contents are incongruent dissolution of feldspars with formation of secondary clays, clay mineral transformations and silica adsorption-desorption reactions in clays. Mixed layer clays of smectite-illite type are the most abundant minerals in water conducting fractures.
- Control by a more stable solid silica phase (chalcedony) occurs in groundwaters with longer residence times (e.g. the old glacial derived groundwaters with a long term hydraulic isolation in the KFR101 borehole).
- However, these types of mineralogical control may be overlapped with mixing, as the effects of marine intrusions with distinctive silica contents (e.g. very high in some Littorina waters and very low in present Baltic waters) are still apparent in the present concentrations of this element in some groundwaters. Mixing processes would be responsible for the present dispersion of silica contents in the shallowest groundwaters of the SFR.

The narrow concentration ranges and the lack of correlation with chloride concentrations observed for the fluoride concentrations in the SFR groundwaters are indicative of the existence of a mineral solubility control:

- Most of the analysed groundwaters at the SFR are equilibrated with respect to fluorite and a similar behaviour has been observed in the PLU or Laxemar groundwaters.
- In the cases for which undersaturation with respect to fluorite has been obtained, the waters correspond mostly to shallow groundwaters affected by the dilution effect associated with the intrusion of present Baltic Sea waters with very low fluoride contents.

The potentiometrical Eh measurements in the SFR groundwaters provide both oxidising and reducing values:

- Reducing values (from -140 to -190 mV) are in line with those measured in the PLU groundwaters. They are apparently controlled by the occurrence of an iron phase with an intermediate crystallinity and/or by clay minerals. The coincidence between the measured values and the results obtained with the $\text{Fe}^{2+}/\text{Fe}(\text{OH})_3$ and the $\text{Fe}^{3+}\text{-clay}/\text{Fe}^{2+}\text{-clay}$ redox pairs, is similar to that observed in the 'Large-Scale Redox Experiment' (Banwart 1999) where the effects of the intrusion of meteoric waters in the Äspö tunnels were studied. Poorly ordered smectite-illite clays with low Mg/Fe ratios are one of the dominant phases in the fracture fillings and iron oxyhydroxides have been detected in the fracture fillings at all depths in the SFR also suggesting their participation in the control of the redox state. However, more detailed studies are needed, especially on the characters of iron-oxyhydroxides.
- The measured oxidising Eh values in the SFR groundwaters (from $+30$ to $+110$ mV) seem to be controlled by amorphous Fe(III)-oxyhydroxides. They could represent the existence of present or very recent oxic environments, since these phases quickly recrystallise to less soluble and more stable phases under reducing conditions. Chemical characters (e.g. pH and Eh values) for those groundwaters are very similar to those observed in the Äspö Underground Laboratory when reducing groundwaters were in contact with the oxygen-rich atmosphere of the tunnel and microbes catalysed the formation of amorphous Fe(III)-oxyhydroxides. Thus, these oxidising conditions would be representative of the groundwater situation close to the oxic environment in the tunnels and they would change to more reducing groundwaters when subsequently pumped. The gradual removal of the groundwater from the tunnel section and the progressive input of pristine formation water may have caused a disequilibrium in the observed long stabilisation periods towards reducing conditions. The more recent measurements performed in the KFR19 and KFR7A boreholes, also displaying long stabilisation periods, would support this interpretation.
- The Eh values calculated for the SFR groundwaters using suitable redox pairs point also towards the existence of overall reducing conditions (below -100 mV), especially in the case of sulphidic and methanic groundwaters (below -200 mV).

The contents and distribution of dissolved Fe(II), S(-II) and Mn in the SFR groundwaters are very similar to the ones reported for the PLU groundwaters, which appears to be related to the presence of similar controlling factors:

- The presence of dissolved Fe(II) and S(-II) in some almost “pure” Baltic type groundwaters would indicate the acquisition of anoxic or reducing characteristics during the infiltration of marine waters through the marine seabed sediments and/or along the bedrock fractures prior to mixing with preexistent, reducing groundwaters.
- Equilibrium situations with respect to amorphous Fe(II)-monosulphides have been achieved in a few groundwaters and they are affected by different uncertainties. Mackinawite equilibrium situations are more frequent which would suggest a low intensity in the sulphate reduction activity; this would be in agreement with the scarce microbiological data. However, taking into account the methodological problems in determining dissolved sulphide contents, much more data are needed to address this question.
- Additionally, siderite could also participate in the control of dissolved Fe(II) in groundwaters with a marine component (i.e. Local Baltic and Littorina types), since most of these groundwaters are in equilibrium with respect to this mineral. However, more detailed studies would be necessary to ascertain whether this equilibrium is effective in the bedrock, or if it is only an inherited feature from the inflow of marine waters through seabed sediments.
- Significant amounts of dissolved manganese have been found in most of the samples, supporting the existence of a generalised anoxic/reducing environment in the SFR groundwaters.
- There is a clear link between manganese concentrations, equilibrium with rhodochrosite and Littorina signatures, also reported for the PLU groundwaters. These relationships can be interpreted as an inheritance of the hydrochemical conditions imposed by rhodochrosite formation during the infiltration of Littorina waters through the marine sediments. Thus, an “old” mixing control on manganese contents is still evident in the SFR groundwaters.
- Groundwaters related to the Southern Boundary Belt show distinctive characteristics with respect to the rest of hydrostructural domains. They show lower and relatively constant values of dissolved iron and manganese, dissolved sulphide below detection limit and undersaturation with respect to siderite and rhodochrosite. All these characteristics point towards a lower marine influence in this zone. This fact may be related to the existence of a thicker sediment cover in this zone, constraining the intrusion of Littorina and Baltic Sea waters, although more data are needed to support this possibility.

With respect to the nitrogen system, higher concentrations of nitrate and nitrite have been detected in some SFR groundwaters compared with those found in Forsmark (PLU) and Laxemar:

- These higher nitrate concentrations may be related to anthropic disturbances linked to the SFR facility and probably favoured by the existence of some localised oxic or suboxic environments, as it occurs in other crystalline rock systems.
- The highest nitrite contents are consistent with the existence of *in situ* bacterial denitrification.
- Ammonium contents are always clearly detectable (except in a few Brackish-glacial and Transition type groundwaters) and, in fact, it is the most common analysed nitrogen component in the SFR groundwaters; this would support the existence of generalised reducing conditions in the SFR groundwaters. On the other hand, the high ammonium concentrations found in Local Baltic type and Littorina type groundwaters seem to be an inherited character from those marine contributions, as also observed in the PLU or Olkiluoto groundwaters.

Thus, most of the hydrochemical evidence indicates the presence of anoxic or reducing environments in the SFR groundwaters. This result would be in agreement with the presence of pyrite at most depths in the fracture fillings, also suggesting the existence of prevailing reducing conditions. Pyrite is only absent in water conductive fractures in the upper 10 metres, probably dissolved during intrusion events of oxygenated fluids, but the amount of data from the upper part of the bedrock is limited. Moreover, the reducing effect of organic matter decay in the marine sediments above the SFR should be clarified by further studies. The extent and thickness of those sediments are rather heterogeneous and on the northern side of the pier there are areas with no, or only partial, sediment coverage. Thus, it is possible that marine waters may penetrate rapidly or, even infiltrate directly

into the bedrock fractures too quickly to allow the development of these reactions. Therefore, a more detailed study of the redox evolution of the intruding Baltic Sea waters and of the redox sensitive mineralogy in the upper part of the bedrock would be very recommendable.

Finally, the presence of iron hydroxides in water conductive zones down to about 500 m depth must be clarified. If they are truly iron hydroxides (difficult to distinguish macroscopically from iron oxides during routine drillcore mapping) they would indicate the presence of probably past oxidising events that have been detected only down to ~110 m in the PLU and Laxemar-Simpevarp areas. A better characterisation of these phases therefore is needed.

7 References

SKB's (Svensk Kärnbränslehantering AB) publications can be found at www.skb.se/publications.

Anderson C R, Pedersen K, 2003. In situ growth of Gallionella biofilms and partitioning of lanthanids and actinides between biological material and ferric oxyhydroxides. *Geobiology*, 1, pp 169–178.

Anderson C R, James R E, Chi Fru E, Kennedy C B, Pedersen K, 2006. In situ ecological development of a bacteriogenic iron oxide-producing microbial community from a subsurface granitic rock environment. *Geobiology*, 4, pp 29–42.

Appelo C A J, Postma D, 2005. *Geochemistry, groundwater and pollution*. 2nd ed. Rotterdam: Balkema.

Auqué L F, Gimeno M J, Gómez J, Nilsson A-C, 2008. Potentiometrically measured Eh in groundwaters from the Scandinavian Shield. *Applied Geochemistry*, 23, pp 1820–1833.

Ball J W, Nordstrom D K, 2001. User's manual for WATEQ4F, with revised thermodynamic data base and test cases for calculating speciation of major, trace, and redox elements in natural waters. Open File Report 91-183, U.S. Geological Survey, Denver, Colorado.

Banwart S A, 1999. Reduction of iron (III) minerals by natural organic matter in groundwater. *Geochimica et Cosmochimica Acta*, 63, pp 2919–2928.

Bath A, Hermansson H-P, 2006. Variability and uncertainties of key hydrochemical parameters for SKB sites. SKI Report 2007:03, Statens kärnkraftinspektion (Swedish Nuclear Power Inspectorate).

Benning L G, Wilkin R T, Barnes H L, 2000. Reaction pathways in the Fe-S system below 100°C. *Chemical Geology*, 167, pp 25–51.

Berner R A, 1981. A new geochemical classification of sedimentary environments. *Journal of Sedimentary Petrology*, 51, pp 359–365.

Burke I T, Kemp A E S, 2002. Microfabric analysis of Mn-carbonate laminae deposition and Mn-sulfide formation in the Gotland Deep, Baltic Sea. *Geochimica et Cosmochimica Acta*, 66, pp 1589–1600.

Canfield D E, 1989. Reactive iron in sediments. *Geochimica et Cosmochimica Acta*, 53, pp 619–632.

Canfield D E, Raiswell R, Bottrell S H, 1992. The reactivity of sedimentary iron minerals toward sulfide. *American Journal of Science*, 292, pp 659–683.

Carman R, Rahm L, 1997. Early diagenesis and chemical characteristics of interstitial waters and sediments in the deep deposition bottoms of the Baltic Proper. *Journal of Sea Research*, 37, pp 25–47.

Chae G-T, Yun S-T, Mayer B, Kim K-H, Kim S-Y, Kwon J-S, Kim K, Koh Y-K, 2007. Fluorine geochemistry in bedrock groundwater of South Korea. *Science of the Total Environment*, 385, pp 272–283.

Chapelle F H, 2001. *Ground-water microbiology and geochemistry*. 2nd ed. New York: Wiley.

Chen W-F, Liu T-K, 2005. Ion activity products of iron sulfides in groundwaters: implications from the Choshui fan-delta, Western Taiwan. *Geochimica et Cosmochimica Acta*, 69, pp 3535–3544.

Christensen T H, Bjerg P L, Banwart S A, Jakobsen R, Heron G, Albrechtsen H-J, 2000. Characterization of redox conditions in groundwater contaminant plumes. *Journal of Contaminant Hydrology*, 45, pp 165–241.

Clark I D, Fritz P, 1997. *Environmental isotopes in hydrogeology*. Boca Raton, FL: Lewis Publishers.

Curtis P, Markström I, Petersson J, Triumf C-A, Isaksson H, Mattson H, 2010. Site investigation SFR. Bedrock geology. SKB R-10-49, Svensk Kärnbränslehantering AB.

Dideriksen K, Christiansen B C, Baker J A, Frandsen C, Balic-Zunic T, Tullborg E-L, Mørup S, Stipp S L S, 2007. Fe-oxide fracture fillings as a palæo-redox indicator: structure, crystal form and Fe isotope composition. *Chemical Geology*, 244, pp 330–343.

Dideriksen K, Christiansen B C, Frandsen C, Balic-Zunic T, Mørup S, Stipp S L S, 2010. Paleoredox boundaries in fractured granite. *Geochimica et Cosmochimica Acta*, 74, pp 2866–2880.

- Deutsch W J, 1997.** Groundwater geochemistry: fundamentals and applications to contamination. Boca Raton, FL: Lewis.
- Drake H, Tullborg E-L, 2009.** Fracture mineralogy Laxemar. Site descriptive modelling, SDM-Site Laxemar. SKB R-08-99, Svensk Kärnbränslehantering AB.
- Drake H, Sandström B, Tullborg E-L, 2006.** Mineralogy and geochemistry of rocks and fracture fillings from Forsmark and Oskarshamn: Compilation of data for SR-Can. SKB R-06-109, Svensk Kärnbränslehantering AB.
- Drake H, Tullborg E-L, Annersten H, 2008.** Red-staining of the wall rock and its influence on the reducing capacity around water conducting fractures. *Applied Geochemistry*, 23, pp 1898–1920.
- Drake H, Tullborg E-L, MacKenzie A B, 2009.** Detecting the near-surface redox front in crystalline bedrock using fracture mineral distribution, geochemistry and U-series disequilibrium. *Applied Geochemistry*, 24, pp 1023–1039.
- Drever J I, 1997.** The Geochemistry of natural waters: surface and groundwater environments. 3rd ed. Upper Saddle River, NJ: Prentice Hall.
- Drew M C, 1983.** Plant injury and adaptation to oxygen deficiency in the root environment: a review. *Plant and Soil*, 75, pp 179–199.
- Döse C, 2009.** Site investigation SFR. Boremap mapping of percussion drilled boreholes HFR101, HFR102 and HFR105 and core drilled borehole KFR27 (down to 147.4 m length). SKB P-09-37, Svensk Kärnbränslehantering AB.
- Döse C, Stråhle A, Mattsson K J, Carlsten S, 2009a.** Site investigation SFR. Boremap mapping of core drilled borehole KFR101. SKB P-09-36, Svensk Kärnbränslehantering AB.
- Döse C, Winell S, Stråhle A, Carlsten S, 2009b.** Site Investigation SFR. Boremap mapping of core drilled boreholes KFR102B and KFR103. SKB P-09-38, Svensk Kärnbränslehantering AB.
- Ferris F G, Konhauser K O, Lyvén B, Pedersen K, 1999.** Accumulation of metals by bacteriogenic iron oxides in a subterranean environment. *Geomicrobiology Journal*, 16, pp 181–192.
- Gascoyne M, 2004.** Hydrogeochemistry, groundwater ages and sources of salts in a granitic batholith on the Canadian Shield, southeastern Manitoba. *Applied Geochemistry*, 19, pp 519–560.
- Gershenfeld N, 1999.** The nature of mathematical modeling. Cambridge: Cambridge University Press.
- Gimeno M J, Auqué L F, Gómez J, 2004a.** Explorative analysis and mass balance modelling. In: Laaksoharju M, (ed). Hydrogeochemical evaluation of the Simpevarp area, model version 1.1. SKB R-04-16, Svensk Kärnbränslehantering AB, pp 121–164.
- Gimeno M J, Auqué L F, Gómez J 2004b.** Explorative analysis and mass balance modelling. In: Laaksoharju M (ed). Hydrogeochemical evaluation of the Forsmark site, model version 1.1. SKB R-04-05, Svensk Kärnbränslehantering AB, pp 113–160.
- Gimeno M J, Auqué L F, Gómez J, 2006.** PHREEQC modelling. In: Hydrogeochemical evaluation. Preliminary site description. Laxemar subarea, version 2.1. SKB R-06-70, Svensk Kärnbränslehantering AB, pp 175–210.
- Gimeno M J, Auqué L F, Gómez J, 2007.** Chemnet's issue report, Forsmark area version 2.1, UZ/SKB/06/02 – Internal report. In: Hydrogeochemical evaluation of the Forsmark site, modelling stage 2.1 – issue report. SKB R-06-69, Svensk Kärnbränslehantering AB, pp 131–187.
- Gimeno M J, Auqué L F, Gómez J, Acero P, 2008.** Water-rock interaction modelling and uncertainties of mixing modelling. SDM-Site Forsmark. SKB R-08-86, Svensk Kärnbränslehantering AB.
- Gimeno M J, Auqué L F, Gómez J, Acero P, 2009.** Water-rock interaction modelling and uncertainties of mixing modelling. Site descriptive modelling, SDM-Site Laxemar. SKB R-08-110, Svensk Kärnbränslehantering AB.
- Glynn P D, Voss C I, 1999.** SITE-94. Geochemical characterization of Simpevarp ground waters near the Äspö Hard Rock laboratory. SKI Report 96-29, Statens kärnkraftinspektion (Swedish Nuclear Power Inspectorate).

- Gómez J B, Laaksoharju M, Skårman E, Gurban I, 2006.** M3 version 3.0: Concepts, methods and mathematical formulation. SKB TR-06-27, Svensk Kärnbränslehantering AB.
- Gómez J B, Laaksoharju M, Skårman E, Gurban I, 2009.** M3 version 3.0: Verification and validation. SKB TR-09-05, Svensk Kärnbränslehantering AB.
- Grenthe I, Stumm W, Laaksoharju M, Nilsson A-C, Wikberg P, 1992.** Redox potentials and redox reactions in deep groundwater systems. *Chemical Geology*, 98, pp 131–150.
- Gustavsson E, Jönsson S, Ludvigson J-E, 2006.** Forsmark site investigation. Pumping tests and flow logging. Boreholes HFM33, HFM34 and HFM35. SKB P-06-193, Svensk Kärnbränslehantering AB.
- Hallbeck L, Pedersen K, 2008a.** Explorative analysis of microbes, colloids and gases. SDM-Site Forsmark. SKB R-08-85, Svensk Kärnbränslehantering AB.
- Hallbeck L, Pedersen K, 2008b.** Explorative analysis of microbes, colloids and gases. Site description model, SDM-Site Laxemar. SKB R-08-109, Svensk Kärnbränslehantering AB.
- Hallberg G R, Keeney D R, 1993.** Nitrate. In: Alley W M (ed). *Regional ground-water quality*. New York: Van Nostrand Reinhold, pp 297–322.
- Heimann A, Jakobsen R, Blodau C, 2010.** Energetic constraints on H₂-dependent terminal electron accepting processes in anoxic environments: a review of observations and model approaches. *Environmental Science & Technology*, 44, pp 24–33.
- Hem J D, 1985.** Study and interpretation of the chemical characteristics of natural water. Water-Supply Paper 2254, U.S. Geological Survey.
- Hoehler T M, Alperin M J, Albert D B, Martens C S, 1998.** Thermodynamic control on hydrogen concentrations in anoxic sediments. *Geochimica et Cosmochimica Acta*, 62, pp 1745–1756.
- Iwatsuki T, Furue R, Mie H, Ioka S, Mizuno T, 2005.** Hydrochemical baseline condition of groundwater at the Mizunami underground research laboratory (MIU). *Applied Geochemistry*, 20, pp 2283–2302.
- Jakobsen R, Cold L, 2007.** Geochemistry at the sulfate reduction–methanogenesis transition zone in an anoxic aquifer: a partial equilibrium interpretation using 2D reactive transport modeling. *Geochimica et Cosmochimica Acta*, 71, pp 1949–1966.
- Jensen D L, Boddum J K, Tjell J C, Christensen T H, 2002.** The solubility of rhodochrosite (MnCO₃) and siderite (FeCO₃) in anaerobic aquatic environments. *Applied Geochemistry*, 17, pp 503–511.
- Jönsson S, Harrström J, Ludvigson J-E, Nilsson A-C, 2008.** Site investigation SFR. Hydraulic tests, flow logging and hydrochemical sampling. Boreholes HFR101, HFR102 and HFR105. SKB P-08-87, Svensk Kärnbränslehantering AB.
- Kehew A E, 2001.** *Applied chemical hydrogeology*. Upper Saddle River, NJ: Prentice Hall.
- Konhauser K, 2007.** *Introduction to geomicrobiology*. Oxford: Blackwell Publishing.
- Konovalov S K, Luther G W, Mustafa Y, 2007.** Porewater redox species and processes in the Black Sea sediments. *Chemical Geology*, 245, pp 254–274.
- Kulik D A, Kersten M, Heiser U, Neumann T, 2000.** Application of Gibbs energy minimization to model early-diagenetic solid-solution aqueous-solution equilibria involving authigenic rhodochrosites in anoxic Baltic Sea sediments. *Aquatic Geochemistry*, 6, pp 147–199.
- Kölling M, 2000.** Comparison of different methods for redox potential determination in natural waters. In: Schüring L, Schulz H D, Fischer W R, Böttcher J, Duijnisveld W H M (eds). *Redox: fundamentals, processes and applications*. Berlin: Springer, pp 42–54.
- Laaksoharju M, Wallin B (eds), 1997.** Evolution of the groundwater chemistry at the Äspö Hard Rock Laboratory. Proceedings of the second Äspö International Geochemistry Workshop, Äspö, Sweden, June 6–7, 1995. SKB ICR-97-04. Svensk Kärnbränslehantering AB.
- Laaksoharju M, Skårman C, Skårman E, 1999.** Multivariate mixing and mass-balance (M3) calculations, a new tool for decoding hydrogeochemical information. *Applied Geochemistry*, 14, pp 861–871.

- Laaksoharju M, Smellie J, Tullborg E-L, Gimeno M, Hallbek L, Molinero J, Waber N, 2008.** Bedrock hydrogeochemistry Forsmark. Site descriptive modeling, SDM-Site Forsmark. SKB R-08-47, Svensk Kärnbränslehantering AB.
- Laaksoharju M, Smellie J, Tullborg E-L, Wallin B, Drake H, Gascoyne M, Gimeno M, Gurban I, Hallbeck L, Molinero J, Nilsson A-C, Waber N, 2009a.** Bedrock hydrogeochemistry, Laxemar. Site descriptive modelling. SDM-Site Laxemar. SKB R-08-93, Svensk Kärnbränslehantering AB.
- Laaksoharju M, Gimeno M, Auqué L F, Gómez J B, Acero P, Pedersen K, 2009b.** Hydrogeochemical and microbiological effects on fractures in the Excavation Damaged Zone (EDZ). SKB R-09-05, Svensk Kärnbränslehantering AB.
- Langmuir D, 1997.** Aqueous environmental geochemistry. Upper Saddle River, NJ: Prentice Hall.
- Langmuir D, Melchior D, 1985.** The geochemistry of Ca, Sr, Ba and Ra sulfates in some deep brines from the Palo Duro Basin, Texas. *Geochimica et Cosmochimica Acta*, 49, pp 2423–2432.
- Lin L-H, Slater G F, Sherwood Lollar B, Lacrampe-Couloume G, Onstott T C, 2005.** The yield and isotopic composition of radiolytic H₂, a potential energy source for the deep subsurface biosphere. *Geochimica et Cosmochimica Acta*, 69, pp 893–903.
- Lindberg R D, Runnells D D, 1984.** Ground water redox reactions: an analysis of equilibrium state applied to Eh measurements and geochemical modeling. *Science*, 22, pp 925–927.
- Lindquist A, Nilsson K, 2010.** Site investigation SFR. Hydrochemical characterisation of groundwater in borehole KFR105. Results from five investigated borehole sections. SKB P-10-02, Svensk Kärnbränslehantering AB.
- Lovley D R, Goodwin S, 1988.** Hydrogen concentrations as an indicator of the predominant terminal electron-accepting reactions in aquatic sediments. *Geochimica et Cosmochimica Acta*, 52, pp 2993–3003.
- Lundin L, Lode E, Stendahl J, Melkerud P-A, Björkvald L, Thorstensson A, 2004.** Soils and site types in the Forsmark area. SKB R-04-08, Svensk Kärnbränslehantering AB.
- Luukkonen A, Pitkänen P, Partamies S, 2004.** Significance and estimations of lifetime of natural fracture mineral buffers in the Olkiluoto bedrock. Posiva Working Report 2004-08, Posiva Oy, Finland.
- Martinez R E, Pedersen K, Ferris F G, 2004.** Cadmium complexation by bacterogenic iron oxides from subterranean environment. *Journal of Colloid and Interface Science*, 275, pp 82–89.
- McKenzie F T, Garrels R M, Bricker O P, Bickley F, 1967.** Silica in sea water: control by silica minerals. *Science*, 155, pp 1404–1405.
- Molinero-Huguet J, Samper-Calvete F J, Zhang G, Yang C, 2004.** Biogeochemical reactive transport model of the redox zone experiment of the Äspö Hard Rock Laboratory in Sweden. *Nuclear Technology*, 148, pp 151–165.
- Neumann T, Heiser U, Leosson M A, Kersten M, 2002.** Early diagenetic processes during Mn-carbonate formation: evidence from the isotopic composition of authigenic Ca-rhodochrosites of the Baltic Sea. *Geochimica et Cosmochimica Acta*, 66, pp 867–879.
- Nilsson A-C, 2009.** Site investigation SFR. Presentation and evaluation of hydrogeochemical data from SFR-boreholes, 1984–2007. SKB P-09-45, Svensk Kärnbränslehantering AB.
- Nilsson A-C, Tullborg E-L, Smellie J, 2010.** Preliminary hydrogeochemical site description SFR (version 0.2). SKB R-10-38, Svensk Kärnbränslehantering AB.
- Nilsson A-C, Tullborg E-L, Smellie J, Gimeno M J, Gómez J, Auqué L, Sandström B, Pedersen K, 2011.** Site investigation SFR. Bedrock hydrogeochemistry. Site descriptive modelling. SKB R-11-06, Svensk Kärnbränslehantering AB.
- Nilsson K, 2011.** Site investigation SFR. Hydrochemical characterisation of groundwater in the SFR repository. Sampling and analysis during 2010. Extended investigations in KFR7A: 48.0 to 74.7 m, KFR08: 63.0 to 104.0 m and KFR19: 95.0 to 110.0 m. SKB P-11-14, Svensk Kärnbränslehantering AB.
- Nordstrom D K, 2005.** Modeling low-temperature geochemical processes. In: Drever J I (ed). *Surface and ground waters, weathering, and soils*. Amsterdam: Elsevier. (Treatise on Geochemistry 5), pp 37–72.

- Nordstrom D K, Jenne E A, 1977.** Fluoride solubility in selected geothermal waters. *Geochimica et Cosmochimica Acta*, 41, pp 175–188.
- Nordstrom D K, Munoz J L, 1986.** *Geochemical thermodynamics*. Palo Alto, CA: Blackwell Scientific Publications.
- Nordstrom D K, Puigdomenech I, 1986.** Redox chemistry of deep groundwaters in Sweden. SKB TR 86-03, Svensk Kärnbränslehantering AB.
- Nordstrom D K, Ball J W, Donahoe R J, Whittemore D, 1989.** Groundwater chemistry and water-rock interactions at Stripa. *Geochimica et Cosmochimica Acta*, 53, pp 1727–1740.
- Nordstrom D K, Plummer L N, Langmuir D, Busenberg E, May H M, Jones B F, Parkhurst D, 1990.** Revised chemical equilibrium data for major water-mineral reactions and their limitations. In: Melchior D C, Basset R L (eds). *Chemical modeling of aqueous systems II*. Washington: American Chemical Society. (ACS Symposium Series 416), pp 398–413.
- Parkhurst D L, Appelo C A J, 1999.** User's guide to PHREEQC (version 2): a computer program for speciation, batch-reaction, one-dimensional transport, and inverse geochemical calculations. Water-Resources Investigations Report 99-4259, U.S. Geological Survey, Denver, Colorado.
- Pedersen K, 2006.** Microbiology of transitional groundwater of the porous overburden and underlying fractured bedrock aquifers in Olkiluoto, Finland. Posiva Working Report 2006-09, Posiva Oy, Finland.
- Pedersen K, 2008.** Microbiology of Olkiluoto groundwater. 2004–2006. Posiva 2008-02, Posiva Oy, Finland.
- Pitkänen P, Partamies S, 2007.** Origin and implications of dissolved gases in groundwater at Olkiluoto. Posiva 2007-04, Posiva Oy, Finland.
- Pitkänen P, Luukkonen A, Ruotsalainen P, Leino-Forsman H, Vuorinen U, 1999.** Geochemical modelling of groundwater evolution and residence time at the Olkiluoto site. Posiva 98-10, Posiva Oy, Finland.
- Pitkänen P, Partamies S, Luukkonen A, 2004.** Hydrogeochemical interpretation of baseline groundwater conditions at the Olkiluoto site. Posiva 2003-07, Posiva Oy, Finland.
- Postma D, 1985.** Concentration of Mn and separation from Fe in sediments. I. Kinetics and stoichiometry of the reaction between birnessite and dissolved Fe(II) at 10°C. *Geochimica et Cosmochimica Acta*, 49, pp 1023–1033.
- Poulton S W, Krom M D, Raiswell R, 2004.** A revised scheme for the reactivity of iron (oxyhydr)oxide minerals towards dissolved sulfide. *Geochimica et Cosmochimica Acta*, 68, pp 3703–3715.
- Rickard D T, 1995.** Kinetics of FeS precipitation. Part 1. Competing reaction mechanisms. *Geochimica et Cosmochimica Acta*, 59, pp 4367–4379.
- Rickard D T, 2006.** The solubility of FeS. *Geochimica et Cosmochimica Acta*, 70, pp 5779–5789.
- Rickard D T, Luther G W, 2007.** Chemistry of iron sulfides. *Chemical Review*, 107, pp 514–562.
- Rivett M O, Buss S R, Morgan P, Smith J W N, Bemmen C D, 2008.** Nitrate attenuation in groundwater: a review of biogeochemical controlling processes. *Water Research*, 42, pp 4215–4232.
- Sandström B, Tullborg E-L, 2009.** Episodic fluid migration in the Fennoscandian Shield recorded by stable isotopes, rare earth elements and fluid inclusions in fracture minerals at Forsmark, Sweden. *Chemical Geology*, 266, pp 135–151.
- Sandström B, Tullborg E-L, 2011.** Site investigation SFR. Fracture mineralogy and geochemistry of borehole sections sampled for groundwater chemistry and Eh. Results from boreholes KFR01, KFR08, KFR10, KFR19, KFR7A and KFR105. SKB P-11-01, Svensk Kärnbränslehantering AB.
- Sandström B, Tullborg E-L, Smellie J, MacKenzie A B, Sukki J, 2008.** Fracture mineralogy of the Forsmark site. SDM-Site Forsmark. SKB R-08-102, Svensk Kärnbränslehantering AB.
- Sasamoto H, Yui M, Arthur R C, 2007.** Estimation of in situ groundwater chemistry using geochemical modeling: a test case for saline type groundwater in argillaceous rock. *Physics and Chemistry of the Earth*, 32, pp 196–208.

- Silver W L, Lugo A E, Keller M, 1999.** Soil oxygen availability and biogeochemistry along rainfall and topographic gradients in upland wet tropical forest soils. *Biogeochemistry*, 44, pp 301–328.
- SKB, 2001.** Site investigations. Investigation methods and general execution programme. SKB TR-01-29, Svensk Kärnbränslehantering AB.
- SKB, 2005.** Preliminary site description. Forsmark area – version 1.2. SKB R-05-18, Svensk Kärnbränslehantering AB.
- SKB, 2006.** Site descriptive modelling. Forsmark stage 2.1. Feedback for completion of the site investigation including input from safety assessment and repository engineering. SKB R-06-38, Svensk Kärnbränslehantering AB.
- SKB, 2008.** Geovetenskapligt undersökningsprogram för utbyggnad av SFR. SKB R-08-67, Svensk Kärnbränslehantering AB. (In Swedish.)
- Smellie J, Tullborg E-L, Nilsson A-C, Sandström B, Waber N, Gimeno M, Gascoyne M, 2008.** Explorative analysis of major components and isotopes. SDM-Site Forsmark. SKB R-08-84, Svensk Kärnbränslehantering AB.
- Stefánsson A, Arnórsson S, Sveinbjörnsdóttir A E, 2005.** Redox reactions and potentials in natural waters at disequilibrium. *Chemical Geology*, 221, pp 289–311.
- Stotler R L, Frappe S K, Ruskeeniemi T, Ahonen L, Onstott T C, Hobbs M Y, 2009.** Hydrogeochemistry of groundwaters in and below the base of thick permafrost at Lupin, Nunavut, Canada. *Journal of Hydrology*, 373, pp 80–95.
- Thorstenson D C, 1984.** The concept of electron activity and its relation to redox potentials in aqueous geochemical systems. Open File Report 84-072, U.S. Geological Survey, Denver, Colorado.
- Thorstenson D C, Fisher D W, Croft M G, 1979.** The geochemistry of the Fox Hills-Basal Hell Creek aquifer in Southwestern North Dakota and Northwestern South Dakota. *Water Resources Research*, 15, pp 1479–1498.
- Thur P, Nilsson K, 2009a.** Site investigation SFR. Hydrogeochemical characterisation of groundwater in borehole KFR101 and results from water sampling and analyses in boreholes KFR02, KFR7A, KFR08 and KFR56. Sampling during winter 2008–2009. SKB P-09-53, Svensk Kärnbränslehantering AB.
- Thur P, Nilsson K, 2009b.** Site investigation SFR. Hydrogeochemical characterisation of groundwater in borehole KFR102A. Results from water sampling and analyses during March 2009. SKB P-09-50, Svensk Kärnbränslehantering AB.
- Thur P, Jönsson S, Harrström J, Ludvigson J-E, 2009.** Site investigation SFR. Hydraulic tests, flow logging and chemical sampling. Borehole HFR106. SKB P-09-54, Svensk Kärnbränslehantering AB.
- Trotignon L, Michaud V, Lartigue J-E, Ambrosi J-P, Eisenlohr L, Griffault L, de Combarieu M, Daumas S, 2002.** Laboratory simulation of an oxidizing perturbation in a deep granite environment. *Geochimica et Cosmochimica Acta*, 66, pp 2583–2601.
- Tröjbom M, Söderbäck B, 2006.** Chemical characteristics of surface systems in the Forsmark area. Visualisation and statistical evaluation of data from surface water, precipitation, shallow groundwater, and regolith. SKB R-06-18, Svensk Kärnbränslehantering AB.
- Tullborg E-L, Smellie J, Nilsson A-C, Gimeno M J, Auqué L F, Brüchert V, Molinero J, 2010.** SR-Site – sulphide content in the groundwater at Forsmark. SKB TR-10-39, Svensk Kärnbränslehantering AB.
- Van Cappellen P, Wang Y. 1996.** Biogeochemical dynamics in aquatic systems. In: Lichtner P C, Steefel C I, Oelkers E H (eds). *Reactive transport in porous media*. Washington, DC: Mineralogical Society of America. (Reviews in Mineralogy 34), pp 335–376.
- Wilkin R T, Barnes H L, 1997.** Pyrite formation by reactions of iron monosulfides with dissolved inorganic and organic sulfur species. *Geochimica et Cosmochimica Acta*, 60, pp 4167–4179.
- Winell S, 2009.** Site investigation SFR. Boremap mapping of core drilled borehole KFR105. SKB P-09-59, Svensk Kärnbränslehantering AB.

- Winell S, Carlsten S, Stråhle A, 2009a.** Site investigation SFR Boremap mapping of core drilled borehole KFR102A. SKB P-09-52, Svensk Kärnbränslehantering AB.
- Winell S, Döse C, Stråhle A, Carlsten S, Selnert E, 2009b.** Site investigation SFR. Boremap mapping of core drilled boreholes KFR104 and KFR27 (from 147.5 m). SKB P-09-39, Svensk Kärnbränslehantering AB.
- Wolthers M, Van der Gaast S J, Rickard D, 2003.** The structure of disordered mackinawite. *American Mineralogists*, 88, pp 2007–2015.
- Wolthers M, Charlet L, van der Linde P R, Rickard D, van der Weidjen C H, 2005.** Surface chemistry of disordered mackinawite (FeS). *Geochimica et Cosmochimica Acta*, 69, pp 3469–3481.
- Yao W, Millero F J, 1993.** The rate of sulfide oxidation by δMnO_2 in seawater. *Geochimica et Cosmochimica Acta*, 57, pp 3359–3365.
- Öhman J, Bockgård N, Follin S, 2011.** Site Investigation SFR. Hydrogeological modelling of SFR. Data review and parameterisation. SKB R-11-03, Svensk Kärnbränslehantering AB.

Searching for suitable compositions of the Baltic and the Old Meteoric end members

M3's End-member Variability Module (Gómez et al. 2006) has been used to find the most suitable composition of two of the end members used in the M3 calculations performed for the SFR. These end members are the Baltic and the Old Meteoric. In the first case, with more than 50 samples of the Baltic Sea available, the most appropriate to be used as end member for the set of samples under study was identified. In the second case, the lack of a measured chemical composition for this kind of waters made the use of a theoretical water necessary. However, the inconclusive results obtained when using this end member together with the other four, led to the possibility to trying to find a more suitable composition for this end member.

What follows is a brief summary of the procedure followed using the End-member Variability Module (implemented in M3), which is based on a Monte Carlo sampling of the compositional space in search of the global minimum of the deviations with respect to the conservative elements.

A1.1 Composition of the Baltic end member

Two different Baltic Sea end-member waters are used in this study. One is an average Baltic Sea water, as defined by Pitkänen et al. (2004); its composition is clearly defined and thus it can be considered as unique. The other Baltic Sea end member is a local sea water from the vicinity of the SFR facilities. More than 50 samples of the Baltic Sea around SFR (sampled during the PLU investigation) were included in the SFR groundwaters dataset to add all the possible geochemical information about these local waters and check their effect on the studied system. The high number of samples and their variability introduced the problem of selecting the most appropriate sample to be used as the local Baltic Sea end member. The procedure followed is presented below.

- 1. Select the compositional range of each end member.** Besides the number of end members, the site investigation should also give an initial guess at the compositional range of each end member. For the local Baltic end member these ranges are listed in Table A1-1; the other end members have a fixed composition. The name "BalL" should be understood as a label attached to the end member, and not as a particular water with a known chemical composition. The final composition of the BalL end member will be given by the procedure itself.

Table A1-1. Initial compositional range of the Baltic Sea end member.

Element	Min value	Max value
Na (mg/L)	1,340.0	1,560.0
K (mg/L)	48.6	63.1
Ca (mg/L)	66.6	79.6
Mg (mg/L)	162.0	189.0
HCO ₃ (mg/L)	70.0	192.0
Cl (mg/L)	2,464.7	2,850.0
SO ₄ (mg/L)	196.0	423.0
Br (mg/L)	7.71	16.4
δ ² H (‰ dev)	-72.5	-58.3
δ ¹⁸ O (‰ dev)	-8.5	-7.6
Tr (TU)	10.6	120.7

- 2. Randomly choose, for each input compositional variable in each end member, a concentration within the range.** It is important to stress here that this selection is completely random and that no correlation between variables is included. A particular, randomly selected, composition of an end member could be absurd from a geochemical point of view. Actually, the *most* randomly selected compositions would be geochemically absurd and the procedure itself would filter them out due to their inherent large residuals.

3. **Perform the PCA on the whole dataset and the randomly chosen composition of the end members, and compute the mixing proportions of each sample.** The code M3 is used for that purpose. Mixing proportions are computed using the information stored in all principal components (Gómez et al. 2008). Following this step a table similar to that in Appendix 2 is obtained, where each sample has either a set of mixing proportions or is blank. Blank samples can not be explained by pure mixing of the chosen end members.
4. **Compute d , the difference between the real and the calculated concentration of each conservative element in each sample.** Calculated concentrations are obtained from the mixing proportions. For example, the Cl concentration in sample i is:

$$Cl_{i,calc} = \%DS_i \times Cl_{DS} + \%Gl_i \times Cl_{Gl} + \%Lit_i \times Cl_{Lit} + \%BaL_i \times Cl_{BaL}.$$

From there, it is straightforward to compute d :

$$d_{i,Cl} = Cl_{i,real} - Cl_{i,calc},$$

and the same for the other of conservative elements (Cl, SO₄, ²H, and ¹⁸O in this case):

$$d_{i,SO4} = SO4_{i,real} - SO4_{i,calc},$$

$$d_{i,2H} = {}^2H_{i,real} - {}^2H_{i,calc},$$

$$d_{i,18O} = {}^{18}O_{i,real} - {}^{18}O_{i,calc}.$$

5. **For the whole dataset, compute Δ_k , the total deviation of the conservative element k .** In other words, each sample's deviation d_i is squared and divided by the measured concentration. The result for each sample is added together and then normalised by the number of samples inside the mixing polyhedron, n :

$$\Delta_{Cl} = \frac{1}{n} \sum_{i=1}^n \frac{d_{i,Cl}^2}{Cl_{i,measured}},$$

$$\Delta_{SO4} = \frac{1}{n} \sum_{i=1}^n \frac{d_{i,SO4}^2}{SO4_{i,measured}},$$

$$\Delta_{2H} = \frac{1}{n} \sum_{i=1}^n \frac{d_{i,2H}^2}{{}^2H_{i,measured}},$$

$$\Delta_{18O} = \frac{1}{n} \sum_{i=1}^n \frac{d_{i,18O}^2}{{}^{18}O_{i,measured}}.$$

This is a chi-square statistics for a variable (the concentration of a conservative element) whose variance is proportional to its mean value (i.e. it is assumed that the concentrations are known with a fixed percent precision). As an example, if the Cl concentration of a sample is 6,000 mg/L, it is assumed that this value is known with an uncertainty of $\sqrt{6000} = 77$ mg/L; and if the Cl concentration is 20 mg/L, its associated uncertainty is $\sqrt{20} = 4.5$ mg/L. This is of course not the *analytical accuracy*, but the sum of all uncertainties, including conceptual ones as the non-constant end-member composition, or the uncertainty in the computed mixing proportions. The number of samples inside the mixing polyhedron, n , is also computed by M3 and output as *coverage* (Gómez et al. 2008).

6. **Repeat steps 5 to 8 usually up to several millions of times.** Each run is composed of five numbers; four Δ s and coverage. Coverage is not only important to compute Δ_k , but also to assess the quality of a particular composition of the end members. If the coverage is low, that means that few samples can be explained as a mixture of the chosen end members, irrespective of the value of the total deviations (think, for example, of a run that only explains 1% of the samples but these have low deviations; Δ_k would be low, but the chosen composition of the end members would be less satisfactory at explaining the dataset as a whole).
7. **Discard all runs with coverage below a critical value.** This value is system-dependent, but should always be close to the maximum coverage. In the present case, only runs with coverage > 97% have been retained.

8. Plot the contents of each conservative element in the Ball end member against the total deviation Δ_k for each run with coverage > 97%, Figure 4 shows graphically the results for the four conservative elements in the SFR dataset (Cl, SO₄, ²H and ¹⁸O).

Each dot in Figure A1-1 represents a different Monte Carlo run with coverage > 97%. The two green lines on each graph mark the input compositional range for each conservative element, and the red arrow points to the concentration for which the deviation is lowest. In other words, the concentration that gives the lowest discrepancy between the measured and calculated concentration for all samples in the dataset. Figure A1-1 shows that the best Cl concentration coincides with the minimum value of the input range (2,465 mg/L); and the best $\delta^2\text{H}$ value coincides with its maximum input value (-58‰). As for sulphate, the best value lies near the middle of the input range: 330 mg/L. Finally, for $\delta^{18}\text{O}$ no value inside the range is better than any other, meaning that the method is not sensitive to this element. However, because it is known that there is a rather good correlation between $\delta^{18}\text{O}$ and $\delta^2\text{H}$ values in groundwaters, from the value $\delta^2\text{H} = -58\text{‰}$, which coincides with the highest value in the input range, an approximate value for $\delta^{18}\text{O}$ of -7.8‰ can be selected, also close to the highest value of its input range.

This “synthetic” composition is plotted in Figure A1-2 together with the 52 Baltic Sea samples in the dataset. All three graphs have chloride in the horizontal axis, while the vertical axis shows the plots of the other three conservative elements (SO₄, $\delta^2\text{H}$, and $\delta^{18}\text{O}$). On each graph the three closest samples to the synthetic BallL composition are labelled. In total, six different samples form the nearest vicinity of BallL, whose compositions are listed in Table A1-2. Only one sample, sample #889, belongs to the nearest vicinity in the three graphs. Thus, ID sample #889¹⁸ is the most similar in composition to the synthetic composition calculated with the Monte Carlo method. Consequently, ID sample #889 has been selected as the BallL end member.

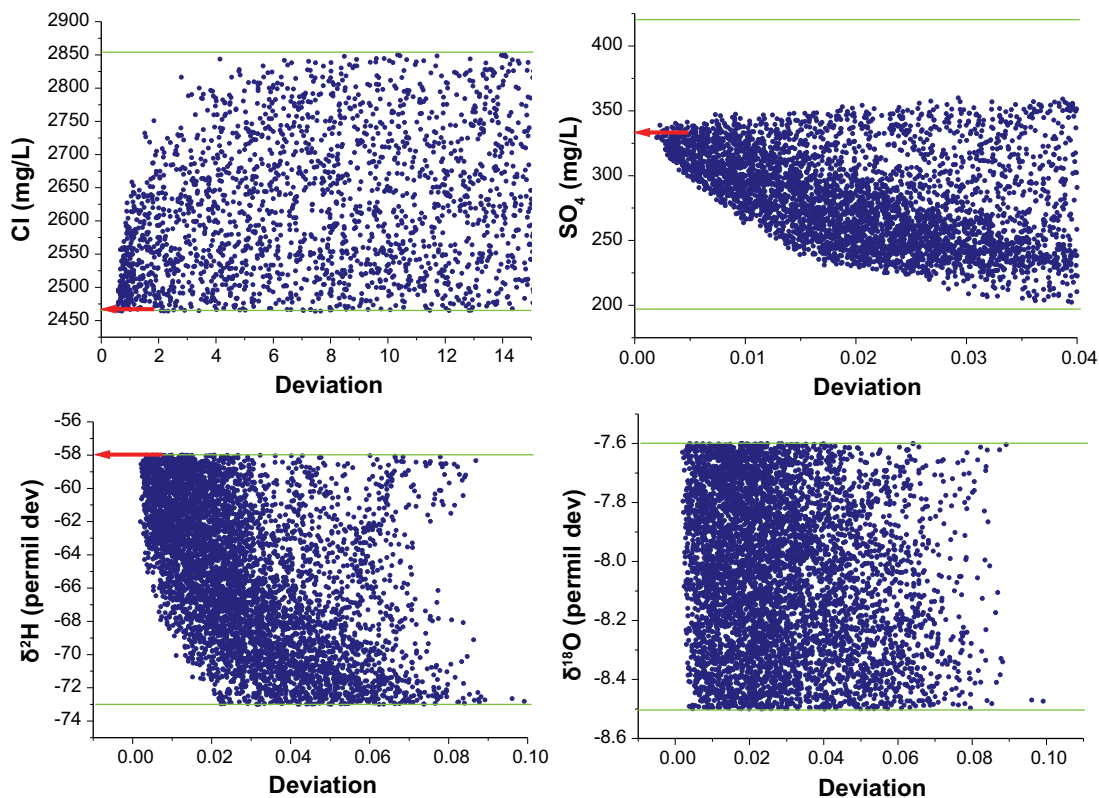


Figure A1-1. Concentration of the conservative elements Cl, SO₄, ²H and ¹⁸O in end member BallL as a function of the total deviation for the 5×10⁶ Monte Carlo runs. The lower the deviation the better at explaining the SFR dataset is the corresponding composition of the BallL end member. Green lines delimit the input range of compositions, while the red arrow points to the composition with the lowest deviation. Note that for oxygen-18 all compositions are equally probable.

¹⁸These numbers correspond to the ID number in the Excel table.

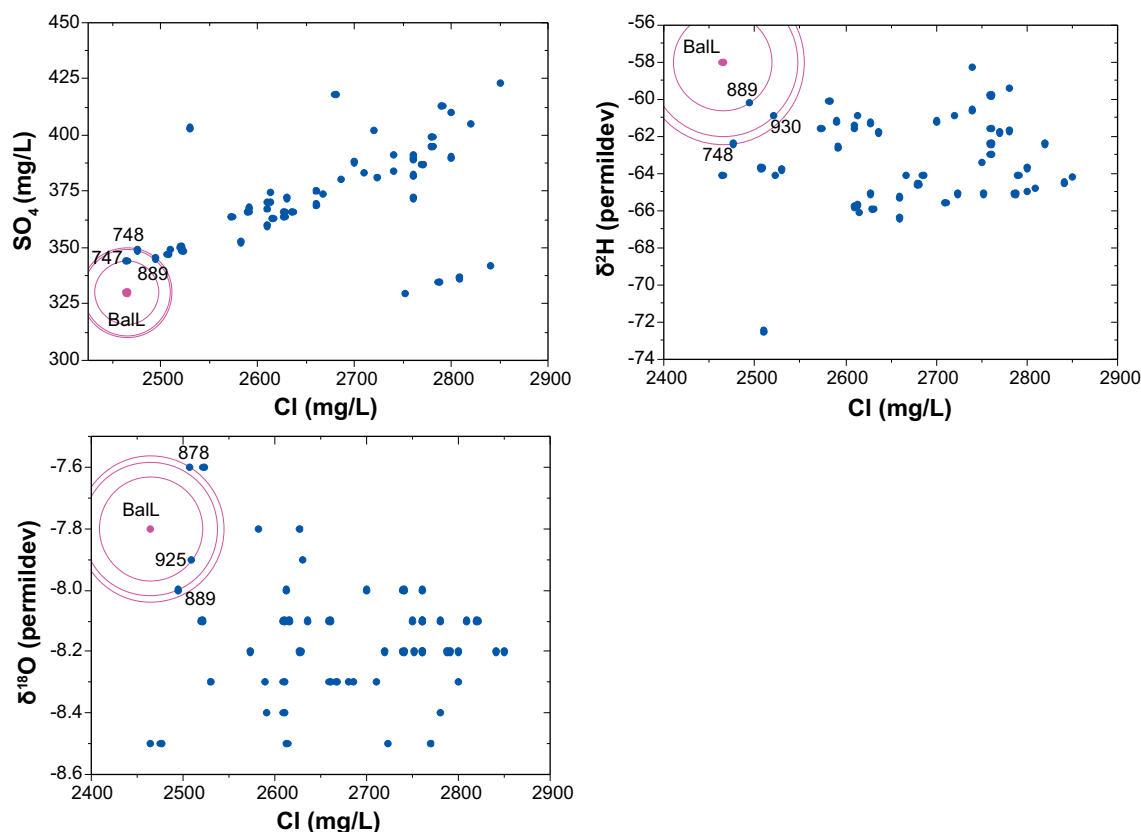


Figure A1-2. Chloride versus the other conservative elements for the 52 Baltic Sea samples in the dataset. The position of the “best” composition for the BalL end member is also shown, together with the distance to the three closest samples (concentric circles centred on the BalL composition).

Table A1-2. Composition of the synthetic BalL and of the most similar Baltic Sea samples.

ID Sample	IDcode	Sample Number #	Cl	SO ₄	δ ² H	δ ¹⁸ O
Ball			2,465.0	330.0	-58.0	-7.80
747	PFM000062	4229	2,464.7	343.93	-64.1	-8.50
748	PFM000062	4230	2,476.4	348.84	-62.4	-8.50
878	PFM000064	4196	2,507.5	347.03	-63.7	-7.60
889	PFM000064	4330	2,494.6	345.16	-60.2	-8.00
925	PFM000065	4212	2,509.5	349.28	-72.5	-7.90
930	PFM000065	4325	2,520.9	350.17	-60.9	-8.10

A2.2 Composition of the Old Meteoric end member

The question that needs to be answered here is: Can a new composition of the Old Meteoric end member be found that increases the coverage of the 5 end-member combination DS+GI+Lit+BalL+OM using the 5 conservative compositional variables Cl+Br+SO₄+²H+¹⁸O?

The procedure followed here is similar for the Baltic end member. Based on knowledge of the system and the experience gained from the site investigations in Forsmark, an initial compositional range for the conservative elements of the Old Meteoric end member was agreed on (Figure A1-3).

Using the ranges shown in Figure A1-3b for Cl, SO₄ and Br and enlarging the range for the isotopes (Figure A1-4a), a set of runs was performed and Figure A1-4b plots the Cl and SO₄ contents in the OM end member against the total deviation for each run with a coverage > 97%. As previously indicated, each dot in Figures A1-4b represents a different Monte Carlo run with coverage > 97%, that is, 97% of the samples are explained using that set of compositions for the end members.

Initial OM ranges		
Element	Min	Max
Cl (mg/L)	4	200
SO ₄ (mg/L)	3	100
Br (mg/L)	0.01	2
δ ² H (‰)	-86	-30
δ ¹⁸ O (‰)	-12	-5

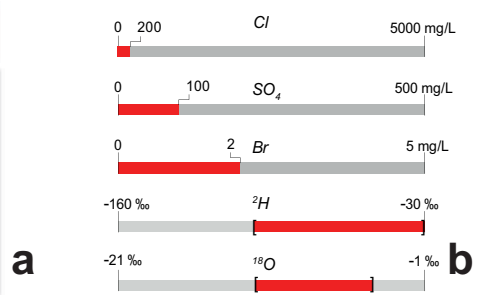


Figure A1-3. Initial compositional range for the conservative elements of the Old Meteoric end member from expert judgment.

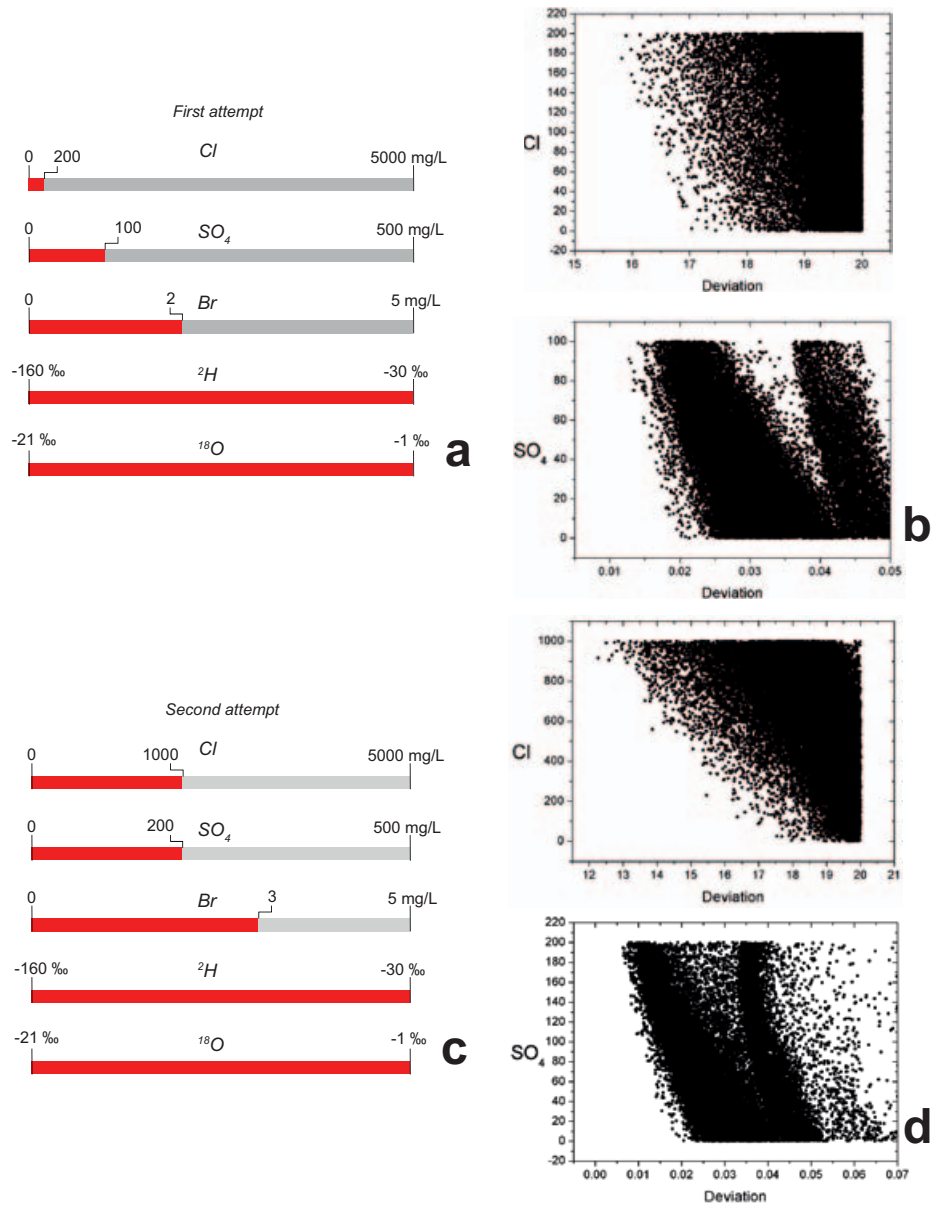


Figure A1-4. (a, c): Compositional ranges selected for the first and second attempt, respectively, for the conservative elements in the Old Meteoric end member; (b, d): Concentration of the conservative elements Cl and SO₄ in the OM end member as a function of the total deviation for the 5×10⁶ Monte Carlo runs in the first and second attempts (b and d, respectively). The lower the deviation the better at explaining the SFR dataset is the corresponding composition of the OM end member. However, none of them find a minimum in the deviation for Cl and SO₄, indicating that higher values of these variables could have been used.

Deviations in the x axis, and concentration of the elements in the y axis, are all in mg/L. It is clear from the plots that for some runs these deviations are quite low, that is, calculated concentrations are very close to the measured ones. However, the distribution of the dots indicate that even for the highest initial values considered for Cl and SO₄ (200 and 100 mg/L respectively), the cloud of dots still tend towards lower deviation values as these concentrations become higher. This suggests that increasing the upper concentration limit for Cl and SO₄ could lower the deviation. This was carried out in a second attempt (Figure A1-4c, d).

This time, the compositional ranges of the three conservative elements Cl, SO₄ and Br were increased to 1,000 mg/L, 300 mg/L and 3 mg/L, respectively (Figure A1-4c). The corresponding deviation plots for Cl and SO₄ are shown in Figure A1-4d. These graphs still show the same trend towards lower deviations as the concentration of Cl and SO₄ increases. So, a third set of runs with increased upper concentration limits was performed again.

This third attempt considered quite a broad compositional range for Cl and SO₄, up to 5,000 and 500 mg/L, respectively, and up to 5 mg/L for Br (Figure A1-5a). In this case, the deviation plots for Cl and SO₄ already include a minimum deviation for concentration values lower than the upper limit (Figure A1-5b).

The two red lines on each graph (Figure A1-5b) mark the compositional range for each conservative element for which the lowest deviations are obtained.

The final set of Monte Carlo runs consisted of fixing the values for Cl, SO₄ and Br (with values near the centre of the range of minimum deviation concentrations), and allowing only the isotopes to change in each run (Figure A1-6a). Figure A1-6b shows the deviation plots for the isotopes and showing all the runs with a coverage > 80% (different colour code). The red arrows point to the δ²H and δ¹⁸O values for which the deviation is lowest. In other words, those values that give the lowest discrepancy between the measured and calculated delta values for all samples in the dataset. Figure A1-6b shows that the best δ²H is -65 (‰ V-SMOW) and the best δ¹⁸O value -4‰. These values, although mathematically correct, are not reasonable from a hydrogeochemical point of view. This is shown in Figure A1-7.

Figure A1-7b plots the calculated delta values in a δ¹⁸O-δ²H graph. The graph also includes the meteoric water line (black line) and several pore water samples analysed in the PLU. Despite some theoretical values coinciding with the pore water samples (which is, in itself, a very interesting finding), in general, most Monte Carlo delta values are located in an area of very low δ²H and very high δ¹⁸O, more so for those runs with the highest coverages.

The graph also plots the location of the minimum-deviation Monte Carlo solution (δ¹⁸O = -4‰; δ²H = -65‰). As a compromise solution, a final composition as indicated in Figure A1-7a (similar to one of the porewater samples, as shown in Figure A1-7b) was taken as the optimal composition for the Old Meteoric end member. Note that the coverage of this “optimal” composition (90%) is not the maximum possible coverage (96%), but is close to it. In any case, this coverage is higher than that of the original OM end member (52%).

A new M3 mixing calculation was performed using the minimum-deviation Monte Carlo composition for the OM end member. The results are shown in Figure A1-8a, whereas Figure A1-8b shows the mixing proportions obtained with the original OM end member (Table 2-3).

Several observations should be made with respect to the “optimal” OM composition:

1. Chloride content has drastically increased in comparison with both the original OM value and the upper limit of the range shown in Figure A1-8b (which was fixed by expert judgment).
2. Sulphate has also increased, although not as drastically as chloride.
3. The isotopes of the new OM composition do not plot on the meteoric water line, but coincide with some of the pore waters sampled in Forsmark (see Figure A1-7b).
4. The Cl and SO₄ contents of the new OM composition are also similar to some of these pore waters.
5. This composition can thus be consistent with the OM having a close relationship with the pore waters stored in the bedrock.

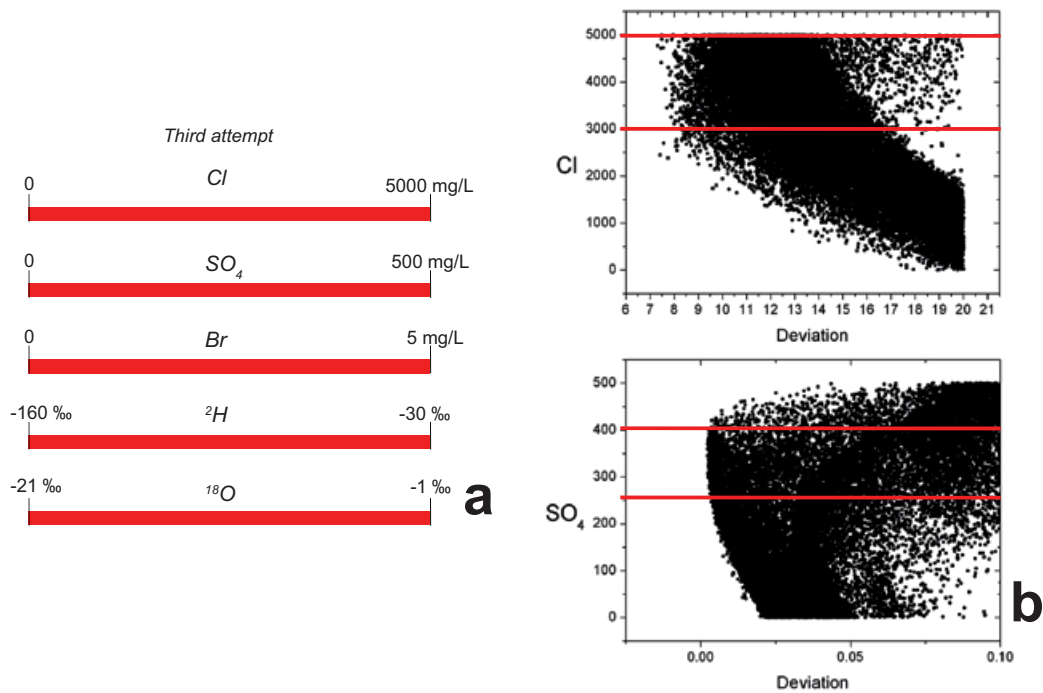


Figure A1-5. (a): Compositional ranges selected for the third attempt, for the conservative elements in the Old Meteoric end member; (b): Concentration of the conservative elements Cl and SO₄ in end-member OM as a function of the total deviation for the 5×10⁶ Monte Carlo runs in the third attempt. The compositional range for Cl and SO₄ which gives a minimum deviation is indicated by two red lines.

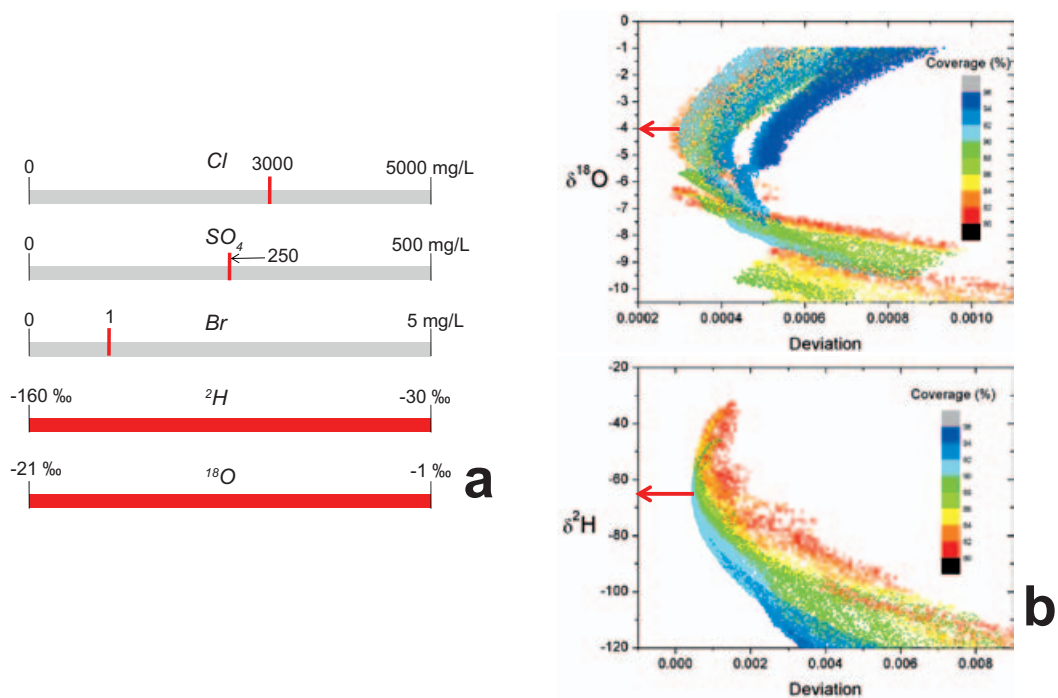


Figure A1-6. (a): Fixed values and isotopic ranges selected for the final attempt, for the conservative elements in the Old Meteoric end member; (b): Values of the isotopes in the OM end member as a function of the total deviation for the 5×10⁶ Monte Carlo runs in the final attempt. The red arrows indicate the isotope values which give the lowest deviation.

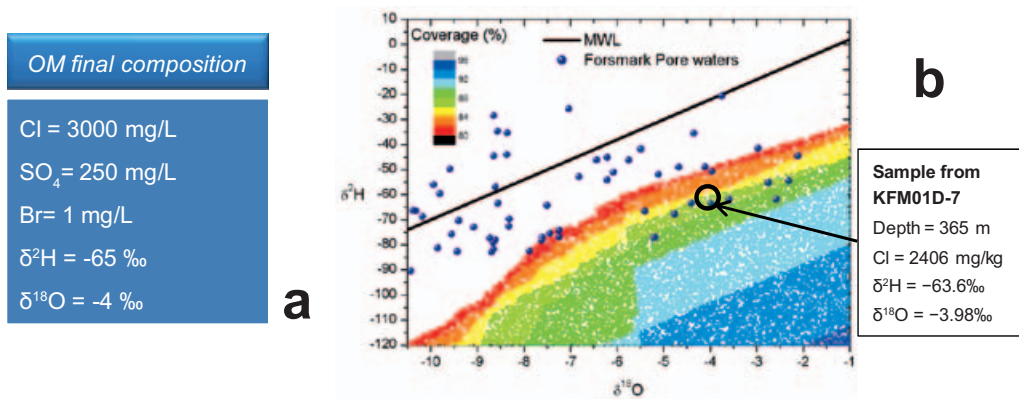
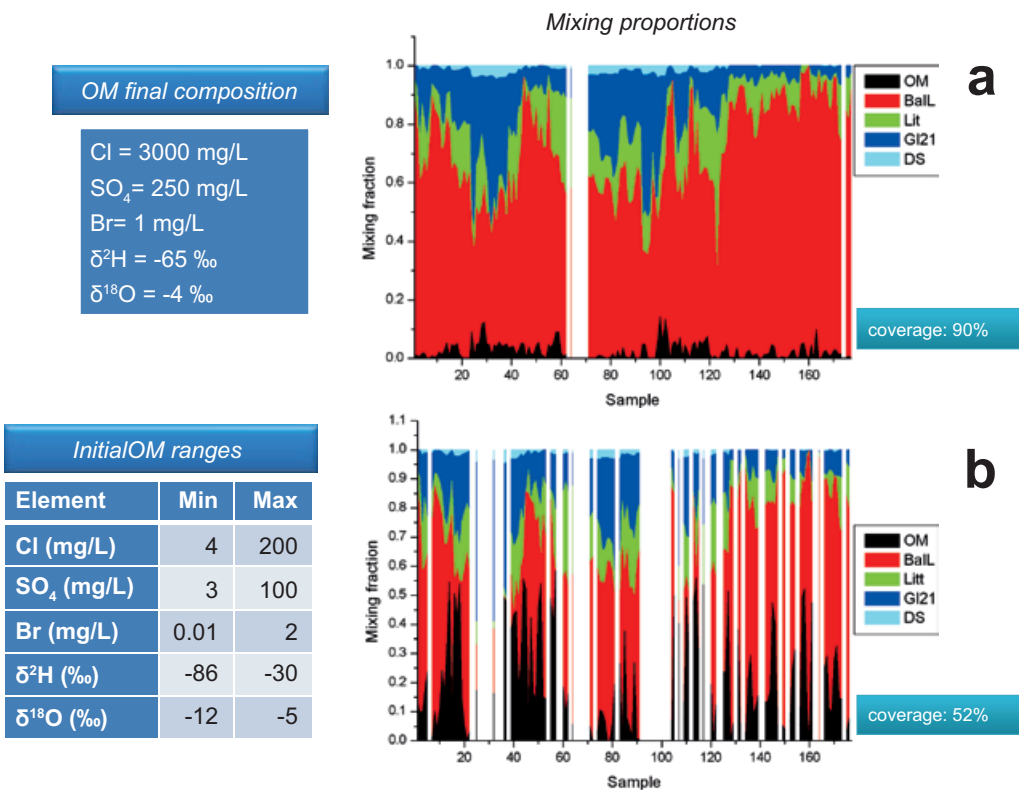


Figure A1-7. (a) Final composition selected for the Old Meteoric end member. (b) Distribution of the obtained values for each Monte Carlo run, coloured by their coverage. The meteoric line and the values corresponding to the porewaters analysed in the PLU are also shown.



M3 results

A2.1 Mixing proportions for the selected mixing models

The selected mixing models are based on four conservative input compositional variables (Cl, SO₄, ²H, and ¹⁸O) and have four end members: Deep Saline (DS), Glacial (Gl), Littorina (Lit), and Baltic Sea local (BalL) in mixing model 1 (MM1) and DS, Gl, Lit and OM in mixing model 2 (MM2).

Tables A2-1 and A2-2 give the mixing proportions for each sample in the dataset as obtained with MM1 and MM2, respectively. Samples with no mixing values in the tables are those not explained by the corresponding mixing model. In both models, samples are grouped by water type and within each group they have been sorted by increasing depth and, for the same depth, by date of sampling. The column with the 'Row' number corresponds to the row number in the Excel file.

Table A2-1. Mixing proportions (in percent) of each end member used in mixing model 1 (MM1) for each sample in the data set.

Row number	Borehole	Sample number	Water type	% Glacial	% Baltic Local	% Littorina	% Deep Saline
69	KFR02	13952	G	47.84	36.89	10.87	4.41
70	KFR02	3215	G	49.53	42.98	2.64	4.85
71	KFR02	12668	G	51.85	35.16	8.11	4.89
75	KFR02	13951	G	40.10	34.60	20.52	4.78
77	KFR02	12667	G	41.40	38.17	15.82	4.61
87	KFR02	13949	G	37.70	40.26	17.68	4.36
91	KFR03	13956	G	47.41	37.55	10.60	4.45
92	KFR03	3231	G	47.50	47.99	0.00	4.51
93	KFR03	12670	G	52.79	40.49	2.67	4.05
95	KFR03	13955	G	52.06	32.27	10.95	4.71
96	KFR03	3230	G	42.61	50.05	2.06	5.28
97	KFR03	12669	G	48.19	44.43	1.86	5.52
101	KFR03	13954	G	51.46	32.03	11.72	4.79
102	KFR03	3229	G	35.45	55.04	4.31	5.20
106	KFR03	13953	G	38.59	40.92	16.07	4.43
107	KFR03	3228	G	34.23	57.42	3.13	5.22
110	KFR04	13959	G	45.49	42.78	7.62	4.11
111	KFR04	3239	G	38.95	55.39	0.77	4.89
112	KFR04	12673	G	42.67	45.43	7.35	4.55
214	KFR101	16145	G				
216	KFR101	16208	G				
217	KFR101	16239	G				
218	KFR101	16240	G				
219	KFR101	16241	G				
220	KFR101	16242	G				
232	KFR105	16371	G	36.62	52.48	7.37	3.53
249	KFR105	16333	G	49.59	36.57	10.34	3.49
250	KFR105	16334	G	47.81	35.91	12.85	3.44
253	KFR105	16337	G	49.78	33.36	13.57	3.29
256	KFR105	16651	G	47.07	38.65	10.65	3.63
264	KFR106	16604	G				
272	KFR13	13969	G	57.44	30.29	7.03	5.24
275	KFR13	3212	G	42.81	45.21	7.01	4.97
221	KFR101	16942	G				
258	KFR105	16918	G				
9	HFR101	16022	T	23.94	59.70	14.13	2.24
13	HFR105	16090	T	18.88	67.17	12.16	1.79

Row number	Borehole	Sample number	Water type	% Glacial	% Baltic Local	% Littorina	% Deep Saline
14	HFR105	16091	T	23.10	60.41	14.55	1.94
15	HFR105	16137	T	14.59	72.84	11.04	1.53
20	HFR106	16328	T	19.30	69.95	9.05	1.70
21	HFR106	16329	T	18.80	73.14	5.82	2.24
39	KFR01	13432	T	25.28	53.16	18.34	3.22
40	KFR01	13436	T	23.72	43.12	31.33	1.83
43	KFR01	13527	T	27.15	43.39	27.61	1.86
45	KFR01	13920	T	20.84	54.38	22.66	2.12
47	KFR01	13937	T	24.00	50.18	23.94	1.88
48	KFR01	13943	T	22.84	51.85	23.31	2.00
51	KFR01	17028	T	22.74	53.30	22.15	1.81
54	KFR01	17068	T	19.84	59.40	19.07	1.70
55	KFR01	3222	T	19.93	63.42	14.57	2.09
56	KFR01	3240	T	18.32	66.46	13.15	2.07
57	KFR01	3243	T	22.36	64.21	11.23	2.20
58	KFR01	17074	T	20.34	50.64	28.71	0.32
59	KFR01	12650	T	20.72	56.01	22.07	1.21
60	KFR01	6228	T	20.79	57.22	20.62	1.37
61	KFR01	6386	T	21.49	53.18	24.16	1.18
62	KFR01	12651	T	13.74	69.43	15.54	1.29
63	KFR01	12652	T	19.18	59.55	19.92	1.35
64	KFR01	12685	T	17.91	63.62	17.21	1.27
65	KFR01	16092	T	19.73	57.81	21.03	1.42
66	KFR01	16588	T	18.56	61.96	17.81	1.66
76	KFR02	3226	T	31.19	50.15	13.72	4.94
79	KFR02	13950	T	31.19	39.54	24.63	4.64
81	KFR02	3225	T	28.24	47.73	19.62	4.42
89	KFR02	12665	T	30.65	58.28	7.02	4.05
88	KFR02	3224	T	34.61	48.19	12.57	4.63
115	KFR04	3238	T	18.92	62.97	14.70	3.41
116	KFR04	12672	T	23.08	50.69	23.07	3.16
118	KFR04	13957	T	18.88	54.14	24.08	2.89
119	KFR04	3237	T	20.68	61.90	13.89	3.53
120	KFR04	12671	T	23.35	51.19	22.37	3.08
222	KFR102A	16234	T	19.28	61.79	15.43	3.50
223	KFR102A	16235	T	19.62	60.76	16.15	3.47
224	KFR102A	16236	T	18.48	62.45	15.60	3.47
225	KFR102A	16237	T	20.32	59.40	16.92	3.36
226	KFR102A	16238	T	21.94	56.72	17.97	3.36
227	KFR102A	16226	T	30.19	56.17	11.00	2.64
228	KFR102A	16227	T	30.08	55.77	11.37	2.78
229	KFR102A	16228	T	27.83	61.05	8.07	3.06
230	KFR102A	16232	T	27.81	61.25	7.76	3.17
231	KFR102A	16233	T	28.61	59.38	8.96	3.05
233	KFR105	16372	T	33.91	44.28	18.60	3.21
235	KFR105	16374	T	30.26	53.95	12.79	3.00
236	KFR105	16361	T	17.56	64.57	16.38	1.48
237	KFR105	16362	T	16.70	65.20	16.67	1.43
239	KFR105	16364	T	16.55	67.09	15.10	1.27
241	KFR105	16367	T	24.49	53.39	20.28	1.84
242	KFR105	16368	T	25.59	52.52	19.70	2.18
244	KFR105	16370	T	24.99	54.03	19.06	1.92
245	KFR105	16357	T	20.45	60.82	17.40	1.34
246	KFR105	16358	T	17.72	64.82	15.96	1.50
248	KFR105	16360	T	19.80	61.89	16.85	1.46

Row number	Borehole	Sample number	Water type	% Glacial	% Baltic Local	% Littorina	% Deep Saline
261	KFR106	16601	T	27.35	57.91	11.45	3.29
276	KFR13	12664	T	34.17	51.97	9.84	4.02
279	KFR13	3213	T	21.94	61.75	11.94	4.36
296	KFR55	12683	T	29.96	54.71	11.95	3.38
299	KFR55	3205	T	25.28	59.54	11.49	3.69
300	KFR55	12682	T	21.63	51.79	23.82	2.77
303	KFR55	3233	T	18.81	64.39	13.95	2.85
304	KFR55	12681	T	22.72	55.71	18.97	2.60
344	KFR7A	12660	T	22.68	46.21	29.24	1.88
347	KFR7A	16094	T	23.75	23.97	52.28	0.00
349	KFR7A	16585	T	17.58	58.01	22.50	1.92
44	KFR01	13661	L	16.92	61.74	19.17	2.17
50	KFR01	13997	L	13.10	68.47	16.55	1.88
52	KFR01	17034	L	20.63	57.37	20.26	1.75
82	KFR02	12666	L	23.63	51.66	20.81	3.90
114	KFR04	13958	L	18.09	56.45	22.53	2.93
122	KFR05	12674	L	13.74	65.33	19.53	1.41
124	KFR05	13960	L	14.63	57.45	26.56	1.36
125	KFR05	3232	L	13.39	72.56	11.82	2.23
207	KFR10	13433	L	9.24	62.17	26.34	2.25
208	KFR10	13437	L	5.81	68.14	24.04	2.01
210	KFR10	13528	L	11.58	57.47	29.65	1.30
213	KFR10	17067	L	6.42	70.27	21.95	1.37
181	KFR10	3208	L	8.06	71.01	19.25	1.68
182	KFR10	3209	L	9.92	67.54	20.86	1.68
183	KFR10	3216	L	10.00	69.08	19.09	1.83
184	KFR10	3217	L	10.19	68.25	19.63	1.92
186	KFR10	12656	L	7.92	67.93	23.07	1.08
187	KFR10	6231	L	10.05	60.40	28.51	1.04
188	KFR10	6384	L	10.46	53.68	34.99	0.87
189	KFR10	12657	L	11.88	54.25	32.80	1.07
190	KFR10	12658	L	8.25	59.56	30.83	1.36
191	KFR10	12687	L	10.77	55.16	32.77	1.29
192	KFR10	16095	L	15.06	47.00	36.44	1.50
193	KFR10	16587	L	10.26	57.81	30.60	1.32
280	KFR13	12663	L	19.96	65.27	10.85	3.92
295	KFR55	3204	L	18.27	63.88	14.51	3.34
302	KFR55	13974	L	14.10	63.89	20.01	2.00
312	KFR7A	3234	L	15.89	65.12	17.53	1.47
322	KFR7A	13434	L	12.68	60.22	21.99	5.11
323	KFR7A	13438	L	14.88	48.66	32.22	4.24
325	KFR7A	13529	L	20.71	38.96	36.39	3.94
326	KFR7A	13663	L	19.23	42.74	33.91	4.12
327	KFR7A	13922	L	15.48	49.97	30.42	4.13
329	KFR7A	13939	L	16.41	47.83	31.96	3.81
330	KFR7A	13945	L	16.00	49.11	31.10	3.79
331	KFR7A	13999	L	9.50	60.45	26.40	3.65
332	KFR7A	17029	L	17.21	50.23	29.02	3.53
333	KFR7A	17036	L	15.08	53.84	28.01	3.06
335	KFR7A	17066	L	14.34	56.84	25.45	3.37
336	KFR7A	3200	L	14.56	61.49	20.72	3.22
337	KFR7A	3203	L	13.79	62.43	20.56	3.22
338	KFR7A	3206	L	13.38	64.21	19.11	3.30
339	KFR7A	3207	L	14.38	63.37	18.90	3.34

Row number	Borehole	Sample number	Water type	% Glacial	% Baltic Local	% Littorina	% Deep Saline
340	KFR7A	17072	L	13.10	57.22	28.41	1.26
342	KFR7A	6229	L	14.66	60.33	23.01	1.99
343	KFR7A	6387	L	14.86	55.91	27.60	1.63
345	KFR7A	12661	L	15.24	60.24	22.21	2.30
346	KFR7A	12688	L	15.99	57.64	24.60	1.77
362	KFR7C	3223	L	13.70	72.69	11.31	2.30
350	KFR7A	16879	L				
351	KFR7A	16882	L				
352	KFR7A	16917	L				
3	HFM34	12291	B	4.83	88.67	6.50	0.00
6	HFM35	12329	B	7.90	81.85	10.25	0.00
12	HFR105	16019	B	12.55	63.05	23.77	0.63
16	HFR106	16330	B	6.30	89.29	4.15	0.26
17	HFR106	16331	B	7.38	85.22	7.06	0.34
18	HFR106	16332	B	8.71	83.36	7.57	0.36
19	HFR106	16327	B	10.36	81.42	7.56	0.67
24	KFR01	12662	B	9.02	78.92	11.99	0.08
127	KFR08	3218	B	4.62	94.46	0.00	0.93
128	KFR08	12679	B	5.49	85.93	8.25	0.33
129	KFR08	16938	B				
131	KFR08	3219	B				
132	KFR08	12678	B	8.72	84.29	6.20	0.79
136	KFR08	13435	B	7.43	74.45	17.90	0.22
137	KFR08	13439	B	3.53	81.36	14.89	0.22
139	KFR08	13530	B	8.36	68.06	23.58	0.00
140	KFR08	13664	B	7.13	74.84	17.76	0.26
141	KFR08	13923	B	4.33	79.04	16.47	0.16
143	KFR08	13940	B	5.13	79.56	15.30	0.00
144	KFR08	13946	B	6.18	77.22	16.56	0.05
146	KFR08	17000	B	22.27	52.15	25.58	0.00
147	KFR08	17026	B	7.75	74.33	17.92	0.00
148	KFR08	17037	B	5.50	81.09	13.40	0.00
150	KFR08	17065	B	7.23	80.07	11.77	0.93
151	KFR08	17069	B	6.98	79.09	13.14	0.79
152	KFR08	3220	B	6.97	84.97	6.89	1.17
153	KFR08	17071	B	4.30	84.75	10.95	0.00
154	KFR08	12653	B	6.35	79.73	13.92	0.00
155	KFR08	6230	B	7.73	78.05	14.14	0.08
156	KFR08	6385	B	6.90	75.71	17.39	0.00
157	KFR08	12654	B	7.37	77.50	15.13	0.00
158	KFR08	12655	B	9.83	72.20	17.95	0.03
159	KFR08	12686	B	6.67	80.00	13.33	0.00
160	KFR08	16093	B	9.97	71.29	18.32	0.43
162	KFR08	16586	B	9.82	71.88	17.82	0.49
164	KFR08	16934	B				
165	KFR08	16943	B				
166	KFR09	3210	B	4.18	91.36	3.75	0.70
170	KFR09	13662	B	6.89	77.74	15.37	0.00
171	KFR09	13921	B	1.83	87.53	10.53	0.11
173	KFR09	13938	B	3.96	83.18	12.86	0.00
174	KFR09	13944	B	4.16	82.83	13.01	0.00
176	KFR09	13998	B	4.99	83.13	11.89	0.00
177	KFR09	17027	B	5.47	82.66	11.88	0.00
178	KFR09	17035	B	4.31	83.25	12.45	0.00

Row number	Borehole	Sample number	Water type	% Glacial	% Baltic Local	% Littorina	% Deep Saline
185	KFR10	17073	B	4.75	78.89	15.51	0.85
282	KFR19	13972	B	5.90	83.00	10.94	0.16
284	KFR19	13971	B	5.98	84.27	9.41	0.35
285	KFR19	3236	B	9.44	86.19	3.69	0.69
286	KFR19	12680	B	6.76	85.91	6.89	0.44
288	KFR19	13970	B	8.05	82.16	9.22	0.56
289	KFR19	3235	B				
290	KFR19	16878	B				
291	KFR19	16892	B				
292	KFR19	16937	B				
307	KFR56	3221	B	5.62	92.38	1.10	0.89
308	KFR56	12684	B	2.62	90.46	6.54	0.39
313	KFR7A	12675	B	8.12	80.05	10.45	1.39
354	KFR7B	12677	B	10.26	69.70	19.29	0.75
360	KFR7B	12676	B	9.63	69.95	19.76	0.66

Table A2-2. Mixing proportions (in percent) of each end member used in mixing model 2 (MM2) for each sample in the data set.

Row number	Borehole	Sample number	Water type	% Glacial	% Old Meteoric	% Littorina	% Deep Saline
69	KFR02	13952	G	53.88	18.09	23.42	4.60
70	KFR02	3215	G	56.50	21.29	17.12	5.08
71	KFR02	12668	G	57.60	17.28	20.05	5.07
75	KFR02	13951	G	45.76	16.99	32.29	4.96
77	KFR02	12667	G	47.64	18.75	28.80	4.81
87	KFR02	13949	G	44.28	19.79	31.36	4.58
91	KFR03	13956	G	53.56	18.40	23.39	4.64
92	KFR03	3231	G	56.05	23.97	15.16	4.82
93	KFR03	12670	G	59.41	19.89	16.44	4.27
95	KFR03	13955	G	57.35	15.82	21.95	4.88
96	KFR03	3230	G	50.77	24.66	19.02	5.54
97	KFR03	12669	G	55.44	21.89	16.92	5.75
101	KFR03	13954	G	56.71	15.70	22.64	4.96
102	KFR03	3229	G	44.43	27.14	22.95	5.48
106	KFR03	13953	G	45.28	20.10	29.97	4.64
107	KFR03	3228	G	43.60	28.27	22.61	5.52
110	KFR04	13959	G	52.48	21.04	22.15	4.34
111	KFR04	3239	G	47.99	27.27	19.56	5.18
112	KFR04	12673	G	50.08	22.40	22.73	4.78
214	KFR101	16145	G	54.85	38.75	2.86	3.54
216	KFR101	16208	G	56.26	39.15	1.34	3.25
217	KFR101	16239	G	58.65	36.25	1.40	3.71
218	KFR101	16240	G	58.52	36.28	1.41	3.80
219	KFR101	16241	G	59.20	35.45	1.59	3.75
220	KFR101	16242	G	59.10	35.75	1.41	3.74
232	KFR105	16371	G	45.20	25.78	25.21	3.80
249	KFR105	16333	G	55.55	18.06	22.71	3.69
250	KFR105	16334	G	53.65	17.72	24.99	3.63
253	KFR105	16337	G	55.26	16.30	24.98	3.46
256	KFR105	16651	G	53.41	18.93	23.83	3.83
264	KFR106	16604	G	53.15	26.62	16.33	3.90
272	KFR13	13969	G	62.39	14.88	17.33	5.40

Row number	Borehole	Sample number	Water type	% Glacial	% Old Meteoric	% Littorina	% Deep Saline
275	KFR13	3212	G	50.17	22.33	22.29	5.21
221	KFR101	16942	G				
258	KFR105	16918	G				
9	HFR101	16022	T	33.71	29.30	34.44	2.55
13	HFR105	16090	T	29.86	32.99	35.00	2.14
14	HFR105	16091	T	33.03	29.54	35.18	2.26
15	HFR105	16137	T	26.52	35.72	35.85	1.91
20	HFR106	16328	T	30.74	34.35	32.84	2.07
21	HFR106	16329	T	30.76	35.95	30.67	2.63
39	KFR01	13432	T	34.00	26.03	36.47	3.50
40	KFR01	13436	T	30.80	21.09	46.05	2.05
43	KFR01	13527	T	34.24	21.32	42.35	2.09
45	KFR01	13920	T	29.74	26.70	41.16	2.41
47	KFR01	13937	T	32.21	24.63	41.02	2.14
48	KFR01	13943	T	31.32	25.47	40.94	2.27
51	KFR01	17028	T	31.45	26.23	40.23	2.09
54	KFR01	17068	T	29.54	29.20	39.25	2.01
55	KFR01	3222	T	30.28	31.22	36.08	2.42
56	KFR01	3240	T	29.17	32.70	35.71	2.42
57	KFR01	3243	T	32.84	31.62	33.01	2.54
58	KFR01	17074	T	28.62	24.89	45.91	0.58
59	KFR01	12650	T	29.89	27.47	41.14	1.50
60	KFR01	6228	T	30.15	28.10	40.08	1.67
61	KFR01	6386	T	30.20	26.06	42.29	1.45
62	KFR01	12651	T	25.10	34.08	39.17	1.65
63	KFR01	12652	T	28.93	29.22	40.19	1.66
64	KFR01	12685	T	28.33	31.20	38.87	1.60
65	KFR01	16092	T	29.20	28.35	40.72	1.73
66	KFR01	16588	T	28.72	30.35	38.94	1.98
76	KFR02	3226	T	39.37	24.72	30.71	5.20
79	KFR02	13950	T	37.68	19.37	38.11	4.85
81	KFR02	3225	T	36.02	23.53	35.78	4.67
89	KFR02	12665	T	40.11	28.88	26.65	4.36
88	KFR02	3224	T	42.47	23.75	28.90	4.88
115	KFR04	3238	T	29.21	30.97	36.08	3.74
116	KFR04	12672	T	31.35	24.96	40.26	3.42
118	KFR04	13957	T	27.74	26.58	42.50	3.18
119	KFR04	3237	T	30.79	30.46	34.90	3.85
120	KFR04	12671	T	31.73	25.14	39.78	3.35
222	KFR102A	16234	T	29.40	30.31	36.46	3.82
223	KFR102A	16235	T	29.57	29.79	36.85	3.79
224	KFR102A	16236	T	28.71	30.61	36.88	3.79
225	KFR102A	16237	T	30.05	29.14	37.14	3.67
226	KFR102A	16238	T	31.23	27.85	37.27	3.66
227	KFR102A	16226	T	39.39	27.58	30.11	2.93
228	KFR102A	16227	T	39.21	27.37	30.35	3.07
229	KFR102A	16228	T	37.82	29.94	28.86	3.38
230	KFR102A	16232	T	37.84	30.04	28.62	3.50
231	KFR102A	16233	T	38.33	29.14	29.16	3.36
233	KFR105	16372	T	41.17	21.70	33.69	3.44
235	KFR105	16374	T	39.07	26.53	31.11	3.29
236	KFR105	16361	T	28.14	31.66	38.38	1.82
237	KFR105	16362	T	27.35	32.07	38.81	1.77
239	KFR105	16364	T	27.53	32.92	37.93	1.62

Row number	Borehole	Sample number	Water type	% Glacial	% Old Meteoric	% Littorina	% Deep Saline
241	KFR105	16367	T	33.24	26.20	38.45	2.12
242	KFR105	16368	T	34.20	25.76	37.59	2.46
244	KFR105	16370	T	33.81	26.56	37.42	2.21
245	KFR105	16357	T	30.41	29.83	38.11	1.66
246	KFR105	16358	T	28.34	31.79	38.03	1.84
248	KFR105	16360	T	29.94	30.34	37.94	1.78
261	KFR106	16601	T	36.87	28.30	31.24	3.59
276	KFR13	12664	T	42.58	25.82	27.29	4.30
279	KFR13	3213	T	32.01	30.42	32.88	4.69
296	KFR55	12683	T	38.89	26.92	30.51	3.67
299	KFR55	3205	T	34.98	29.38	31.64	4.00
300	KFR55	12682	T	30.10	25.42	41.44	3.04
303	KFR55	3233	T	29.32	31.69	35.80	3.18
304	KFR55	12681	T	31.82	27.39	37.89	2.90
344	KFR7A	12660	T	30.24	22.67	44.97	2.12
347	KFR7A	16094	T	27.74	11.66	60.60	0.00
349	KFR7A	16585	T	27.09	28.42	42.27	2.22
44	KFR01	13661	L	27.00	30.36	40.14	2.49
50	KFR01	13997	L	24.30	33.63	39.83	2.24
52	KFR01	17034	L	29.98	28.28	39.69	2.05
82	KFR02	12666	L	32.01	25.61	38.21	4.17
114	KFR04	13958	L	27.32	27.73	41.73	3.22
122	KFR05	12674	L	24.41	32.11	41.72	1.75
124	KFR05	13960	L	24.02	28.24	46.07	1.67
125	KFR05	3232	L	25.24	35.72	36.44	2.61
207	KFR10	13433	L	19.42	30.48	47.52	2.58
208	KFR10	13437	L	16.97	33.42	47.24	2.37
210	KFR10	13528	L	20.95	28.33	49.12	1.60
213	KFR10	17067	L	17.90	34.55	45.81	1.74
181	KFR10	3208	L	19.66	34.92	43.37	2.05
182	KFR10	3209	L	20.94	33.26	43.76	2.04
183	KFR10	3216	L	21.25	34.09	42.46	2.19
184	KFR10	3217	L	21.31	33.69	42.72	2.28
186	KFR10	12656	L	19.05	33.32	46.21	1.43
187	KFR10	6231	L	19.93	29.67	49.04	1.36
188	KFR10	6384	L	19.25	26.31	53.28	1.16
189	KFR10	12657	L	20.75	26.65	51.24	1.36
190	KFR10	12658	L	18.00	29.23	51.10	1.67
191	KFR10	12687	L	19.80	27.09	51.53	1.58
192	KFR10	16095	L	22.81	22.89	52.56	1.74
193	KFR10	16587	L	19.73	28.37	50.28	1.63
280	KFR13	12663	L	30.55	32.33	32.85	4.27
295	KFR55	3204	L	28.69	31.47	36.16	3.68
302	KFR55	13974	L	24.54	31.39	41.73	2.34
312	KFR7A	3234	L	26.51	32.07	39.61	1.81
322	KFR7A	13434	L	22.55	29.50	42.52	5.43
323	KFR7A	13438	L	22.86	23.84	48.81	4.50
325	KFR7A	13529	L	27.07	19.17	49.61	4.14
326	KFR7A	13663	L	26.21	21.02	48.42	4.35
327	KFR7A	13922	L	23.65	24.55	47.41	4.39
329	KFR7A	13939	L	24.21	23.54	48.19	4.06
330	KFR7A	13945	L	24.02	24.14	47.79	4.05
331	KFR7A	13999	L	19.38	29.73	46.92	3.97
332	KFR7A	17029	L	25.41	24.75	46.05	3.80

Row number	Borehole	Sample number	Water type	% Glacial	% Old Meteoric	% Littorina	% Deep Saline
333	KFR7A	17036	L	23.86	26.56	46.24	3.35
335	KFR7A	17066	L	23.62	27.98	44.74	3.67
336	KFR7A	3200	L	24.59	30.31	41.56	3.55
337	KFR7A	3203	L	23.98	30.74	41.74	3.55
338	KFR7A	3206	L	23.86	31.64	40.87	3.64
339	KFR7A	3207	L	24.71	31.27	40.35	3.68
340	KFR7A	17072	L	22.45	28.14	47.84	1.56
342	KFR7A	6229	L	24.53	29.64	43.52	2.31
343	KFR7A	6387	L	24.02	27.41	46.65	1.92
345	KFR7A	12661	L	25.11	29.54	42.73	2.62
346	KFR7A	12688	L	25.42	28.30	44.21	2.07
362	KFR7C	3223	L	25.57	35.77	35.98	2.68
350	KFR7A	16879	L				
351	KFR7A	16882	L				
352	KFR7A	16917	L				
3	HFM34	12291	B	19.36	43.56	36.70	0.38
6	HFM35	12329	B	21.32	40.22	38.14	0.32
12	HFR105	16019	B	22.87	30.97	45.21	0.96
16	HFR106	16330	B	20.91	43.82	34.53	0.73
17	HFR106	16331	B	21.33	41.81	36.07	0.79
18	HFR106	16332	B	22.36	40.91	35.94	0.80
19	HFR106	16327	B	23.67	39.99	35.24	1.10
24	KFR01	12662	B	21.94	38.73	38.85	0.49
127	KFR08	3218	B	20.27	46.97	31.32	1.44
128	KFR08	12679	B	19.56	42.16	37.50	0.78
129	KFR08	16938	B				
131	KFR08	3219	B	23.98	45.29	28.55	2.18
132	KFR08	12678	B	22.51	41.38	34.88	1.23
136	KFR08	13435	B	19.63	36.51	43.26	0.61
137	KFR08	13439	B	16.86	39.90	42.59	0.65
139	KFR08	13530	B	19.56	33.56	46.88	0.00
140	KFR08	13664	B	19.38	36.72	43.24	0.65
141	KFR08	13923	B	17.27	38.78	43.38	0.57
143	KFR08	13940	B	18.14	39.10	42.35	0.40
144	KFR08	13946	B	18.80	37.94	42.80	0.45
146	KFR08	17000	B	30.79	25.65	43.30	0.25
147	KFR08	17026	B	19.94	36.63	43.27	0.16
148	KFR08	17037	B	18.76	39.92	40.95	0.37
150	KFR08	17065	B	20.32	39.37	38.96	1.35
151	KFR08	17069	B	19.91	38.87	40.02	1.21
152	KFR08	3220	B	20.86	41.78	35.75	1.61
153	KFR08	17071	B	18.18	41.67	39.81	0.34
154	KFR08	12653	B	19.45	39.18	41.16	0.22
155	KFR08	6230	B	20.50	38.32	40.69	0.49
156	KFR08	6385	B	19.38	37.26	43.35	0.00
157	KFR08	12654	B	20.10	38.12	41.60	0.18
158	KFR08	12655	B	21.61	35.54	42.44	0.41
159	KFR08	12686	B	19.79	39.32	40.59	0.29
160	KFR08	16093	B	21.64	34.99	42.57	0.80
162	KFR08	16586	B	21.60	35.23	42.31	0.86
164	KFR08	16934	B				
165	KFR08	16943	B				
166	KFR09	3210	B	19.11	44.93	34.78	1.18
170	KFR09	13662	B	19.59	38.24	41.77	0.41

Row number	Borehole	Sample number	Water type	% Glacial	% Old Meteoric	% Littorina	% Deep Saline
171	KFR09	13921	B	16.15	42.99	40.30	0.57
173	KFR09	13938	B	17.57	40.92	41.17	0.34
174	KFR09	13944	B	17.71	40.70	41.18	0.40
176	KFR09	13998	B	18.59	40.92	40.17	0.31
177	KFR09	17027	B	18.99	40.65	39.98	0.38
178	KFR09	17035	B	17.96	41.08	40.84	0.12
185	KFR10	17073	B	17.65	38.76	42.33	1.26
282	KFR19	13972	B	19.48	40.77	39.16	0.59
284	KFR19	13971	B	19.77	41.35	38.09	0.79
285	KFR19	3236	B	23.50	42.47	32.90	1.14
286	KFR19	12680	B	20.83	42.13	36.15	0.89
288	KFR19	13970	B	21.50	40.34	37.17	0.99
289	KFR19	3235	B	21.36	46.92	30.09	1.63
290	KFR19	16878	B				
291	KFR19	16892	B				
292	KFR19	16937	B				
307	KFR56	3221	B	20.72	45.42	32.48	1.38
308	KFR56	12684	B	17.45	44.30	37.39	0.86
313	KFR7A	12675	B	21.21	39.32	37.66	1.81
354	KFR7B	12677	B	21.66	34.24	42.99	1.11
360	KFR7B	12676	B	21.07	34.37	43.54	1.03

A2.2 Calculated chemical composition theoretically controlled by mixing for the set of SFR groundwaters

Table A2-3 shows the chemical composition for the main components as obtained with mixing models MM1 and MM2.

Despite the different end members and mixing proportions obtained with these two mixing models, it is quite remarkable that the predicted chemical composition, as a result of mixing (without reaction), is very similar irrespective of the model used.

This fact would allow a hypothetical composition due to mixing to be calculated for the whole set of samples, including not only the conservative elements, but also other more reactive ones such as magnesium, sodium, calcium or potassium. These compositions could then be used to calibrate the hydrogeological models of mixing over time, which would add a very important additional constraint that cannot be included in this statistical analysis.

The range of composition for all the major elements and isotopes is listed below in Table A2-3.

pH uncertainties in speciation-solubility calculations

The available hydrochemical dataset corresponds to the 1.0 version, including also groundwater data from the recent SFR extension project. Detailed data quality assurance, selection and categorisation of the samples were performed by Nilsson (2009) and Nilsson et al. (2010, 2011). Most of the data correspond to general groundwater analyses, including major and minor ions and isotopes although some analytical results about gasses, microbes and redox data are also available (see Section 1.3). For the speciation-solubility calculations, samples with a charge balance error exceeding $\pm 5\%$ have been eliminated, as also done for the Site Descriptive Models for Forsmark, Laxemar-Simpevarp and SFR (Nilsson 2009, Nilsson et al. 2010).

An important source of uncertainty associated with the available hydrochemical data is related to the pH determinations. Apart from the pH measurements obtained with the Chemmac probe (see Appendix 4) for 7 borehole sections (53 samples¹⁹), field measurements for pH are available only for 78 of the 416 samples from the studied area (i.e. 19% of the total number of samples). For the rest of the samples, pH was either not measured (10% of cases) or measured in the laboratory (59% of the pH determinations).

This situation represents an important limitation for the development and interpretation of speciation-solubility calculations, affecting especially the characterisation of redox processes and to the carbonate system. Thus, as described below, an analysis of the effects of pH uncertainty on the results and interpretations has been performed for each of the speciation-solubility calculations presented in this work.

A3.1 Dealing with pH uncertainties

Groundwaters in crystalline rock environments from the Fennoscandian sites (e.g. Laxemar-Simpevarp, Olkiluoto, Stripa, etc) display CO₂ partial pressures both higher and lower than the atmospheric value. Therefore, apart from other problems (see Gimeno et al. 2009 for a review) laboratory pH measurements or even on-line pH field measurements can be affected by CO₂-exchange with the atmosphere (CO₂ outgassing or ingassing).

In- and out-gassing problems prior or during the pH measurements have been taken into account since the initial stages of the Site Characterisation Programmes, especially when pH was measured in the laboratory. Gimeno et al. (2004a, b) calculated the theoretical original pH for these groundwaters, apparently over- or undersaturated with respect to calcite, by adding or extracting the amount of CO₂ gas necessary to reach calcite equilibrium (SI = 0), which was assumed to represent the original groundwater conditions.

This approach, which may not always be reasonable (see Gimeno et al. 2009 for further discussion on this topic), was also used by Pitkänen et al. (2004) for the Olkiluoto groundwaters and, more recently, by other research groups (e.g. Bath and Hermansson 2006, Sasamoto et al. 2007) and it will be used in the speciation-solubility calculations presented in the following sections.

Both the measured pH and the calculated pH using this approach will be used to obtain an uncertainty range in the speciation-solubility results and in the rest of key parameters discussed below.

A3.2 Results in the carbonate system

Speciation-solubility calculations performed with the available measured pH data for the SFR area suggest that all sampled groundwaters show CO₂ partial pressures higher than the atmospheric value (Figure A3-1a). Most of them are in equilibrium or slightly oversaturated with respect to calcite (Figure A3-1b) and 45 of the 128 samples with field pH data (field and Chemmac) show calcite saturation indices higher than +0.3 units. These oversaturation values may be either “real” or resulting from CO₂-outgassing in groundwaters originally equilibrated with respect to calcite, both under laboratory and under field conditions.

¹⁹ For modelling purposes when Chemmac data were available, the selected pH and Eh values were used for all the samples corresponding to the same section and date. Thus, a total of 53 samples have *in situ* pH values.

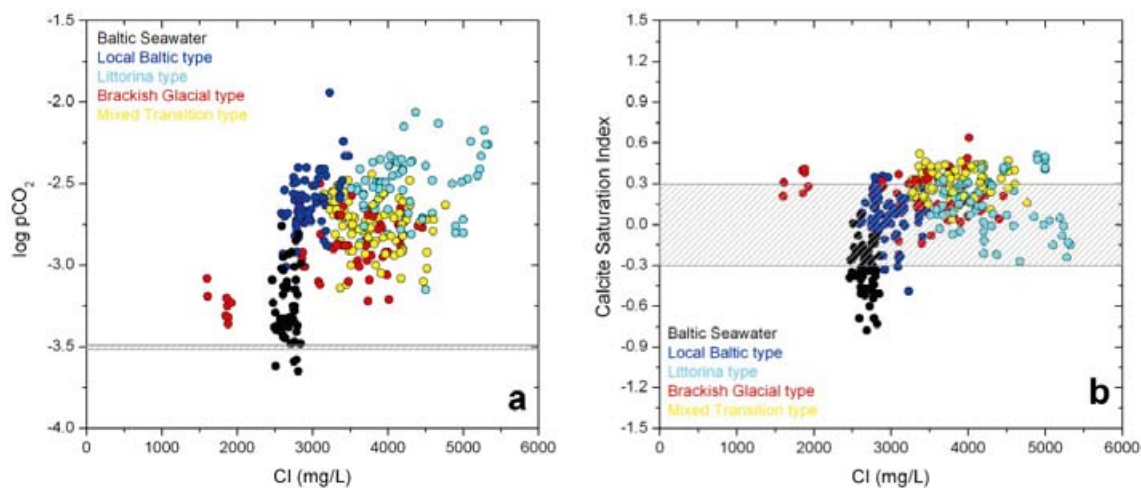


Figure A3-1. Speciation-solubility calculation results of $\log p\text{CO}_2$ (a) and calcite saturation index (b) versus chloride contents for the SRF groundwaters and the Baltic Sea waters used in this work (black dots). Measured pH data are used. Rastered area in panel 'b' corresponds to the uncertainty range (± 0.3 units) associated with the calcite saturation index calculations.

A small set of groundwater samples, also with CO_2 partial pressures higher than the atmospheric value, seem to be undersaturated with respect to calcite. Even in these cases, some CO_2 outgassing during sampling and pH measurement cannot be discarded, leading to measured pH values and saturation indices higher than under original groundwater conditions, which could have corresponded to undersaturation with respect to calcite²⁰.

Moreover, it is also possible that other samples in that set were initially equilibrated with respect to calcite and had suffered some unknown in-gassing process during pH measurements. Furthermore, the existence or other unrecognised influences on pH, in addition to or instead of CO_2 ingassing-outgassing, is also possible for some samples and measurements²¹.

Figure A3-2a shows the comparison between the measured and the calculated pH values in the SFR waters. The calculated pH values in equilibrium with calcite are usually lower than the measured ones as the set of groundwaters oversaturated with respect to calcite (with the measured pH values) is larger, and therefore to reach the equilibrium situation they have to gain CO_2 , decreasing the pH.

The $p\text{CO}_2$ values calculated using the pH in equilibrium with calcite (Figure A3-2b) are higher than the atmospheric value. Thus, this characteristic of the SFR groundwater situation is not affected by pH uncertainties.

Measured pH in the SFR groundwaters range from 6.6 to 8.0 and the calculated values (assuming calcite equilibrium) are within a narrower range, between 7 and 7.7. No clear correlation with depth, neither for measured nor for calculated pH values (Figure A3-3a, b), is apparent and, thus, this conclusion is not affected by the pH uncertainties. This situation may be the result of the heterogeneity of the system and the frequent horizontal dispersion of this parameter in the examined sections, possibly due to the groundwaters evolution over the time.

²⁰ For example, groundwater samples from borehole HFM34 are slightly undersaturated with respect to calcite and display a hydrochemistry similar to present Baltic Sea waters in the surroundings of the SFR area. Most of these Baltic waters show a clear undersaturation with respect to calcite (the same situation has been usually described for Baltic samples in the PLU and Laxemar-Simpevarp areas) and thus, the undersaturation state in the HFM34 groundwaters could be real, or even more marked.

²¹ For example, the lowest measured pH values (6.6, in sample 17063 from KFR10 at section 63–104.4 m, and 6.8, in sample 17069 from KFR08 at section 87–107.8 m) are “anomalously” low in the long time series of measurements (13–20 years) performed at those sections (at least 0.4–0.5 units below the rest of measurements) without any apparent change in the rest of the compositional characters.

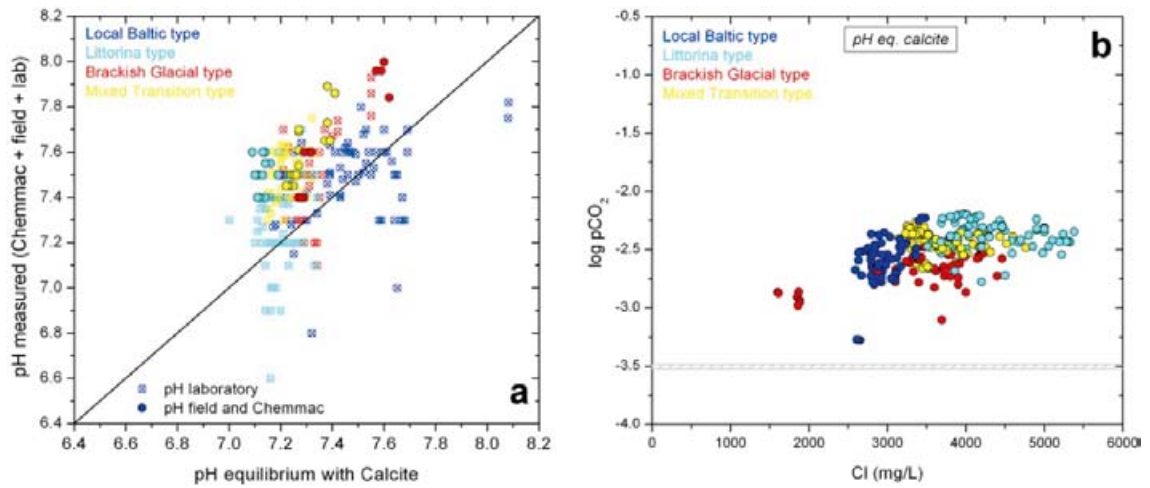


Figure A3-2. Comparison between the measured (both in laboratory and in situ) and calculated (assuming calcite equilibrium) pH values (a) and log pCO₂ values in equilibrium with calcite values versus chloride concentrations for the SRF groundwaters (b).

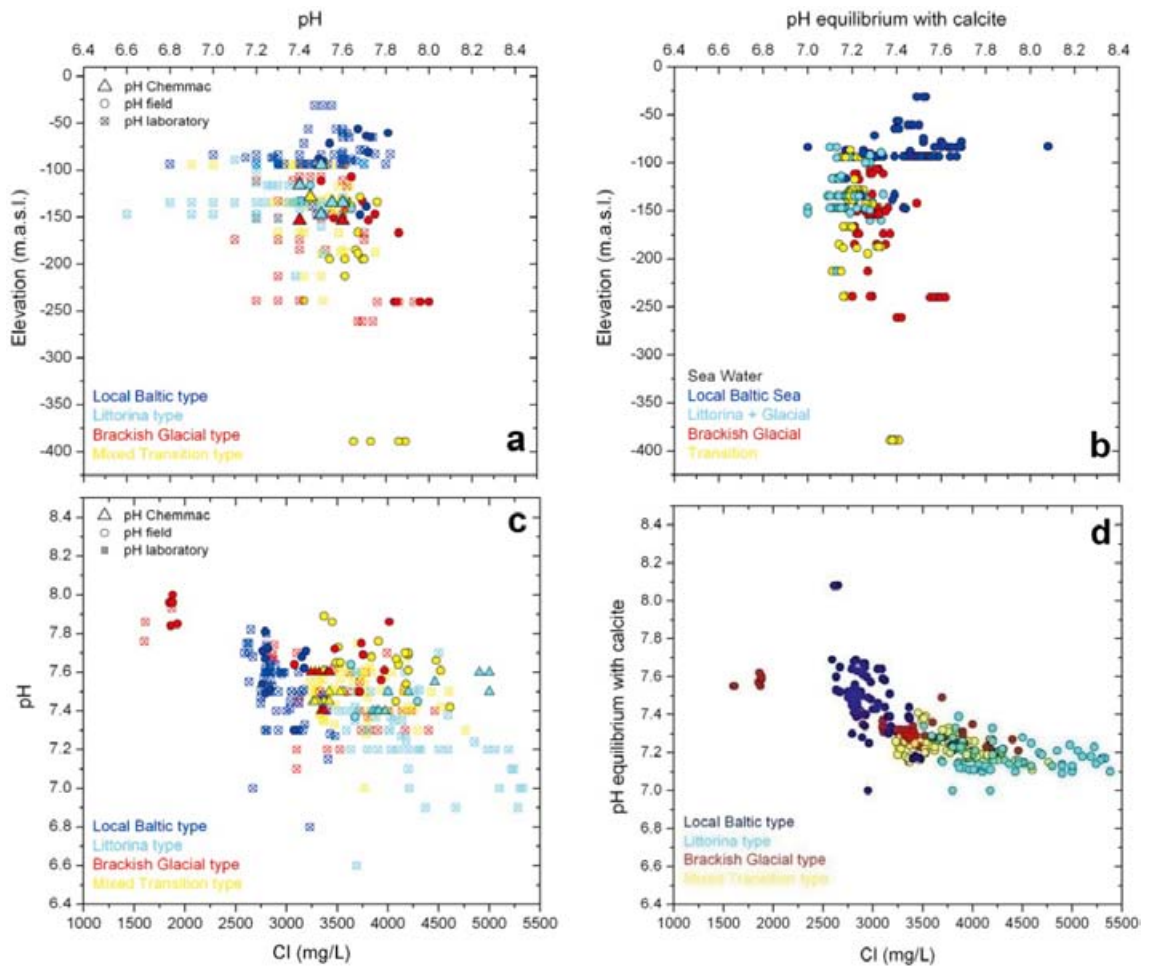


Figure A3-3. Measured pH values (a, c) and pH values calculated in equilibrium with calcite (b, d) with respect to depth (a, b) and chloride (c, d) in the SRF groundwaters.

The roughly negative trend between measured pH and chloride contents (Figure A3-3c), is apparently better defined by the calculated pH values (Figure A3-3d). It would suggest that the Baltic Sea water intrusion and mixing with the older and more saline groundwaters at depth, may promote a pH increase. However, this trend is not so evident with the measured pH values and is clearly affected by the uncertainties in the pH measurements. This aspect would merit further study in future works.

The overall results on the carbonate system presented in the Section 4.1 are not affected by the uncertainties in the pH measurement. This is mainly due to the fact that, when using these pH measurements, most groundwaters are already in equilibrium with calcite (inside the usually accepted uncertainty range of 0.3 SI units).

However, under or over saturation situations with respect to calcite, found in some of the groundwaters, could be affected by the uncertainty associated with the pH measurement. Especially remarkable is the undersaturation found in some of the Local Baltic type groundwaters (Figure A3-1b) as this fact could be attributed to an infiltration time for present Baltic Sea waters too fast to allow equilibration with respect to this mineral. Thus, this aspect merits further detailed study (and *in situ* pH measurements).

A3.3 Results of the redox pair calculations

Redox pair calculations have been performed with pH values determined by Chemmac in order to compare the results with the potentiometric Eh measurements (also measured with the same probe). However, as the available potentiometric Eh measurements are still scarce, some redox pairs calculations have also been performed for the whole set of groundwaters (with laboratory and field pH measurements). Thus, redox pair potentials have been obtained both with the measured and the calculated pH to evaluate the associated uncertainty. Results are shown in Figure 5-2 (Section 5.2.2).

Redox potentials obtained from the sulphur and Fe^{3+} -clay/ Fe^{2+} -clay redox pairs show similar ranges and mean values for both situations. The potential values obtained with the measured pH values usually show a slightly larger range than those obtained with the calculated pH values (as shown above, assuming calcite equilibrium, pH values are within a narrower range). Therefore, the results obtained with these redox couples are not drastically affected by pH uncertainties in calculations.

From the scarce data available for methane (five samples) values for the CO_2/CH_4 redox pair (not shown in Figure 5-2) are very similar to the ones obtained with the sulphur couples (from -208 to -233 mV) and the differences promoted by the use of measured or calculated pH values are lower than 11 mV.

The redox potential defined by the $\text{Fe}^{2+}/\text{Fe}(\text{OH})_3$ heterogeneous redox pair depends on the character of the mineral phase (solubility, particle size, etc.) of the specific ferric oxyhydroxide included in the calculations. Results for a crystalline phase such as hematite or goethite (using the solubility data obtained by Grenthe et al. (1992), for an iron phase with intermediate crystallinity (using the data provided by Banwart (1999) and for microcrystalline and amorphous ferric oxyhydroxides (with data from Nordstrom et al. 1990) are presented in Figure 5-2. The pH variation effects, when using measured or calculated values over the redox potentials obtained for each of these phases are more important than in the case of the sulphur and Fe^{3+} -clay/ Fe^{2+} -clay redox pairs. The range of values obtained with the measured pH is significantly larger than the range obtained with the calculated pH values. Differences in the mean values are also higher than those observed for the other redox couples.

This higher sensitivity of the potentials obtained with the $\text{Fe}^{2+}/\text{Fe}(\text{OH})_3$ redox pair to the pH values is a consequence of the steeper slope of the involved equilibrium (with respect to those involved in the sulphur and Fe^{3+} -clay/ Fe^{2+} -clay redox pairs) in the classical pH-Eh diagrams (see, for example, Drever 1997 or Kölling 2000).

Due to this fact, and just in case, the pH effects on the redox potentials obtained by the $\text{Fe}^{2+}/\text{Fe}(\text{OH})_3$ redox pairs also have been performed when compared with the potentiometrical Eh measurements (though in these cases Chemmac pH measurements were available; see Section 5.2.2.1).

The results indicate that variations in the calculated redox potentials due to the different pH values used would not change the type of iron oxyhydroxide, presumably involved in the control of the potentiometrically measured Eh. Thus, for example, in the case of the oxidising values potentiometrically measured in some of the analysed sections, redox pair calculations would support a control by amorphous Fe(III)-oxyhydroxides (Table 5-3), within the usual ± 50 mV uncertainty range for Eh measurements (see Section 5.2.2.1), independently of the pH value used in the calculations.

The potentiometric value obtained for the $\text{Fe}^{2+}/\text{Fe}(\text{OH})_3$ redox pair using the equilibrium constant for a microcrystalline phase provide too low (reducing) values with respect to the potentiometric measurement.

A3.4 Results in the saturation indices for the redox minerals

As stated before, many of the available pH data for groundwater samples were measured in the laboratory and selecting samples with available *in situ* pH values would result in an extremely reduced set of samples to deal with the redox systems (see Section 5.1). Thus, as samples with both field and laboratory pH values have been selected, uncertainties related to the pH measurement may propagate to the saturation index results with respect to some key redox minerals in the studied system, i.e. siderite, rhodochrosite and amorphous or crystalline monosulphides (see Sections 5.3 and 5.4).

To verify the effects of the pH measurement, saturation index calculations for those minerals have also been performed both using the measured and calculated pH values. Results are presented in Figures A3-4 to A3-6.

Results obtained with the measured pH indicate that most of the Littorina type and Local Baltic type groundwaters are in equilibrium with respect to siderite (Figure A3-4a). This situation is even more clearly seen in the results obtained with the pH values calculated in equilibrium with calcite (Figure A3-4b). Some Mixed transition and Brackish-glacial type groundwaters are affected by the pH data used, changing from being in an equilibrium situation with respect to siderite when using the measured pH, to being slightly undersaturated when using the calculated values (Figure A3-4 a, b). However, these changes do not affect:

- The SFR groundwaters with the clearest glacial signatures, the less saline groundwaters from the KFR101 borehole at section 271.5–341.76 m.b.l. (with a long-term hydraulic isolation), which are undersaturated with respect to this mineral both with the measured and the calculated pH. This is consistent with the undersaturation observed in the most saline and deep groundwaters (not affected by marine intrusion) in the PLU and Laxemar systems (Gimeno et al. 2009); and to
- The groundwaters associated with the Northern Boundary Belt, which are also undersaturated with respect to siderite, supporting a minor influence of past (Littorina) and present (Baltic) marine intrusions.

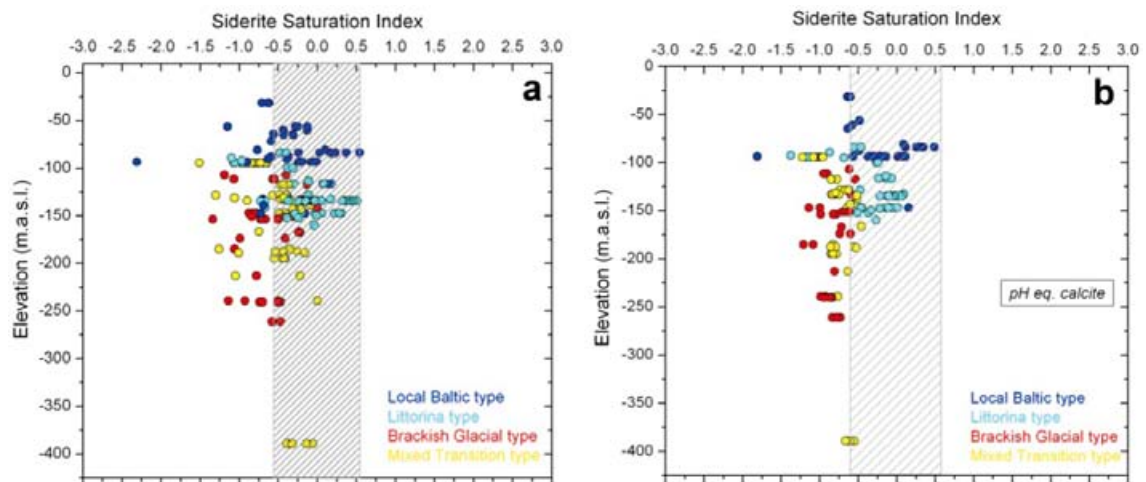


Figure A3-4. Siderite saturation indices obtained with measured (a) and calculated (b) pH values versus depth for the SFR groundwaters.

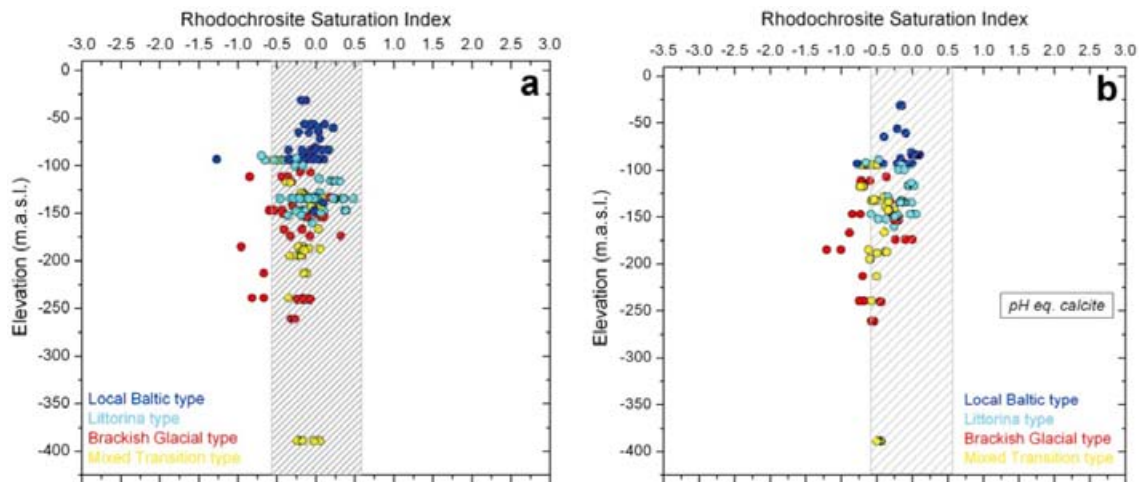


Figure A3-5. Rhodochrosite saturation indices obtained with measured (a) and calculated (b) pH values versus depth for the SFR groundwaters.

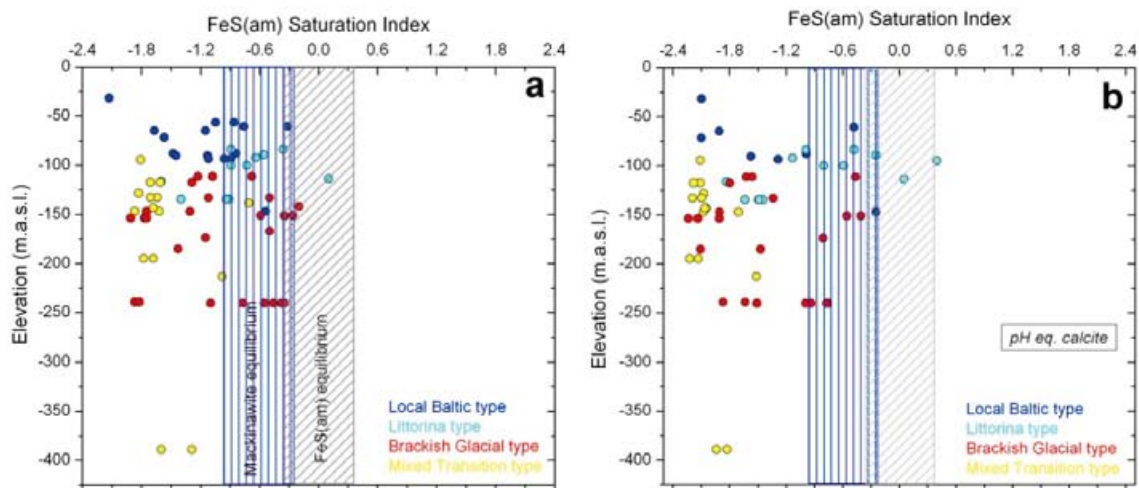


Figure A3-6. Amorphous monosulphide and mackinawite saturation indices obtained with measured (a) and calculated (b) pH values versus depth for the SFR groundwaters.

Therefore, the uncertainties associated with the pH measurement do not affect the main conclusions related to the siderite equilibrium in this work. Moreover, siderite equilibrium situations in the SFR groundwaters, mainly associated with groundwaters with marine signature, were also observed in the PLU groundwaters with clear Littorina contributions (Gimeno et al. 2008).

Most of the groundwaters in the SFR are also in equilibrium with rhodochrosite (Figure A3-5 a, b). Only some Local Baltic type and, especially, Brackish-glacial type groundwaters are undersaturated with respect to this mineral. Although some specific samples are affected by the pH value used in calculations (measured or calculated), the overall picture does not change. Moreover, the clear link between rhodochrosite equilibrium situations and Littorina signatures (Figure A3-5 a, b) in the groundwaters from the SFR was also observed in the groundwaters with similar characters in the PLU and Laxemar-Simpevarp areas (Gimeno et al. 2008, 2009).

Equilibrium situations with respect to the amorphous Fe(II)-monosulphides are scarce in the SFR groundwaters. Only some groundwater samples of Local Baltic, Littorina or Brackish-glacial types are in equilibrium with this mineral when measured pH values are used in the calculations (Figure A3-6a). When calculated pH values are used, only some Local Baltic and, mainly, Littorina-type groundwaters are in equilibrium (Figure A3-6b) and the Brackish-glacial type groundwaters, previously in equilibrium, are now undersaturated.

Thus, in detail, the reduced set of samples in equilibrium with respect to the amorphous Fe(II)-monosulphides is affected by the pH uncertainty and only some Littorina type groundwaters remain in equilibrium. But the overall picture does not change; this type of equilibrium situation is scarce in the SFR groundwaters, as it occurs in the PLU groundwaters (Gimeno et al. 2008). More studies are needed in order to decide whether this situation corresponds to the real one or if it has been produced by sampling conditions (Gimeno et al. 2009, Nilsson et al. 2010, Tullborg et al. 2010).

More groundwaters are in equilibrium with respect to mackinawite but the number of samples is also affected by the pH used in calculations (Figure A3-6). However, a meaningful number of Littorina type groundwaters are in equilibrium, independently of the pH values and the same occurs for the long term hydraulically isolated groundwaters of Brackish-glacial type from the KFR101 borehole at section 271.5–341.76 m.b.l. In any case, as stated above, uncertainties related to possible sampling modifications of dissolved sulphide concentrations still remain.

A3.5 Conclusions

Laboratory measurements of pH represent a source of uncertainty in speciation-solubility calculations related to the carbonate and redox systems. The sensitivity analysis performed in this Appendix has used measured and calculated (in equilibrium with calcite) pH values to evaluate their effects on the carbonate system (calcite saturation index, log pCO₂ values), redox pair calculations and siderite, rhodochrosite and Fe(II)-monosulphides as key redox phases in the studied system.

Overall, the main trends, interpretations and conclusions related to these parameters are not importantly affected by the pH uncertainty. However, some aspects have been influenced by this uncertainty, mainly the undersaturation state situations in some Local Baltic type groundwaters and the equilibrium with respect to the amorphous Fe(II)-monosulphides.

Considering the present degree of knowledge of the system, the effects of the pH uncertainties in these two situations are not a critical point as both are also conditioned by more critical uncertainties due to the lack of information; no information about the marine sediments, hydrochemical features of the infiltrating marine waters, sampling effects on the dissolved sulphide contents, lack of microbiological data, etc. However, *in situ* determination of pH is an indispensable procedure to minimise the set of uncertainties associated with this kind of studies, to make more detailed studies in the future.

Review of on-line Eh measurements in the SFR

It is well known that potentiometric Eh measurements in groundwaters can be subjected to both technical and interpretative problems (Auqué et al. 2008 and references therein), even with the sophisticated methodology for Eh measurement developed by SKB over the last 25 years. Thus, the group of the University of Zaragoza (UZ) has reviewed the available information and continuous logs compiled and supplied by SKB's geodatabase SICADA, as well as the P-reports related to this subject.

The aim of this work is to select the best quality Eh (and pH) values based on a common and well defined set of criteria, as it has been done in the Site Characterisation Programmes from Forsmark and Laxemar (Auqué et al. 2008, Gimeno et al. 2008, 2009).

This appendix presents the final Eh and pH values selected by the UZ group from on-line measurements performed in the SFR site (and based on the work done by Nilsson (2009) and Lindquist and Nilsson (2010)), explaining, when necessary, the differences with the values suggested, reported or rejected by other authors.

A4.1 Available data

Potentiometric Eh measurements have been performed in a few borehole sections at the SFR site in 1987, 2000 and 2009–2010. The mobile chemistry unit with the surface Chemmac measurement system was used for the measurements in all occasions, but none of the measurements were conducted in the same fashion as the Site Characterisation Programmes in Forsmark or Laxemar-Simpevarp. During the Site Characterisation Programme, the measurement methodology involved continuous logging of Eh for long periods of time in isolated packed-off sections in the boreholes. Eh was measured simultaneously by different electrodes (usually three; gold, platinum and glassy carbon electrodes) in the borehole and at the surface, and against Ag/AgCl double junction gel-filled reference electrodes in both cases. Apart from Eh, the logging also included other parameters such as pH, dissolved oxygen, conductivity and temperature.

For the SFR programme, the outlet in the tunnel from each borehole section was connected directly to the Chemmac measurement cell where pumping was not required since the groundwater was discharged by natural over-pressure and the electrodes were located outside the borehole. Although these measurements were technically not as complex as the measurements performed during the Site Characterisation Programme, they may even have some advantages (e.g. no air contaminated equipment is introduced into the borehole section; see Nilsson 2009).

The available data in SFR were recorded at different moments, with intervals of around ten years (1986–87, 2000, 2010). During this time, different modifications and improvements of the Chemmac system have been carried out regarding computerisation, electronics, electrode design, data treatment routines and borehole investigation methodology.

Therefore, the specific methodology and the information level on the on-line measurements are rather heterogeneous:

- Detailed documentation regarding the experiment set-up is not available for the old SFR data (Nilsson 2009).
- On-line measurements of pH, Eh and electrical conductivity (but not dissolved oxygen) are available from three borehole sections (KFR01, KFR10 and KFR7A) and from two different sampling campaigns in each borehole (1986–1987 and 2000 respectively). However, the number of Eh-electrodes used in the measurements varies from two to four, depending on the borehole and on the year of measurement (as reviewed by Nilsson 2009).
- Recent on-line measurements of pH, Eh, electrical conductivity and dissolved oxygen are available for two sections from the KFR105 borehole drilled from the SFR construction tunnel within the SFR extension project. In this case, three Eh electrodes were used and detailed documentation exists on the experiment set-up and protocols (Lindquist and Nilsson 2010).

- Finally, during the autumn campaign in 2010, a further three sections were studied in order to check the previously measured values and on-line measurements with Chemmac probe are available, although no written documentation is available yet.

Most of these pitfalls have been also mentioned in previous reviews of Chemmac logs performed during the Site Characterisation Programme from Forsmark and, specially, at Laxemar where, for example, data from sampling campaigns, quite separate in time, were also included (Gimeno et al. 2008, 2009). Thus, the selection criteria for Eh values defined by the University of Zaragoza group in those exercises can be mostly applied in the SFR.

A4.2 Selection criteria defined by the University of Zaragoza

Chemmac methodology of measurement and the selection criteria used by UZ have been described in detail in Auqué et al. (2008) and more briefly in Gimeno et al. (2008, 2009).

As stated above, the measurement methodology in the SFR involves continuous logging of Eh for long periods of time. Eh is measured simultaneously by different electrodes (usually, gold, platinum and glassy carbon electrodes; i.e. Eh_{au}, Eh_{pt} and Eh_{gc}) against Ag/AgCl double junction gel-filled reference electrodes. Apart from Eh, the logging also includes other parameters such as pH (usually by different electrodes simultaneously; pH_y), conductivity, temperature and, only in some cases, dissolved oxygen. The selection of a potentiometric Eh value from logs must be based on a careful analysis of the readings obtained with the different electrodes, the logging time, the pH, the conductivity, and the dissolved oxygen values.

The basic assumption is that the measured potential corresponds to the equilibrium potential and this fact can only be demonstrated when the different electrodes give identical readings (Christensen et al. 2000). Ideally, the Eh values selected as representative should only be those obtained simultaneously and within a small Eh range (± 50 mV²²) by all used electrodes over a long period of time. However this criterion is too restrictive; there might be undesirable effects or technical problems selectively affecting several electrodes or, as it occurs in this case, the measurements could have been performed with a different number of electrodes over the time. Taking into account all these issues, the following selection criteria were applied:

- Eh logs longer than 3 days (actually, most logs are longer than a week);
- Eh logs with stable (i.e. not changing over time) and similar readings (range smaller than ± 50 mV) for, at least, two electrodes in the long term; and
- Eh logs with simultaneous and stable pH readings (in order to minimise the uncertainty associated with pH in geochemical modelling).

A4.3 Review of the existing information

As stated above, potentiometric Eh measurements were conducted in three of the early SFR boreholes (KFR01 at 44.5–62.3 m.b.l. KFR7A at 48.0–74.7 m.b.l. and KFR10 at 87.0–107.28 m.b.l.) in 1986–1987 and repeated in the same three borehole sections in 2000 (Nilsson 2009). These data are presented in section A4.3.1. Additionally, recent potentiometric Eh measurements were conducted in two sections from the KFR105 borehole drilled from the SFR construction tunnel within the SFR extension project (Lindquist and Nilsson 2010, Nilsson et al. 2010) (data presented in section A4.3.2) and in three sections of three different boreholes (KFR19, KFR7A and KFR08) during the last autumn campaign (2010). These latest data are presented in section A4.3.3.

²²This value (± 50 mV) corresponds to the precision of Eh measurement in borehole sections for the SKB methodology (SKB 2001) and also to the precision usually considered in the scientific literature (e.g. Kölling 2000).

A4.3.1 On-line measurements in KFR01, KFR7A and KFR10 during 1987 and 2000

KFR01, borehole section 44.5–62.3 m.b.l.

The first measurement was performed in 1987 with two electrodes (glassy carbon and platinum electrodes, *Ehcy* and *Ehpty*, respectively) for about 15 days. Readings follow a decreasing trend with time and both electrodes seem to reach a relatively stable value (around –133 to –139 mV) at the end of the measurement period (Figure A4-1a). Thus, in agreement with Nilsson (2009) and Nilsson et al. (2010), a value of –140 mV has been selected.

The corresponding pH values were stable around 7.5 during the extent of the measurement period (Figure A4-2a). Laboratory measured values in groundwater samples taken during this period range between 7.4 and 7.5, thus, this pH value (7.5) can be selected for this section. Conductivity also shows a stable value around 1,290 mS/m during the measurement period.

The second measurement was performed in 2000 with three Eh electrodes (glassy carbon, platinum and gold *Ehcy*, *Ehpty*, and *Ehauy* respectively). All of them stabilised at positive values between 80 and 120 mV for about a 12 day period before starting to decrease after a further 20 days (the steeper decrease is marked by the carbon electrode towards –100 mV; Figure A4-1b). An Eh value for this section was not proposed by Nilsson (2009) or Nilsson et al. (2010). However, as it was indicated by Nilsson (2009), these Eh values might be representative of the groundwater situation at that time rather than erroneous measurements (as the long stabilisation period defined by three different electrodes suggests). Thus, a value of +110 mV was selected; note that the value selected for the same section in 1987 was –140 mV.

Measured pH values by two different electrodes show stable readings around 7.5 (with variations lower than 0.05 pH units, Figure A4-2b) during the same time interval when also stable Eh readings were obtained (Figure A4-1b). This value is the same as the one measured in 1987. The pH values measured in the laboratory for the groundwater samples taken during this period range from 7.5 to 7.6 and the value selected in the SICADA database is 7.46. Thus, a pH value of 7.5 was selected for this section where conductivity values were also stable around 938 mS/m.

KFR7A, borehole section 48.0–74.7 m.b.l.

Two electrodes (glassy carbon and platinum electrodes) were used during the first measurement time (1987) in borehole KFR7A. During the first three days significant differences in the readings were observed but gradually both electrodes stabilised at a potential around –180 mV (Figure A4-1c). Therefore, this value has been selected in agreement with Nilsson (2009) and Nilsson et al. (2010).

Stable conductivity values (around 1,530 mS/m) were recorded during the logging period and the measured pH values, provided by two different electrodes (squares and diamonds in Figure A4-2c), were also stable but at different values, 7.6 and 8.0. A pH value of 7.58 was proposed for this section in SICADA although lower pH values were measured in the laboratory for groundwater samples taken in the same section (between 7.3 and 7.5). Thus, in this case, the selection of a representative pH value is more problematic. A value of 7.6 ± 0.2 was proposed with the proviso that it is handled with caution.

During the measurements performed in 2000, the three Eh electrodes used stabilised at a positive value between 20 and 40 mV after about six days. Even the minor divergences observed over these six days were restricted to a narrow range (between +10 and +50 mV; Figure A4-1d). The following long period when stable readings were achieved by the three different electrodes, strongly suggests that a positive Eh might be representative of the true groundwater situation at that time. Thus, a value of +30 mV was selected in agreement with the value (+20 mV) proposed by Nilsson (2009). Note again the difference in the selected value for this period and the one found in 1987.

Conductivity shows a continuous decrease during the logging period (from 1,600 to 1,420 mS/m) and a decrease also occurs for the pH values recorded by two different electrodes (Figure A4-2d). However, the decreasing pH trend is very subtle, showing variations from only 7.6 to 7.5 over the 20 days of measurement. Laboratory pH values measured in the groundwater samples from this period were around 7.65. Thus, a pH value of 7.55 was selected (in agreement with the value indicated in SICADA).

Overall, the measurements performed in this section during 2000 appear to correspond to groundwaters (of Littorina type, Nilsson et al. 2010) that were subject to slight dilution processes during the logging period but with “stable” Eh and pH conditions.

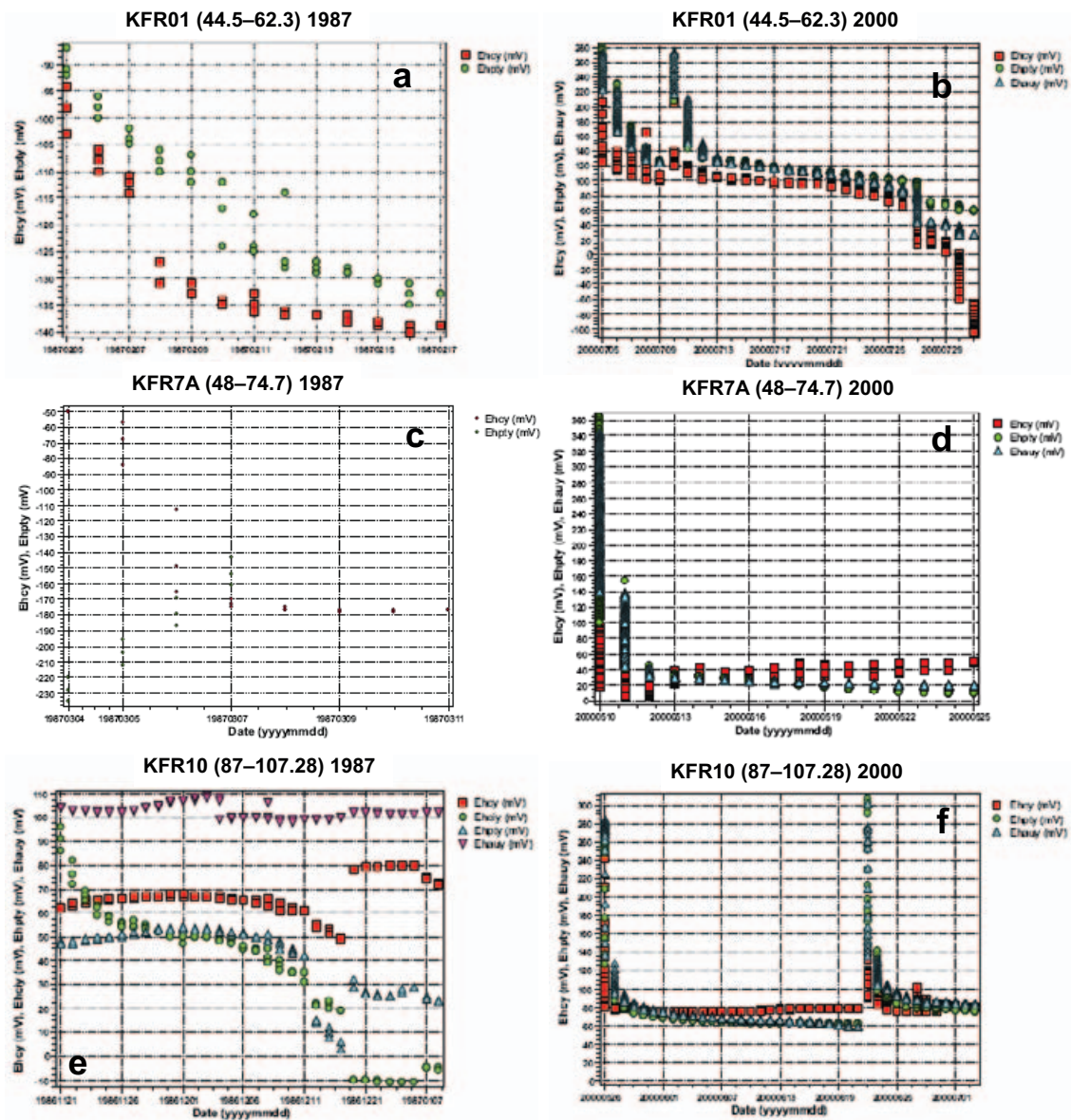


Figure A4-1. Results of on-line redox potential measurements in the KFR01, KFR7A and KFR10 boreholes. Eh values measured in the KFR01 borehole at section 44.5–62.3 m.b.l. by platinum (Ehpty) and glassy carbon (Ehcy) electrodes during 1987 (a) and by platinum, glassy carbon and gold (Ehaay) electrodes during 2000 (b) ; Eh measurements in the KFR7A borehole at section –48.0 to –74.7 m.a.s.l. carried out by platinum and glassy carbon electrodes during 1987 (c) and by platinum, glassy carbon and gold electrodes during 2000 (d).; Eh values measured in the KFR10 borehole at section –87.0 to –107.28 m.a.s.l. by platinum, gold and two glassy carbon electrodes (Ehcy and Ehcay) during 1986 (e) and by platinum, glassy carbon and gold electrodes during 2000 (f) . Data from Nilsson (2009).

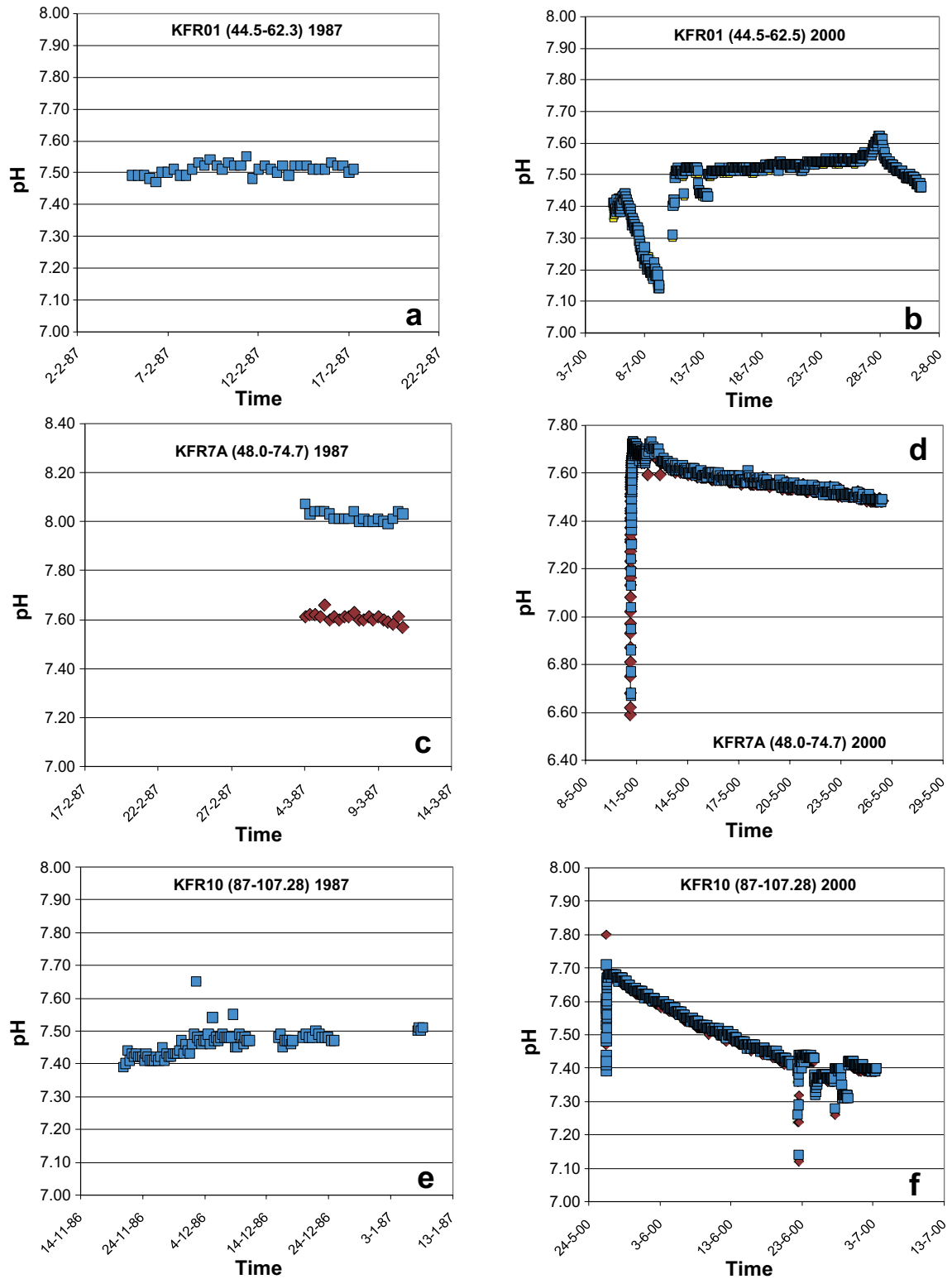


Figure A4-2. Results of on-line pH measurements in the KFR01, KFR7A and KFR10 boreholes. pH measurements during 1987 (a) and during 2000 with two electrodes (b) in the KFR01 borehole at section 44.5–62.3 m.b.l.; pH measurements during 1987 with two electrodes (c) and during 2000 also with two electrodes (d) in the KFR7A borehole at section 48.0–74.7 m.b.l.; pH measurements during 1986 (e) and during 2000 with two electrodes (f) in the KFR10 borehole at section 87.0–107.28 m.b.l.

KFR10, borehole section 87.0–107.28 m.b.l.

The first measurements in 1987 were performed with four electrodes (two glassy carbon electrodes – Ehcy and Ehcy –, a platinum electrode – Ehpty – and a gold electrode – Ehauy –) over almost 50 days. At the end of the logging period the electrodes stabilised at different potential values ranging from positive to close to zero (–10 to +105 mV). However, stable and coincident readings were obtained for 10 days at the middle of the measurement period for three electrodes (the platinum and the two glassy carbon electrodes) between +50 and +70 mV (Figure A4-1e). The other electrode (the Au electrode) provided a value around +100 mV although not perfectly stable.

Thus, in this logging period two redox potential trends seem to exist. A value of +60 mV could be proposed from the aforementioned agreement between the three electrodes during the ten day period. However, during the final period, overall stable values appear for all electrodes but at a wider range of potentials. In general, the main observation is that all recorded Eh data suggest the existence of positive potentials, and the selection of an Eh value therefore will be a compromise. A value of +60 mV was chosen subsequently for comparative or discussion purposes.

Recorded pH values reached stable readings between 7.45 and 7.52 during the last month of measurement (Figure A4-2e) in common with conductivity (around 1,534 mS/m). Thus, a pH value of 7.5 was selected in agreement with the value indicated in SICADA.

The late measurements in 2000 showed stable and positive redox potentials (+60 to +90 mV) by three electrodes almost since the beginning of the logging. Moreover, after an interruption of the measurements, the three electrodes quickly stabilised in the same range of values (Figure A4-1f). Thus a value of +70 mV was selected in agreement with the value (+80 mV) proposed by Nilsson (2009) and close to the one selected in 1987.

Conductivity shows a subtle decreasing trend during the complete measurement period (between 1,140 and 1,050 mS/M) and the same is observed for the recorded pH values. However, following the measurement interruption (Figure A4-2f), the pH values obtained by two electrodes appear to stabilise between 7.35 and 7.45 over a period of a week. Thus a pH of 7.4 was selected in agreement with the value in the SICADA database.

A4.3.2 On-line measurements in KFR105 in 2009

KFR105, borehole section 120.0–137.0 m.b.l.

In this section, Chemmac measurements were performed more recently in 2009 within the SFR extension project (Lindquist and Nilsson 2010). Redox potential values measured by three different electrodes (gold, glassy carbon and platinum electrodes) provide positive values reaching stable readings between +30 and +50 mV (Figure A4-3a). Dissolved oxygen data indicate a value of 0 mg/L during the measurement period. A value of +40 mV was selected for this section.

Recorded conductivity and pH values (the latter measured by two different electrodes) are very stable since beginning the logging (Figure A4-3b). There is no selected pH value in the SICADA database; however, a pH value of 7.45 is proposed here for this section. Laboratory pH measurements in the groundwater samples from this period range between 7.49 and 7.54.

KFR105, borehole section 265.0–306.8 m.b.l.

Chemmac measurements for this section were also performed within the SFR extension project. Two sets of logs are available, one performed in 2009 and other repeated at the beginning of 2010 (Lindquist and Nilsson 2010).

Recorded Eh values in 2009 by three electrodes stabilised between +40 and +60 mV (Figure A4-3c) and the dissolved oxygen contents were below the detection limit; thus, a value of +50 mV was selected for this period. Measured pH values (by two different electrodes; Figure A4-3d) were very stable over the logging period and a value of 7.6 was selected (laboratory pH measurements in the groundwater samples from this period are between 7.54 and 7.57).

The repeated Eh measurements in 2010 used, once again, three different electrodes. However, the platinum electrode gave erroneous values that are not shown here. At the beginning of this new logging

period, the gold and carbon electrodes provided similar and stable readings around +80 mV for over a week (Figure A4-3e), very similar to the values obtained in 2009. From then on, the potential values decrease, reaching stable and reducing readings at the end of the measurement period (around -190 mV).

The pH measurements appear to show some electrical disturbances but a value of 7.4 ± 0.1 was proposed for the end of the recording period (Figure A4-3f). However, for some unknown reason(s), a pH value of 7.7 has been included in SICADA for this section and for the same measurement period. Thus, this value needs to be corrected.

Overall, the Eh values appear to change from oxidising to reducing conditions in the two successive measurement periods in this section. The stable and similar potential readings by different electrodes and the good link between these measurement periods would suggest that the observed changes correspond to a “real” situation” in the analysed groundwater rather than to erroneous measurements in the logs. This will be discussed in the discussion section.

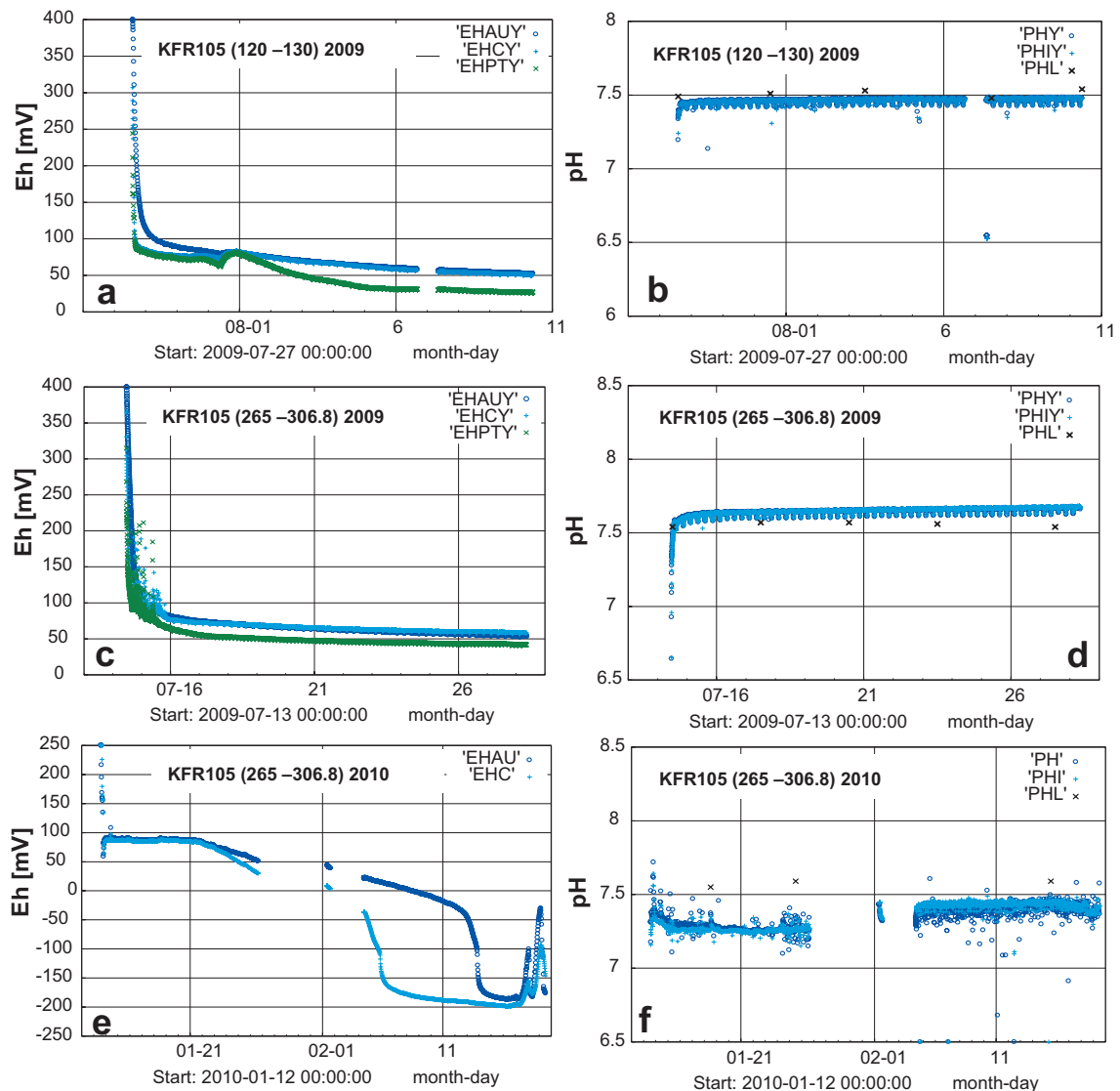


Figure A4-3. Results of on-line redox potential and pH measurements in the KFR105 borehole. (a) Eh measurements by platinum (Ehpty), glassy carbon (Ehcy) and gold (Ehauy) electrodes, and (b) pH measurements by two electrodes (pHy and pHiy) s during 2009 at section 120.0–130.0 m.b.l.; (c) Eh measurements by platinum (Ehpty), glassy carbon (Ehcy) and gold (Ehauy) electrodes, and (d) pH measurements by two electrodes (pHy and pHiy) during 2009 at section 265.0–306.8 m.b.l.; (e) Eh measurements by glassy carbon (Ehc) and gold (Ehau) electrodes and (f) pH measurements by two electrodes (pH and pHi) during 2010 at section 265.0–306.8 m.b.l. Data from Lindquist and Nilsson (2010).

A4.3.3 On-line measurements in KFR07A, KFR08 and KFR19 boreholes in autumn 2010

Five out of the nine redox measurements reviewed above (mostly, “old” measurements without detailed information) show a mildly reducing character whereas the rest indicate slightly oxidising conditions. Two of the sections with repeated measurements (in 1986–87 and in 2000) have changed from reducing to oxidising values (KFR01 and KFR7A) whereas one section (in the KFR10 borehole) appears to maintain an oxidising character. The hydrochemistry of the groundwaters in these sections has also evolved with time; their initial composition, mainly that of Littorina type groundwaters, has been modified by the intrusion of present Baltic Sea water. A general “dilution” of all dissolved components (including the redox sensitive elements such as Fe or Mn) and an increment in the tritium contents are clearly shown between 1986–87 and 2000.

Thus, an increase in Eh with time, due to the input of shallow marine waters (promoted by the change in hydraulic conditions, i.e. drawdown caused by the repository), could be possible. However, oxygen diffusion into tubes connecting the borehole outlet and the measurement cell (e.g. due to long tubing or poor choice of tubing material) can not be entirely discarded; unfortunately, there is no data on dissolved oxygen during these measurement periods. Moreover, effects of the oxic environment in the tunnels may influence these oxidising measurements (e.g. in the section groundwater) as suggested by the results obtained in the KFR105 borehole at section 265.0–306.8 m. Here, the opposite Eh trend is observed showing a change from oxidising to reducing conditions in the measurements performed in 2009 and 2010. In addition, significant changes in groundwater composition were also observed with increasing iron contents between the measurement campaigns.

In order to determine which of these possibilities would be the responsible for the oxidant character measured, three new sections were selected (based on a thorough analysis of the different possibilities) where additional measurements were made available at the end of 2010. Two sections in KFR08 and KFR19 were selected for these measurements because their groundwaters were of the Baltic type in both cases and they represent two different situations; (1) a major deformation zone, and (2) the bedrock between deformation zones. Section in KFR08 is located in a conductive major vertical zone (Zone 8) and it seems to correspond to a preferential flow path of Baltic Sea waters (the groundwaters at this section were of the “Baltic type” already since the beginning). Thus, if the intrusion of Baltic Sea waters were responsible for the oxidant Eh values measured, this section would be especially suitable to investigate.

The section in KFR7A at 48 74.7 m.b.l. was also selected. This section was previously monitored in 1986–87 and in 2000 and measurements have changed from reducing to oxidising values. Furthermore, the hydrochemistry of the groundwaters in this section also has evolved with time, although still retaining the initial Littorina type character.

These results are very recent and therefore there is to date no available documentation. However, below is included a preliminary presentation of the data provided by Nilsson (Pers. comm.) containing important additional information for understanding the redox-system at the SFR site.

Results obtained *in the KFR19 borehole at section 95–110 m.b.l.* indicate that during the first twenty days of measurements, the Eh values recorded by three electrodes do not stabilise. However, by the end of the measurement period, the Eh values stabilised to about –165 mV (Figure A4-4a). Measured pH values (by one electrode; Figure A4-4b) were very stable during the logging period and a value of 7.7 was selected.

Measurements *in the KFR08 borehole at section 63.0–104.0 m.b.l.* also provided reducing Eh values of about –157 mV by three electrodes whereas pH values of 7.3 were determined by two electrodes (Figure A4-4c and A4-4d).

Therefore, with respect to these two borehole sections which correspond to preferential flow paths of Baltic Sea water, reducing conditions have been measured.

In the KFR7A borehole at section 48.0–74.7 m.b.l. the Eh values were also recorded by three electrodes but failed to stabilise during the first twenty five days of measurement (Figure A4-4e). During this time two of the electrodes provided oxidising values (as occurred in the measurements performed in 2000; Figure A4-2d); however, by the end of the measurement period, Eh values measured by all three electrodes stabilised to about –150 mV (Figure A4-4e). The overall trend of the measured redox potential is similar to that obtained during the second measurement campaign made in borehole KFR105 (Figure A4-3e).

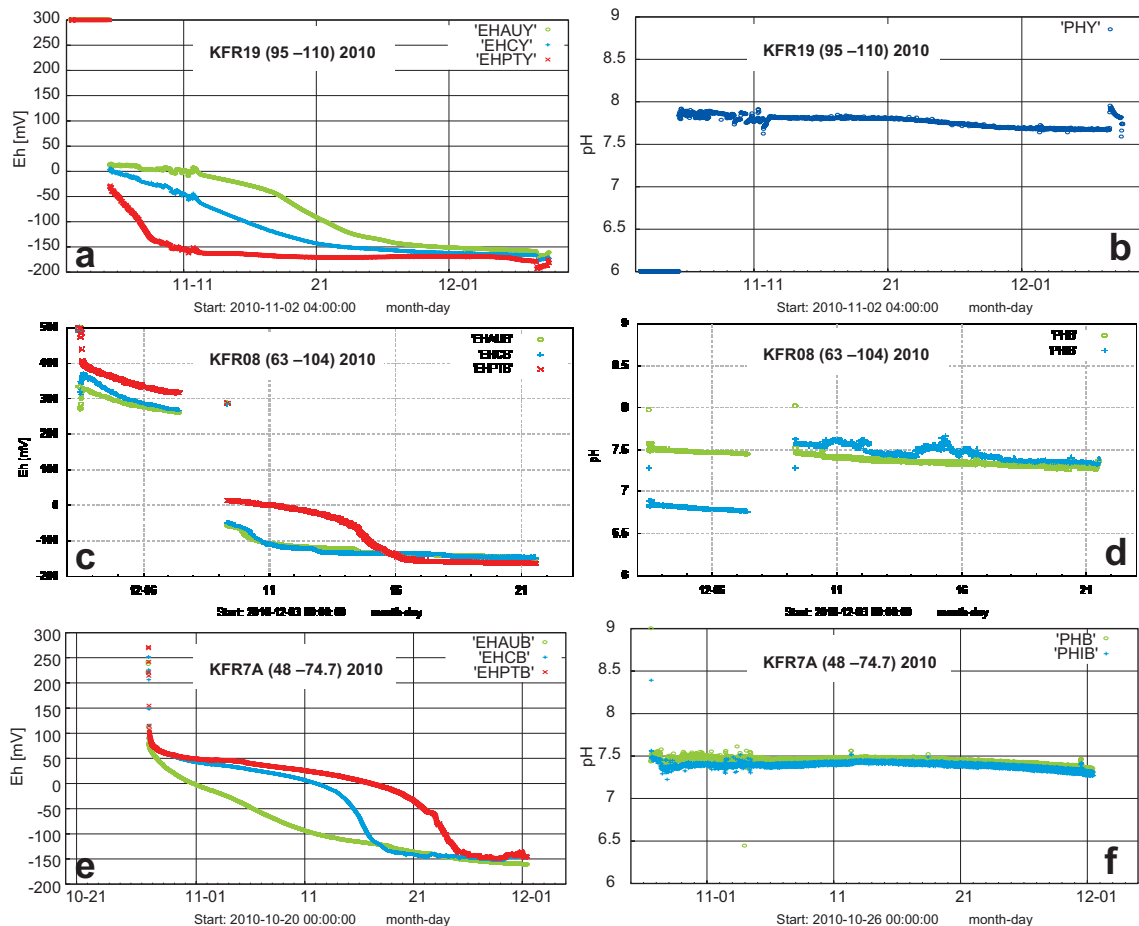


Figure A4-4. Results of on-line redox potential and pH measurements in the KFR19 (a, b), KFR08 (c, d) and KFR7A (e, f) boreholes, measured during the autumn campaign in 2010. Data provided by Nilsson A-C.

Measured pH values (by two different electrodes; Figure A4-4f) were very stable during the logging period and a value of 7.4 was selected.

This section, therefore, appears to recover the “original” reducing character (measured in 1986–1987) after a more or less prolonged pumping period in 2010. This reducing redox potential would be in agreement with the still retained “Littorina type” groundwaters found at this borehole section.

A4.4 Discussion and conclusions

Eight of the twelve reviewed redox measurements, performed at depths between 94 and 154 m in the SFR, show a mildly reducing character, whereas the rest indicate slightly oxidising conditions.

Two of the sections with repeated measurements (in 1986–87 and in 2000) have changed from reducing to oxidising values (in KFR01 and KFR7A), whereas one section (in KFR10) appears to maintain an oxidising character. The hydrochemistry of the groundwaters in these sections have evolved with time, mainly the “dilution” of Littorina type groundwaters by the intrusion of present Baltic Sea water. A general decrease of all dissolved components (including the redox sensitive elements Fe or Mn) and an increment in the tritium contents are clearly shown between 1986–1987 and 2000. Positive Eh values were also measured in the KFR105 borehole at section 120.0–137.0 m.

Other section with repeated measurements in the KFR105 borehole (section 265.0–306.8 m) shows the opposite trend with changes from oxidising to reducing conditions in the measurements performed in 2009 and 2010. Significant changes in groundwater composition, with increasing iron contents between these measurement campaigns, were also observed. This change occurred during measurements performed in 2010 (Figure A4-3e) and there is a similarity to the trend observed in

the KFR01 borehole at section 44.5–62.3 m.b.l. (Figure A4-1b) during 2000. However, the observed decreasing trend towards reducing conditions at the end of the measurements in this last section might have stabilised had the measurements continued.

Positive Eh values and also changes from reducing to oxidising values can be caused by;

- the intrusion of young oxidising marine waters (promoted by the change in hydraulic conditions, i.e. drawdown caused by the repository),
- oxygen diffusion into tubes connecting the borehole outlet and the measurement cell (e.g. due to long tubing or poor choice of tubing material) especially during the old campaigns, or
- the measurements were influenced by the oxic environment in the tunnels (i.e. reflected in the initial borehole section groundwater samples).

The rapid penetration of oxidising Baltic Sea waters could be possible as there are only small amounts of deposited fine-grained material in the sea bed above the SFR. Therefore, the reducing effect of organic debris on oxygen may remain incomplete. In such case, the oxidation of ferrous minerals within bedrock fractures would be the most probable oxygen consumer. At present, there are no data on the oxidising or reducing character of the infiltrating waters in the marine sediments above the SFR.

The most recent measurements performed in preferential “Baltic type” groundwaters paths (KFR08 and KFR19 boreholes) would indicate that this type of “recent” marine groundwater is anoxic and shows a clear reducing character. The presence of circulating recent marine-derived reducing groundwaters at the SFR may to some extent be supported by the results obtained in the Aspö HRL REX project where young oxidising meteoric waters intruding into the bedrock became reducing in a few weeks.

With respect to the tunnels, the influence of the oxic environment could explain the oxidising measured Eh values. These oxidising conditions would be representative of the groundwater situation close to the oxic environment in the tunnels, but would change to reducing conditions due to pumping from sources into the bedrock away from the tunnels. In addition, the gradual removal of the groundwater from the analysed section, and the progressive introduction of reducing formation water into the section, could possibly cause disequilibrium and may explain the observed long stabilisation periods towards achieving reducing conditions. Results from the more recent measurements performed in the KFR19 and KFR7A boreholes, also characterised by long stabilisation periods, would support this hypothesis (see Chapter 5 for further discussion).